European Journal of Scientific Research

ISSN: 1450-216X **Volume 18, No 3 October, 2007**

As of 2005, European Journal of Scientific Research is indexed in ULRICH, DOAJ and CABELL academic listings.

European Journal of Scientific Research

http://www.eurojournals.com/ejsr.htm

Editorial Policies:

1) European Journal of Scientific Research is an international official journal publishing high quality research papers, reviews, and short communications in the fields of biology, chemistry, physics, environmental sciences, mathematics, geology, engineering, computer science, social sciences, medicine, industrial, and all other applied and theoretical sciences. The journal welcomes submission of articles through ejsr@eurojournals.com.

2) The journal realizes the meaning of fast publication to researchers, particularly to those working in competitive & dynamic fields. Hence, it offers an exceptionally fast publication schedule including prompt peer-review by the experts in the field and immediate publication upon acceptance. It is the major editorial policy to review the submitted articles as fast as possible and promptly include them in the forthcoming issues should they pass the evaluation process.

3) All research and reviews published in the journal have been fully peer-reviewed by two, and in some cases, three internal or external reviewers. Unless they are out of scope for the journal, or are of an unacceptably low standard of presentation, submitted articles will be sent to peer reviewers. They will generally be reviewed by two experts with the aim of reaching a first decision within a three day period. Reviewers have to sign their reports and are asked to declare any competing interests. Any suggested external peer reviewers should not have published with any of the authors of the manuscript within the past five years and should not be members of the same research institution. Suggested reviewers will be considered alongside potential reviewers identified by their publication record or recommended by Editorial Board members. Reviewers are asked whether the manuscript is scientifically sound and coherent, how interesting it is and whether the quality of the writing is acceptable. Where possible, the final decision is made on the basis that the peer reviewers are in accordance with one another, or that at least there is no strong dissenting view.

4) In cases where there is strong disagreement either among peer reviewers or between the authors and peer reviewers, advice is sought from a member of the journal's Editorial Board. The journal allows a maximum of two revisions of any manuscripts. The ultimate responsibility for any decision lies with the Editor-in-Chief. Reviewers are also asked to indicate which articles they consider to be especially interesting or significant. These articles may be given greater prominence and greater external publicity.

5) Any manuscript submitted to the journals must not already have been published in another journal or be under consideration by any other journal, although it may have been deposited on a preprint server. Manuscripts that are derived from papers presented at conferences can be submitted even if they have been published as part of the conference proceedings in a peer reviewed journal. Authors are required to ensure that no material submitted as part of a manuscript infringes existing copyrights, or the rights of a third party. Contributing authors retain copyright to their work.

6) Submission of a manuscript to EuroJournals, Inc. implies that all authors have read and agreed to its content, and that any experimental research that is reported in the manuscript has been performed with the approval of an appropriate ethics committee. Research carried out on humans must be in compliance with the Helsinki Declaration, and any experimental research on animals should follow internationally recognized guidelines. A statement to this effect must appear in the Methods section of the manuscript, including the name of the body which gave approval, with a reference number where

appropriate. Manuscripts may be rejected if the editorial office considers that the research has not been carried out within an ethical framework, e.g. if the severity of the experimental procedure is not justified by the value of the knowledge gained. Generic drug names should generally be used where appropriate. When proprietary brands are used in research, include the brand names in parentheses in the Methods section.

7) Manuscripts must be submitted by one of the authors of the manuscript, and should not be submitted by anyone on their behalf. The submitting author takes responsibility for the article during submission and peer review. To facilitate rapid publication and to minimize administrative costs, the journal accepts only online submissions through ejsr@eurojournals.com. E-mails should clearly state the name of the article as well as full names and e-mail addresses of all the contributing authors.

8) The journal makes all published original research immediately accessible through www.EuroJournals.com without subscription charges or registration barriers. European Journal of Scientific Research indexed in ULRICH, DOAJ and CABELL academic listings. Through its open access policy, the Journal is committed permanently to maintaining this policy. All research published in the. Journal is fully peer reviewed. This process is streamlined thanks to a user-friendly, web-based system for submission and for referees to view manuscripts and return their reviews. The journal does not have page charges, color figure charges or submission fees. However, there is an article-processing and publication charge.

Further information is available at: http://www.eurojournals.com/ejsr.htm

European Journal of Scientific Research

Volume 18, No 3 October, 2007

Contents

European Journal of Scientific Research
ISSN 1450-216X Vol.18 No.3 (2007), pp.354-359

http://www.eurojournals.com/ejsr.htm

Complexation of Nicotinohydroxamic Acid with Nickel (II)

Aliyu A.O
Department of Chemistry, Research Laboratory
Nigerian Defence Academy, PMB 2109, Kaduna
E-mail: salimatadetutu@yahoo.com

Nwabueze J.N
Department of Chemistry, Research Laboratory
University of Abuja, PMB 117, FCT, Abuja, Nigeria

Abstract

A spectroscopic investigation of the reaction of nicotinohydroxamic acid with N_i^{11} in aqueous solution reveals the sole formation of 1:2 complex at equilibrium. Spectra and magnetic studies of the isolated complex indicate octahedral mixed coordination mode (N,O). Microbial sensitivity test on 8 microorganisms show no activity.

Keywords: Nickel (II), spectroscopic investigation, octahedral and mixed coordination.

Introduction

The biological importance of hydroxamic acids is well established[1]. They are known as constituents of antibiotics, growth factors, food additives, tumor inhibitors and cell division factors. Hydroxamic acids have been shown to possess diverse biological activities, many of which are due to their complexing properties towards transition metal ions[2-4]. Data have been published on the inhibitory activity of hydroxamic acid derivatives of amino acids and peptides on metalloproteinases[5,6]. The mechanism of inhibition appears to involve chelation of metals at their active sites. Some amino hydroxamic acids have been investigated with the aim of designing metal chelates as suitable sources of various trace element essential in animal nutrition[7].

A few complexes of Ni (II) have been synthesized with hydroxamic acids. The greenish-yellow bis (hydroxamato) Ni (II) has been prepared[(8)]. The greenish yellow nickel (II) complexes are paramagnetic having magnetic values of 2.78-3.15 B.M and are presumably octahedral. It has equally been reported that Ni (II) forms square planar complex probably with ground state[8].

Due to the nature of the nickel (II) ion, one can expect some preference for the formation of an N-N chelate. This prediction has been widely confirmed, both in solid state and in solution[8]. The same coordination mode is especially favoured when square-planar complexes are formed. However N,O bonding mode has been reported in dinuclear complex of copper (II)[9].

With regards to the strong ability of hydroxamic acids to form chelates, clarification of their interactions with metal ions is of particular importance in terms of biological effects. This paper is therefore a report on the work carried out on the complexation of nickel (II) with nicotinohydroxamic acid with special emphasis on the structure and nature of bonding involved. In addition, some physico-chemical properties were investigated and included in this report.

Experimental

Ethylnicotinate was obtained from Aldrich. All other reagents were of Analar R-grade. $NaNO_3$ was used for the preparation of the background electrolyte and stock solutions. Water was doubly distilled, degassed using purified N_2 and stored in glass stoppered flasks. KOH and HNO_3 used for adjusting pH were stored in glass ampoules and were standardized with potassium hydrogen phthalate and tris (hydroxymethyl) methyl amine respectively. The pH measurements were made using a radiometer Copenhangen Research pH meter calibrated with standard buffer tablets (2,4,9).

Electronic spectra were recorded on ATI Maltson Genesis series. FTIR^{TM} machine as Nujol mull in the 4000-200cm^{-1} spectra region. Room temperature magnetic susceptibility measurements were made on MSB Auto magnetic susceptibility balance. All these analysis were done at National Research Institute for Chemical Technology (NARICT) Zaria and University of Abuja.

Preparation of the Ligands

Nicotinohydroxamic acid (NHA) was prepared as described in literature[10].

Preparation of the Complex

$[Ni(NHA)_2].2H_2O$ complex was prepared as follows:

$NiSO_4.6H_2O$(0.53g, 0.002 mol) in EtOH was added with stirring in NHA (0.556g, 0.004 mol) in EtOH (20cm^3). To this mixture a 10% solution of $NaHCO_3$ was added until a lemon green precipitate appeared. The precipitate was removed by filtration, washed with small aliquots of Et_2O and dried over silica gel in a vacuum dessicator. Yield 55%.

Equilibrium Studies

The pKa values for the ligands was determined spectrophotometrically by the method of Albert and Sergent[11] using Boric acid and borax of ionic strength 0.1 moldm^{-3} and 0.025 moldm^{-3} buffer for NHA ligand. In this case, the ligand stock solution was 5 x 10^{-4} mol dm^{-3} diluted five folds in buffer solution for NHA. Measurements were made in eight boric/borax buffer solutions used for NHA at analytical wavelength of 215nm. The number of complexes present in solution at equilibrium was determined by the isosbestic point method and graphic Matrix rank analysis using nine solutions containing 1:1 – 1:5 metal ligand ratio (ligand concentration increasing in units of 0.5). A solution of I = 0.1 mol dm^{-3} made up of 0.01 mol dm^{-3} HNO_3 and 0.09 mol dm^{-3} $NaNO_3$ was used to prepare equimolar solution of Ni^{2+} and the ligands 2.5 x 10^{-3} mol dm^{-3}; the same solution was used for all dilutions. In all cases, the solutions were thermostated at 25ºC 2 hr in an ultrasonic bath.

Evaluation of the Antimicrobial Activity

The antimicrobial activity of the test compound was assayed against eight bacteria. *S.aureus, E-coli, Salmonella-typhy, Klebsiella, Streptocococcus, Pseudomonias, Corrynebacterium* and *Neisseria.* Among these organisms, four of them are Gram +ve. While others are Gram -ve. All are regarded as phatogenic to humans and animals. All media and bacteria suspensions were prepared using a method adapted from that of cruicksahank[12].

About 15-20cm^3 of molten nutrient agar was poured into sterile Petri plates about 10cm in diameter. After solidification of the agar, three cups (10mm in diameter and 5mm deep) were removed from each agar dish and fresh bacteria suspension was then uniformly spread on each cup. At this point, each of the cups was spotted three times with test solution at concentration of 50, 100 and 200 μg/cm^3 in dimethyl sulphoxide DMSO. After incubating the plates at 37ºC overnight, the diameter of the zone of inhibition of the bacteria growth was then recorded.

A 5% phenol solution was used as a positive control and DMSO as solvent control each time the experiments were performed.

Results and Discussion

Table 1: Analytical data and Physicochemcial Properties of the Isolated Complexes () Calculated %.

Compound	Form.wt	Mp/Dec ^{o}C	Colour	Found M	μ eff B.M	λ max x 10^3	Assignment
$Ni(NHA)_2.2H_2O$	370.17	211	Lemon	15.46	3.27	25.64	$^3A_{2g} \rightarrow {}^3T_{1g}P$
			Green	(15.86)		19.61	$^3A_{2g} \rightarrow {}^3T_{1g}P$
						12.35	$^3A_{2g} \rightarrow {}^3T_{2g}$

Key: M = metal, Formwt = Formular weight, MP/dec = Melting Point/Decomposition, B.M = Borh Magneton

Table 2: Diagnostic I.R Data for the Complex (cm^{-1})

Compound	ν (NH) cm^{-1}	$\Delta\nu$ (NH) cm^{-1}	ν (C=0) cm^{-1}	$\Delta\nu$ (C=0)cm^{-1}
NHA	3418.00		1659.61	
$Ni(NHA)_2.2H_2O$	3343.18	-74.82	1566.96	-89.65

Key: NHA = Nicotinohydroxamic acid

Table 3: Microbial Sensitivity Test for the Ligands and its isolated Nickel (II) Complex.

Ligand/ Complex	*Staph. Aureus*	*S. Typhylium*	*E.Coli*	*Klebsiella*	*α hemolytic strep.*	*Neisseria*	*Pseudo-nomias*	*Coryne-bacteria*
Gram	+ve	+ve	-ve	-ve	+ve	-ve	-ve	+ve
NHA	-	-	-	-	-	-	-	-
$Ni(NHA)_2.2H_2O$	-	-	-	-	-	-	-	-

Figure 1: Isosbestic point search for Ni^{II}-NHA system

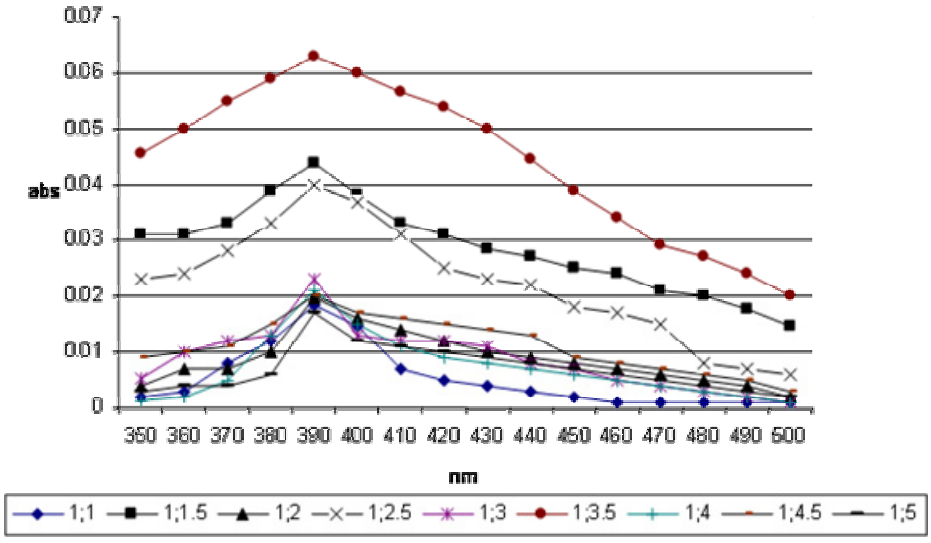

Figure 2: Graphical rank Matrix analysis for Ni^{II}-NHA system (one specie test)

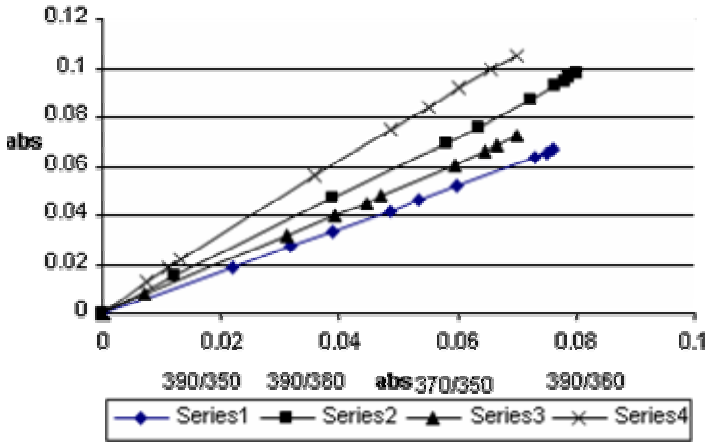

Figure 3: Continuous variations (Job's plot) for Ni^{II}-NHA system

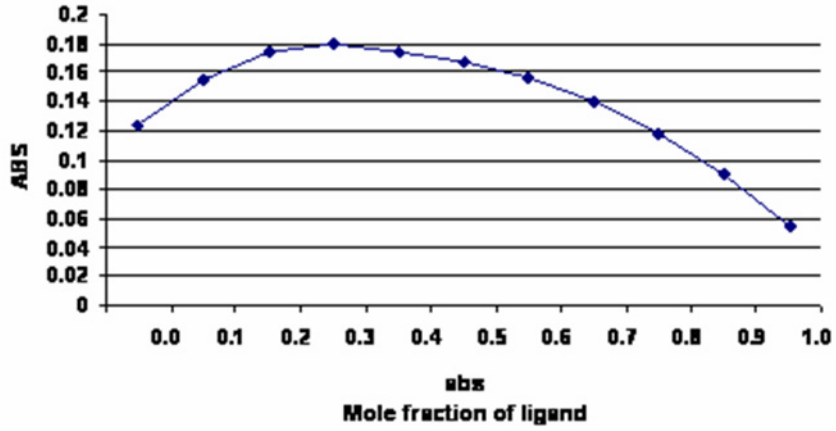

Figure 4: Visible Spectrum of $[Ni(NHA)_2].2H_2O$ Complex.

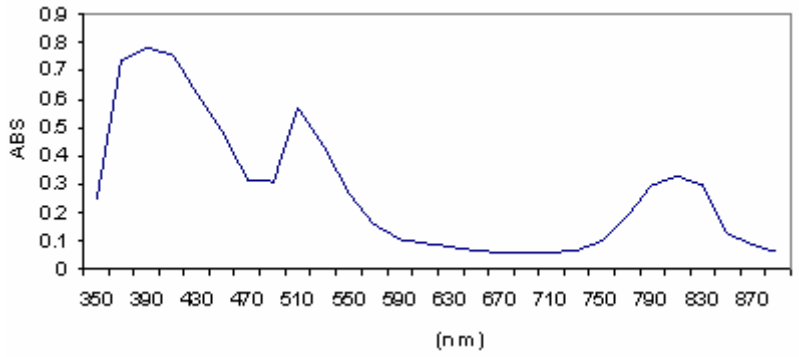

The various stages in the preparation of NHA are as represented by the reactions below:

$$2Na + 2MeOH \rightarrow 2MeONa + H_2\uparrow$$

$$NH_2OH.HCl + MeONa \rightarrow NH_2OH + NaCl\downarrow + MeOH$$

$$NH_2OH + RCO_2Et \rightarrow RCON(H)OH + EtOH$$

$$RCON(H)OH + MeONa \rightarrow RCON(H)O^-Na^+ + MeOH$$

$$RCON(H)O^- - Na^+ + HCl \rightarrow RCON(H)OH + NaCl\downarrow$$

where R = Pyridine ring for the complex of NHA model.

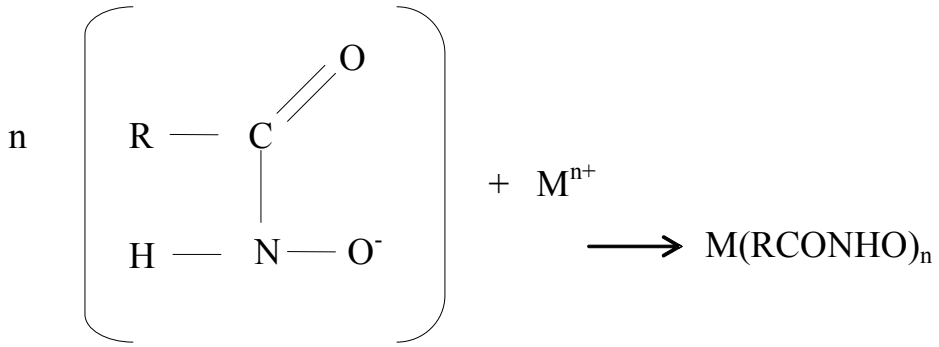

where n is a neutral monodentate ligand.

The pKa value of NHA is 8.68 0.05. The high basicity of the ligand may be ascribed to the positive inductive effect of the bulky pyridine ring attached to the functional group. Figure 1 shows the absorption spectra of solutions containing a constant metal but variable ligand molar concentration for NHA system, while Figure 2 shows graphical Matrix rank analysis of the absorbance data generated from similar solutions for NHA system. The absence of an isosbestic point and the shape of the graph is typical of systems containing only one complex specie. In this regard, the system show similar behaviour[13].

Several equilibrium models were tried but it was only with ML_2 model that convergence was achieved. The composition of the complex as determined by Job's plot is shown in Figure 3. The ratio of N_1[11] to the ligand under investigation was ML_2 i.e. N_i[11] – NHA[13].

The colour of Nickel(II) complex is lemon green. The analytical data and some physico-chemical properties are shown in Table 1. The spectrum of $[Ni(NHA)_2].2H_2O$ shows three bands located at about 25.64 x 10^3 cm^{-1}, 19.61 x 10^3 cm^{-1} and 13.35 x 10^3 cm^{-1} which are due to transition from the $^3A_{2g}$ ground term to the $^3T_{1g}(P)$ and $^3T_{2g}$ levels respectively. This spectrum and the observed magnetic moment indicate a magnetically dilute octahedral nickel(II) complex[14, 15]. The diagnostic i.r band in the free ligand was compared with the complex reported in Table 2. the ν (c-=0) vibration located at 1659.61cm-1 in the ligand is lowered by 89.65cm^{-1} in the complex, this together with decrease in the ν(NH) band indicates mixed bonding mode (N,O) i.e. coordinating via both the carbonyl oxygen and the amide nitrogen of the hydroxamate group[9]. The microbial sensitivity test carried out on the ligand and its isolated nickel(II) complex show no activity on the microorganism under investigation. On the basis of its physioco-chemical properties, the shown structure in Scheme 1 is proposed for the complex.

Proposed structure for (N,O) bonding mode for octahedrally coordinated complex.

Scheme 1

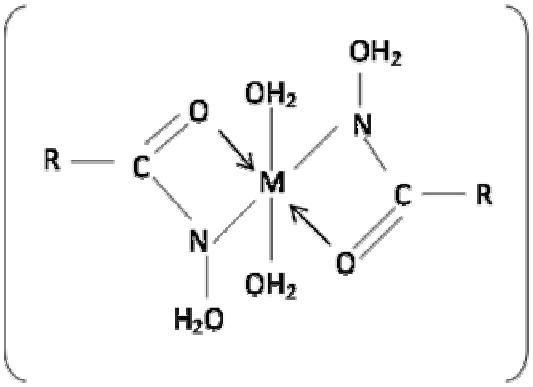

Key: $M^{2+} = Ni^{2+}$

References

[1] Kehl, H. (1982) Chemistry and Biology of Hydroxamic acids; Karger, New York.
[2] Raymon, K.N. (1990) Coord. Chem. Rev. 105, 135.
[3] Crumblis, A.L. (1991) Handbook of Microbial Iron Chelate; Ed. G. Winkelmann, CRC Press, New York.
[4] Raymond, K.N. (1994) Pure Appl. Chem. 66, 773.
[5] Yatabe, T.; Kawai, Y.; Oku, T; Tanaka, H. (1998) Chem. Pharm. Bull. 46, 966.
[6] Mock, W.L; Cheng, H. (2000) Biochemistry. 39, 13945.
[7] Brown, D.A.; Roche, A.L. (1983) *Inorg. Chem*. 22, 2199.
[8] Brown, Derrilla, makeith and W.K Glass (1979) Inorg. Chemica Acta 35,5-10.
[9] Biljana Nigovic, Nicola Kujundzic, Kresimir Sankovic 2002, 49, 525.
[10] L.W. Jones and A.W. Scott (1922). J.Am. Chem. Soc. 44, 407.
[11] Albert A and E.P Sergent (1971). The determination of Ionization Constants, 2nd Edition, Chapman and hall, London. pp 44.
[12] Cruickshank R. (1965) Medical Microbiology Eds. Church and Livinstone U.K pp 75-85.
[13] F.R. Hartley, C. Burgess and R.M. Alcock, (1980) Solution equilibra. Ellis Horwood, Sussex p 33.
[14] A.P. Boadanov, V.V. Zelenstov and V.M. Padalko (1972) Russ. J. Inorg. Chem. 22, 1417.
[15] D. Nicholls, (1974) Complexes and First Row Transition Elements, Macmillan, London pp 89-95.

European Journal of Scientific Research
ISSN 1450-216X Vol.18 No.3 (2007), pp.360-368

http://www.eurojournals.com/ejsr.htm

Adsorption Study of Phenol on Activated Carbon Made from Coffee Grounds. Determination of Adsorption Capacity

K. Benrachedi
Laboratory of food's Technology, Faculty of Engineer's Science
University of BOUMERDES, Algeria
E-mail: benrachedik@yahoo.fr

A. Mekarzia
Laboratory of food's Technology, Faculty of Engineer's Science
University of BOUMERDES, Algeria

M.Z. Boureghda
Laboratory of food's Technology, Faculty of Engineer's Science
University of BOUMERDES, Algeria

Abstract

To show the adsorptive capacities of the granular activated carbon produced from coffee grounds by chemical activation, the adsorption of different phenols, acid and basic colorants have been carried out. Comparison to a commercial activated carbon has been made.

The adsorption isotherms of phenol and dyes (acid and basic) onto granular activated carbon product, and commercial were experimentally determined by batch tests. Both the Freundlich and the Langmuir models [1, 2] are well suited to fit the adsorption isotherm data. As a result, the coffee ground- based activated carbon may be promising for phenols and dyes removal from aqueous streams.

Keywords: Adsorption, coffee grounds, wastewater treatment, dyes, Organic pollutants.

1. Introduction

Water pollution is a very persistent problem in fact, the intensive throwing up of different toxic substances without control constitutes a real danger.

Phenolic compounds are common contaminants in wastewater. They are widely used for commercial production of a wide variety of resins [3].

These are harmful to organisms at low concentrations, and US. Environmental Protection Agency (EPA) call for phenol's content in wastewater to less than 1 mg/l [4].

Effluents from dyeing and finishing processes, the dyestuff manufactory and some similar industries are generally highly colored with a large amount of suspended organic solids. They are important sources of water pollution because dyes in wastewater undergo chemical as well as biological changes, consume dissolved oxygen, and destroy aquatic life. Therefore, it is necessary to treat textile effluents prior to their discharge into the receiving water.

The removal of synthetic dyes (may be carcinogens), has became an important aspect of textile wastewater treatment and many studies have been conducted on the toxicity of dyes and their impact on the ecosystem , as well as the environmental issues associated with the manufacture and subsequent usage of dyes [5].

To remove organic pollutants and/or dyes many treatments have been proposed such as: coagulation, sedimentation, filtration, oxidation ($KMnO_4$, H_2O_2, Cl_2, O_3…), adsorption, [6,7, 8, 9, 10, 11]. Biological treatment processes are reported to be efficient in the reduction of organic pollutants concentration, but ineffective in removing colour [12, 13]

Of these methods, adsorption has been found to be (i) an efficient and economic process, (ii) an effective and widely employed mean of water and wastewater treatment.

Despite its prolific use in water and wastewater treatment, commercial activated carbon remains an expensive material. This leads to a search for low coast materials as alternative adsorbents.

Of these alternatives, agricultural and/or wood wastes such as , sawdust, maize cob, coconut husk fiber's, fruit kernel, and nut shells appear to be more economically attractive in certain countries because abundant [14, 15, 16].

Algeria annually consumes an average of one hundred thousand tons of coffee (Algerian national office of statistics, 2000). Aside from some unimportant losses, all these quantities of coffee end up in the form of grounds-coffee in the discharges. Hence, the interest to recover and to develop them by transforming them into activated carbon material to be used in the water treatment.

The purpose of this paper is to investigate the feasibility of manufacturing carbonaceous adsorbents from coffee ground,(i) the produced material could be usable as adsorbent of pollutant and color producing, (ii) the reduction of the solid waste.

2. Materials and Methods

2.1. Production of activated carbon

The supply of Activated carbon commercial (ACC) is unknown. Raw material for the preparation of activated carbon (ACP) is produced locally (coffee grounds).

The experimental procedure used in the activation process is as follows: the carbonaceous material is washed with hot water first to eliminate the impurities, dust and water-soluble substances, second with distillated water and then dried for 24 h at 105°C in the oven (*MEMMERT, DIN 40050-IP20*).

After drying to constant weight, it goes through a chemical activation step using ($ZnCl_2$+H_3PO_4) as activating agent. The activated sample is obtained by putting 50 g of grounds-coffee in contact with adequate volume of an aqueous equal-molecular solution of ($ZnCl_2$+H_3PO_4) 3N/l for 24 hours in a continuous reactor. Activated sample is subsequently dried in the oven at 100°C for one hour. The resulting sample is then carbonised for a given time in a horizontal cylindrical furnace (*PROLABO, VOLCA MC18*) at a temperature ranging from 500 to 700°C. After cooling, the char is washed with diluted HCl (10% by weight) to eliminate the excess of dehydrating agents and the fraction of soluble ash, followed by distillate water to remove the residual organic and mineral matters. Washing with water will easily remove most of the residues from activating agents.

However, this usually takes time, and the completion of washing is done when the conductivity measurements become stable.

It is then dried at 105°C for 48 hours. The carbon product is crushed and sieved to a uniform size (30 μm) and stored in closed bottles [17].

Chemical and physical characterization of granular activated carbon produced from coffee grounds (ACP) has been made.

2.2. Characterization of the produced activated carbon

Chemical and physical characterization of granular activated carbon produced from coffee grounds (ACP) has been made. This characterization enables us to better apprehend the behaviour of our adsorbent with respect to certain substances.

A measurement of specific area has been made by nitrogen adsorption (at 77K), with a discontinuous volumetric apparatus*"Micrometrics model 2100"*, [18].

For a better Knowledge of the nature of the mineral components, a spectrographic analysis (*soviet spectrograph UEI N°ICA5*) and by fluorescing (*A fluorescing X sequential spectrometer, Phillips PW1480*) have been accomplished.

To provide information on the chemical structure of the activated carbon, a study the surface functional groups has been done by IR analysis *"NICOLET 560 FT-IR"*.

A Zeta potential is a physical parameter, which enables us to quantify the electrical potential of the solid particle surface. It is determined by using a *"Micrometrics Zeta Potential Analyzer"*

The determination of acidic and basic surface functional groups of the activated carbon has been done according to the protocol established by Boehm et al [19].

2.3. Adsorption test

To characterize the adsorption capacity of an activated carbon, different adsorbates are commonly used. Iodine and methylene blue are among these and are frequently used to characterize activated carbons used in wastewater treatment.

We must notice that the results from these "commercial" tests like the iodine, methylene blue or phenol indices give a technical estimate of the adsorption capability of a carbon but they do not provide any insight on the intrinsic properties of the material.

In general iodine number and amount of methylene blue adsorbed are considered as a measure of adsorption capability of adsorbents for low and high molar mass solutes respectively.

The iodine number corresponding to the produced adsorbent is determined according to the procedure established by the American Society for Testing Materials (1980) (ASTM).

The iodine number and amount of methylene blue are obtained as follows:

The activated carbon (0,1 g) was placed in the 250 cm^3 dry Erlenmeyer flask and fully wetted by 10 cm^3 by diluted HCl (5% by weight). 100cm^3 of iodine solution (0,1 mol/l) was poured into the flask and the contents was vigorously shaken for 30s. After filtration, 50cm^3 was titrated with 0,01mol/l sodium thiosulfate.

For the amount of methylene blue, the activated carbon (1g) was added into a 100 cm^3 solution containing 0,5 g/l de methylene blue (Merck) and has been stirred for 5 days at 30°C. After filtration, the aqueous phase concentration of methylene blue was analyzed with a U.V visible spectrophotometer at 663nm.

To characterize the adsorption ability of the produced activated carbon in the wastewater treatment, adsorption tests were carried out.

Two dyes (acid blue 25 and basic yellow 2) and phenols were chosen as adsorbates. We used for that phenol (C_6H_5OH) and phenol di -substituted [$C_6H_4(OH)_2$] in *"ortho", "para" and "meta"* positions, to evaluate the behavior of our adsorbent with respect to the size of our molecule (substitution position involving a starch effect and a preferential uptake causing by the inductive effect of the radicals -OH). The combined effect of the two mechanisms gave us information on the size of the pores. All tests were compared with a commercial activated carbon (ACC).

Activated carbon used in this study is commercially available but its physical and chemical properties are not known, therefore a characterization was done.

Dyes and other chemicals used in this study were reagent grade. Stocks of dyes (CI Acid Blue 25, and CI basic yellow 2) and phenols were prepared and suitable diluted to the required initial concentration adsorption.

The initial concentration was obtained by measuring O.D at wavelength maximal for each chemical reagent considered, using a Beckman UV-Visible spectrophotometer DU-6.

The wavelengths maximal were 597nm and 406 nm for acid blue and basic yellow. Respectively.

The amount adsorption at time was calculated by: $q_t = x/m = (C_0 - C_t).V/m$

With C_0 (mg/l) and C_t (mg/l) are the liquid-phase concentration initially and at time t (min), V (l) the volume of solution and m (g) the weight of the dry adsorbent.

If adsorption occurs, concentration is expected to decrease with time until reaching a certain value without further decrease, it may be said that equilibrium has been reached.

The kinetic experiments were carried out in order to find out the adsorption equilibrium time. The concentration variation over the time was obtained as follows. The aqueous solution of dyes or phenol was agitated at a stirring speed of 150rpm.

At given time intervals, aqueous samples ($5cm^3$) were taken and the concentrations of dyes and phenol were spectrophotometrically determined after filtration. Each experiment was repeated at least once.

The isotherms were obtained as follow: exactly 100ml of solutions of known initial concentration was shaken at the constant agitation speed (150rpm) with a required dose of ACP (or ACC) for a specific period of contact time (60mn, determinate experimentally.) Experiments were carried out at room temperature (25 ± 2°C) under batch mode.

3. Results and Discussion

The main physical properties of the activated carbons are listed in *Table n°1*

Table 1: Characteristics of Activated Carbon

Characteristics	**Values**	
	ACP	**ACC**
Real Density	1,56	1,48
apparent Density	0,72	0,73
Pore volume	0,95 cm^3/g	1,29 cm^3/g
specific Surface area	640 m^2/g	950 m^2/g
Porosity	0,48	0,64
Isoelectric point	5,80	4,35
surface Function	Weakly Acid PH = 6,35	Weakly Acid PH = 5,70
iodine number	440 mg/g	590 mg/g
decolourisation of methylene blue	> 90%	> 90%

The results of spectrographic analysis indicates that the sample contains very small quantities (% by weight is the order of 10^{-4} to 10^{-2}) of copper, zinc magnesium, nickel, cobalt, chromium, molybdenum, barium and tin. And, it permitted us to identify oxides of calcium, magnesium, iron, phosphate (% by weight is about a 10^{-1})

When using the prepared adsorbent in batch tests the concentration in solution of each compound (phenols and dyes) considered decreased continuously with time until an equilibrium point was reached, characteristic of each adsorbate.

Figure 1: Adsorption of different phenols onto ACP with time Co = 20 mg/l; T = 25 °C Hydroquinol (1, 4); phenol, catechol (1, 2) ; resorcinol(1,3)

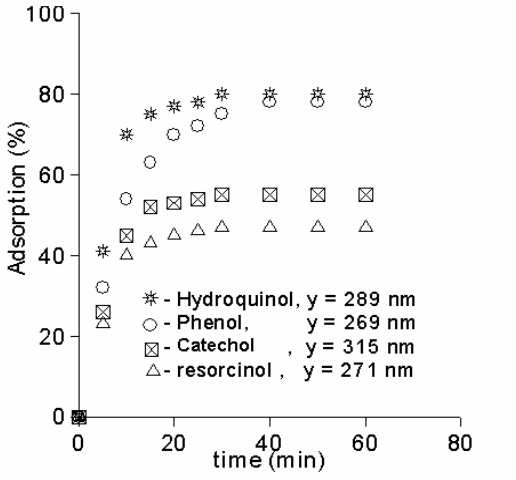

Figure 2: Adsorption of Acid blue dye onto ACP at different concentrations, T = 25°C.

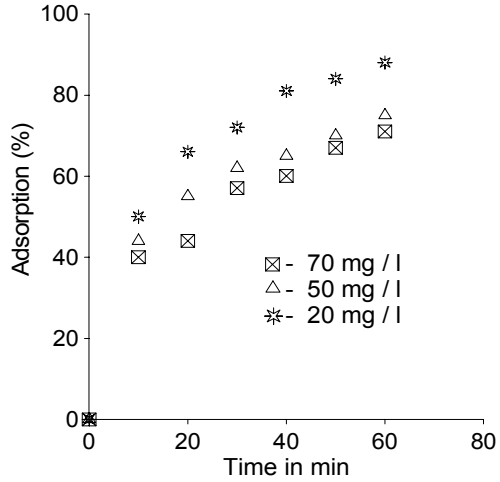

Figure 3: Adsorption of Basic yellow dye onto ACC at different concentrations, T = 25°C.

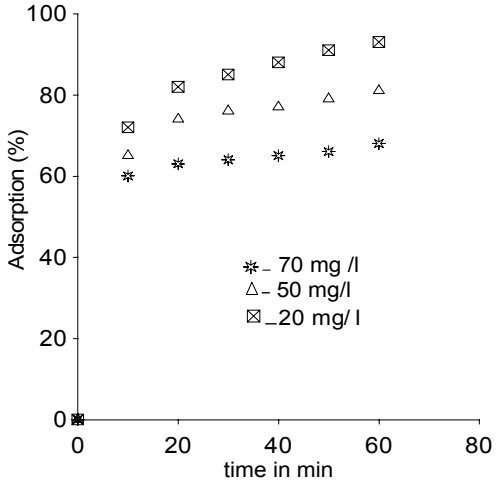

As it can be noticed, equilibrium times are not dependent on the nature of the adsorbates. The quantity of solute adsorbed depends, concerning the phenols, on the position of the radical hydroxyl

(OH).More adsorbed is the hydroquinol, the radicals (-OH) substituted in position *"para"* give the molecule a linear position, The attractive effect of functional surface groups (weakly acid) of the activated carbon is helping the radical hydroxyl (-OH) to move towards the pore. For the phenol, the adsorption is facilitated by one substitution, but the random position of the molecule makes less adsorption compared to the hydroquinol. The adsorption of both hydroquinol and phenol indicates a preferential orientation of the molecules and it is the radical (-OH) that is ahead of the adsorption. Naturally resorcinol is more adsorbed than catechol (the molecule being bulkier and not having a preferential position) the comparative study involving the Isotherms corresponding to the adsorbates removal from solutions by produced activated carbon (ACP) and commercial activated carbon (ACC) are showed in graphs *[Graphs N° 4,5,6]*

Figure 4: Adsorption isotherms of phenol of both activated carbons. Co = 20 mg/l; T = 25 °C

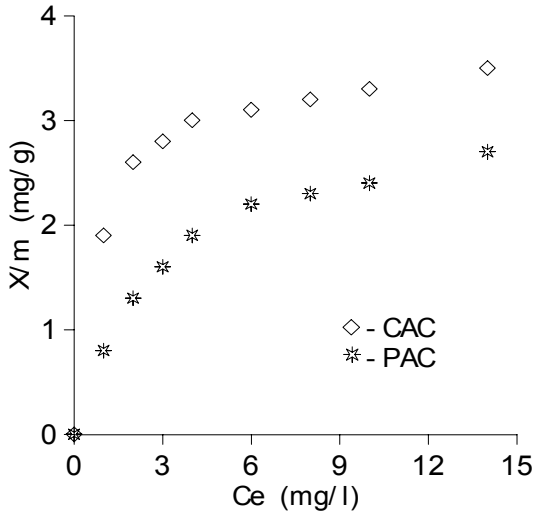

Figure 5: Adsorption isotherms of basic dye of both activated carbons. Co = 20 mg/l; T = 25°C

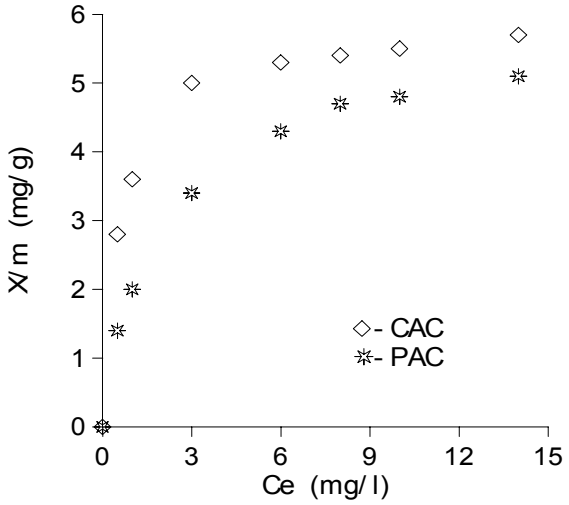

Figure 6: Adsorption isotherms of Acid dye of both activated carbons. Co = 20 mg/l; T = 25 °C

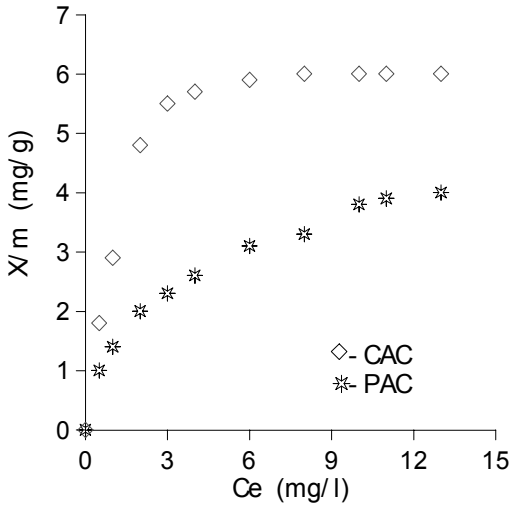

One can notice that,it can be seen, each compound adsorption data corresponds to isotherms of type 1 [18], i.e. convex upward curves, who are considered to be of a strong adsorption.

Results obtained for each adsorbate adsorption were fit to two adsorption isotherm models, those of Langmuir and freundlich.

A least square fitting procedure was followed to get for each model the characteristic parameters and the determination coefficients corresponding to experimental data.

Langmuir equation is based on a theoretical model and assumes that the maximum adsorption corresponds to a monolayer saturated with adsorbate molecules on the adsorbent surface that is energetically homogeneous $q_e = K_L.q_m.C_e/(1+K_L.C_e)$

Were K_L is a parameter which makes reference to the adsorption energy and q_m is a constant relative to the maximum adsorption capacity.

However, the freundlich equation is an empirical model that considers heterogeneous adsorptive energies on the adsorbent surface.

$q_e = K_F.C_e^{1/n}$ Were K_F is relative to the adsorption capacity and n refers to the process intensity. The coefficients of determination of the data fitting to each of the above models are shown in table 2 together with the values of the characteristic parameters for each of the two models studied. According to the CD, both Langmuir and Freundlich models have provided good fittings for the data of phenol and dyes adsorption.

A characteristic of the Langmuir isotherm is the definition on a dimensionless factor *r* defined as $(1+K_L.q_m)^{-1}$, Rozada and al (2001) and called a separation factor.

Adsorption is considered favourable when $r < 1$ which is the case in all experiments.

As for values obtained from the freundlich model, the *n* value indicates a favourable adsorption when $1 < n < 10$, thus the adsorption is better as smaller values are obtained, namasivayam and Sunthilkumar (1998) support this conclusion.

Table 2: Results from fitting to Langmuir and Freundlich models.

Adsorbats	Adsorbents	Langmuir model				Freundlich model		
		K_L	q_m	CD	r	K_F	n	CD
Phenol	ACP	0,33	3,22	0,998	0,48	1,07	2,70	0,964
	ACC	1,08	3,70	0,987	0,20	2,41	7,14	0,980
Acid blue	ACP	0,74	3,57	0,979	0,27	2,27	1,40	0,993
	ACC	0,57	8,33	0,991	0,17	2,27	2,89	0,900
Basic yellow	ACP	1,70	10	0,978	0,06	2,04	2,56	0,982
	ACC	1,32	4	0,989	0,16	3,49	4,76	0,931

The study of the parameters obtained shows that activated carbon produced has a good affinity for basic substances than activated carbon commercial.

For dyes adsorption, the kinetic of basic yellow is faster and has better uptake than acid blue.

4. Conclusion

The materials produced from coffee grounds confirm their adsorbents properties. The activated carbon produced being able to remove organic pollutants and dissolved dyes. In batch discontinuous tests, both adsorption kinetic studies and the isotherms determination indicated that, the adsorbents have the same behaviour and do not depend on the nature of compound to be removed from the solution.

Adsorption of phenol and di-substitutes shows that the radical (OH) have a significant influence, and give us information on the forms and the dimensions of the pores.

The Freundlich and the Langmuir equations appropriately fitted all isotherm adsorption data. The study of the factors in the table 2 , shows that the two activated carbon are comparable in adsorption capacity, but the activated produced carbon appears to be better against the basic substances.

The removal by activated carbon produced is found to be favourable according to the separation factor related to the Langmuir isotherm mode.

References

[1] H. Freundlich . Colloid and Capillary Chemistry .Methuen. London 1925.

[2] I. Langmuir . The adsorption of gases on plane surfaces of glass, mica, and platinum. Journal American Chemical Society. 40 (1918) 1361-1403.

[3] H.H. Fang, and O. Chen. Toxicity of phenol towards aerobic biogranules. Water Research. 31 (1997) 2229-2242.

[4] US Environmental Protection Agency. Toxicological review 2000. No 108-95-02. http://www.epa.gov/epaoswer/general/risk/emrad.htm

[5] M. Ajmal, and A.U. Khan . Effect of a textile factory effluent on soil and crop plants. Environmental pollution Series A: Ecological and biological. 37 (1952) 131-148.

[6] G.R. Brower, and G.D. Reed. Economical pre-treatment for color removal from textile dye wastes in Proc. 41st industrial waste conference, Purdue university: West Lafayette, Indiana, 1985.

[7] J. Hoigne. Organic micropollutants and treatment processes: Kinetics and final effects of ozone and chlorine dioxide Science of the Total Environment 47 (1985) 169-185.

[8] J. Bandara, J. Kiwi, C. Pulgarin and G. Pajonk . catalytic oxidation and photo-oxidation of nitrophenol by strong oxidants generated in situ via Cuo -aerogel. Journal of molecular catalysis A : chemical. 111 (1996) 333-339.

[9] J. KOCHANY AND J.R. BOLTON. Mechanism of photodegradation of aqueous organic pollutants. 2. Measurement of the primary rate constants for reaction of hydroxyl radicals with benzene and some halobenzenes using an EPR spin-trapping METHOD FOLLOWING THE photolysis of hydrogen peroxide. Environmental Science and Technology. 26 (1992) 262-265.

[10] K. MAJEWSKA -NOWAK . Effect of flow conditions on ultra filtration efficiency of dyes solutions and textiles effluents. Desalination. 71 (1989) 127-135

[11] A.R. Khan, T.A. Al-Bahri and A. Al-Haddad. Adsorption of phenol based organic pollutants on activated carbon from multi-component dilute aqueous solutions Water research. 31(1997)2102-2112.

[12] K.D.D. Bandyopadhyay, B.R. Maiti. Kinetics of phenol degradation using *Pseudomonas putida* MTCC 1194, Bioprocess and biosystems Engineering.18 (1998) 373–377.

[13] A.A.M.G. Monteiro, R.A.R. Boaventura, A.E. Rodrigues. Phenol biodegradation by *Pseudomonas putida* DSM 548 in a batch reactor, Biochemistry. Engineering Journal. 6 (2000)4 5-49

[14] J.W. Hassler. Activated carbon. New York. Chemical Publication.1963. S.E. Bailey , T.J.R. Olin, M. Bricka and D.D. Adrian. **A** review of potentially low-cost sorbents for heavy metals, Water Research. 33 (1999) 2469-2479.

[15] S.J.T. Pollard, G.D. Fowler, C.J. Sollars R. Perry. low cost adsorbents for waste and wastewater treatment: a review. The Science Total Environment. 116 (1992) 31-52.

[16] F. Julien, M. Baudu, M. Mazet, J.Water. Relationship between chemical and physical surface properties of activated carbon. Water research. 32 (1998) 3114-3124.

[17] S. Brunauer, P.H. Emmet, E. Teeller . Adsorption of gases in multimolecular layers. Journal of the American Chemical Society. 60 (1938) 309-319.

[18] H.P. Boehm, E. Diehl, W. Heck and R. Sappok. Identification of functional groups in surface oxides of soot and others carbons. 1966. Angew .Chem. Int Ed 3; 669.

[19] F. Rozada, L.F. Calvo, A.I. Garcia, J. Martin-Villacorta, M. Otero. Dye adsorption by sewage sludge-based activated carbons in batch and in fixed-bed systems. Bioressource technology. 87 (2001) 221-230.

[20] C. Namasivayam, S. Senthikumar. Removal of arsenic (V) from aqueous solution using industrial solid waste: adsorption rates and equilibrium studies. Industrial and Engineering Chemistry research. 37 (1998) 4816-4822.

European Journal of Scientific Research
ISSN 1450-216X Vol.18 No.3 (2007), pp.369-388

http://www.eurojournals.com/ejsr.htm

Geological Setting and Integrated Geophysical Exploration for Pb- Zn Sulphide Mineralization in Baban Tsauni Area Federal Capital Territory Abuja, Central Nigeria

Okunlola, O.A
Department of Geology, University of Ibadan, Ibadan

Oladunjoye, M.A
Department of Geology, University of Ibadan, Ibadan

Osinowo, O.O
Department of Geology, University of Ibadan, Ibadan

Abstract

An integrated geological and geophysical investigation was undertaken at Baban Tsauni area of Federal Capital Territory, Central Nigeria with the aim of determining and dilineating potential areas of base metal (Pb-Zn) mineralization. From systematic geological mapping on a scale of 1:25000, the study area is underlain mainly by varieties of migmatite gneisses, ultamafites which have all been intruded by semi concordant N-S trending pegmatites and quartz veins. Cataclastic deformation with intense shearing is a common feature. Disseminated sulphide mineralization is noticed in some of the pegmatite veins and quartz bodies

Geophysical investigation involved gravity, electromagnetic, self potential and electrical resistivity techniques. For the first three geophysical techniques, a station interval of 10 m was employed while the current electrode separations for Schlumberger array for resistivity determination ranged from 2 to 75 m.. Measurements were taken in W – E direction for the first three geophysical techniques while investigation using the fourth technique was carried out at selected points. In all, ten gravity profile lines, three electromagnetic profile lines and six vertical electrical sounding stations were established. The gravity data were reduced using a computer programme for transformation to absolute gravity, the VLF-EM raw data were converted to filtered real data using a filter operator. The SP data were presented in form of profiles while a computer-assisted one-dimensional inversion algorithm of the Schlumberger sounding data was carried out for quantitative interpretation.

The results of the geophysical investigations show that the southern zone near Baban Tsauni village is characterized by high positive gravity anomalies with their long axes parallel to the structural grain of the underlying rocks and were thus delineated as prospect “A” while the central part shows significant but less peak anomalies and were designated as prospect “B”. Also the EM data shows major and minor linear features suspected to be geological interfaces which also correspond to the structural grain controlling mineralization in the study area.

The fresh bedrock in most of the study area is overlain by 2 layers of overburden – the top soil of about 1.5 m and weathered basement of about 3 – 7 m suspected to host the Pb-Zn mineralization.

Introduction

Integrated approach involving a combination of geological, geophysical and geochemical methods have proved useful in revealing concealed mineralization especially in Nigeria (Okunlola et.al.,2003; Elueze and Okunlola, 2003; Oluyide and Okunlola 2007;). Employing this approach therefore, geological and integrated geophysical investigations were undertaken at Baban Tsauni village, near Izom, in the north-western part of the Federal Capital Territory, Abuja, Nigeria to delineate areas of Pb-Zn sulphide mineralization and thus attempt a preliminary economic evaluation of the occurrence.

Geophysical investigation involved gravity, electromagnetic, self potential and electrical resistivity techniques .Gravity prospecting which is a passive geophysical technique that involves measurements of gravitational field force on the surface of the earth and it is used to investigate the subsurface geology on the basis of variations in the earth's gravitational field generated by differences in density between subsurface rocks is employed in this study because of the expected density contrast between the suspected Pb-Zn ore body and host lithological associations Electromagnetic method (EM) survey detects zones of conductivity anomalies in the subsurface (Sharma, 1997). The geophysical investigation involved the Very Low Frequency (VLF) electromagnetic method. This technique was used to corroborate information obtained from the gravity prospecting method.

The electrical resistivity method has been employed for various applications in the Nigerian terrain such as overburden characteristics over a concealed ore body, groundwater exploration and shallow engineering investigations. (Ako et. al., 1986; Olorunfemi and Mesida, 1987; Olayinka and Barker, 1990; Osella, et.al.,2002) This method is also expected to reveal overburden characteristics and the ore body geometry, This technique was employed to determine the thickness of subsurface lithologic units within the study area.

The study area located at the south-eastern corner of sheet 185 (Paiko) is bounded by grid references $6^0$57'15'' to $6^0$58'3^0'' and $9^0$08'15'' to $9^0$11'00'' covering a total surface area of 11.587455 square kilometers (Fig. 1). The area could be approached from the northern end through a motorable road connecting Izom – Baban Tsauni to Gwagwalada. The relief is generally undulating and slopes moderately to the south. However, the western and the eastern sides are characterized by ridges and inselberg topography ranging from 195m to 650m above sea level. The streams are seasonal and flow southward. They cut fairly deep valleys as they are apparently controlled by the structure and lithology of the underlying bedrock. Hence a trellis drainage pattern has been developed on the geology. Vegetation ranges in character from deciduous to woodland savannah, fairly thick forest grows along the banks of the streams. Gwari Farmers and cattle Fulanis inhabit this area in small villages and hamlets. Baban Tsauni is the biggest of these settlements.

Figure 1: Location map of the study area

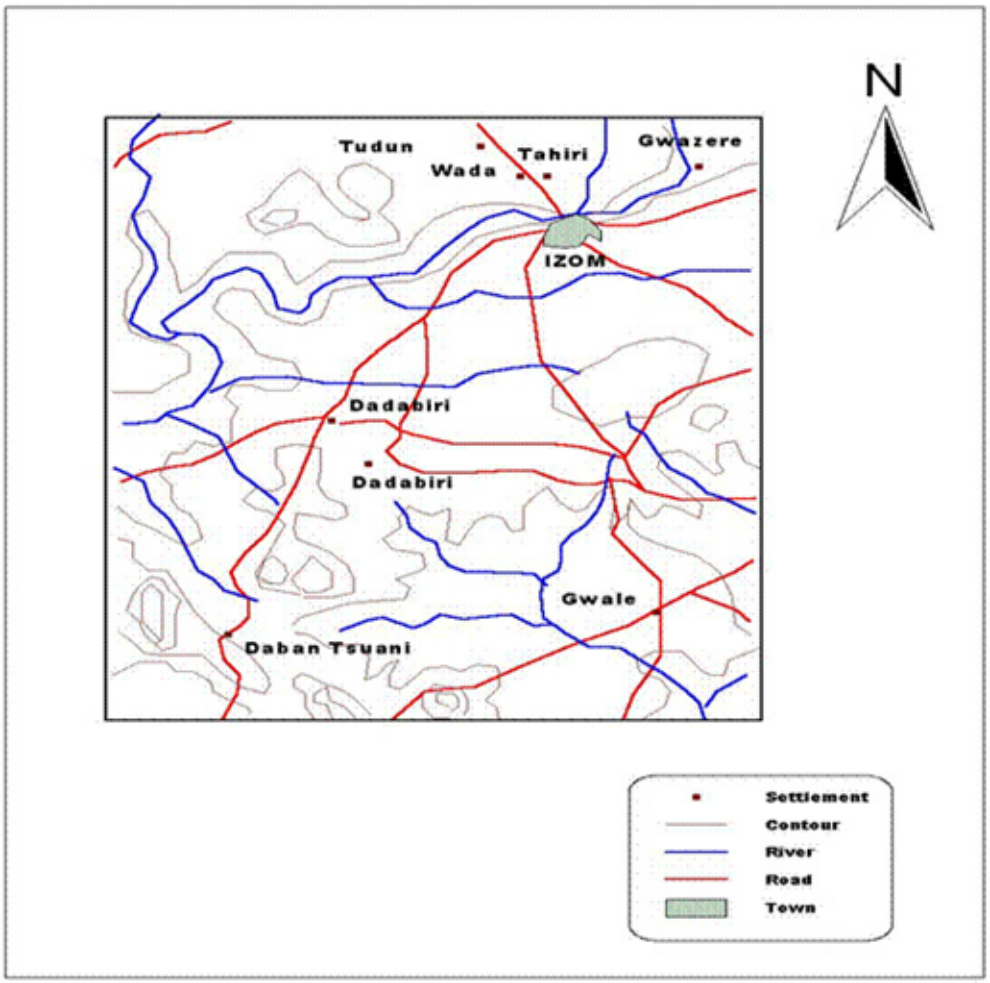

Previous Work

Previous studies in the area include those of Russ (1957), and Truswell and Cope (1963) who carried out reconnaissance geological survey of the area. while Hunting (Geology and Geophysics) of England (1975) carried out Airborne Geophysical Surveys of the area under the auspices of the Geological Survey of Nigeria. Woakes and Bafor (1984) also studied aspects of gold mineralization in the area.

Methods of Study

A detailed systematic field mapping on a scale of 1: 25,000 was first carried out. This was then followed by the Geophysical investigations.

A Worden gravity meter of appropriate sensitivity, sensitive enough to pick small as well as large perturbations in the subsurface was employed to carry out the gravity measurements. This aims at determining localized regions of gravitational field disturbance as a result of excess density which may be interpreted as regions corresponding to zones of anomalous mineralization. A total of 288 gravity stations were occupied; all in W-E traverses, which are perpendicular to the identified general geologic strike of the area. The traverse lines were carefully selected to cover three areas of the study area. In order to have a fair coverage of the field, five traverse lines were occupied at the southern part of the field, four at the central and two at the northern extreme, where mineralization enrichment was found to be least. Traverse length ranges from 180m – 400 m and station interval of 10m was used to

accomplish resolution of small anomalies. Measurements such as equipment's dial readings, time of measurement, longitude, latitude as well as station elevations from GPS equipment were recorded at all the stations.

Observed gravity (raw) data in milligals (mGals) were obtained by multiplying equipment's dial readings by the equipment's constant. Obtained raw data were processed and corrected for latitude, free air, bouguer and drift. The purpose of this was to remove variations in gravity not resulting from localized gravity effect. The processed/reduced data were finally fed into a gravity modelling program which determined the gravity anomaly in mGals, 2^{nd} derivative as well as residual anomaly for each of the eleven traverses. The program also modelled the gravity anomalies. The program presents the results of all the above listed parameters and compares them with the absolute gravity value in the region. Isogravity, gravity relief maps and gravity field vector plot of the investigated part of the study area were also produced from the processed/refined data.

VLF-EM measurements were made at 10 m interval along three traverses along W-E direction perpendicular to the strike of the rock in the area. Traverse length ranges between 250 - 430 m. The VLF-EM unit was used for the data acquisition. The equipment measures the real and imaginary components of the vertical to horizontal magnetic field ratio. Most commonly, the presence of conductive overburden suppresses response from deeper targets of interest and relatively small variations in overburden conductivity can by themselves generate significant VLF anomalies.

To resolve the problem of anomaly interference, a filter operator was applied to the real component of the VLF-EM data to transform it to filtered real VLF-EM data (Karous and Hjelt, 1983). The filtered real data transformed every genuine crossover or inflection points of the real anomaly to positive peaks while reverse crossover become negative peaks. A double plot of the real and filtered real anomaly curves enabled qualitative identification of possible target areas in the subsurface.

Six vertical electrical sounding using the Schlumberger electrode array were carried out at selected locations within the study area. The field data are expected to give information on the probable lithological units in the subsurface and their thicknesses, variations in the degree of saturation and depth to weathered/fresh rock. The electrodes were expanded from a minimum current electrode spacing (AB/2) of 1.0 m to a maximum of 42 m. The Geopulse Tigre resistivity meter was used for resistance measurements. Good quality data were obtained with the observational errors being less than 1%. The field data obtained were plotted on bilogarithmic coordinates and a preliminary interpretation was carried out using partial curve matching involving two-layer master curves and the appropriate auxiliary charts. The layered model thus obtained served as input for an inversion algorithm as a final stage in the quantitative data interpretation.

Results and Discussion

Geological setting

The study area is underlain by rocks of the Precambrian basement complex of Nigeria. Generally the Precambrian rocksof Nigeia have been loosely categorized into three main subdivisions. These are the migmatite – gneiss complex, the schist belts and the Pan African Older Granite Series (Okunlola and Jimba, 2006). Specifically, the Baban Tsauni area is underlain mainly by migmatite gneiss complex rocks namely banded gneiss, pegmatised migmatite, granite gneiss, migmatised amphibolite, pegmatites, quartz veins and dolerite dyke.. All these rocks grade imperceptibly into each other except where they are demarcated by discontinuities (faults and fractures) [Fig.2,]

Figure 2: Geological map of the study area around Baban sauni Federal Capital Territory Nigeria

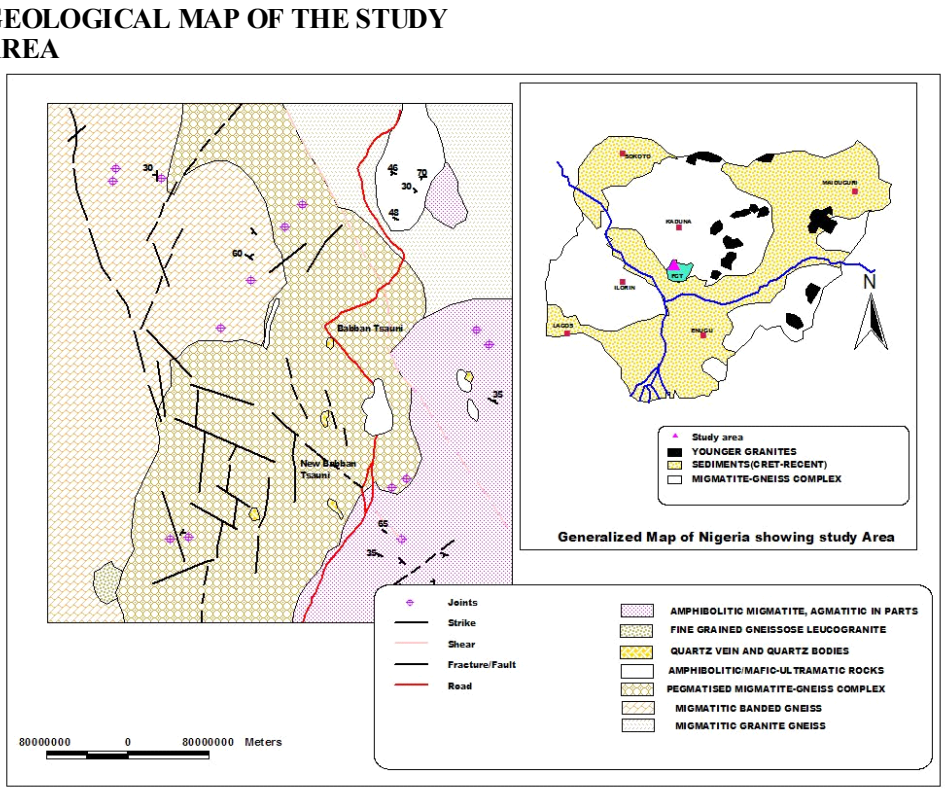

The pegmatised migmatite constitutes by far the most widely occurring rock type in the area. It outcrops mainly in the central portion of the study area. It is either gneissose and banded in structure in the southern parts; or the gneissose structure is dominated by augen of feldspar porphyroblasts, as observed in the middle and northern parts. Some of these potassic feldspar porphyroblasts measure up to 5cm. Apart from the abundant quartz, about 30% of the mineral assemblage is biotite while hornblende constitutes about 43 per cent. Orthoclase feldspar, augite and zircon are present in subordinate amounts. The host migmatite is invaded pervasively by several bodies of medium to coarse grained complex pegmatites and quartz vein thus resulting in its field lithological characterization as a pegmatised migmatitic rock.. The pegmatites are distinctively coarse-grained and sometimes tend to inherit the gneissic structure of the host rock. The sheared varieties of the pegmatites often appear falsely schistose. Field measurements indicate that the pegmatites were emplaced along fracture/shear zones. They trend dominantly northwest-southeast although a few are aligned in the north-south and northeast – southwest direction. Discrete Pb- Zn sulfide mineralization of the galena and spalerite varieties are noticed as embedded crystals within the pegmatite veins and the quartz bodies. The occurrence is more concentrated in regions of intense shearing and noticeably along fracture zones.

Banded gneiss occurs to the western margin of the mapped area as semi continuous inselbergs. It is medium to coarse-grained in texture with an alternation of fine bands of quartzo-feldspathic and mafic materials. Its contact with the pegmatised migmatite to the east is marked by flow structures and a fairly regional but narrow fault zone. The mineralogy consists mainly of quartz, orthoclase, biotite and hornblende. Augite, zircon and opaque ore are present as accessories.

Migmatitic granite gneiss occurs in the north-eastern corner of the study area. The rock trends in an E-W direction. Small bodies of granite and pegmatite forming the neosome are emplaced parallel or discordant with the foliation. Feldspar porphyroblasts also develop along the foliation and are deformed into augen or banded structures. Small pegmatites veins are emplaced in this rock unit as

sheet-like body, medium-grained in texture and less brecciated. Quartz, biotite and plagioclase feldspars are the main minerals with accessory tourmaline.

Amphibolitic migmatite occurs to the south-eastern parts of the study area. It is in contact with the pegmatised migmatite and outcrops in ridges, broken by valleys of fracture-controlled streams. The rock is predominantly greenish in colour due to the masking effect of the prepondarant amphibolite palaeosome. It is characterized by soapy feel. The neosome consists of granitoids and quartzo-feldsapathic veins. Both the amphibolitc and the felsic constituents develop into lit-per-lit and more often agmatitic fabric. The rock is profusely sheared/mylonitised thus exhibiting conchoidal fracture surfaces and cataclastic textures. Microscopic study of the rock confirms that the amphibolite palaesome is composed predominantly of actinolite, hornblende, quartz and minor amount of andesine and accessory sphene.

Ultramafic rocks occur as small bodies, distinctly medium to coarse-grained and weakly foliated. Small discontinuous Quartzo-feldspathic and quartz veins intrude the rock. The rock exhibits conchoidal surfaces and shapes resembling pillow lavas. Dolerite dyke which trends north-south occurs almost at the contact of pegmatised migmatite with the banded gneiss. In hand specimen, the rock is characterized by disseminated roundish specks of magnetite which occur along foliation and joint surfaces. The rock is composed predominantly of pyroxene, olivine, labradorite, magnetite, minor quartz and accessory sphene and zircon.

Fine-grained leucocratic granite occurs to the south-west corner as a small stock. The rock is composed predominantly of quartz in addition to albite, biotite minor hornblende and accessory zircon. The rock grades into the banded gneiss. The pegmatites and quartz vein occur intimately together in the pegmatised migmatite terrain. They are emplaced as small bodies, outcropping in ridges of low hummocky topography. The extent of the ridges accommodates sheared rubbles and boulders most probably derived from these rocks.

Structures

Field investigation shows that the crystalline basement rocks have undergone at least three episodes of deformation, the latest being associated with the Pan African 550 ± 100 ma thermotectonic event (Burke and Dewey, 1972). The resulting fabrics are manifested in the forms of foliations, lineations, folds, joints and fractures. Foliation in the the gneisses and migmatites are characterized by preferred alignment of minerals into alternating bands hence manifesting in differentiated layering of melanocratic and leucocratic materials of these rocks. However the lit-per-lit layering is frequently disturbed by augen boudins, xenoliths of older rocks and quartzo-feldspathic veins. All these define different foliation directions of relatively different ages (Fig.3). Also the geological map of this area depicts the foliation trends in various directions-NNW-SSW and E-W (Fig. 2). These are indications that the crystalline rocks have experienced multiple folding. On the outcrops, the style of folding varies from very tight intra folia folds structures in the migmatites to well rounded open folds in the banded gneiss. The axial traces of the open folds plunge in the NNW/SSE direction.

Figure 3: Deformation and metamorphic fabrics in the migmatites

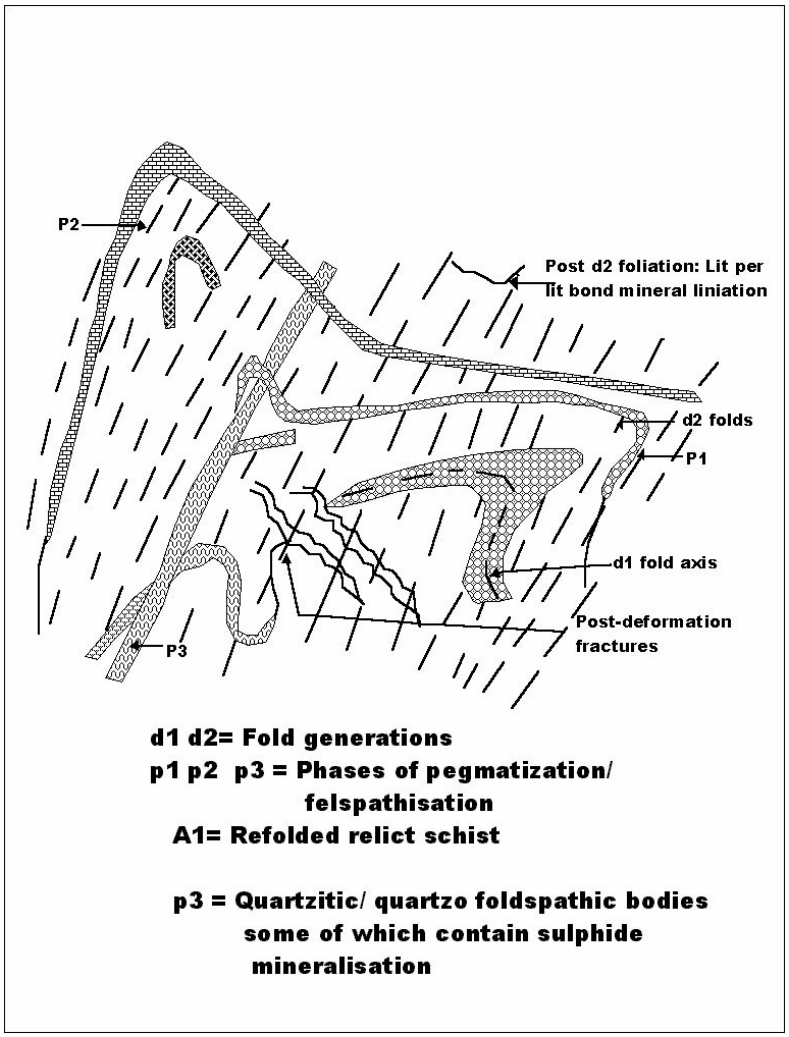

Lineation is defined by the preferred orientation morphology of the inequant mineral grains such as mica, feldspar and hornblende. The major plunge directions are the NNW/SSE directions in the banded gneisses and the pegmatised migmatite. It is pertinent to note that the quartz veins which show indications of sulphide mineralization also trend in the NNW/SSE direction. On many outcrops lithologic layerings are displaced along planar surfaces and jointing is very well-marked on the pegmatised migmatite gneisses; some of these range in width from 2cm to 25cm. There are other fairly inconspicuous joint systems, some of which are microscopic along which the rocks are sheared. Some of these joint surfaces measured in the field are shown in the frequency strike diagram (Fig.4). This figure depicts two dominant directions NNW/SSE and WNW/ESE. Important minor trends are NNE/SSW and ENE/WSW.

Figure 4: Strike frequency diagram of joints in the study area

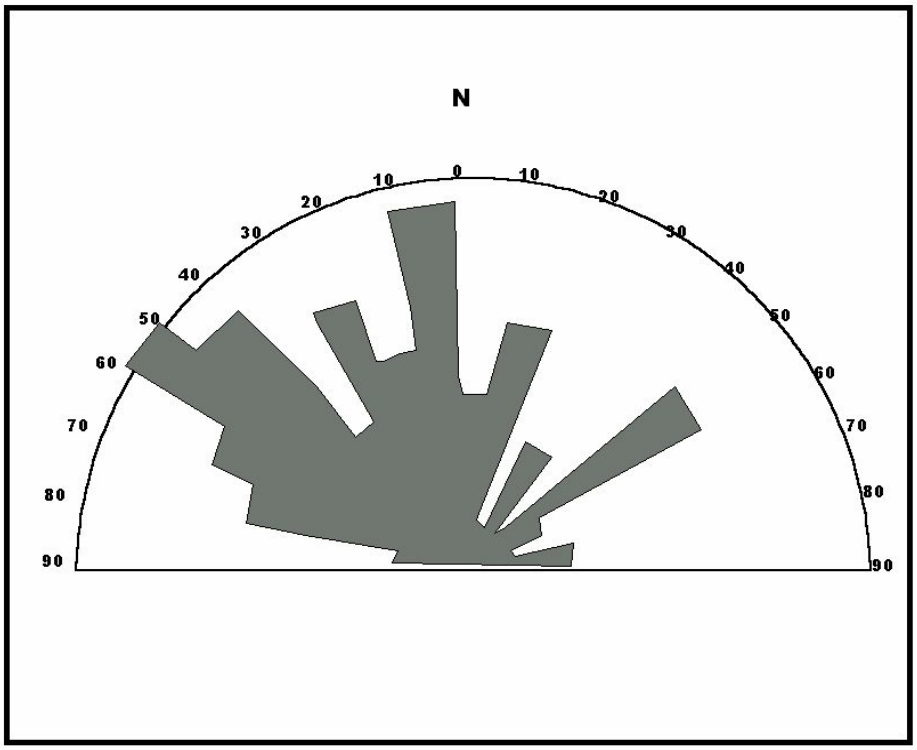

Regional fractures are clearly depicted on Fig 2, the geologic map. These features are marked in the field by cataclastic textures and silicification, indicating that movement had taken place along the shear zones. The regional fractures trend dominantly in the NW-SE, NNW-SSE and NNE-SSW. The pegmatised migmatite gneiss appears to be the most susceptible to the fracturing and all streams developed on this lithology appear to be controlled by the fractures.

Geophysical investigation

All the stations show strong positive and negative gravity anomaly that ranges from 1480 to 1560mgals. The strong positive anomalies result from disturbance in gravitational field in the area due probably to mineralization enrichment of geologic materials of excess mass or high specific gravity or density

The profiles of the eleven occupied traverse stations (Figures 5-15) and other field observations revealed that the mineralization enrichment exists in a pegmatitic vein which runs across the study area in a N-S trend. The thickness of the vein varies from about 15m to 80m. The southern part toward Baban Tsauni village is richest in the mineralization concentration and gradually decreases away to the north towards Izom.

Figure 5: Baban Tsauni Lead Sulphide Minaralization

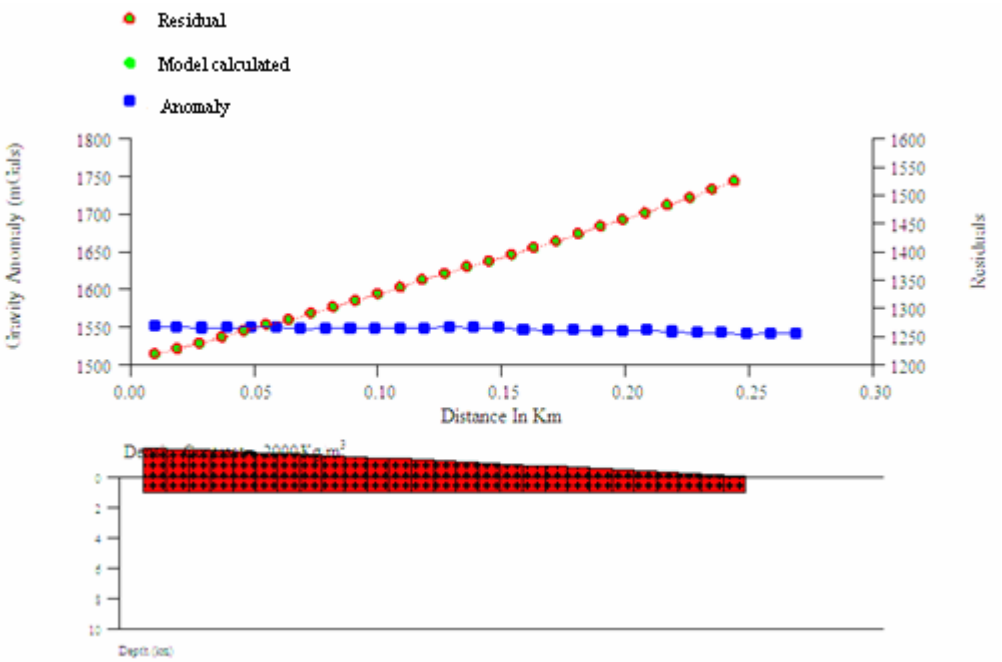

Figure 6: Baban Tsauni Lead Sulphide Minaralization 2

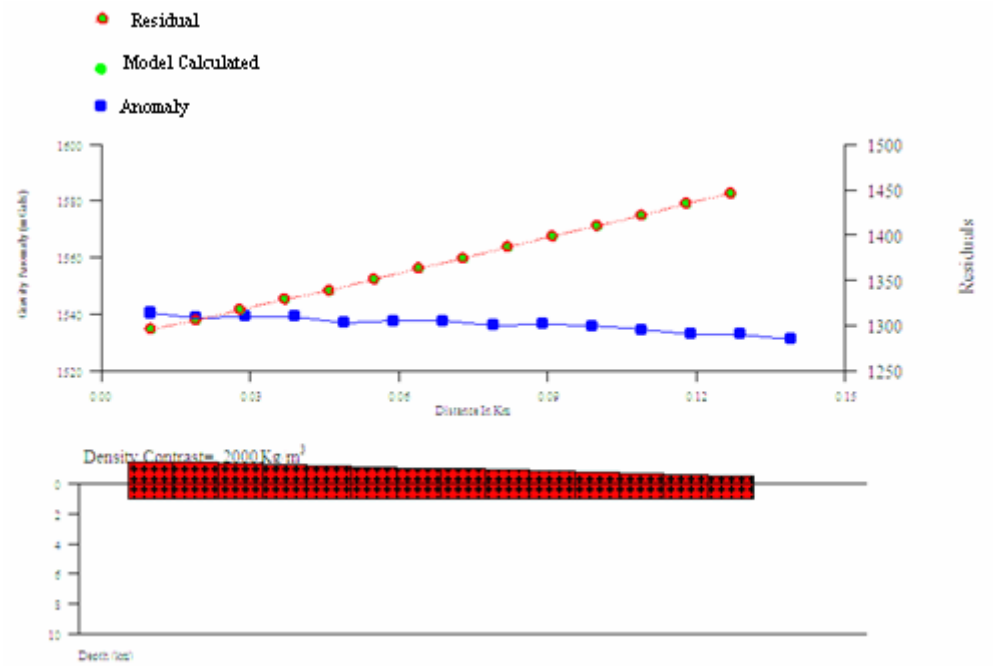

Figure 7: Baban Tsauni Lead Sulphide Minaralization 3

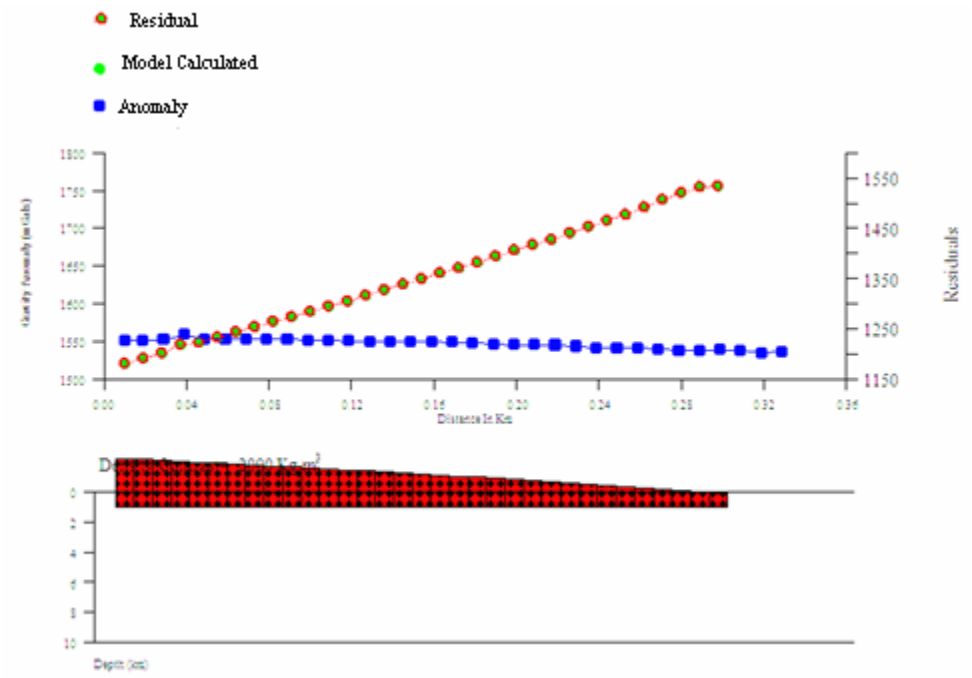

Figure 8: Baban Tsauni Lead Sulphide Minaralization 4

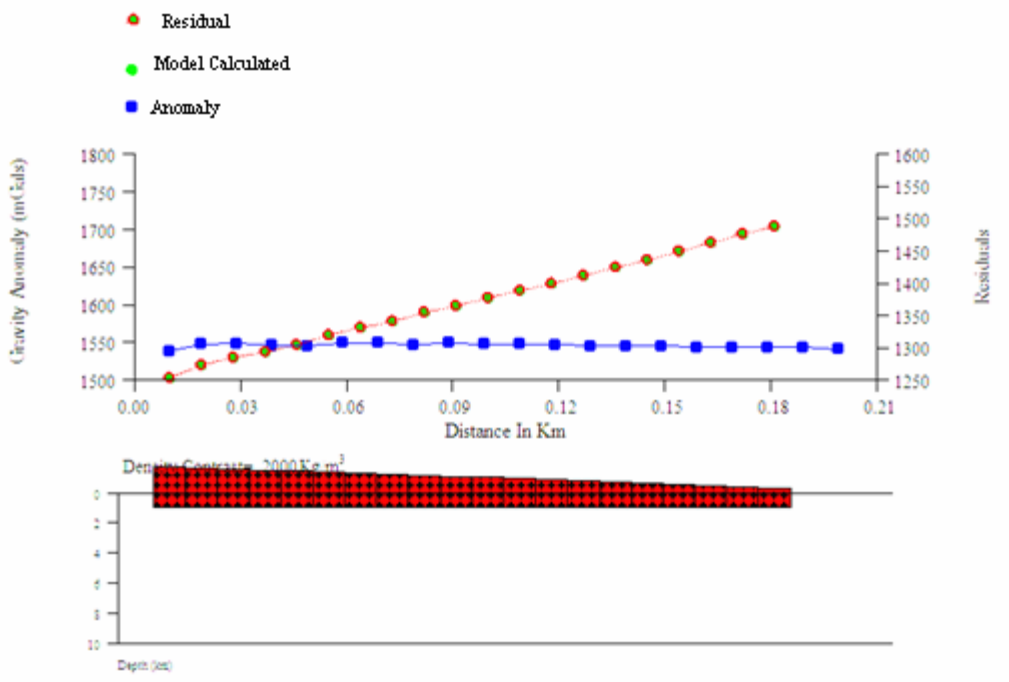

Figure 9: Baban Tsauni Lead Sulphide Minaralization 5

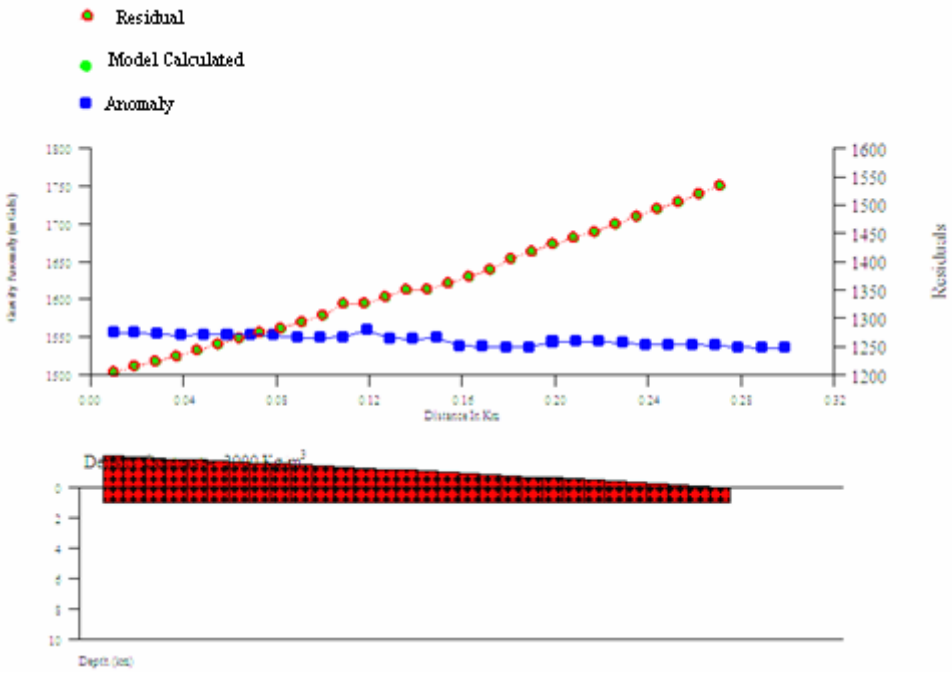

Figure 10: Baban Tsauni Lead Sulphide Minaralization 6

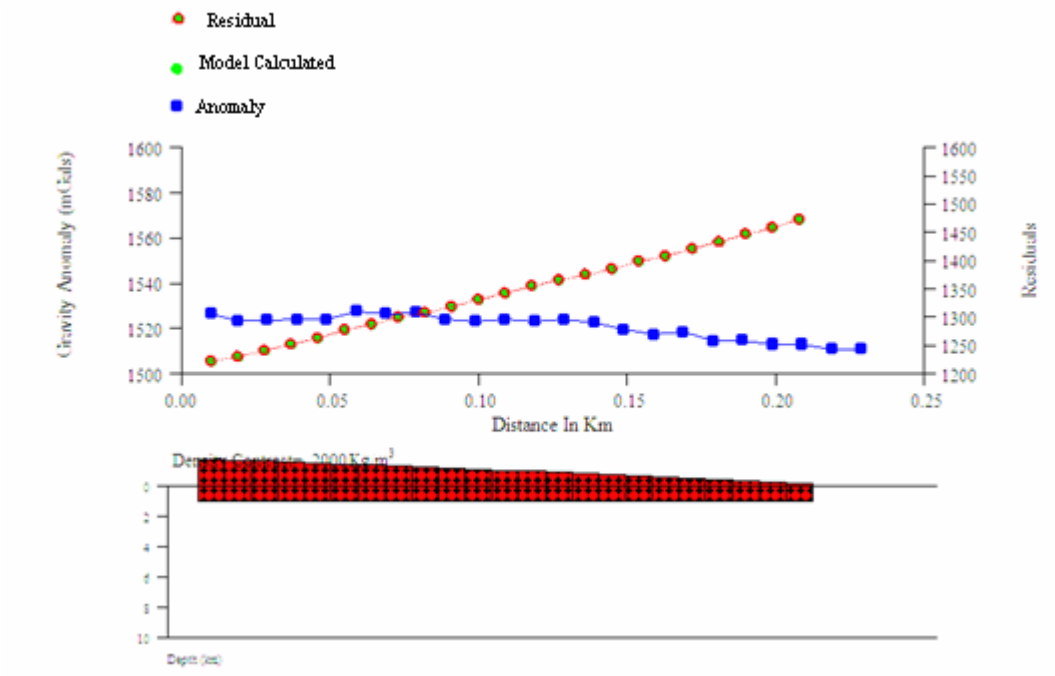

Figure 11: Baban Tsauni Lead Sulphide Minaralization 7

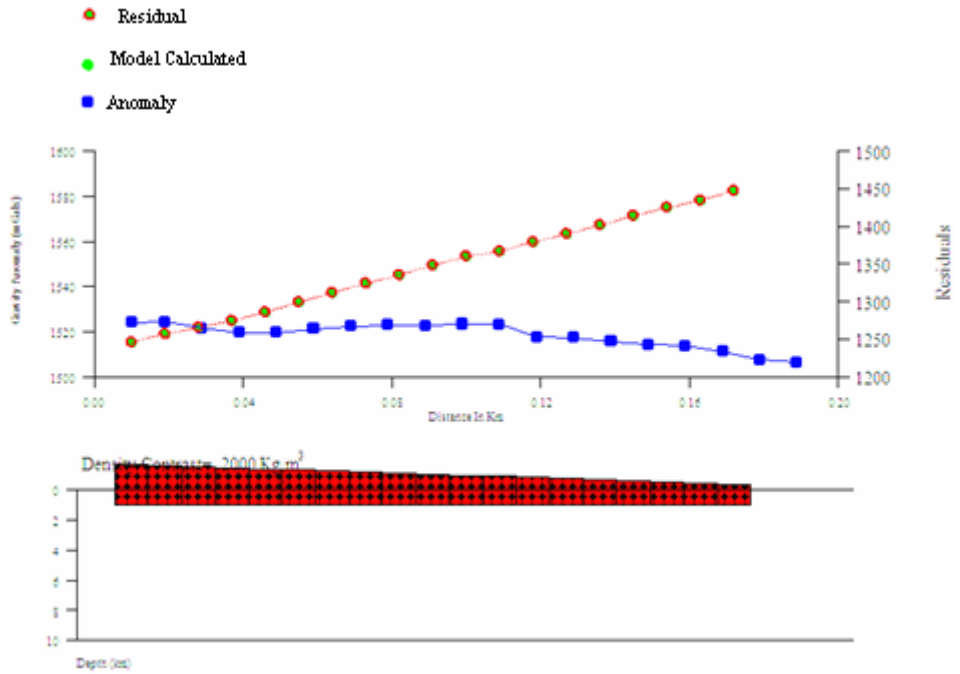

Figure 12: Baban Tsauni Lead Sulphide Minaralization 8

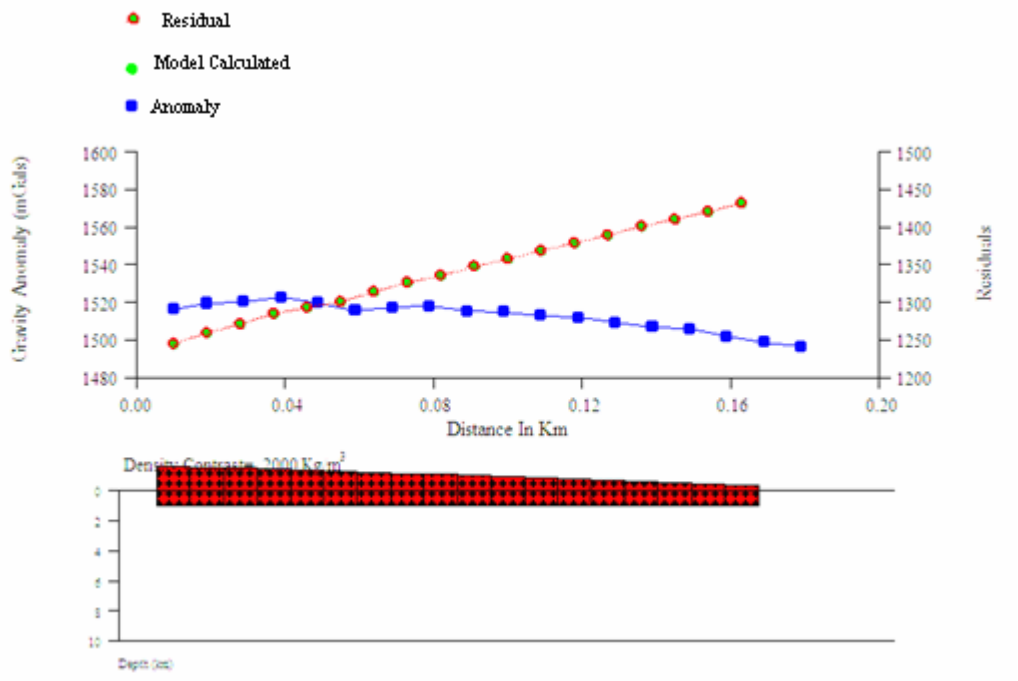

Figure 13: Baban Tsauni Lead Sulphide Minaralization 9

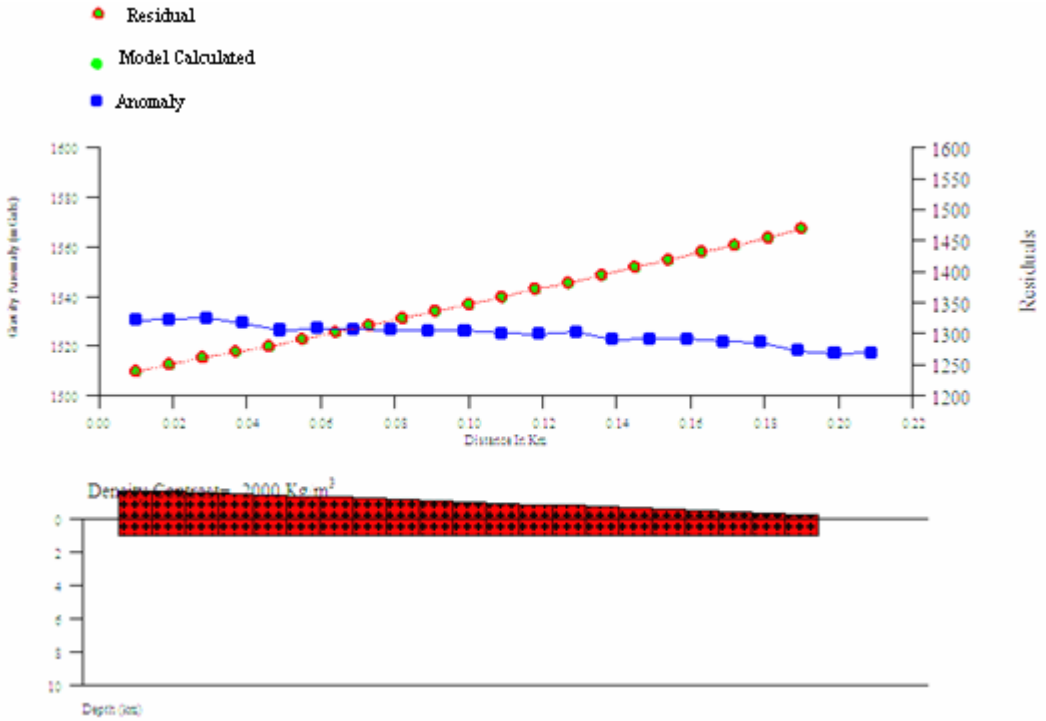

Figure 14: Baban Tsauni Lead Sulphide Minaralization 10

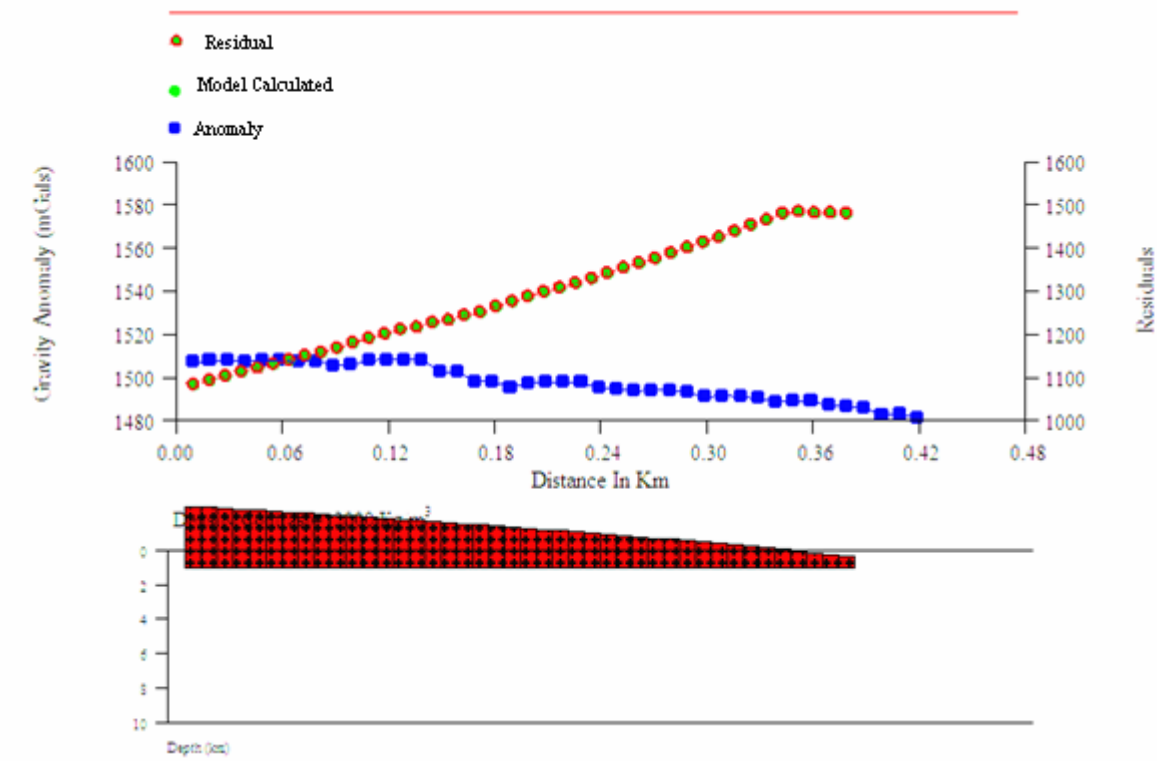

Figure 15: Baban Tsauni Lead Sulphide Minaralization 11

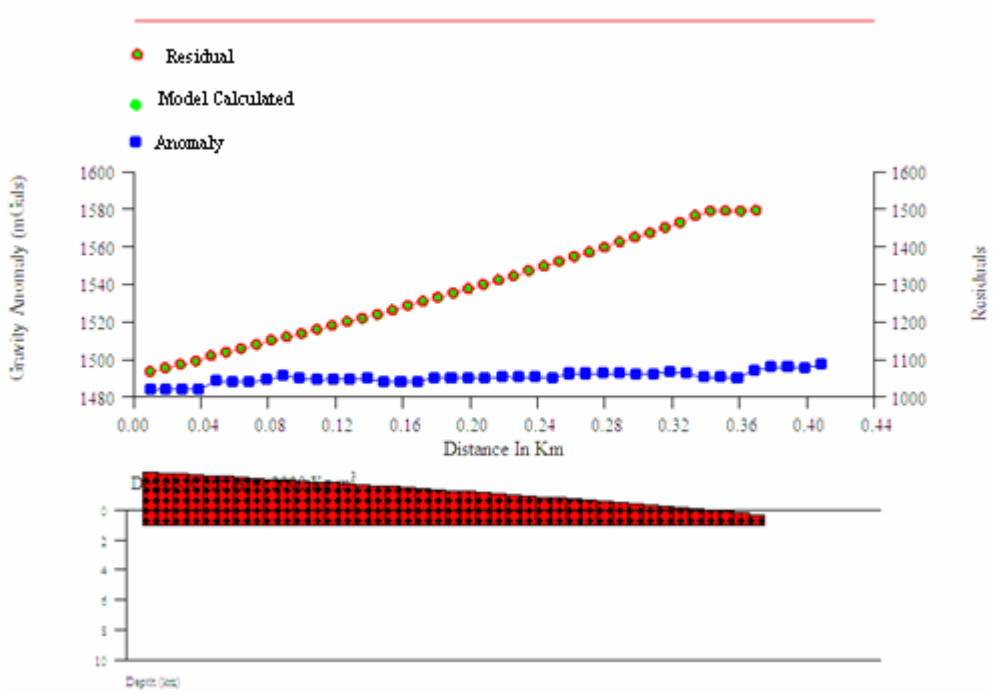

Likewise, an east to west enrichment trend was also established. Gravity values in all the traverse stations decrease from peak values (1570m Gals) in the west towards the east (1460m Gals), the implication of which is that the Lead Sulphide mineralization enrichment is higher and closer to the surface at the western end away from Baban Tsauni village and gradually decreases towards the village. The two identified trends isolate the southwestern part of the field as the most enriched region with potential economic prospect.

Gravitational field vector map of the area (Figure 16) revealed acute gravitational field perturbation in four regions of the Cadastral field. The magnitude of the perturbation is highest and most directional in the western and central part of the field. The gravitational field disturbances agree well with the established E-W enrichment trend, as determined from the profiles.

Figure 16: Gravitational Field Vector Map of Study Area.

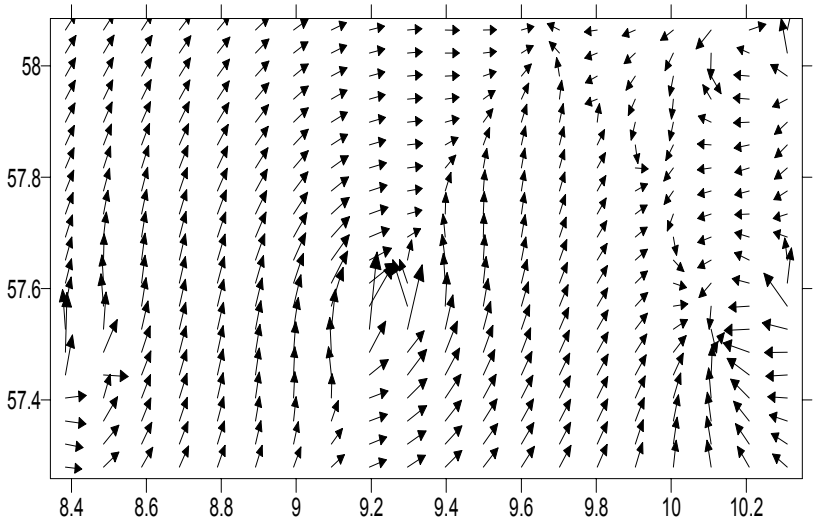

The isogravity map as well as the gravity relief map (Figure 17) of the area identified the southwestern part of the study area as region of high gravity relief, that stand out relative to others and this may result from embedded geologic materials of high density as earlier stated above.

Figure 17: Isogravity and Gravity Relief Maps of the Study Area.

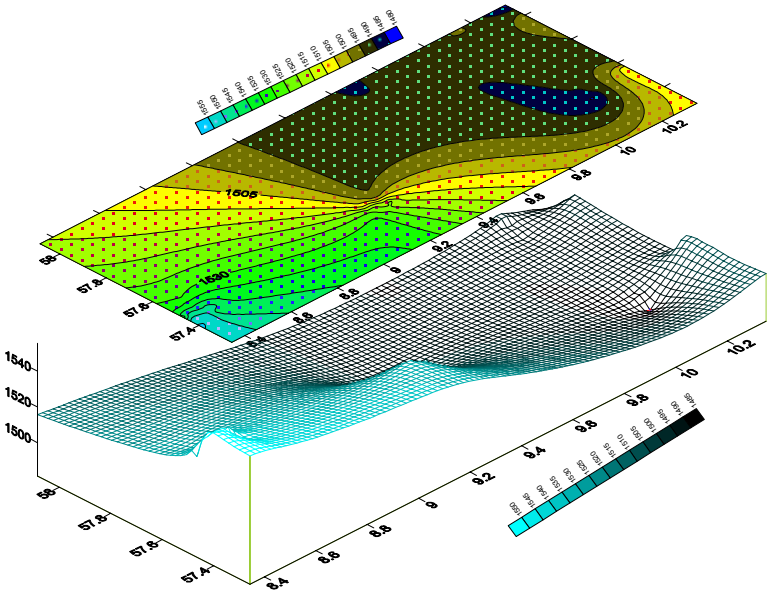

Figures 18 – 20 represent the VLF-EM anomaly curves (real and filtered real) along traverses $EMTR_1$ – $EMTR_3$. Major and minor linear features (suspected geological interfaces) with positive peak filtered real amplitudes ranging between 5- 60% were delineated using characteristic feature curves of coincident inflections on real component anomaly curves with positive peaks on filtered real anomaly curves.

Figure 18: Plot of real and filtered real component of the VLF along traverse $EMTR_1$

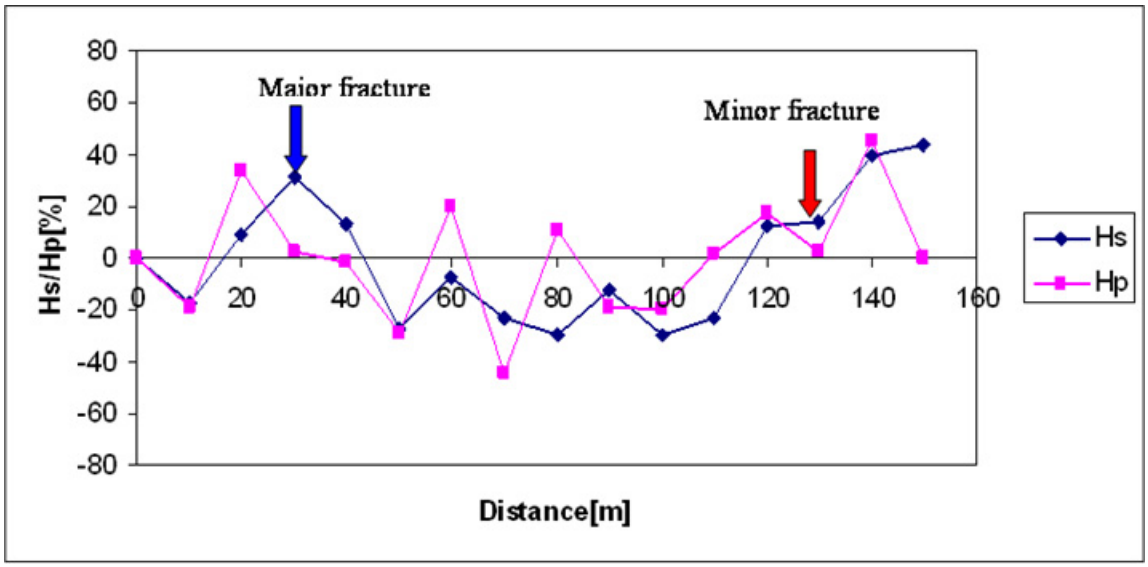

Figure 19: Plot of real and filtered real component of the VLF along traverse $EMTR_2$

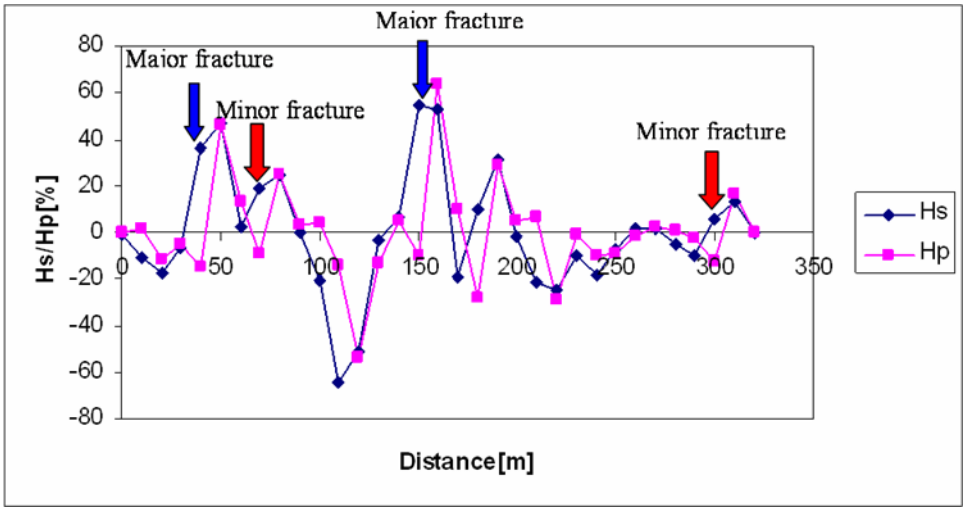

Figure 20: Plot of real and filtered real component of the VLF along traverse $EMTR_3$

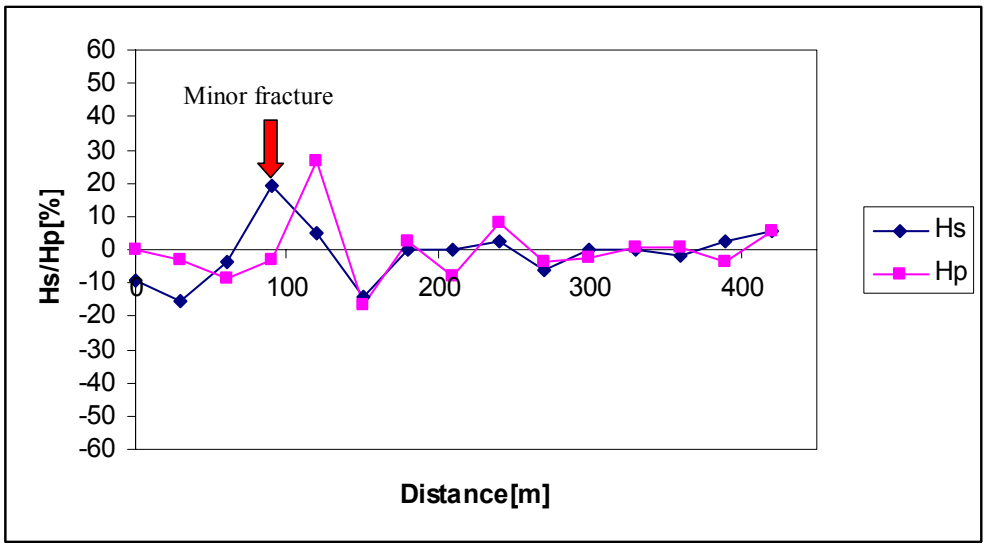

Along traverse $EMTR_1$ (W-E direction), major linear features with amplitude greater than 30% were located at distance 40 m while minor linear features (amplitude less than 20%) occurs at distance 130 m along the profile line. The major fracture corresponds to zone where artisanal workings are currently in progress. Along traverse $EMTR_2$ (W-E direction), two major and minor shear zones were identified and from field observations they are associated with zones of sulfide mineralisation . There was no major shear zone observable along traverse $EMTR_3$ (W-E direction).

The results of the sounding data show a system of three geo-electric layers. Representative VES curve is shown on Figure 21. The sequence comprises, from top to bottom - the topsoil, saturated clay/clayey sand and the weathered basement. A summary of the VES interpretation is shown in Table 1. The results indicate that overburden thickness is generally shallow at less than 7 m. This is in agreement with the presence of outcrops in the study area. This therefore suggests that mining activity in the area will not involve too much excavation of the overburden on top of the host rock.

Figure 21: Layer model interpretation for VES 4

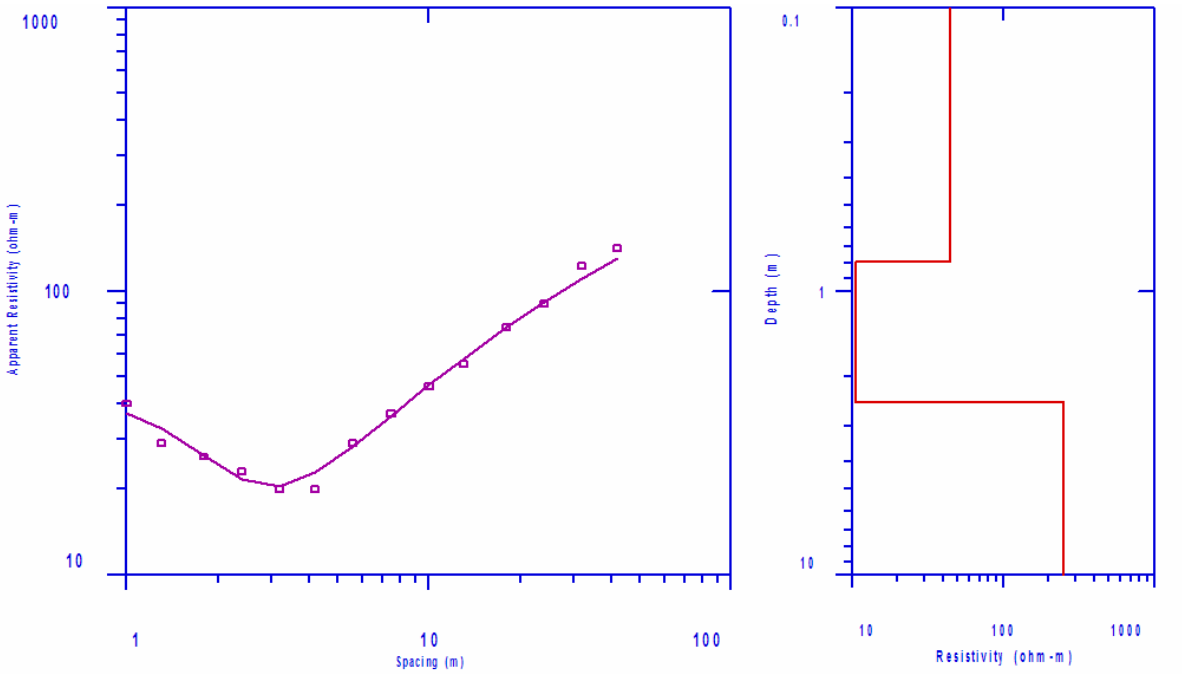

Table 1: Summary of VES Interpretation

Layer	Resistivity (ohm-m)	Thickness (m)	Depth (m)	Probable Lithology
VES1				
1	73	0.4	0.4	Topsoil
2	9	2.7	3.1	Saturated clay
3	290	-	-	Weathered basement
VES2				
1	13	1.6	1.6	Topsoil
2	114	5.0	6.6	Clayey sand
3	250	-	-	Weathered basement
VES3				
1	24	0.4	0.4	Topsoil
2	12	2.0	2.4	Saturated clay
3	200	-	-	Weathered basement
VES4				
1	44	0.8	0.8	Topsoil
2	11	1.7	2.5	Saturated clay
3	250	-	-	Weathered basement
VES5				
1	86	0.6	0.6	Topsoil
2	10	1.1	1.7	Saturated clay
3	360	-	-	Weathered basement
VES6				
1	238	0.8	0.8	Topsoil
2	31	1.1	1.9	Saturated clay
3	420	-	-	Weathered basement

Prospect areas

This study show that the most favourable environments for mineralization are the fractures and fault zones in the south western and south central portion of the study area. The most favourable host rocks are the pegmatised migmatite gneiss and the ultramafic bodies . Lead sulphide was found to occur as disseminated crystal within quartz and/or pegmatites in the pegmatised migmatite terrain. Two

prospect areas (A and B) have thus been delineated based on this investigation (Figure 22). The southern end is more enriched, followed by the central portion while the northern end shows no significant enrichment.

Figure 22: Map showing the prospect areas

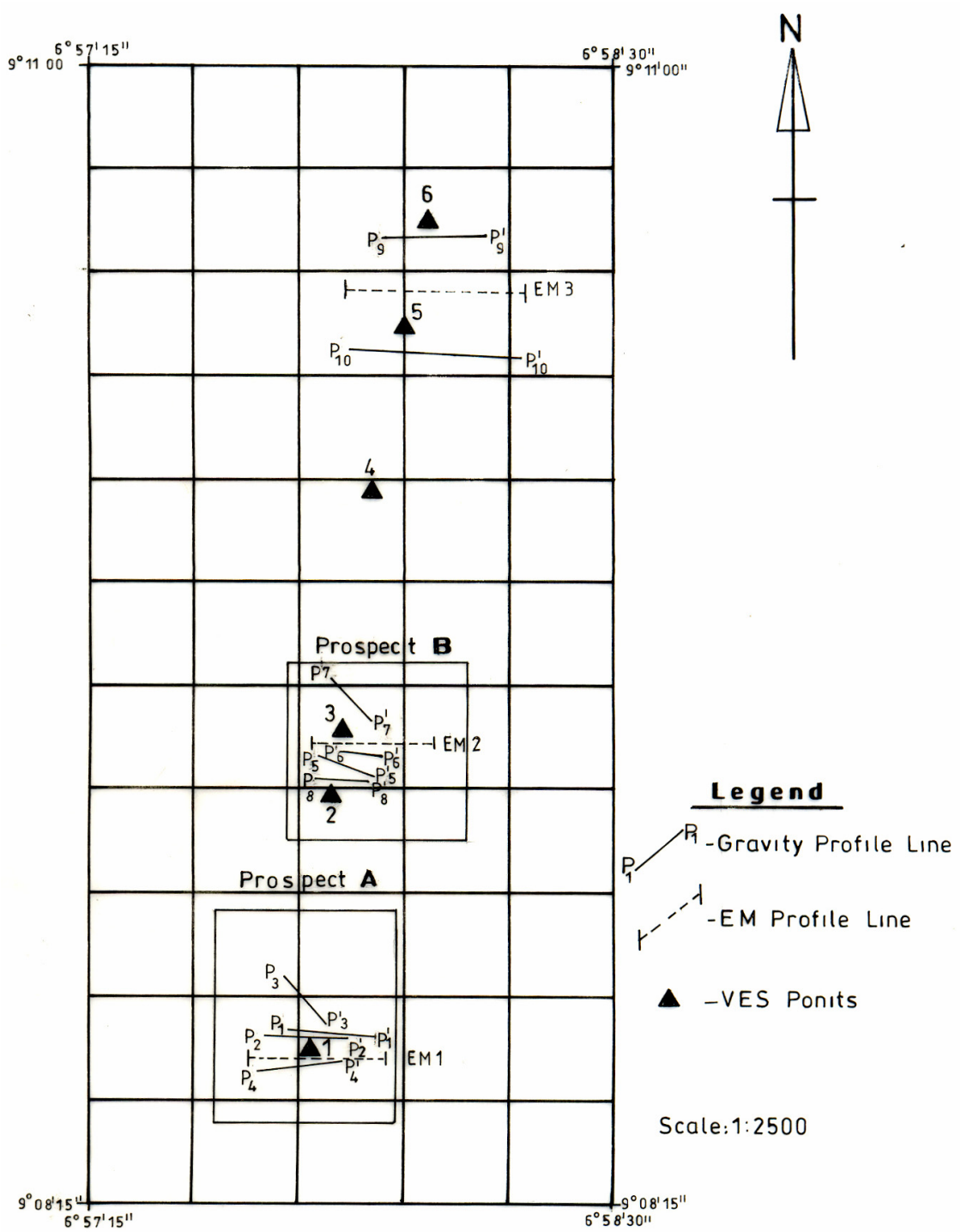

Summary and Conclusions

This present studies consisting of systematic geological mapping and geophysical investigations have shown that Baban Tsauni area is underlain by Precambrian Basement rocks consisting of migmatite-

gneiss complex, ultramafics, pegmatized migmatites and pegmatites. These rocks have been folded and fractured. The fractures trends dominantly in the NNW/SSE and NNE/SSW conjugate directions. Such fractures are more intensely exposed in the pegmatised migmatites and they are indicated by the linearity of the streams. Quartz vein and pegmatites are emplaced along and parallel to these zones of discontinuity, thus acting as mineral traps in the study area. The geologic studies indicate that the pegmatised migmatites and the ultramafites are the most favourable host rocks for the Pb-Zn mineralization. Evidence from the old mine pits and dumps point to the fact that the Pb-Zn mineralization are associated with the late quartz veins associated with the pegmatites which are usually characterized by low ridges and often covered with pebbly materials. Minor sulphide mineralization is also associated with the ultramafites. The Pb-Zn mineralization in the host assemblages is thought to be lithologically and structurally controlled.

Geophysical techniques, especially the gravity techniques apart from determining the occurrence and geometry of the ore bodies have revealed three distinct zones of mineralization,viz: the southern zone (near Baba Tsauni village) which is characterized by high positive anomalies, with their long axes parallel to the structural grain of the underlying rocks; the central portion where high anomalies are indicated with associated gold mineralization and the northern parts which shows indistinct and low level of mineralization. From the resistivity survey, the fresh bedrock is overlain by 2 layers of overburden – the top soil of about 1.5 m and weathered basement of about 3 – 7 m.

References

[1] Ako, B.D., Adegoke, O.S., Ajayi, T.R., Ajayi, J.O. and Rahaman, M.A., 1986: Groundwater prospecting and exploitation in Nigeria. In: Proceedings of the First Annual Symposium and Exhibition on Groundwater Resources in Nigeria, NIWASA, Lagos, Nigeria pp. 3-44.

[2] Burke, K.C. and Dewey, F.J., 1972: Orogeny in Africa. In: African Geology. Ibadan, Eds. Dessauvagie, A and Whiteman, C. Geol. Dept. Univ. Ibadan Nigeria, pp 583-608.

[3] Elueze,A.A. and. Okunlola, O.A., 2003: Petrochemical and Petrogenetic Characteristics of metasedimentry rocks of Lokoja – Jakura Schist belt Central Nigeria. Journal of Mining and Geology Vol.39, No 1 pp21 – 28.

[4] Huntings (Geology and Geophysics Ltd), 1975: Airborne – magnetometer and Gama-Ray Spectrometer survey over central Northern (Katsina – Jos) area.

[5] Karous, M.R. and Hjelt, S. E., 1983: Linear Filtering of VLF dipole-angle measurements. Geophysical Prospecting, 31: 782 – 794.

[6] Okunlola,O.A., Ogedengbe,O. and Ojutalayo,A., 2003; Compositional features and industrial appraisal of the Baba Ode talc Occurrence, South Western Nigeria .Global Journ. Of Pure and Applied Sciences Vol. 9 No. 1 2003 pp63-72

[7] Okunlola, O.A. and Jimba, S., 2006: Compositional trends in relation to Ta-Nb mineralization in Precambrian pegmatites of Aramoko-Ara- Ijero area, southwestern Nigeria, Jour. Min. Geol. Vol.42, No 2, pp. 113 – 126.

[8] Okunlola,O.A. and Oluyide, P.O. 2007; Integrated exploration for polymetallic mineralization, Jibiya area , Northwestern Nigeria. Technical report Nigerian Geological surveys Agency 100p.

[9] Olayinka, A.I. and Barker, R.D., 1990: Borehole siting in crystalline basement areas of Nigeria with a micro processor-controlled resistivity traversing system. Groundwater, 28, 178-83.

[10] Olorunfemi, M.O. and Mesida, E.A., 1987: Engineering geophysics and its application in engineering site investigation – Case study from Ile-Ife area. The Nigerian Engineer, 22, pp.57-66.

[11] Osella, A., Matias de la Vega and Eugenia, L., 2002: Characterization of a contaminant plume due to a hydrocarbon spill using geoelectric methods, JEEG, Vol.7, Issue 2, pp. 78-87.

[12] Oyawoye, M.O., 1972: The Basement Complex of Nigeria. In African Geology Ibadan, Eds. Dessaauvagie and Whiteman. Geol. Dept. Univ. Ibadan Nigeria, pp 67- 99.

[13] Russ, W., 1957: The geology of parts of Nigeria, Zaria and Sokoto provinces. Geological Survey of Nigeria Bulletin No. 27, 43p.

[14] Sharma, P.V., 1997: Environmental and Engineering Geophysics, Cambridge University Press, 173p.

[15] Truswell, J.F. and Cope, R.N., 1963: the geology of parts of Niger and Zaria provinces. Geological Survey of Nigeria Bulletin No. 29, 53p.

[16] Woakes, M. and Bafor, B.E., 1984: Primary Gold Mineralization in Nigeria. In Foster R.P. (Ed) : Geology, Geochemistry and Genesis of Gold Deposits, pp 661 – 671.

European Journal of Scientific Research
ISSN 1450-216X Vol.18 No.3 (2007), pp.389-401

http://www.eurojournals.com/ejsr.htm

Melissopalynologic and Physicochemical Analysis of Some North-East Algerian Honeys

Chefrour Azzedine
Laboratoire de Botanique
Département de Pharmacie- Faculté des Sciences Médicales
Université de Badji Mokhtar- Annaba, BP 205 Ezzafrania, Annaba (23000) Algérie
E-mail: azchefrour@yahoo.fr

Battesti Marie-José
Association « Miel et Pollen » - BP 48 - Campus Grossetti - 20250 Corte- France

Ait Kaki Yasmina
Laboratoire de Botanique
Département de Pharmacie- Faculté des Sciences Médicales
Université de Badji Mokhtar- Annaba, BP 205 Ezzafrania, Annaba (23000) Algérie

Bennadja Salima
Laboratoire de Botanique
Département de Pharmacie- Faculté des Sciences Médicales
Université de Badji Mokhtar- Annaba, BP 205 Ezzafrania, Annaba (23000) Algérie

Tahar Ali
Laboratoire de Biologie Végétale et Environnement
Institut de Biologi, Faculté des Sciences, Université Badji Mokhtar-Annaba, Algérie

Abstract

The qualities of thirteen honey samples harvested from the North-East areas of Algeria were evaluated by determining the pollen spectrum and physicochemical attributes. The following determinations were carried out: pH, density, acidity (free, lactone and total), moisture, electrical conductivity, hydroxymethylfurfural, diastase activity, apparent sucrose, and proteins.

The results obtained in the present study show the variability of chemical composition of the honey samples. It proved that nine natural honeies are of origin floral, suitable for consumption and that one can be used with fine dietetics.

On the other hand, the remainders (four honeies) are non in conformity with the standards, their sugar contents (Sucrose) and in hydroxymethylfurfural. Exceed the international standards, this probably due to the use of syrup for the over-feeding the bees with sugar during the spring.

Keywords: honey, pollen, melissopalynology, sucrose, Hydroxymethylfurfural, physico-chemical analyses, pH, HMF, total acidity.

Introduction

Honey is natural complex food product produced by bees from nectar of plants and also from honeydew. It is a unique sweetening agent that can be used by humans without processing. Honey of honeybees has significant nutritional and medicinal benefits. It is a rich source of readily available sugars, organic acids, various amino acids and in addition source of many biologically active compounds. [1]

The quality and biochemical properties of honey are related to honey maturity, production methods, climatic conditions, processing and storage conditions, as well as the nectar source of the honey [2, 3, 4, 5, 6].

However, quality and composition of honey are negatively affected by the other factors such as overfeeding with sucrose and other sucrose variants, harvesting prior to maturity, unhealthy storage conditions, and overused veterinary drugs. [7, 8, 4, 9]

Considering the dietetic importance of this product and its scarcity on the market, it is exposed to the frauds.

For that, the European and international Commissions proposed methods of analyses followed by standards of the food codex [10, 11] or European standards for the honeies quality control.

In Algeria, the bee-keeping is practised in many areas, characterized by a remarkable richness of honey plants.

The Algerian East is one of the zones of the most significant bee-keeping in the country.

The production of honey will be in the process of one year progression with another. There for, the present study was undertaken to characterise the physicochemical properties and the botanical origin (blossom and/or honey-dew honeys) of the Northeast Algerians samples honey.

Material and Methods

Honey samples

Thirteen samples of honeys produced in various regions of North-East of Algeria (Fig. 1) were collected from beekeepers between July 2001 and September 2001. The samples were stored in a refrigerator at 4-6°C in airtight plastic containers until analysis.
The regions from which the samples of honey were collected are indicated in Table 1.

Table 1: General information on the collected honey samples

Samples	Location	Botanical origin	Harvested period	Mode of extraction
M1	Guerguour	Eucalyptus	sept-01	centrifugation
M2	Boutheldja	Polyfloral	sept-01	pressage
M3	Bouhadjar	Polyfloral	jul-01	centrifugation
M4	Chihani	Polyflora	sept-01	pressage
M5	Bougous	Polyfloral	sept-01	pressage
M6	Drean	Citrus	sept-01	centrifugation
M7	Bouhachana	Polyfloral	sept-01	centrifugation
M8	Hamam N'Bail	Polyfloral	sept-01	pressage
M9	Mekfel	Polyfloral	jul-01	pressage
M10	Megasmia	Polyfloral	jul-01	centrifugation
M11	Bouhdid	Polyfloral	jul-01	centrifugation
M12	Ain Barbar	Polyfloral	sept-01	pressage
M13	Oued El Aneb	Polyfloral	sept-01	pressage

The botanical origin of the samples of honey was based on the pollen spectrum (45% and above), which is the ratio of the frequency of each pollen type in the honey. [12]

The analysis was based on the principle that microscopic elements were concentrated by centrifuging the honey dissolved in water, examining the sediments and evaluating them under the microscope after acetolysis. The method followed for pollen analysis was described by Louveaux et al. [1978].

Briefly, a sub-sample of 10 g of honey was dissolved in 20 ml of warm distilled water (around 40°C) and centrifuged twice (2000 rpm) for 10 min. The dry sediment was mounted on a slide with glycerine/gelatine slightly stained with an alcoholic solution of fuchine. Slides were microscopically observed and compared with the reference for identification.

The following terms were used for frequency classes: predominant pollen (more than 45% of pollen grains counted), secondary pollen (16–45%), important minor pollen (3–15%), minor pollen (less than 3%).

Figure 1: Distribution of the samples analysed in the studies regions (northeast Algeria) Localisation des échantillons de miels récoltés de l'Est Algérien

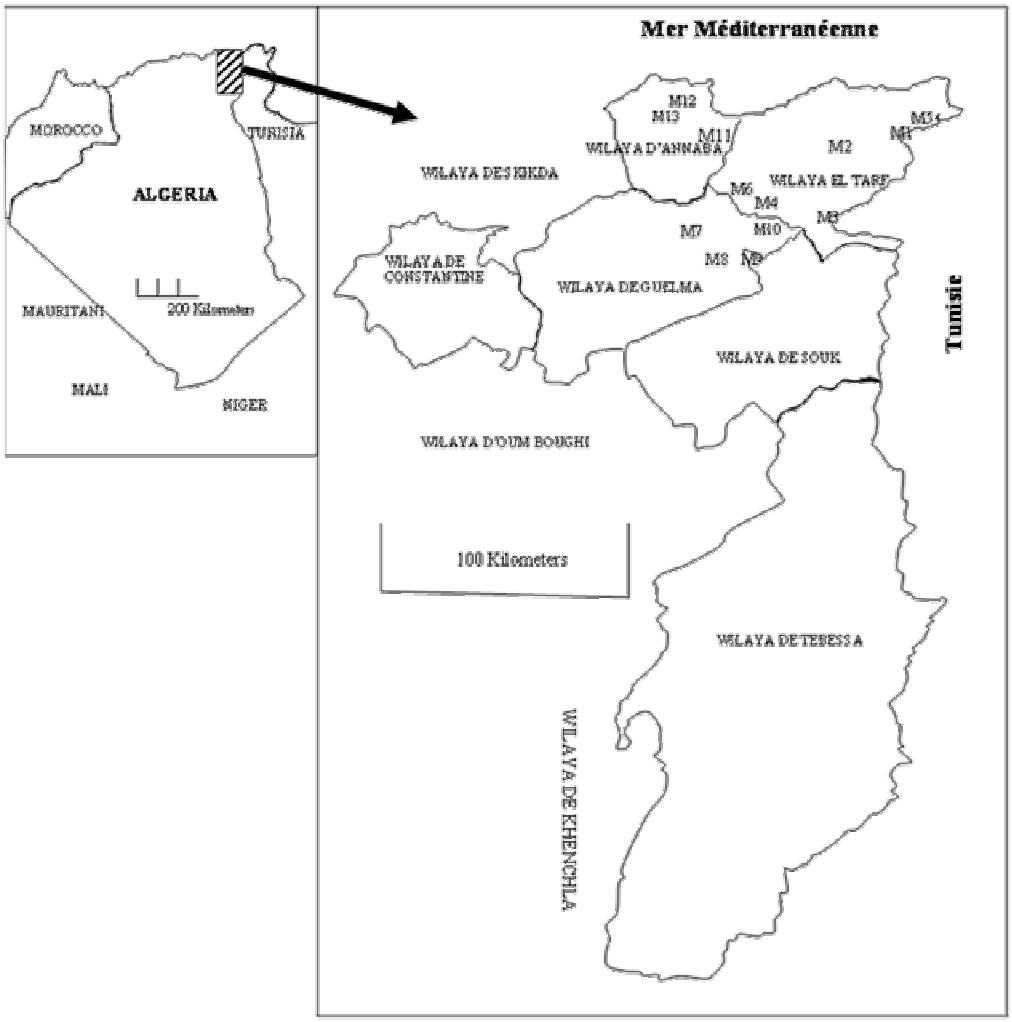

Honey properties

The samples of honey were analysed according to the European Commission of honey methods in order to determine: [13, 14, 10, 11, 15, 16]

The specific gravity of honey (density) was determined by dividing the weight of specific gravity bottle (50 ml) filled with honey by the weight of the same bottle, filled with water. [23]

Moisture was determined by refractometry method [17].

Electrical conductivity was measured in a 20% (w/v) solution of honey in deionized water using Leibohld model conductimeter.

The pH was assessed in a 10% (w/v) solution of honey in distilled water [17].

Lactone and total acidity were determined by the titrimetric method: first add 0.05N NaOH and stop at pH 8.5 (free acidity), immediately pipette in 10 ml 0.05N NaOH, and without delay back-titrate with 0.05N HCL to pH 8.3 (lactone acidity).

Total acidity results from adding free plus lactone acidities [22]. Results were expressed as meq/kg.

Apparent sucrose determined by the methods described in the French official journal [17].

The protein content was determined by the method of Azeredo, Azeredo, De Souza, and Dutra [2003]. A volume of 0.1 ml of protein extract (honey sample 50% w/v) was added to 5 ml of Coomassie Brillant Blue. After 2 min of incubation, the quantity of proteins was estimated at 595 nm in relation to bovine serum albumin standard curve. [25]

Hydroxymethylfurfural (HMF) was determined after dilution with distilled water and addition of p-toluidine solution according [18] and Saoudi Arabian Standard organization [19]. Absorbance was determined at 550 nm using a 1 cm cell in a Biochrom spectrometer. Results were expressed as mg/kg.

Diastase activity was measured with Phadebas, according to the Harmonized Methods of the European Commission of Honey [14].

A buffer solution of soluble starch and honey which was incubated in a special glass test tube. The unit of Diastase Activity, the Gothe unit, is defined as that amount of enzyme which will convert 0.01 gram of starch to the prescribed end-point in one hour at 40 °C under the conditions of test. Results are expressed in Gothe units (or Schade units) per gram of honey. [18, 20, 21]

Results and discussion

Pollen analysis

The absolute numbers of pollen grains indicate the richness of the samples in sediments. [26] The number of pollen grains in 10 g of honey ranged between 8 000 and 2 424 000. (Table 2)

According to the total number of plant elements, honeys are distributed into four classes [27]:

Table 2: quantitative analysis of samples and their class according to Maurizio classifications **(Maurizio, 1979)**

Samples	Location	Pollen grain number (PG/g)	Class
M1	Guerguour	6,220,000	V
M2	Boutheldja	24,832,000	V
M3	Bouhadjar	240,000	IV
M4	Chihani	3,774,000	V
M5	Bougous	7,300,000	V
M6	Drean	76,000	II
M7	Bouhachana	1,376,000	V
M8	Hamam N'Bail	646,000	IV
M9	Mekfel	6,190,000	V
M10	Megasmia	30,000	II
M11	Bouhdid	8,000	I
M12	Ain Barbar	1,200,000	V
M13	Oued El Aneb	5,800,000	V

Class I: include A1 with low pollen grains (8,000PG/10g).

Class II: two samples (M6, M10) with a number 76,000 and 30,000 pollen grain. two samples included in class IV; M3 (240,000 pollengrain) and M8 (646,000 pollen grain).

The remainders of the samples are classified in class V with a pollen number higher than one thousand.

The results from the pollen analysis (pollen spectrum) summarised in **Table 3,** show that the predominant pollen is not found in all honeys.

In our case, Honey can never be derived from a single botanical source, because the bee-keepers collect the honey of each apiaries only once per year. To obtain a unifloral honey, it is necessary to make harvest after the end of each flowering of a flower honey.

The term `unifloral' honey is used to describe honey produced mostly from one plant species. Generally, the pollen content for a honey to be called `unifloral' should be at least 45% of the total pollen content. [28]

More than 10 pollen types are found in honey sample of Guergour (M1), and Megasmia (M10).

In other samples the pollen type number limited between 10 and 6.

The determination of the floral origin of honey has been achieved by the analysis of the pollen present in honey. The different pollen types are described in the literature [29, 30, 31, 32, 33, 34, 35, 36, 37].

The results from the quality analysis are shown in Table 3

Table 3: Qualitative analysis of pollen types in honey samples, represented as percentages

Samples	Predominant Pollen (> 45%)	Secondary pollen (16 – 45%)	Minor pollen (3 – 15%)	Important minor Pollen (<3%)
M1	-	*Hedysarum coronarium* 24, *Eucalyptus spp* 22, Type Rosaceae 17	Apiaceae 15,*Thymus spp* 12, *Geranium* 7, Asteraceae 3	-
M2		*Eucalyptus* 33, *Daucus* 28, Urticaceae 16	*Eucalyptus* 10, *Trifolium spp* 7, *Rubus* 4	*Lavandula stoechas* 2
M3		*Hedysarum coronarium* 25, *Cistus spp* 20	*Rubus ulmifolius* 14, *Eucalyptus* 10, *Allium cepa* 8, *Ornithogalum* 10, *Asphodelus aestivus* 9	*Apium graveolens* 2, *Myrtus* 2
M4		*Eucalyptus* 34, *Cucurbita spp* 30	*Hedysarum coronarium* 12, *Trifolium spp* 8, *Allium spp* 6 , Iridaceae 4	*Myrtus communis* 2, *Potentilla spp* 2, *Taraxacum* 2
M5		*Eucalyptus* 37, *Pyrus /Malus* 29	Liliaceae 14, Euphorbiaceae 8, *Trifolium spp* 7, *Geranium* 3	*Anethum spp, Malva sylvestris*
M6		*Eucalyptus* 19	*Rubus* 15, *Daucus* 13, *Erica arborea* 13, *Foeniculum spp* 11, *Liliaceae* 10, *Citrus* 5, *Borago spp* 5, Euphorbiaceae 4	*Iris* 2, *Myrtus communis* 2, *Juniperus* 1
M7		*Hedysarum coronarium* 40, *Pyrus/Prunus* 25, *Trifolium spp* 18	*Anethum* 9, *Eucalyptus* 6	Liliaceae 2
M8		*Eucalyptus* 26, *Apiaceae* 22	*Trifolium spp* 13, *Myrtus* 12, *Genista* 9, *Rubus* 8, *Thymus vulgaris* 7, Asteraceae type *Centaurea* 3	
M9		*Eucalyptus* 35, *Hedysarum coronarium* 21, *Trifolium spp* 19	*Iris* 9, *Malva sylvestris* 7, *Prunus spp* 3	Chenopodiaceae 2, *Brassica* 2, *Euphorbia* 2
M10		*Prunus* 19, *Rubus* 16, *Apiaceae* 16 *Crataegus* 10	Liliaceae 14, *Cistus spp* 8, *Brassica nigra* 6, *Trifolium spp* 4, *Eucalyptus* 3, *Allium* 3	*Myrtus communis*
M11		Papilionaceae 40, *Eucalyptus* 27	*Anethum spp* 13, Campanulaceae 10, *Salix* 6, *Sinapis spp* 4	
M12		*Hedysarum coronarium* 32	*Inula viscosa* 13, *Eucalyptus* 11, *Echinops spinosus* 10, *Cichorium intybus* 7, *Rubus* 6,*Malva* 5, *Cistus* 4, *Salix* 3, *Erica arborea* 3	Poaceae 1, *Allium spp* 2, *Cucurbita sp, Beta vulgaris* 2
M13		*Echium* 23, *Brassica spp* 16	*Borago officinalis* 15, *Cistus* 12, *Pyrus* 8, *Lavandula stoechas* 12, *Erodium spp* 6, *Myrtus communis* 4, *Daucus carota* 4	

Fourty nine pollen types had identified from 26 families.

Three families (Asteraceae, Rosaceae and Apiaceae) are best represented with a number of taxa which is respectively 8, 7 and 5 types. The anemophilus pollen grains observed in tree samples (M6, M9 and M12).

The only type of pollen present in almost all the samples is the *Eucalyptus*; this species is a polliniferous plant which has a very broad surface of distribution.

Physicochemical parameters

Mean results for physicochemical analysis (moisture content, density, pH, total acidity, electric conductivity, sugar, diastase index, protein content) are summarised in **Table 4.**

Density

The physical parameter density values ranged from 1.37 to 1.5.

Indeed, the samples M8, M3, M6 and M11 have values exceeding the average standard (1,39 to 1,44 at 20°C) and do not exceed the maximum limit which is 1,5.They are very dense honeies.

The samples M1, M7 and M13 have density slightly lower than the standard, because they have a high water contents.

Moisture content

Water content, a parameter related to the maturity degree, is an indicator of the mode of extraction of honey and density. Analyzed honeies have values limit between 16.4-20.4%.

According to Gonnet [1986], honeies having a water content higher than 18% are regarded as lower quality (preserves itself badly), and are suspect with falsification.

The water contents obtained for various honeies go from 16 to 20.4%.The honey having a value ranging between 16- 18% are regarded as best honeies with respect to the conservation and of storage. [2]

Only one honey sample (M7) was found to be higher in moisture content (> 20%) than the maximum allowable content for honey determined by the International Honey Commission. [2]

Electric conductivity

All honeies are in conformity with the international standard (1 to 15 X10 $^{-4}$ S/cm). In this interval, honeies are classified in two groups: (Table 4)

- Ten honeies result from nectar, because their electrical conductivities limited between 1-5 X10 $^{-4}$ S/cm. [43]; [44]
- Honeies (M7, M8 and M6) having of the median values between 5 and 10 X10 $^{-4}$ S/cm are of two origins (Honeydews and floral honey).

This parameter depends on the ash, organic acids, proteins, some complex sugars and polyols content, and varies with botanical origin [45].

The conductivity measurement is easy. It is widely used for discrimination between honeydew and blossom honeys and also for the characterisation of unifloral honeys [2].

The honeydew honeys are characterised by their very dark colour and high values of pH, ash content and electrical conductivity [46, 47].

Table 4: Results of some physicochemical parameters of honey samples. (mean±S.D.) Samples

Samples	Densité	Moisture (%)	Electrical conductibility (10-4S/cm)	pH	Free acid (meq/kg)	Lactone (meq/kg)	Total acidity (meq/kg)	Sucrose (%)	Proteins (%)	HMF (mg/kg)	Diastase
M1	1.37 ± 0.01	19.6 ± 0.00	4.21 ± 0.2	3.29 ± 0.01	63.5 ± 0.32	23.96 ± 0.22	87.46 ± 0.49	11.02	0.92 ± 0.03	4.416 ± 0.14	25.21 ± 0.02
M2	1.40 ± 0.011	18 ± 0.27	3.55 ± 0.1	3.3 ± 0.3	38.5 ± 0.29	21.49 ± 0.28	59.99 ± 0.55	1.06	0.96 ± 0.06	2.304 ± 0.04	3.55 ± 0.04
M3	1.46 ± 0.008	17 ± 0.29	2.01 ± 0.2	3.39 ± 0.01	27.25 ± 0.41	17.73 ± 0.28	44.98 ± 0.53	2.28	0.72 ± 0.01	6.72 ± 0.15	19.05 ± 0.35
M4	1.41 ± 0.008	17.6 ± 0.51	2.36 ± 0.0	3.82 ± 0.04	11.5 ± 0.32	25.99 ± 0.3	37.49 ± 0.62	9.14	0.87 ± 0.06	14.016 ± 0.05	114 ± 0.69
M5	1.4 ± 0.009	17.8 ± 0.24	2.96 ± 0.3	3.71 ± 0.02	12.25 ± 0.38	22.73 ± 0.27	34.98 ± 0.63	0	0.93 ± 0.03	5.184 ± 0.053	22 ± 0.06
M6	1.48 ± 0.01	16.8 ± 0.44	8.25 ± 0.6	4.09 ± 0.01	13 ± 0.31	3.75 ± 0.21	16.75 ± 0.49	2.92	0.63 ± 0.02	14.97 ± 0.0	6.86 ± 0.32
M7	1.38 ± 0.009	20.4 ± 0.43	9.22 ± 0.5	3.8 ± 0.05	7.5 ± 0.28	39.98 ± 0.21	47.48 ± 0.45	3.42	0.66 ± 0.01	4.992 ± 0.061	34.17 ± 0.74
M8	1.48 ± 0.013	16 ± 0.25	6.47 ± 0.7	3.5 ± 0.04	26.25 ± 0.29	21.23 ± 0.21	47.48 ± 0.47	3.3	0.79 ± 0.00	1.728 ± 0.046	13.68 ± 0.31
M9	1.39 ± 0.007	18.1 ± 0.4	3.1 ± 0.2	4.05 ± 0.03	12 ± 0.29	15.49 ± 0.24	27.49 ± 0.53	1.14	0.28 ± 0.01	4.032 ± 0.01	22.01 ± 0.05
M10	1.44 ± 0.009	17.4 ± 0.51	2.36 ± 0.3	3.84 ± 0.01	12.5 ± 0.22	14.99 ± 0.12	27.49 ± 0.32	0	0.22 ± 0.01	5.952 ± 0.04	19.63 ± 0.053
M11	1.5 ± 0.012	16 ± 0.32	2.46 ± 0.3	3.92 ± 0.03	15.75 ± 0.47	14.24 ± 0.23	29.99 ± 0.67	14.78	0.64 ± 0.06	480 ± 0 .00	2.84 ± 0
M12	1.39 ± 0.009	18.6 ± 0.46	2.01 ± 0.2	3.68 ± 0.03	29 ± 0.22	18.49 ± 0.1	47.49 ± 0.3	2.28	0.53 ± 0.00	5.568 ± 0.0	23.08 ± 0.7
M13	1.38 ± 0.007	18.8 ± 0.29	2.49 ± 0.4	3.86 ± 0.04	21.5 ± 0.38	19.24 ± 0.28	40.74 ± 0.66	8.96	0.77 ± 0.03	4.608 ± 0.016	25.21 ± 0.065

pH

According to the standards [22, 11], honeies whose pH is located between 3,5 and 4,5 results from honeydews and blossom honey. It is the case of all the analyzed samples xcepted the samples M1, M2 and M3.

The pH values located between 4,5 and 5,5 indicate that it is about a honey of honeydew. [38]

Moreover, a honey with a low pH of about 3,5 is regarded as a fragile product for the conservation, whose great precautions must be taken.

Total acidity

Total acidity of M1 was higher than the other honeys. This sample has a value out the international standard average; it had the highest free acid content (Table 4).

The acidity of honey is due to the presence of organic acids, particularly the gluconic acid, in equilibrium with their lactones or esters and inorganic ions such as phosphate and chloride [39, 40]. The variation in acidity among different honey types may be attributed to variation in these constituents due to extraction season [41]. El-Sherbiny and Rizk [1979] reported that total acidity was higher in cotton honey than in clover honey which indicates the influence of floral types in total acidity.

Sugar

Sucrose Content of four samples (M11, M13, M1 and M4) is not conforming. A high content of this sugar means most of the time, an early harvest of the honey, i.e. a product in which the sucrose has not been fully transformed into glucose and fructose by the action of invertase. Generally, the sucrose content does not exceed 5% for authentic honey samples. [24]

The bee-keepers explain this value with the using of syrup for over-feeding the bees with sugar during the winter season.

Protein Contents

The protein contents of analysed honey samples were between 0, 22% and 0, 96%. These results indicate that the colorimetric determination of the protein content of honey samples using the method of Bradford, was efficient and it allowed the detection of high values in the samples M1, M2 and M5, compared to the mean of the other analyzed honeys.

The results of this study are higher than those obtained by Azeredo et al. [2003] for honeys of Borreria verticillata (0,223 %), whereas they are close to the results obtained by Ouchemoukh et al. [2007] for some Algerian honeys.

The samples M1, M2 and M5 have contents exceeding the standard [11], this is explained by the strong content of pollen in these inconceivably collected honeies. [49, 53, 54]

Hydroxymethylfurfural (HMF)

The results obtained (Table 4) showed that, in just one case, the content was higher than the maximum allowed, which is 40 mg/kg [48] As this one sample (M11) was harvested after a relatively long time, then it has been submitted to high temperatures, knowing that its content sucrose (14,78%) is very higher.

Diastase index (I.D)

Only one sample (M11) has a lower diastase index than the minimum standard value (superior than 8). this can be due either, with overheating at the time of the extraction, or with the natural poverty of the sample on amylase, but the higher HMF content confirm that this honey has undergoes an overheating.

Diastase index and HMF content are the indicators of the freshness degree of honey. [15, 49, 50, 51, 12]

Conclusion

In conclusion, the physico-chemical characteristics of the honeies analyzed in this study generally were not in agreement with the requirements of European Community Directive. Because according to results' obtained, an abnormal sucrose rate was detected in four honey samples, with a very low pH for three samples and a Rate of significant HMF.

The harvest of the old honeycombs (frameworks of the winter detected by the very high content of saccharose), with pollen and honeycombs of the year in hive body (brood chamber) with others of the shallow super (very significant content of pollen) and the realization of an extraction (manual or mechanical) without letting the product rest in maturator (very low pH for some samples, shows that the bee-keepers of these areas are not professional person.

Normally, the beekeeper does not collect the frame comb of the hives body, because this space is reserved for the bees to rear brood and store honey for their own use.

The remainders of the samples are good quality, characterized by a remarkable floristic variability. it allowing to be used in dietetics and with the fine therapeutic ones.

References

[1] **Jasim A, Prabhu S T, Raghavan G S V. and M Ngadi** Physico-chemical, Rheological, Calorimetric and Dielectric Behavior of Selected Indian Honey. *Jour. of Food Engin.* 2007; **79**: 1207–1213.

[2] **Bogdanov S, Lüllman C, Martin P, Von Der OheW, Russmann H, Vorwohl G, Persano-Oddo L, Sabatini A G, Marcazzan G L, Piro R, Flamini C, Morlot M, Heritier J, Borneck R, Marioleas P, Tsigouri A, Kerkvliet J, Ortiz A, Ivanov T D, Arcy B, Mossel B & P Vit** Honey quality and international regulatory standards: review by the international honey commission. *Bee World* 1999; **80(2)**: 61–69.

[3] **Crane E** Honey: A comprehensive survey. *Heinemann Intern. Bee Res. Ass. (IBRA)*. London 1979: 3-76.

[4] **Persano Oddo L and S Bogdanov** Determination of Honey Botanical Origin: Problems and Issues. *Apidologie* 2004; **35**: S2–S3.

[5] **White J W** Honey. *Advances in Food Res.* 1978; **24**: 287–374.

[6] **White J W** Spectrophotometric Method for Hydroxymethylfurfural in Honey. *J. Ass. Off. Anal. Chem.* 1979; **62**: 509.

[7] **Bakan A** Balda Kristallenme Sorunu. Gıda 2002; 86–87.

[8] **Bogdanov S, LullmannC, Martin P, Ohe W V D, Russmann H, Vorwohl G et al.** Honey Quality, Methods of Analysis and International Regulatory Standards: Review of the Work of the International Honey Commission. Liebefeld Switzerland. *Swiss Bee Res. Center* 2000. FAMwww.fam.admin.ch.

[9] **Sahinler N, Sahinler S, and A Gul** Biochemical Composition of Honeys Produced in Turkey. *J. of Apic. Res.* 2004; **43(2)**: 53–56.

[10] **Codex Standard for Honey.** *European Regional Standard.* **12**-1981.

[11] **Codex Alimentarius Commission Standards** 2001 CODEX STAN 12- 1981. Rev. 1 (1987), Rev. 2.

[12] **Louveaux J Maurizio A et G Vorwohl** Methods of Melissopalynology. *Bee World* 1978; **59**: 139-157.

[13] **Bogdanov S and S E Baumann** Bestimmung von Honigzucker mit HPLC. *Mitt Geb. Lebensmittelunters Hyg.* 1988; **79**: 198-206.

[14] **Bodganov S, Martin P and C Lüllmann** Harmonised Methods of the European Honey Commission. *Apidologie.* Elsevier, France 1997:1-59

[15] **Codex Alimentarius Commission** Recommended European Standard for Honey. CAC/RS-12-1969. Jt. FAO/WHO Food Stand. Program. Rome. Reprinted *in Bee World* 1969; **51**, 79-91. Directive 74/409/EEC.

[16] **Pourtallier J** Les Analyses dans le Contrôle de la Qualité des Miels. 23ème *Congrès international d'apiculture*. Moscou 1971.

[17] **Journal Officiel Français** Arrêté du 15/02/77 Relatif aux Méthodes Officielles d´Analyse du Miel (Journal Officiel de la République Française - N.C. du 22/04/77). 1977.

[18] **Association Official Analytical Chemists** *Official Methods of Analysis of AOAC International*, 16th ed..1995; Vol. II. Method 969.38b.

[19] **SASO** Test Methods of Honey. Saudi Arabian Stand. Org. 1990; n°102. Saudi Arabia: Ministry of Commerce.

[20] **Bogdanov S and P Lischer** Phadebas and Schade Diastase Determination Methods, Humidity by Refractometry and Invertase Activity: Report for the participants. *Interlaboratory Trial of the International Honey Commission* 1993.

[21] **Persano Oddo L and P Pulcini** A Scientific Note on the Phadebas Method for Honeys with Low Enzyme Content. *Apidologie*. 1999; **30**: 347-348.

[22] **AOAC** Acidity of Honey. Official Methods of Analysis. 1990; **962.19**: 1033.

[23] **Bogdanov S, Bieri K, Figar M, Figueiredo V, Iff D, Känzig A, Stöckli H and K Zurcher** Miel: Définition et Directives pour l'Analyse et l'Appréciation. *In* Livre Suisse des Denrées Alimentaires, OCFIM. 1995: 1–26.

[24] **Azeredo L da C , Azeredo M A A , De Souza** S R and V M L Dutra Protein Contents and Physicochemical Properties in Honey Samples of *Apis mellifera* of Different Floral Origins. *Food Chemistry* 2003; **80**:249–254.

[25] **AOAC International** Official Methods of Analysis of AOAC International. 2000; Vol. **II**, 17th Edition.

[26] **Von der Ohe W, Persano Oddo L, Piana M L, Morlot M and P Martin** Harmonized Methods of Melissopalynology. *Apidologie*. 2004; **35**: S18- S25.

[27] **Maurizio A** Microscopy of Honey. **In: Crane E** (Ed.), Honey: A Comprehensive Survey London: Heinemann **in** Cooperation with *International Bee Res. Ass*., 1979: 240–257.

[28] **Maurizio A** How Bees Make Honey. **In: Crane E** (Ed.), Honey: A Comprehensive Survey. Heinemann, London, UK, 1975: 77–105.

[29] **Lieux M H** A Melissopalynological Study of 54 Louisiana (U.S.A.) honeys. *Rev. Palaeobot. Palynol*.1972 ; **13**: 95-124.

[30] **Louveaux J** Annexes Microphotographiques aux Méthodes Officielles d'Analyse. Tome III : Atlas Photographique d'Analyse Pollinique des Miels. Service de Répression des Fraudes et du Contrôle de Qualité. Commission Générale d'Unification des Méthodes d'Analyse. Paris VII, France ; 1970: 24-52.

[31] **Louveaux J** Caractérisation Botanique et Géographique des Miels. *Bull. Apicole*. 1972; Vol.**15** n°1.

[32] **Moore P D and Webb J A In** An Illustrated Guide to Pollen Analysis. Hodder and Stoughton, London. 1978.

[33] **Reille M** Leçon de Palynologie et d'Analyse Pollinique. Ed. CNRS, Paris. 1990 ; 199 pages

[34] **Renault-Miskovsky J et M Petzold** Pollen et spores. Ed. Duraulie. 1976; 248 pages.

[35] **Ricciardelli D'Albore G**. Mediterranean Melissopalynology. Perugia: Institute of Agricultural Entomology, University of Perugia. 1998.

[36] **Ricciardelli D'Albore G and L P Oddo** Flora Apistica Italiana. Federazione Apicoltori Italiani. 1978.

[37] **Sawyer R** Honey Identification. *Cardiff Academic Presse*, UK. 1988.

[38] **Gonnet M** L'Analyse des Miels. Description des Quelques Méthodes de Contrôle de qualité. *Bull. Tech. Apicole* 1986 ; **13(1)**: 17-36.

[39] **Echingo T and T Takenaka** Production of Organic Acids in Honey by Honey bees. *J. of Agric. Chem. Society*, Japan. 1974; **48**, 225–230.

[40] **Nandaa V, Sarkara B C, Sharmaa H K and A S Bawab** Physico-Chemical Properties and Estimation of Mineral Content in Honey Produced from Different Plants in Northern India. *J. of Food Composition and Analysis*. 2003; **16**: 613–619.

[41] **Perez-Arquillue C, Conchello R, Arino A, Juan T and A Herrero** Quality Evaluation of Spanish Rosemary (*Rosmarinus officinalis*) Honey. *Food Chem.* 1994; **51**: 207–210.

[42] **El-SherbinyG A and S S Rizk** Chemical Composition of Both Clover and Cotton Honey Produced in A.R.E. Egypt. *J. of Food Sci.* 1979 ; **7** : 69–75.

[43] **Gonnet M** Le Miel, Composition, Propriétés et Conservation. 2ème Ed., OPIDA, France. 1982 ; 31 pages.

[44] **Jean-Prost P** Apiculture. Ed. *Tec. et Doc.*, 6ème édition. 1987: 310-346.

[45] **Terrab A, Diez M J and F J Heredia** Palynological, Physicochemical and Colour Characterisation of Moroccan Honeys. I. River Red Gum (*Eucalyptus camaldulensis* Dehnl.) Honey. *International J. of Food Sci and Tech.* 2003a; **38**: 379-386.

[46] **Diez MJ, Andrés C and A Terrab** Physicochemical Parameters and Pollen Analysis of Moroccan Honeydew Honeys. *International J. of food Sci. and Tech.* 2004; **39**: 167-176.

[47] **Thrasyvoulou A and J Manikis** Some Physicochemical and Microscopic Characteristics of Greek Unifloral Honeys. *Apidologie* 1995; **26**: 441–452.
[48] 48- AOAC Official Methods of Analysis. (14th Ed.) *Association of Official Analytical Chemists.* Washington DC; 1984.
[49] **Louveaux J** Les Abeilles et leur Élevage (Nouvelle Encyclopédie des Connaissances Agricoles). Ed. Hachette, Paris. 1980: 164-199.
[50] **Louveaux J** Le Miel. *Cah. Nutr. Diét.* 1985 ; **20**: 57-70.
[51] **Louveaux J, Maurizio A et G Vorwohl** Méthodes de la Mélissopalynologie. Commission internationale de la botanique apicole de l'U.F.S.B. *Apidologie* 1970 ; **1(2)**:211-227.
[52] **Ouchemoukh S, Louaileche H and P Schweitzer** Physicochemical Characteristics and Pollen Spectrum of Some Algerian Honeys. *Food Control* 2007; 18: 52-58.
[53] **Philippe** Le Guide de l'Apiculture. Ed. ÉDISUD, Paris 1988: 200-295.
[54] **Philippe** Le guide de l'apiculteur. 3ème Ed., ÉDISUD, La Caade, Aix-en-Provence –France 1999 : 203-219.

European Journal of Scientific Research
ISSN 1450-216X Vol.18 No.3 (2007), pp.402-416

http://www.eurojournals.com/ejsr.htm

Enhancing Senior Secondary School Students' Cognitive Achievement in Mathematics Through Self and Cooperative Instructional Strategies

Francis A. Adesoji
Department of Teacher Education
Faculty of Education, University of Ibadan, Ibadan, Nigeria
E-mail: francisadesoji@yahoo.com

Ifamuyiwa Adebola S
Lecturer, Curriculum Studies and Instructional Technology Department
Faculty of Education, Olabisi Onabanjo University, Ago-Iwoye, Nigeria
E-mail: saji_38@yahoo.com

Abstract

This study investigated the effects of self and cooperative instructional strategies on senior secondary school students' cognitive achievement in Mathematics. The moderating effects of locus of control and gender were also investigated.

The study adopted pre-test, post-test, control group quasi-experimental design using a 3x2x2 factorial matrix with two experimental groups and one control group. Three hundred and fifty (350) SSS II students from six purposively selected secondary schools in Ijebu-North Local Government Area of Ogun State were the subjects. Three instruments were developed, validated and used for data collection. Analysis of Covariance (ANCOVA) and Scheffé post-hoc analysis were the statistics used for data analysis. Findings showed that the treatments had significant main effect on students' cognitive achievement in Mathematics. The participants exposed to cooperative instructional strategy recorded the highest post-test mean achievement score. The study, however, found no significant main effects of locus of control and gender on the participants' cognitive achievement. It was therefore concluded that Mathematics teachers should be trained to use self and cooperative learning packages in the classroom since the strategies were found to be more effective in enhancing students' achievement in Mathematics than the conventional teaching method.

Keywords: Self-Instructional Strategy, Cooperative-Instructional Strategy, Gender, Locus of Control, Cognitive Achievement.

Introduction and Related Literature

The Federal Government of Nigeria, through the Federal Ministry of Education, gave prominence to Mathematics by making it a core subject (because of its importance) at the secondary school level, as clearly spelt out in section 5 (items 24 & 25, pages 19 – 21) of the National Policy on Education (Federal Republic of Nigeria, 2004) and accorded it a central place in the school curriculum. Today, Mathematics is taught every school day in both primary and secondary schools in Nigeria.

In spite of the importance of Mathematics world wide, the annual reports of the West African Examination Council (WAEC) Chief Examiners in Mathematics indicated that students' performance in the Senior School Certificate Mathematics Examinations remains very low, as many of the candidates scored zero or marks within zero range (West African Examination Council, 1997; 2000 - 2005). In 2005 for instance, part of the Chief Examiner's report says, "the performance of the candidates did not improve significantly. The standard of candidates' performance was still low. This showed lack of preparedness on the part of the candidates" (Page 157). Insufficient preparation of students for the examination, computation error involving the four rules of arithmetic and students' failure to observe the rubrics were the factors identified by the Chief Examiners as being responsible for the dismal performance.

In addition, the following table speaks volume about students' poor performance in Mathematics between 1997 and 2004 in Nigeria.

Table 1: Statistics of Entries and Results in 'O' Level Mathematics for the May / June Senior Secondary School Certificate Examination (SSCE) Between 1997 and 2004 in Nigeria

Number and Percentage Obtaining Crade						
Year	**Total Enrolled for Exam**	**Distinction**	**Credit**	**Pass**	**Failure**	**Number Absent**
1997	616,923	8,883 1.50%	38,369 8.95%	161,526 26.20%	408,145 66.20%	4,921 0.81%
1998	635,686	13,962 2.20%	56,896 8.95%	159,000 25.01%	390,962 61.50%	4,938 0.72%
1999	756,680	30,907 4.08%	107,191 14.17%	212,514 28.09%	381,029 50.36%	4,408 0.58%
2000	634,604	55,683 8.78%	152,561 24.04%	196,080 30.92%	230,280 30.29%	8,767 1.36%
2001	1,023,102	103,094 10.07%	270,861 26.47%	334,907 32.73%	314,240 30.71%	17,015 1.64%
2002	908,235	67,698 7.43%	241,711 26.50%	308,359 33.95%	290,457 31.98%	17,053 1.84%
2003	926,212	71,955 7.75%	269,973 29.50%	331,348 35.78%	229,878 24.81%	13,294 1.41%
2004	832,689	88,590 10.63%	198,894 23.78%	245,071 29.43%	300,134 36.04%	11,836 1.40%

Source: West African Examination Council, Yaba, Lagos (2005).

It is pathetic to note that for the years under review in table 1, while about 60% of the students who wrote the examination failed Mathematics (i.e. percentage of those that recorded pass and outright failure), only about 10% of the students recorded distinctions in Mathematics for the years 2001 and 2004 and less than 10% for the remaining years.

Akinsola (1999), Adetunji (2000), Popoola (2002), Ojo (2003) and Olowojaiye (2004) are researchers that have attributed the problems hindering Mathematics teaching and learning in Nigerian schools to teachers' inability to help students learn Mathematics in a meaningful way. These authors were unanimous in their submissions that there is need for Mathematics teachers to understand classroom practices that could facilitate the processes leading to effective learning of Mathematics. This is necessary in order to de-emphasize the prevailing learning activities in schools that presupposes learning of Mathematics to be 'information absorption' in which knowledge is acquired independent of the social and physical environment from which Mathematics as a subject derives its meaning and usefulness. Such approach to teaching and learning of Mathematics according to DeCorte (1992), does not equip students with the necessary skills, beliefs, motivation and knowledge to approach mathematical problems and learning tasks in an efficient and successful way.

The process of teaching and learning Mathematics at the secondary school level, which gives students less opportunity to learn at their own rate, is a potent factor hindering students' cognitive

achievement in Mathematics. The prevailing learning activities in schools that often times do not give consideration to learners' experiences and which consist mainly the use of textbook and chalkboard as instructional materials, listening, watching and imitating the teacher, are not supportive of efficient learning of Mathematics. It thus appears that the conventional method of teaching Mathematics, which is prevalent in Nigerian secondary classrooms, has been shown to be ineffective and has not been yielding the desired result (Akinsola, 1994; Ojo, 2003). There is therefore the need to search for alternative methods of teaching Mathematics that would be effective in helping learners to understand and retain what is learnt. Akinsola (1994) pointed out that when searching for such alternatives, it should be remembered that the basic ingredient that has been identified as necessary for effective learning is the active participation of the learner in the learning situation. Strategies associated with self-instruction and student's self-regulatory learning (Udousoro, 2000; Popoola, 2002; Ojo, 2003), cooperative instructional strategy and peer tutoring assisted instruction (Alebiosu, 1998; Ogundipe, 2004) and meta-cognitive instructional strategy (Ekwere, 1998; Akinsola & Igwe, 2002) have been acclaimed to be effective.

Learning, according to Farrant (1982), is the process by which human beings acquire and retain attitudes, knowledge, understanding, skills and capabilities that cannot be attributed to inherited behaviour patterns or physical growth. There are times a student needs to be left alone, exposed neither to teaching by a teacher nor interaction with his peers, in order to think things out for himself. This is because learning itself, according to Head (1974), occurs at an individual level. One instructional strategy that provides learners with the opportunity to learn at such individual level is self-instructional strategy. The attendant problem that followed the astronomical increase of students in a classroom and which often leads to a reduction in the frequency with which any member of the class can interact with the teacher was a reduction in the learning opportunities of the learners. Self-instructional strategy was one of the strategies that evolved to combat and resolve this problem.

Self-instructional strategy is a learner-centered strategy, which involves individual students' use of instructional packages or learning packages (especially programmed instructional package, which consist of stimuli, provision for responses, feedback, and testing) with which the student can learn either without teacher's intervention or with a minimum of teacher's guidance. According to Jenkins and Keefe (2001), self-instruction focuses specifically on the needs, talents, learning style, interests, and academic background of each learner, and also challenges each learner to grow and advance. The basic premise is that with the learners being in control of instruction, it affords them the opportunity to have time to think things through, structure the task of learning and to decide on the meaningfulness of what is learned. The materials so programmed are presented in a well arranged and organized form (learning package) that lead the students from a body of known principles to the unknown, from simple to complex concepts within the same content area. Despite the heavy theoretical emphases in recent years on learner-centered types of instruction, self-learning is yet to be formally introduced into the Nigerian educational system as a useful instructional strategy for her primary and secondary classes.

Several studies have been undertaken to investigate the effectiveness of self-instructional strategy on students' academic achievement. The strategy has been extensively used in Europe, America, Asia and Nigeria, and in various school subjects and programmes.

Adesoji (1991) reported that problem-solving technique, as a self-learning text, was more effective in learning problem solving in chemistry than the lecture method. Ajiboye (1996) reported that the self-learning programme was found to be most effective in enhancing the cognitive achievement of subjects in the learning of selected concepts in population education. Similar finding was discovered by Ajelabi (1998) who reported that both computer-assisted and text-assisted programmed instructions were found to be superior and much more effective in terms of academic achievement of learner's in Social Studies. Popoola (2002) also found that the students exposed to programmed instructional strategy, with an adjusted post-test mean score of 17.5, performed significantly better in Mathematics than the students exposed to conventional teaching method who recorded a post-test mean score of 11.9. Some of the results of with no significant outcomes include the works of Smith (1966) and Watkins (1991). The present study, which made use of a self-learning

package, is a further attempt at investigating the inconclusiveness of effectiveness of individualized instruction particularly in Mathematics.

An important basic assumption about children learning Mathematics is that children learn both independently and through collaboration (Oyedeji, 1997). This implies that the learning environment during the teaching-learning process should accommodate students' active interaction with one another if they are expected to exhibit optimum achievement in Mathematics especially at the secondary school level. One learning strategy that readily affords learners such collaborative learning environment is the cooperative instructional strategy. This strategy is a complete departure from the self-learning strategy, which focuses mainly on each student learning independently. Cooperative learning refers to a set of instructional strategies in which students are encouraged to work together on academic tasks. Johnson and Johnson (1986), when distinguishing between the goals structures of individualistic, competitive and cooperative instructional strategies, explained that: in a cooperative learning environment, there is positive interdependence among students' goal attainments; students perceive that they can reach their learning goals if and only if other students in the learning group also reach their goals. The theory of cooperative learning is based upon the fact that when individuals work together towards a common goal, they are dependent on one another's effort to achieve that goal. Cooperative instructional strategy stresses academic achievement and clearly defined curricular goals. The teacher's focus is more on how to enhance student-student interaction towards achieving instructional goal. The social training that results from cooperative learning is one of its most valuable features. By working in groups, students learn how to deal with disagreement, how to accept others who hold different views, how to co-operate in order to achieve a bigger output, and how to work as a team. By working as a team, students learn the sense of belonging that comes from being a member of a group and they learn how to accept in a mature fashion the elation of success in competitive tasks and also the pains of defeat.

The effect of interaction patterns on students learning outcomes has been a major focus of many studies. While some reported that cooperative strategy resulted in better academic achievement than others (Alebiosu, 1998; Veenman, Benthum, Bootsma, Dieren & Kemp, 2002; Ojo, 2003; Oladunjoye, 2004) a few other studies (Jordan & Joanna, 1997; Joyce, 1999; Slavin & Hurley, 2000) reported that pure cooperative strategy alone do not. Ojo (2003) reported a statistically significant difference between the mean achievement scores in Mathematics of students exposed to cooperative learning strategy and those not exposed to the strategy. Slavin and Hurley (2000) on the other hand, argued that 'pure cooperative strategy' on its own could not improve learning outcomes of students except when used with some other effective learning strategies. These conflicting results have shown the need to further investigate the efficacy or otherwise of cooperative instructional strategy in the teaching and learning of Mathematics at the secondary school level. The present study utilized a cooperative learning package, using the "student team learning" cooperative strategy presented by Slavin (1994), to investigate the effectiveness of cooperative instructional strategy on students' cognitive achievement in secondary school Mathematics.

Literature is replete with evidence to show that some learners' personality variables could influence students' learning outcomes irrespective of the instructional strategy used. Such students' personality variables include sex (Ogwuazor, 1992; Ifamuyiwa, 2003), self-concept (Akinsola, 1994), locus of control and attribution style (Onabanjo, 2000; Popoola, 2002; Ojo, 2003), cognitive style (Igwe, 1991; Ajelabi, 1998), cognitive entry behaviour (Igwe, 1991; Ogunkola, 2000), and numerical ability (Udousoro, 2000; Adegoke, 2003).

Locus of control refers to individually perceived sources of control over certain behaviours and events (Ogunkola, 2000). The construct, 'locus of control', is an important personality dimension worthy of study as it is helpful in understanding a student's view of placement of responsibility for his or her academic successes or failures; whether a student's perception of the locus of events is determined internally by his/her own behaviour or by fate, luck, or external circumstances. Many studies classified students as either internals or externals. Igwe (1991) states that locus of control expectancy, which explains individual perception, is believed to vary along the internals-externals (I-E)

continuum. Internal locus of control is associated with the perception of events, whether positive or negative as being a consequence of one's own actions and thereby potentially under personal control. External locus of control, on the other hand, refers to the perception of positive or negative events as being unrelated to self-behaviour and accordingly beyond personal control. Reeves (1993) suggests that what underlies the internal locus of control is the concept of "self as agent". This means that a person's thoughts control his or her actions and that a realization of this executive function of thinking can positively affect one's beliefs, motivation, and academic performance. A link between locus of control and learning would seem logical given that school achievement requires a degree of effort and persistence in academic tasks and that such behaviours are unlikely to occur if the student sees little relationship between his efforts in learning and the outcomes.

Ogunkola (2000) reported that research efforts on locus of control in the last three decades have been conducted primarily with adults and school children, and most of the research efforts have focused on the relationship between locus of control and school achievement. Ogunkola (2000) found a significant main effect of locus of control on student's achievement in and attitude towards Biology and reported that successful senior secondary school one (SSS I) students tended to indicate more internal control perception than unsuccessful students. Popoola (2002) reported no significant main effect of locus of control on senior secondary school two (SSS II) students' achievement in and attitude towards Mathematics but found a significant interaction effect of treatment and locus of control on the students' attitude towards Mathematics.

Apart from the influence of locus of control, gender is one other learner characteristic that has been shown to exert considerable influence on students' learning outcomes. Gender differences in educational outcomes, including achievement in Mathematics are well known phenomena (Yoloye, 1994, Bolaji, 1996; Akinsola, 2001; Ifamuyiwa, 2003). There are various interests in the investigation of the role of gender in secondary school students' achievement, school engagement, and attitude to schoolwork and peers. Abundant evidence in literature shows that gender is a strong predictor of human conduct and that many differences have been documented between the attitudes, behaviours and achievement of boys and girls (Etukudo, 2002; Popoola, 2002; Ojo, 2003; Olowojaiye, 2004). Etukudo (2002) reported a significant gender difference between the performances of junior secondary school students in Mathematics in favour of the boys with a mean score of 65.3 as against 52.9 scored by the girls. The same study however, found no significant gender difference between the performance of boys and girls in the experimental group taught with the help of the computer. Ojo (2003) reported significant main effect of gender on students' attitude towards Mathematics but found that there was no significant difference between the post-test mean achievement scores of male and female students in Mathematics in the same study.

It is evident from the literature reviewed that research findings on self and cooperative instructional strategies still raise questions and doubts regarding their effectiveness and preference to the conventional method of teaching Mathematics at the secondary school level in varying cultural settings. In addition, the use of programmed textual materials by cooperating students working in groups in comparison with students working individually on the programmed text is not common among researchers in Nigeria. It is also obvious from the literature reviewed that researchers who have investigated the effects of locus of control and gender revealed diverse conflicting reports on the possible influence of locus of control and gender on the learning outcomes of secondary school students in Mathematics. Thus, the need to improve students' cognitive achievement in secondary school Mathematics and the fact that self and cooperative instructional strategies and some learner characteristics (locus of control and gender) could influence the learning outcomes of students informed this study whose problem is posed below.

Statement of the Problem

This study investigated the effects of self and cooperative instructional strategies on senior secondary school students' cognitive achievement in Mathematics. The study also investigated the moderating effects of locus of control and gender on the dependent measure.

Hypotheses

Ho 1: There is no significant main effect of treatment on students' achievement in Mathematics.
Ho 2: There is no significant main effect of locus of control on students' achievement in Mathematics.
Ho 3: There is no significant main effect of gender on students' achievement in Mathematics.
Ho 4: There is no significant interaction effect of treatment, locus of control and gender on students' achievement in Mathematics.

Research Method

Design

This study adopted a pre-test, post-test control group quasi-experimental design adopting a **3×2×2** factorial matrix. Learning strategies (conventional method, self and cooperative instructional strategies) were crossed with locus of control (internal and external) and gender (male and female).

Target Population

The target population for this study comprised all the second year students in public Senior Secondary Schools in Ijebu-North Local Government Area, Ogun State. Ijebu-North Local Government Area was considered for the study because it has a relatively large number of public secondary schools. Thirteen out of the nineteen public secondary schools in the Local Government Area are located in the urban areas while 6 are located in the rural areas. All the 19 schools are coeducational with at least one arm of SSS II class. The number of SSS II students in each of the schools ranged from 85 to 245. Senior secondary school two (SSS II) students were considered for the study because:

(i) The researchers believed that the students have attained some level of maturity and confidence needed for self and cooperative use of learning packages with little or no teacher assistance.
(ii) The students were not being prepared for any external examinations that could distract them from full participation in the study.
(iii) The Trigonometry aspect of Mathematics treated in the learning packages used as treatment is contained in the students' (SSS II) Mathematics curriculum.

Sampling Procedure and Sample

The following criteria, using the judgmental sampling technique, were used to select the schools that took part in the study.

(a) The school must be a public co-educational secondary school;
(b) The SSS II students in the school have not been taught the trigonometric topics treated in the package used as treatment;
(c) The school has/have graduate Mathematics teacher(s) teaching SSS II students; and
(d) The school had accessible records of the candidates presented for the Senior School Certificate Mathematics Examination in the last ten years.

From the eight secondary schools that met the criteria above, six were randomly selected to participate in the study. In each of the six chosen secondary schools, one intact class (an arm of SSS II) was randomly picked and assigned to the experimental and control groups. Thus, a sample of three hundred and fifty (350) SSS II students (183 males, 167 females; 140 internals and 210 externals) participated in the study.

Instruments: Three research instruments were used in this study. These are:

(i) Mathematics Achievement Test (MAT)
(ii) Locus of Control Scale (LOCS)
(iii) Teacher's Instructional Guide (TIG)

Mathematics Achievement Test (MAT)

The MAT is a 30-item multiple-choice Mathematics achievement test with four options per item. The MAT was constructed and validated by the researchers to measure students' academic achievement in Mathematics. The topics covered by the MAT were taken from the scheme of work for SSS II classes in Ogun State and were the topics treated in the learning packages used as treatments in the study. An initial pool of sixty multiple-choice objective-test items was developed from a table of specification drawn to reflect knowledge, understanding and thinking levels of cognitive domain in line with the suggestion of (Yoloye, 1982), and five content areas from which the lessons and objectives specified in the packages used for the study were drawn. The items were reduced to thirty after the item analysis procedure. The thirty items that survived the item analysis stage constitute the Mathematics Achievement Test. The 30-item MAT was administered on a sample of 150 SSS II students (80 males and 70 females) in two schools that were not part of the study, but whose students are similar in age and class to the students involved in the study. From the students' responses, a reliability coefficient of 0.88, using the Kuder-Richardson Formula 21 was obtained. The average item difficulty score was 54.

Locus of Control Scale (LOCS)

This study adapted Igwe's (1991) locus of control personality scale to measure the extent to which an individual possesses internal or external reinforcement beliefs. The original scale having twenty-nine pairs of statements including six filler statements was reduced to twenty-six pairs with three filler statements. Three pairs of statements that are not appropriate for SSS II students were removed from the original scale. Filler statements are those, which did not reveal any locus of control pattern or dimensions. The pairs of statements are organized in such a way that internal statements are arranged as option **'a'** while external statements are arranged as option **'b'**. Students are expected to endorse one of the two statements making a pair. The modified LOCS was administered to a sample of 150 SSS II students (80 males and 70 females) in two schools that were not part of the study, but whose students are similar in age and class to the students involved in the study in order to re-establish the reliability of the scale. A Cronbach alpha was used for reliability determination and it yielded reliability index of 0.86.

Teacher's Instructional Guide (TIG)

The TIG is an operational guide that was used by the trained teachers in the experimental and control groups to ensure uniformity. The TIG consists of the activities, behaviours and specific instructions guiding the teachers. The TIG was used in training the six SSS II Mathematics teachers that participated in the study (before the commencement of treatment). This was done to ensure that the participating teachers master how to use the three instructional guides adequately and consistently. It also helped to minimize the teachers' biases during the treatment period. Experts, comprising three experienced SSS II Mathematics teachers, adjudged the TIG adequate and useful in creating the type of environments needed in the experimental and control groups.

Learning Packages: Two learning packages developed and validated by the researchers were used as treatment in the experimental groups.

A Self-Instructional Package (SELP)

This is a branching model text-assisted programmed instruction which covered five broad topics in Trigonometry aspect of SSS II Mathematics. It was the treatment used by the first experimental group (Self-instructional strategy, T_1). It contained 25 lessons covering five weeks of five periods per week as contained in the scheme of work for SSS II classes in Mathematics. Students can use the SELP with little or no teacher intervention, because it provides opportunity for immediate feedback. Each learner works on the SELP at his/her own pace without any pressure from either the teacher or his/her classmates. The SELP was trial-tested on a group of 80 SSS II students (42 boys and 38 girls) having characteristics similar to the intended students for the main study. The feedback obtained from the learners, as it concerned the length and timing of the lessons, the simplicity or otherwise of the examples and solutions provided as well as the workability of the package for the study, was used to further modify the SELP in order to make it suitable for the main study.

Instructional Package for the Co-operative Group (LPCG)

The LPCG is similar to the Self-Instructional Package (SELP) in content and model. It was the treatment used by the second experimental group (Cooperative-instructional strategy, T_2). The LPCG is different from the SELP in the format of its course content (the stimulus) and its test-yourself exercises (i.e. the response/feed back). In the LPCG, the stimulus part were prepared together, week by week, to be led by each group leader, while the response part was produced separately. Each student received the response part in all the groups after each lesson in other to solve the relevant exercises individually first, before group discussions and solutions, in line with the instructions in the package. This is also done to ensure that the 'student team learning' cooperative model chosen for the study is properly utilized during the treatment and data collection period. The LPCG was also trial-tested on a different group of 84 SSS II students (comprising of 44 boys and 40 girls distributed into 21 groups of 4 students per group) having characteristics similar to that of the intended subjects for the main study. This was done in order to find out its suitability for the main study. The feedback obtained from the learners, as it concerned problems encountered and the workability of the package for group study, was used to further modify the package.

Data Collection Procedure

The research procedure was divided into three phases:

(a) pre-treatment phase
(b) treatment phase
(c) post-treatment phase.

(a). Pre-Treatment Phase

The actual pre-treatment phase was done in the following steps:

The researcher, as the resource person, trained the six participating teachers and two research assistants for two weeks. With the TIG, the participating teachers were trained on the use of the learning packages (SELP and LPCG), how to create the right type of environment for the experimental and control groups and how to administer the other instruments (MAT and LOCS). The participating teachers used the third week for trial testing. This was done to ensure that the teachers master the right treatment for the experimental and control groups and apply the same during the treatment period. The two research assistants were asked to rate the participating teachers during the trial testing. The exercise produced inter-rater reliability values of between 0.77 and 0.81 range.

(b). Treatment Phase

The fourth week was used for pre-test. The researchers, with the help of the research assistants and the trained teachers administered the pre-test on the participating students in the following order: Locus of Control Scale (LOCS) before the Mathematics Achievement Test (MAT). The treatment period took five weeks in each of the six schools. This involved the use of the SELP for students in the experimental group 1, the use of the LPCG for those in the experimental group 2 and the use of the conventional method of teaching for the students in the control group. No interaction was allowed between the students in the treatment and control groups, whose schools were located in different areas, during the treatment period.

(c). Post-Treatment Phase

The tenth week was used for post-test which comprised the administration of the Mathematics Achievement Test (MAT) in both the experimental and control groups.

Data Analysis

The hypotheses raised in the study were tested using the Analysis of Covariance (ANCOVA) statistic. The Multiple Classification Analysis (MCA) was used to explain the magnitude of the post test achievement scores of the different categories of students while Scheffe post-hoc analysis was used to explain the direction of possible significant effects.

Results and Discussion

The sequence of the presentation and discussion of the results obtained in this study is in accordance with the hypotheses formulated for the study.

Hypothesis 1: There is no significant main effect of treatment on students' cognitive achievement in Mathematics.

Table 1: Summary of Analysis of Covariance of Students' Achievement According to Treatment, Locus of Control and Gender

Source of Variation	Sum of Squares	df	Mean Squares	F	Significance of F
1.Covariates (Pre-test)	**1135.002**	**1**	**1135.002**	**174.451**	**.000**
Main Effects	301.235	4	75.309	11.575	.000
Treatment	295.139	2	147.570	22.682	.000*
Locus of Control (LOC)	1.238	1	1.238	.190	.658
Gender	.143	1	.143	.022	.882
2 Way Interactions	**48.651**	**5**	**9.730**	**1.496**	**.191**
Treatment X LOC	21.029	2	10.515	1.616	.200
Treatment X Gender	33.165	2	16.583	2.549	.080
LOC X Gender	0.004	1	.004	.001	.980
3 Way Interactions	**36.400**	**2**	**18.200**	**2.797**	**.062**
Treatment X LOC X Gender	36.400	2	18.200	2.797	.062
Explained	1521.288	12	126.774	19.485	.000
Residual	2192.566	337	6.506		
Total	**3713.854**	**349**	**10.641**		

* Denote significance at $P < 0.05$

Table 1 revealed the result of the main effect of treatment on students' achievement in Mathematics. It showed significant main effect of treatment on students' achievement in Mathematics ($F_{(2, 337)} = 22.68$, $P < 0.05$). The result implied that the achievement scores of the students exposed to

the different treatment conditions are significantly different. Therefore, the null hypothesis 1 is rejected.

In order to determine the magnitude of the mean achievement scores of students exposed to the different treatment conditions, the result of the Multiple Classification Analysis (MCA) presented in table 2 was used.

The results in table 2 revealed that, with a grand mean of 10.289, the students exposed to the cooperative learning package (use of cooperative instructional strategy) had the highest adjusted post-test mean achievement score of 11.139 (10.289 + 0.85).

Table 2: Multiple Classification Analysis of Students' Achievement According to Treatment, Locus of Control and Gender

Grand Mean = 10.289					
Variable + Category Instructional Strategy	**N**	**Unadjusted Deviation**	**Eta**	**Adjusted for Independent + Covariates**	**Beta**
1. Self [T_1]	100	-.36		.35	
2. Cooperative [T_2]	140	.65		.85	
3. Conventional [T_3]	110	-.50	.45	-1.40	.60
Locus of control					
1. Internal	140	.13		.07	
2. External	210	-.08	.03	-.05	.02
Gender					
1. Male	183	-.27		.02	
2. Female	167	.25	.08	-.02	.01
Multiple R squared					**.387**
Multiple R					**.622**

The students exposed to the self-learning package (use of self-learning strategy) had the next higher adjusted post-test mean achievement score of 10.639 (10.289 + 0.35) while the students in the control group (use of conventional teaching method) obtained the least post-test mean achievement score of 8.889 (10.289 - 1.40). This result showed that the cooperative instructional strategy had the greatest potency at effecting student's achievement in Mathematics. The result in table 2 further revealed that treatment alone accounted for 36% $(0.60)^2$ of the variance observed in the students' achievement scores in Mathematics. In order to trace the source of the significant difference recorded in table 2 the Scheffe post-hoc analysis presented below was carried out.

Table 3: Scheffe Multiple Range Test of Achievement on Treatment Groups

Mean	**Group**	**Self-Instructional Strategy**	**Cooperative Strategy**	**Conventional Teaching Method**
9.930	**Self-Instructional Strategy**			
10.936	**Cooperative Strategy**			*
9.791	**Conventional Teaching Method**		*	

* Denote pairs of groups, which are significantly different at $P < 0.05$

The result in table 3 showed that the source of the observed significant difference was due to the difference between experimental group 2 (cooperative instructional strategy) and control group (conventional teaching method). This implied that the post-test mean achievement scores of students exposed to the use of cooperative instructional strategy differ significantly from the post-test mean achievement scores of students exposed to the conventional method.

The results presented above showed that learning packages through the use of self and cooperative instructional strategies have the potentials to improve students' cognitive achievement in secondary school Mathematics than the conventional method of teaching. This finding provides

empirical support to earlier findings that established that programmed instruction improves students' achievement in Mathematics (Popoola, 2002; Ojo, 2003). The finding that treatment had significant effect on students' achievement in Mathematics is explicable considering the views of Akimoyewa (1983) that learner centred instructional strategies (such as self and cooperative instructional strategies) are capable of effecting remarkable impact on instructional practices in Nigerian educational system. Cooperative instructional strategy was found to be more effective in facilitating achievement in Mathematics in this study because the strategy provided learners with adequate time and opportunity to discuss and work together, share views and opinions, and iron out problem areas with one another. This finding further gives empirical support to earlier findings on the usefulness of cooperative instructional strategy over and above other instructional strategies (Ojo, 1992; Esan, 1999; Adeyemi, 2002).

Hypothesis 2: There is no significant main effect of locus of control on students' cognitive achievement in Mathematics.

The result of the main effect of locus of control in table 1 revealed no significant main effect of locus of control on students' achievement in Mathematics ($F_{(1, 337)} = 0.19$, $P > 0.05$). This result shows that the post-test mean achievement scores of internal and external students in Mathematics are not significantly different. Therefore, the null hypothesis 2 is not rejected. However, the result of the MCA in table 2, showed that the internal students recorded a better adjusted post-test mean achievement score of 10.359 than the externals who had an adjusted post-test mean achievement score of 10.239. The result in table 2 further revealed that locus of control alone accounted for just .04% $(0.02)^2$ [less than 1%] of the variance observed in the students' achievement scores in Mathematics.

The finding that the main effect of locus of control on the students' achievement in Mathematics was not significant as indicated by the results in table 1 is at variance with the findings of Igwe (1991) and Ogunkola (2000) who both reported that achievement creates positive locus of control (internals) and probably not the reverse. The outcome however, confirmed the findings of Onabanjo (2000) and Popoola (2002) who reported that the effect of locus of control on students' achievement in Mathematics was not significant. The insignificant main effect of locus of control on students' achievement in Mathematics in this study is attributable to higher negative locus of control effect. This means that the achievement scores of the two hundred and twenty externals (students with negative locus of control) who participated in this study cancels out the possible positive effect of the one hundred and forty internals (those with positive locus of control) that took part in the study. Perhaps the situation would not have been the same if equal numbers of internal and external students have participated in the study.

Hypothesis 3: There is no significant main effect of gender on students' cognitive achievement in Mathematics.

The result of the main effect of gender in table 1 revealed no significant main effect of gender on students' achievement in Mathematics ($F_{(1, 337)} = 0.022$, $P > 0.05$). This implied that the post-test mean achievement scores of male and female students in Mathematics are not significantly different. Therefore, the null hypothesis 3 is not rejected. Table 2 however revealed that the adjusted post-test mean achievement score (10.309) of the male students was higher than that of the females whose adjusted post-test mean achievement score was (10.269). The result in table 2 further revealed that gender alone accounted for just .01% $(0.01)^2$ [less than 1%] of the variance observed in the students' achievement scores in Mathematics.

The non-significant main effect of gender on students' achievement in Mathematics obtained in this study and presented in table 1 conforms with some previous studies (Sullivan, 1995; Popoola 2002) but at variance with some others (Yoloye, 1994; Odogwu, 2002; Ojo, 2003). This finding, though at variance with the belief that gender stereotyping is still very much in the Nigerian educational system and could be hindering the education of girls in Science, Technology and Mathematics courses, is actually in support of the view that the gender differences being observed in students' achievement in secondary school Mathematics are not statistically significant. As a result,

one could conveniently say that gender difference in students' learning outcomes in secondary school Mathematics is diminishing at a speedy rate. This finding tends to suggest that the efforts of Mathematics educators towards eliminating gender differences in students' learning outcomes in Mathematics are perhaps yielding the desired result.

Hypothesis 4: There is no significant interaction effect of treatment, locus of control and gender on students' cognitive achievement in Mathematics.

The result of the 3-way interaction effects in table 1 revealed no significant interaction effect of treatment, locus of control and gender on students' achievement in Mathematics ($F_{(2, 337)} = 2.797$, $P > 0.05$). This result means that there is no significant difference in students' group achievement (based on treatment) among the entire possible locus of control–gender combinations: internal–boys; internal–girls; external–boys; and external–girls. Hence, the null hypothesis 4 is not rejected. Taking the independent and moderator variables (i.e. treatment, locus of control and gender) together, the results of the MCA in table 2 revealed that the variables jointly accounted for 38.7% of the variation in students' achievement in secondary school Mathematics

This non-significant 3-way interaction effect is explicable considering the finding that only treatment was found to produce significant effect on the achievement of the students that participated in this study. This outcome confirms the views of Ogunkola (2000) that the performance of students with different locus of control patterns and of different gender tends to be consistent under any instructional strategy.

Conclusion and Recommendation

Specifically, this study investigated the effects of two instructional strategies (self and cooperative) on students' achievement in secondary school Mathematics. The study is an extension of the frontiers of knowledge in the use of learning packages that emphasized the active participation and intellectual involvement of learners. The results of the study revealed that self and cooperative instructional strategies through the use of learning packages are effective strategies for learning Mathematics. The cooperative instructional strategy was found to be more effective in promoting student achievement in Mathematics than the self-instructional strategy. The study is thus recommending the use of self and cooperative instructional strategies involving the use of learning packages for learning secondary school Mathematics. It is further recommended that Mathematics teachers should explore the use of cooperative instructional strategy for Mathematics teaching at the secondary school level since it has the potential of enhancing students' achievement in Mathematics. Moreover, appropriate courses need be introduced into teacher education programmes for the training teachers in the skills of designing and developing useful learning packages for Mathematics instructions.

References

[1] Adegoke, A. B. (2003). Teacher Influence as a Determinant of Dependent-Prone Students' Learning Outcomes in S.S.S. Geometry in Ibadan, Nigeria. *Unpublished Ph.D. Thesis,* University of Ibadan.

[2] Adesoji, F. A. (1991). A Comparative Analysis of Problem Solving and Self-Learning Techniques in Teaching Electrolysis. *Unpublished Ph.D. Thesis,* Obafemi Awolowo University, Ile-Ife.

[3] Adetunji, F. O. (2000). A Study of Some Nigerian Primary School Teachers' Attitude to Mathematics. *African Journal of Educational Research*, 6 (1 & 2), 93-99.

[4] Adeyemi, S. B. (2002). Relative Effects of Cooperative and Individualistic Learning Strategies on Students' Declarative and Procedural Knowledge in Map work in Osun State, Nigeria. *Unpublished Ph.D. Thesis,* University of Ibadan.

[5] Ajelabi, P. A. (1998). The Relative Effectiveness of Computer Assisted and Text Assisted Programmed Instruction on Students' Learning Outcomes in Social Studies. *Unpublished Ph.D. Thesis,* University of Ibadan.

[6] Ajiboye, J. O. (1996). A Self-Learning Programme, the Modified Lecture Method and Students' Cognitive and Affective Outcomes in Some Population Education Concepts. *Unpublished Ph.D. Thesis,* University of Ibadan.

[7] Akinmoyewa, J. O. (1983). *"Self-Instruction: An Effective Instructional Mode."* Seminar paper, School of Education, OYSCE, Ilesa, page 2.

[8] Akinsola, M. K. (1994). Comparative Effects of Mastery Learning and Enhanced Mastery Learning Strategies on Students' Achievement and Self-concept in Mathematics. *Unpublished Ph.D. Thesis,* University of Ibadan.

[9] Akinsola, M. K. (1994). Effects of using Mother Tongue on Students Achievement and Attitude in Mathematics. *Nigerian Journal of Development Issues: Education, Socio-Political and Economic Development,* 1 & 2, 96 – 106.

[10] Akinsola, M. K. (1999). Factors Inhibiting the Learning of Mathematics. In Obemeata, J. O., Ayodele, S. O., Araromi, M. A. (Eds.) *Evaluation in Africa in Honour of E. A. Yoloye.* Ibadan: Stirling-Horden Publishers (Nig.) Ltd. 192-211.

[11] Akinsola, M. K. & Igwe, I. O. (2004). The Relative Effects of Meta-cognitive Strategy of Framing on Students' Achievement in Selected Difficult Chemistry Concepts. *Journal of the Science Teachers Association of Nigeria,* 37 (1 & 2), 20 – 28.

[12] Akinsola, O. S. (2001). The Extent of Dominant Factors of Girls and Women's Low Participation in Mathematics Education: Mathematics Educators' Views. *Proceedings of the 42nd Annual conference of the Science Teachers Association of Nigeria,* Mathematics Panel. 295 – 298.

[13] Alebiosu, K. A. (1998). Effects of Two Co-operative Learning Models on Secondary School Students' Learning Outcomes in Chemistry. *Unpublished Ph.D. Thesis*, University of Ibadan.

[14] Bolaji, C. (1996). Gender Difference and the use of Two Approaches in the Teaching of Algebra. *Kano Journal of Education*, 3 (1), 24 – 35.

[15] DeCorte, E. (1992). On the Learning and Teaching of Problem Solving Skills in Mathematics and Logo Programming. *Applied Psychology,* 41, 317 – 331.

[16] Ekwere, O. J. (1998). Meta-cognitive Instructional Strategies and Students' Concept Attainment in, and Attitudes towards Chemistry in Ibadan Municipality. *Unpublished Ph.D. Thesis,* University of Ibadan.

[17] Esan, A. O. (1999). Effects of Cooperative and Individualistic Problem-Solving Strategies on Students' Learning Outcomes in Secondary School Mathematics. *Unpublished Ph.D. Thesis,* University of Ibadan.

[18] Etukudo, U. E. (2002). The Effect of Computer Assisted Instruction on Gender and Performance of Junior Secondary School Students in Mathematics. *ABACUS. The Journal of the Mathematics Association of Nigeria,* 27 (1), 1 – 8.

[19] Federal Republic of Nigeria (2004). *National Policy on Education (4th Edition),* Lagos: N.E.R.D.C. Press.
[20] Farrant, J. S. (1982). *Principles and Practice of Education*. England: Longman group limited.
[21] Head, J. O. (1974). Methods and Techniques of Teaching. In Sutton, C. R. & Haysam, J. T. (Eds.) *The Art of the Science Teacher.* London: McGraw Hill Company.
[22] Ifamuyiwa, A. S. (2003). Girls' Participation and Performance in Senior Secondary Further Mathematics in Ijebu-Ode, Ogun State, Nigeria. In Baiyelo, T. D. & Busari, O. O. (Eds.) *Standards for Science, Technology & Mathematics Educational Research (A book of readings)*. Lagos: Victory Printers Nig. Ltd., 97-109.
[23] Igwe, G. O. (1991). Impact of Behavioural Objectives, Cognitive Entry Behaviour and Locus of Control Paradigm on Students' Learning Outcomes. *Unpublished Ph.D. Thesis,* University of Ibadan.
[24] Jenkins, J. M. & Keefe, J. W. (2001). Strategies for Personalizing Instruction: A typology for Improving Teaching and Learning. *NASSP Bulletin,* 85, 69. Retrieved April, 2004, from (*http://www.principals.org.html*).
[25] Johnson, D. W. & Johnson, R. T. (1986). Computer Assisted Cooperative Learning. *Educational Technology*, XXVI (1), 12 - 18.
[26] Jordan, D. W. & Joanna, L. M. (1997). Social Skiling through Co-operative Learning. *Educational Research*, 39 (1), 3 – 21.
[27] Joyce, B. W. (1999). On the Free Rider Problem in Cooperative Learning. *Journal of Education Business,* 45 (5), 271 – 274.
[28] Odogwu, H. N. (2002a). The Effect of Computer Assisted Instruction on Students' Performance in Mathematics. *Proceedings of September 2002 Annual National Conference of Mathematical Association of Nigeria (M.A.N),* 1 – 9.
[29] Odogwu, H. N. (2002b). Female Students' Perception and Attitude to Mathematics: A Bane to their S.M.T Education. *ABACUS. The Journal of the Mathematics Association of Nigeria,* 27 (1), 19 – 29.
[30] Ogundipe, B. D. (2004). Effect of Peer tutoring-assisted Instruction, Class Size, and Test Anxiety on Senior Secondary School Students' Achievement in Physics. *Unpublished Ph.D. Thesis,* University of Ibadan.
[31] Ogunkola, B. J. (2000). Instructor Expressiveness, Student Locus of Control and Cognitive Entry Behaviour as Measures of Students' Achievement in and Attitude towards Biology. *Unpublished Ph.D. Thesis*, University of Ibadan.
[32] Ogwuazor, K. E. (1992). Nigerian Women and Science Education: The situation so far. *Lagos Journal of Science Education*, 1 (1), 76 – 82.
[33] Ojo, M. O. (1992). The Differential Effectiveness of Cooperative, Competitive and Individualistic Classroom Interaction Patterns on Students' Chemical Problem Solving Skills. *The Nigerian Teacher Today,* 1 (2), 121 – 129.
[34] Ojo, O. J. (2003). Relative Effects of Self-regulatory and Cooperative Learning Strategies on Learning Outcomes in Senior Secondary School Mathematics, Ibadan-North, Nigeria. *Unpublished Ph.D. Thesis,* University of Ibadan.
[35] Oladunjoye, O. (2004). Effects of Two Collaborative Learning Strategies on Students' Performance in and Attitude to Verbal Communication in the English Language in Ogun State, Nigeria. *Unpublished Ph.D. Thesis,* University of Ibadan.
[36] Olowojaiye, F. B. (2004). Effects of Behavioural Objective-based and Study Question-based Instructional Strategies on Students' Learning Outcomes in Senior Secondary Mathematics in Lagos State. *Unpublished Ph.D. Thesis,* University of Ibadan.
[37] Onabanjo, I. O. (2000). Peer-tutoring-assisted Instruction, Parent Supportiveness and Students Locus of Control as Determinants of Learning Outcomes in S.S.S. Mathematics. *Unpublished Ph.D. Thesis*, University of Ibadan.

[38] Oyedeji, O. A. (1997). The Effect of the use of Project Method on Students' Affective Learning Outcome in Secondary Mathematics. *Studies in Curriculum*, 1, 25 – 31.

[39] Popoola, A. A. (2002). Effects of Heuristic Problem-solving and Programmed Instructional Strategies on Senior Secondary School Student Learning Outcomes in Mathematics in Ekiti State, Nigeria. *Unpublished Ph.D. Thesis,* University of Ibadan.

[40] Reeves, T. C. (1993). Pseudoscience in Computer-based Instruction: The Case of Learner Control Research. *Journal of Computer-Based Instruction*, 20 (2), 39 – 46.

[41] Slavin, R. E. (1994). Students Motivating Students to Excel: Incentives, Cooperative Tasks and Students' Achievements. *The Elementary School Journal,* 85, 53 – 62.

[42] Slavin, R. E. & Hurley, E. A. (2000). *Cooperative Learning and Achievement; Research, and Future Directions*. Paper presented at the office of Educational Research and Improvement, U. S. Department of Education.

[43] Smith, N. (1966). Conventional Method and Programmed Instruction in Teaching History. *Journal of Educational Research,* 55, 417 – 420.

[44] Sullivan, M. M. (1995). Analysis of Conceptual Understanding in Undergraduate Descriptive Statistics across Learning Style and Gender after Student-centred and Activity Oriented Instruction. *Dissertation Abstract International.* 39, 1697A.

[45] Udousoro, U. J. (2000). The Relative Effects of Computer and Text-assisted Programmed Instruction on Students' Learning Outcomes in Mathematics. *Unpublished Ph.D. Thesis,* University of Ibadan.

[46] Veenman, S., Benthum, N. V., Bootsma, D., Dieren, J. V. & Kemp, N. V. (2002). Cooperative Learning and Teacher Education. *Teaching and Teacher Education*, 18 (1), 87–103.

[47] Watkins, B. T. (1991). Using Computers to Teach Basic Skills. *Chronicle of higher Education,* 38 (6), 23 – 26.

[48] West African Examination Council (1997; 2000-2005). *Chief Examiners' Reports*. Yaba, Lagos: Amao press Limited.

[49] Yoloye, E. A. (1982). Science Education in the Nigerian primary schools: A need for radical approach. *Keynote address at the 23rd Annual Conference of STAN, Akure,* 11 – 17.

[50] Yoloye, T. W. (1994). Attitude of Some Female Nigerian Secondary School Students towards Science and Technology. *Journal of Studies in Education,* 1 (1), 73-79.

European Journal of Scientific Research
ISSN 1450-216X Vol.18 No.3 (2007), pp.417-426

http://www.eurojournals.com/ejsr.htm

Complexation of Vanadium (IV) with Some Hydroxamic Acids

Nwabueze J.N
Department of Chemistry, University of Abuja
PMB 117, FCT, Nigeria

Aliyu A.O
Department of Chemistry, Nigerian Defence Academy
PMB 2109, Kaduna

Abstract

Hydroxamic acids, RCONHOH, form highly stable complexes with vanadium (IV) in 1:2 molar ratio in aqueous solution at equilibrium. Cyclohexylacetohydroxamic acid (CHAH), Nicotinohydroxamic acid (NHA) and Isonicotinohydroxamic acids (INHA) were selected for the study. A spectroscopic investigation of reaction of some hydroxamic acids with Vanadium (IV) shows that their pKa's are 9.86 ± 0.03, 8.68 ± 0.02 and 8.68 ± 0.05 respectively. Spectra and magnetic studies of the isolated complexes indicates five coordinate square pyramidal coordination via (N) bonding mode for VO^{IV}-CHAH and oxygen atom of the hydroxamate group for VO^{IV} in isonicotin and nicotinohydroxamates. Microbial sensitivity test shows no activity.

Keywords: Oxovanadium (IV), spectroscopic, square pyramidal, cyclohexylacetohydroxamic acid, (CHAH) isonicotinohydroxamic acid (INHA) and nicotinohydroxamic acid (NHA), Isosbestic point.

Introduction

Hydroxamic acids are a family of organic acids of general formular RCONHOH and are much weaker acids than the structurally related carboxylic acids. RCOOH Monohydroxamic acids form typical octahedral complexes with transition metals via coordination through the oxygen atoms with formation of reasonably ionic metal oxygen bonds[2] accompanying the complexation. Simple hydroxamate analogue (acetohydroxamic, benzohydroxamic and salicylhydroxamic acids) Fig (1) on the other hand can undergo two deprotonation processes and act as either hydroxamato^{-} or hydroxamato^{2-} ligand, which behave as monodentate as well as bidentate ligands[3]. Among numerous siderophore structures, the hydroxamates are of interest due to their ability to form stable transition metal complexes through the formation of a five membered chelate ring as shown in scheme 1[4].

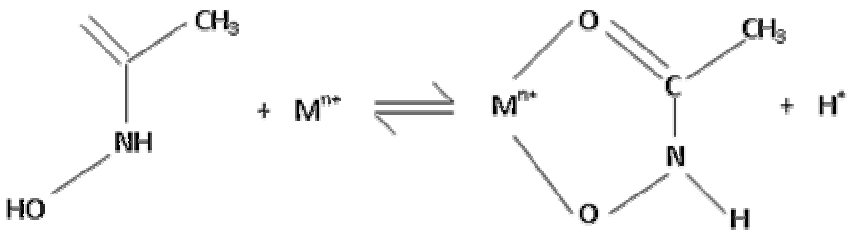

Catechols and N-hydroxylated (such as L-Glutathione) ligands which can be considered as biological sequestering agents for a large class of metal ions, are particularly effective in stabilizing high oxidation state for elements such as vanadium and molybdenum[5]. These ligands can utilize the capability of free vanadium ions to activate glucose uptake and glucose metabolism in rats adipocytes in vitro by 4-5 folds and to lower blood glucose levels in hyperglycemic rats in vivo by 5-7 folds[(6)].

They form an intense ultra violet – absorbing complexes upon associating with vanadium (IV) at 1 to 3 mole ratio i.e.vanadium (IV): ligand [(7)].

In both +5 and +4 oxidation states, vanadium can form complexes of fairly high stability with ligands being able to displace partly or fully, oxygen from the stable VO^{2+} and VO_2^+ oxocations[5]. In highly acidic media, reversible oxygen displacement occurs from the metal ion to yield monoxo V(IV) or V(V) complexes, which exhibits distinct EPR and ^{51}V NMR spectra features, respectively. In these species, the bare vanadium ions are coordinated to the three hydroxamic functions of the ligands. With increasing pH, oxocoordination is restored and normal VO(IV) and VO_2(V) complexes formed with metal bonding to one or two hydroxamic functions of the ligands[7]. Hydroxamic acids have been used as therapeutic agents in chelation therapy and as metalloenzyme inhibitors[8]. Other medical applications of the hydroxamates which utilize their affinity for high charge density metal ion, include the possible use of their metal complexes as imaging agents[9].

VO^{2+} complexes have extensive clinical applications. A new turning point appeared in 1985, when a scientist claimed that oral administration of vanadate to type-1 diabetic rats lowered the high levels of blood glucose to normal values. Unlike insulin, which is not absorbed orally, vanadate as a low-molecular weight substance and a phosphate analog can permeate plasma membranes and intestinal wall with relative ease[10].

N bonding was first observed by Brown et al in 1982 in nickel (II) complexes with glycine hydroxamic acid and since then only a few examples have been cited[11]. However, complexation of vanadium (IV) with some hydroxamic acids have not as yet been studied.

This paper is therefore a report on the work carried out on the complexation of vanadium (IV) with some hydroxamic acids namely cyclohexylacetohydroxamic acid (CHAH), nicotinohydroxamic acid (NHA) and isonicotinohydroxamic acid (INHA) ligands with special emphasis on the structure and nature of bonding involved in each case. In addition, some physico-chemical properties of the isolated complexes were investigated and included in this report.

Experimental

Ethylcyclohexylacetate, ethylisonicotinate and ethylnicotinate were obtained from Aldrich. All other reagents used were Analar.R. grade. $NaNO_3$ was used for the preparation of the background electrolyte and stock solutions. Water was doubly distilled, degassed using purified N_2 and stored in glass stoppered flasks. KOH and HNO_3 used for adjusting pH were stored in glass ampoules and were standardized with potassium hydrogen phthalate and tris (hydroxymethyl) methyl amine respectively. The pH measurements were made using a Radiometer Copenhagen Research pH meter calibrated with standard buffer tablets (2, 4 and 9). Electronic spectra were recorded on ATI Maltson Genesis Series FTIR^{TM} machine as Nujol mull in the 4000-200cm^{-1} spectra region. Room temperature magnetic susceptibility measurements were made on MSB Auto magnetic susceptibility balance. All these analyses were done at National Research Institute for Chemical Technology (NARICT) Zaria and University of Abuja, Nigeria.

Preparation of the Ligands[12]

Cyclohexylacetohydroxamic acid was prepared as described in the literature[13], Nicotinohydroxamic and isonicotinohydroxamic acids were prepared as follows:

Na metal (2.3g, 0.1 mol) in MeOH (50cm^3) was added to $NH_2OH.HCl$ (6.9g, 0.1mol) in MeOH (100cm^3). The mixture was cooled to room temperature and ethyl nicotinate (15.12g, 0.1 mol) was added. The mixture was stirred for 40 minutes and a further solution of Na (2.3g, 0.1 mol) in MeOH was added and stirring continued for another 10 minutes. The mixture was filtered to remove the precipated NaCl and the filterate acidified with concentrated HCl and the precipitated NaCl was removed by filteration. The filterate was concentrated using a rotary evaporator (without heating) and left overnight in the open laboratory and then kept in a refrigerator to crystallize. The crystals were removed by filtration and recrystalized from EtOH, yield 55%. Similarly, isonicotinohydroxamic acid was prepared by using (15.12g, 0.1mol) of Ethyl isonicotinate (2.3g, 0.1mol) Na and (6.9g, 0.1mol) $NH_2OH.HCl$ in 50cm^3 and 100cm^3 respectively.

Preparation of the Complexes

$VO(CHAH)_2.2H_2O$ was prepared as follows:

$VOSO_4.H_2O$(0.326g,0.002mol) in cold water was added with stirring to CHAH (0.629g, 0.004mol) in EtOH (20cm^3). The mixture was allowed to precipitate out as black crystals. The precipitate was washed, dried over silica gel in a vacuum dessicator. Yield 58% $VO(NHA)_2.2H_2O$ and $VO(INHA)_2.2H_2O$ were similarly prepared using (o.556g, 0.004 mo 1) of NHA and INHA respectively.

Equilibrium Studies

The pKa values for the ligands were determined spectrophotometrically by the method of Albert and Sergent[13] using sodium bicarbonate with ionic strength of 0.02 mol dm^{-3} and sodium bicarbonate of ionic strength 0.01mol dm^{-3} buffers for CHAH. Boric acid and borax of ionic strength 0.1 mol dm^{-3} and 0.025 mol dm^{-3} buffers for NHA and INHA ligands. In each case, the ligand stock solution was 5 x 10^{-4}M diluted five folds in buffer solution for CHAH, measurements were made in seven sodium bicarbonate/sodium carbonate buffer solutions at the analytical wavelength of 220nm while eight boric/borax buffer solutions were used for NHA and INHA at analytical wavelengths of 215nm and 200nm respectively. The number of complexes present in solution at equilibrium was determined by the isosbestic point method and graphical Matrix rank analysis using nine solutions containing 1:1 – 1:5 metal; ligand ratio (ligand concentration increasing in units of 0.5). A solution of I=0.1 moldm^{-3} made up of 0.01Moldm^{-3} HNO_3 and 0.09 Moldm^{-3} $NaNO_3$ was used to prepare equimolar stock solution of VO^{2+} and the ligands 2.5 x 10^{-3} Moldm^{-3}; the same solution was used for all dilutions. In all cases, the solutions were thermostated at 25^{o}C 2h in an ultrasonic bath.

Evaluation of the Antimicrobial Activity

The antimicrobial activity of the test compounds was assayed against eight bacateria; *S.aureus, E-coli, Salmonella-typhy Klebsiella, Streptococcus, Pseudomonias, corrynebacterium* and *Neisseria*. Among these organisms, four of them are gram-positive i.e. *S-aureus, Salmonellatyphy*, Streptococus and Corynebacteria, while others are gram-negative. All are regarded as pathogenic to humans and animals. All media and bacterial suspensions were prepared using a method adapted from that of Cruickshank[15].

About 15-20cm^3 of molten nutrient agar was poured into sterile petri plates about 10cm in diameter. After solidification of the agar, three cups (10mm in diameter and 5mm deep) were removed from each agar dish and fresh bacterial suspension was then uniformly spread on each cup. At this point, each of the cups was spotted three times with test solution at concentration of 50, 100 and 200 μ g/cm^3 in dimethyl sulphoxide (DMSO). After incubating the plates at 37^{o}C overnight, the diameter of the zone of inhibition of the bacterial growth was then recorded.

A 5% phenol solution was used as a positive control and DMSO as solvent control each time the experiments were performed.

Figure 1a: Spectra of solutions of different M:L retios for the VO^{IV}-INHA system showing the absence of isosbeotic points

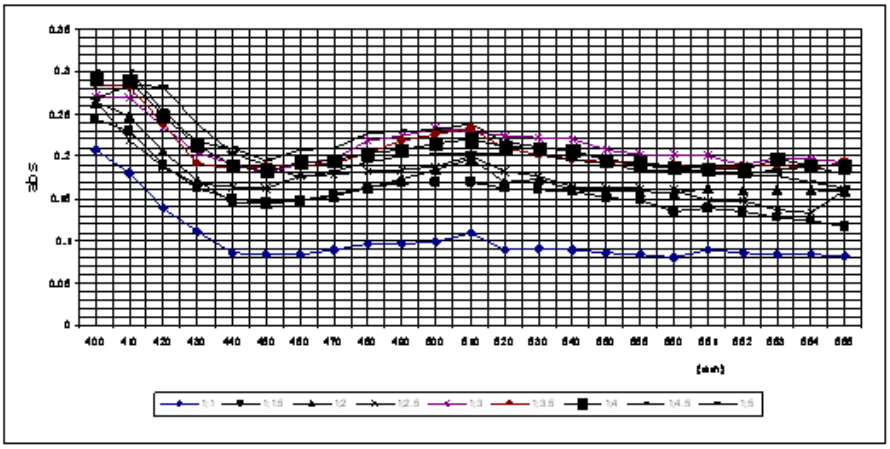

Figure 1b: Spectra of solutions of different M:L ratios for the VO^{IV}-NHA system showing the absence of isosbeotic points

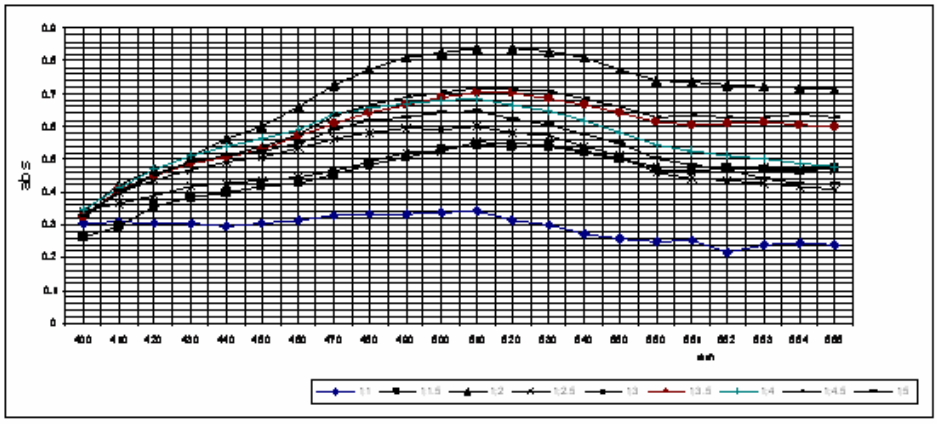

Figure 1c: Spectra of solutions of different M:L ratios for the VO^{IV}-CHAH system showing the absence of isosbeotic points

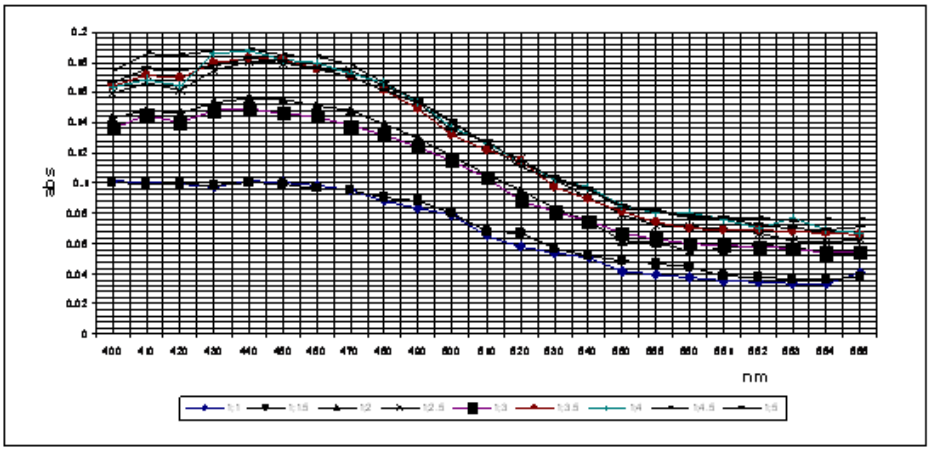

Figure 2a: Graphical rank Matrix analysis for VO^{IV}-NHA system (one specie test)

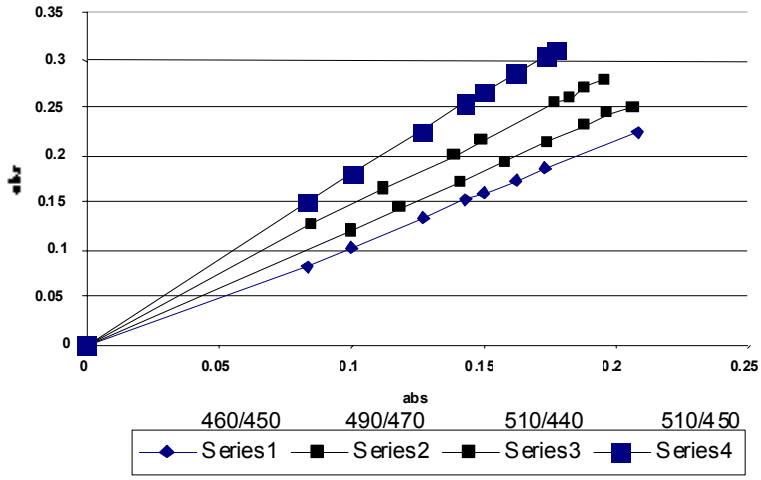

Figure 2b: Graphical rank Matrick analysis for VO^{IV}-INHA system (one specie test)

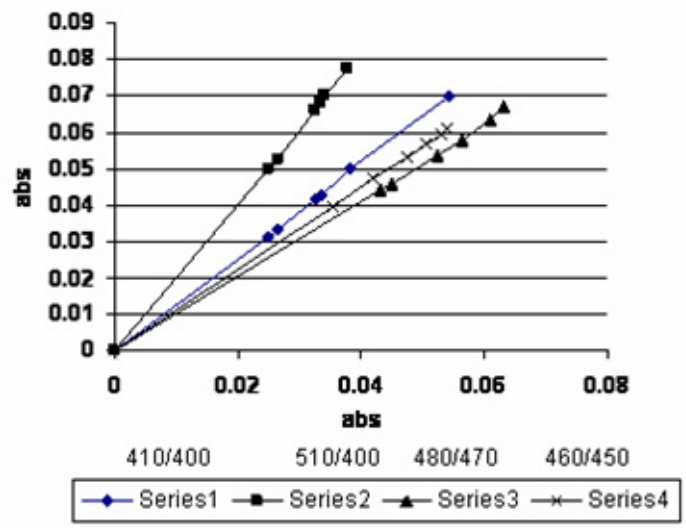

Figure 2c: Graphic rank Matrix analysis for VO^{IV}-CHAH system (one specie test)

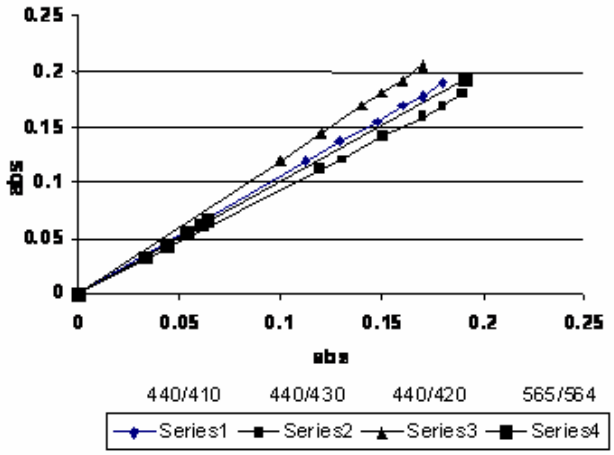

Figure 3a: Continuous variations (Job's plot) method for VO^{IV}-NHA system

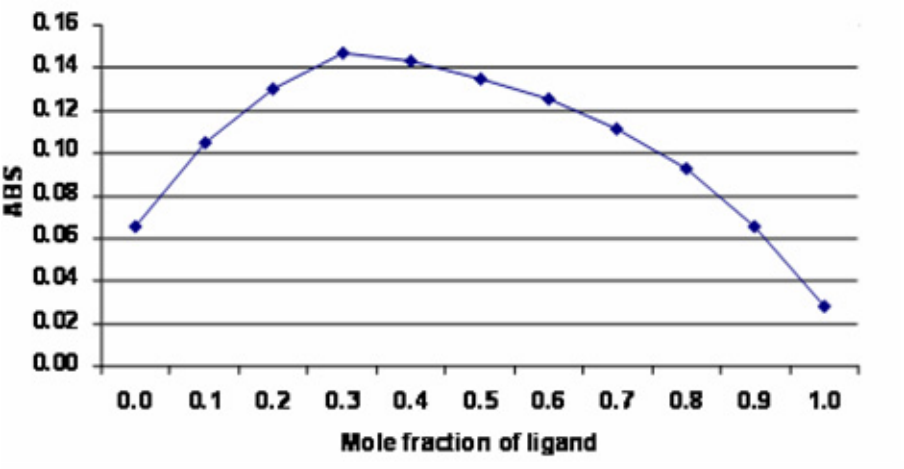

Figure 3b: Continuous variations (Job's plot) method for VO^{IV}-INHA system

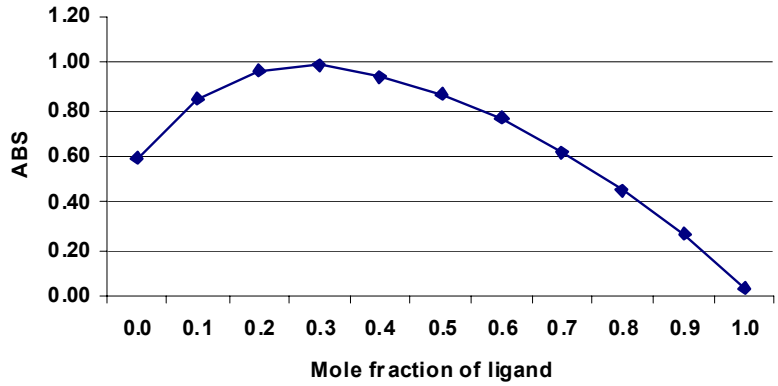

Figure 3c: Continuous variations (Job's plot) method for VO^{IV}-CHAH system

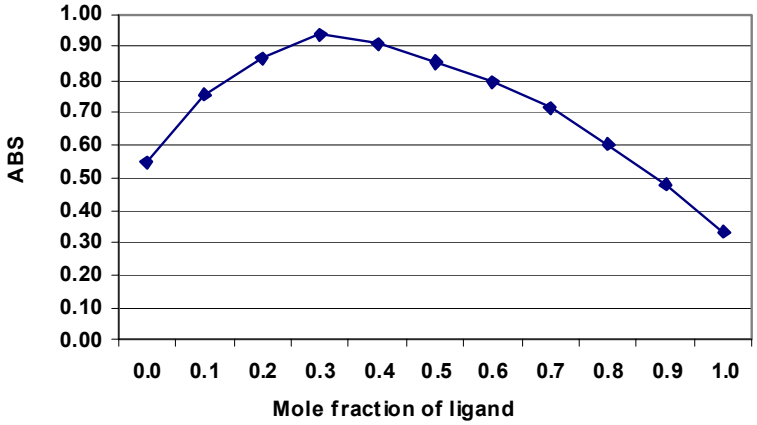

Figure 4a: Visible Spectrum of $[VO(NHA)_2].4H_2O$ Complex.

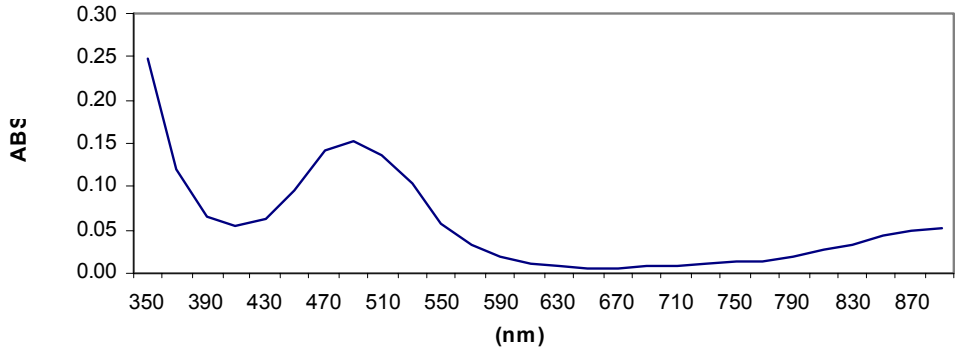

Figure 4b: Visible Spectrum of $[VO(INHA)_2].4H_2O$ Complex

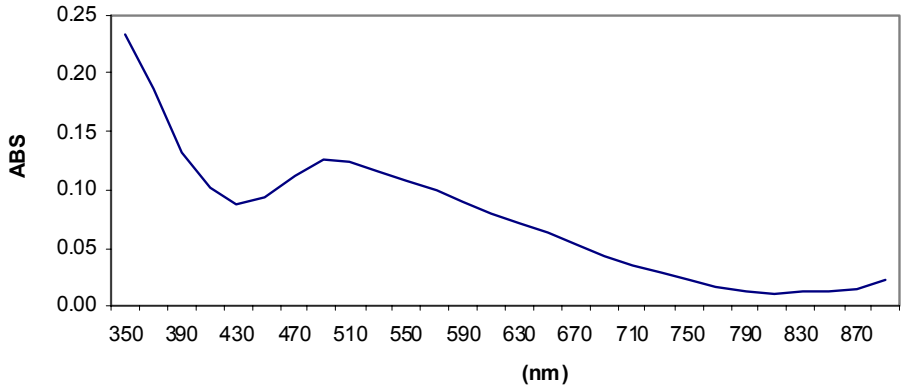

Figure 4c: Visible Spectrum of $[VO(CHAH)_2].4H_2O$ Complex

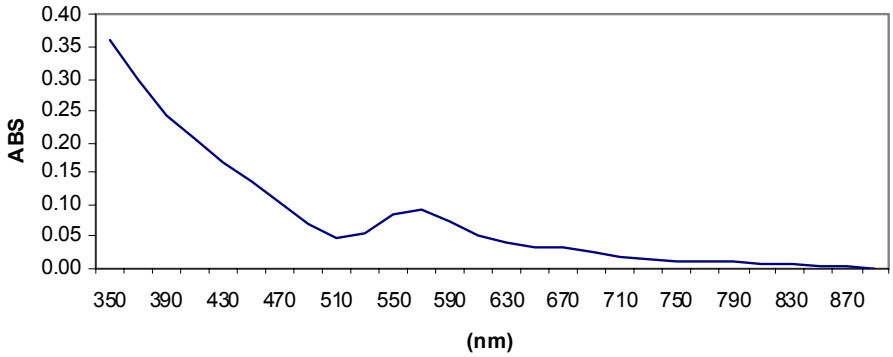

Results and Discussion

Table 1: Analytical data and Physicochemcial Properties of the Isolated Complexes () Calculated %.

Compound	Form.wt	Mp/Dec ^oC	Colour	Found M	μ eff B.M	λ max x 10^3	Assignment
$VO(CHAH)_2.2H_2O$	452.9	223	Grayish Black	11.96 (11.24)	1.79	17.54	$^1T_1 \rightarrow {}^1A_1$
$VO(INHA)_2.2H_2O$	414	200	Grayish Black	11.79 (12.29)	1.68	16.95	$^1B_2 \rightarrow {}^1A_1$
$VO(NHA)_2.2H_2O$	414	201	Grayish Black	11.80 (12.29)	1.88	19.61	$^1B_1 \rightarrow {}^1A_1$

Key: M = metal, Formwt = Formular weight, MP/dec = Melting Point/Decomposition, B.M = Borh Magneton

Table 2: Diagnostic I.R Data for the Complexes (cm^{-1})

Compound	ν (NH) cm^{-1}	ν (NH) cm^{-1}	ν (C=0) cm^{-1}	D ν (C=0) cm^{-1}	ν (V-0)cm^{-1}
CHAH	3433.14		1561.53		
$VO(CHAH)_2.2H_2O$	3354.35	-78.79	1628.60	67.07	962.76
INHA	3422.59		1605.01		
$VO(INHA)_2.2H_2O$	3424.30	+1.71	1545	-60.01	954.18
NHA	3418.00		1659.61		
$VO(NHA)_2.2H_2O$	3438.59	+20.59	1590.53	-69.08	933.76

Key: CHAH = Cyclohexylacetohydroxamic acid
INHA = Isonicotinohydroxamic acid
NHA = Nicotinohdroxamic acid

Table 3: Microbial Sensitivity Test for the Ligands and their Oxovanadium (IV) Complexes.

Ligands/Comlexes	Staph. aureus	S. Typhylium	E. Coli	Klebsiella	α hemolytic strep.	Neisseria	Pseudo-nomias	Coryne-bacteria
CHAH	-	-	-	-	-	-	-	-
INHA	-	-	-	-	-	-	-	-
NHA	-	-	-	-	-	-	-	-
$VO(CHAN)_2.2H_2O$	-	-	-	-	-	-	-	-
$VO(INHA)_2.2H_2O$	-	-	-	-	-	-	-	-
$VO(NHA)_2.2H_2O$	-	-	-	-	-	-	-	-

The various stages in the preparation of CHAH, INHA and NHA are as represented by the reactions below:

$$2Na + 2MeOH \rightarrow 2MeONa + H_2\uparrow$$

$$NH_2OH.HCl + MeONa \rightarrow NH_2OH + NaCl\downarrow + MeOH$$

$$NH_2OH + RCO_2Et \rightarrow RCON(H)OH + EtOH$$

$$RCON(H)OH + MeONa \rightarrow RCON(H)O^-Na^+ + MeOH$$

$$RCON(H)O^- - Na^+ + HCl \rightarrow RCON(H)OH + NaCl\downarrow$$

where R = Cycloalkyl group and pyridine ring for the complexes of CHAH, INHA and NHA model.

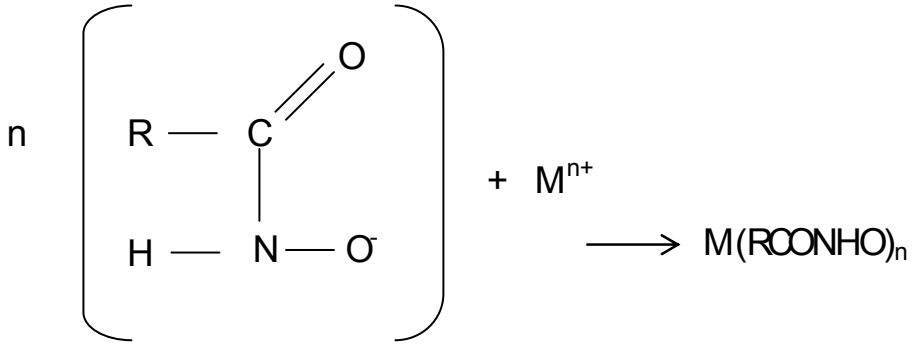

where n is a neutral monodentate ligand.

The .pka values for the ligands are 9.86 ± 0.03, 8.68 ± 0.02 and 8.68 ± 0.05 for CHAH, INHA and NHA respectively. The high basicity of the ligands may be ascribed to the positive inductive effect of the bulky groups attached to the functional group i.e. cyclohexyl ring and methylene group in the case of CHAH and pyridine group in the case of NHA and INHA. Figures 1(a– c) show the absorption spectra of solutions containing a constant metal but variable ligand molar concentration for the CHAH, NHA and INHA systems, while figures 2(a-c) show graphical Matrix rank analysis of the absorbance data generated from similar solutions for CHAH, NHA and INHA system. The absence of an isosbestic point and the shape of the graph is typical of systems containing only one complex specie. In this regard, the systems show similar behaviour[16].

Several equilibrium models were tried but it was only in ML_2 model that convergence was achieved. The composition of the complexes as determined by Job's plot is shown in figures 3(a-c). The ratio of VO^{IV} to the ligands under investigation were ML_2 ie VO^{IV} – CHAH, VO^{IV} – NHA and VO^{IV} – INHA[16].

The colours of all oxovanadium IV complexes are grayish black. The analytical data and some physico-chemical properties are shown in Table 1.

The visible spectra of oxovanadium (IV) complexes i.e $[VO(CHAH)_2]. 2H_2O$, $[VO(NHA)_2] . 2H_2O$ and $[VO(INHA)_2]. 2H_2O$ show bands located at 17.54 x 10^3cm^{-1}, 16.95 x 10^3cm^{-1} and 19.61 x 10^3cm^{-1} respectively. The position of these bands together with the magnetic moments of the complexes are consistence with square pyramidal coordination. The bands are therefore being assigned to these transitions: ${}^1T_1 \rightarrow {}^1A_1$ for $[VO(CHAH)_2]. 2H_2O$, ${}^1B_{21} \rightarrow {}^1A_1$ for $[VO(INHA)_2]. 2H_2O$ and ${}^1B_1 \rightarrow {}^1A_1$ for $[VO(NHA)_2]. 2H_2O$. All these bands are $d \rightarrow d$ transition of oxovanadium (IV) ions.[16]

The diagnostic i.r bands in the free ligands and their corresponding complexes are shown in Table 2. The υ (C=0) vibration located at 1561.53 (CHAH), 1605.01 (INHA) and 1659.61cm^{-1}(NHA) in the ligands is higher by 67.07cm^{-1} in the oxovanadium IV complex of CHAH but lowered by between 60.01 – 69.08cm^{-1} in the oxovanadium (IV) complexes of NHA and INHA. The υ (V-0)cm^{-1} band in the complexes ranges between 933.76 – 962.76cm^{-1}. This together with decrease in υ (NH) in the complex of CHAH and increase in υ (NH) band in the NHA and INHA complexes indicates coordination via Nitrogen atom of the hydroxamic acid[11] for CHAH complex while for NHA and INHA complexes shows coordination via the carbonyl oxygen.[16]

The microbial sensitivity test carried out on the ligands and the oxovanadium IV complexes shows no activity on the microorganism under investigation. Table 3.

On the basis of their physico-chemical properties the shown structure in scheme 2 are proposed for the complexes.

Proposed Structures for (O,O) bonding mode in square pyramidal complexes of oxovanadium (IV) hydroxamate.

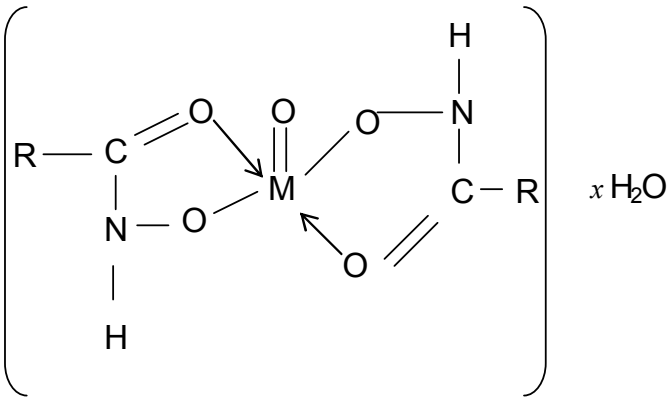

Proposed structure for (N) bonding mode in square pyramidal complexes of oxovanadium (IV) hydroxamate.

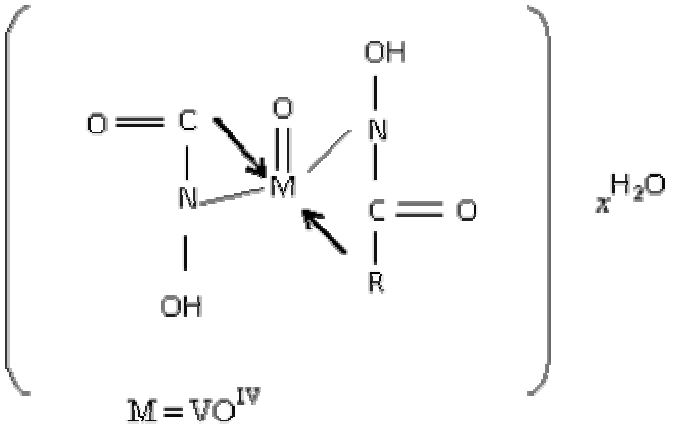

References

[1] Nwabueze, J.N, (1996) Trans. Met. Chem 21.
[2] K. Ali, N. Fatima, Z.T. Maqsood and S.A Kazmi (2004) J. Iranian Chemical Society. 1, 1.
[3] A. Sigel, H. Sigel (Eds) (1998) Iron Transport and Storage in Micro Organism, Plants and Animals; Metal Ions and Biology Systems, M. Dekker Inc., New York.
[4] A Dessi, G. Micera, D. Sanna, L.S. Erre (1992) J. Inorganic Biochem 48, 273.
[5] I. Goldwaser J. Li, E. Gershonov, M. Armoni, E. Karnieli, M. Fitkin, Y. Shechter, (1999) J. Biol. Chem. 274, 26617.
[6] B. Peter, C. Nicola, T. Kiss, M. Giovanni, S. Daniee, (1995) J. Inorganic Biochem, 60, 45.
[7] Rockwell, M. Melden, R.A. Copeland, K. Hardman, C.P. Decicco, W.W. Degrado (1996) J. Am Chem. Soc. 118, 10337.
[8] M.J. Miller, F. Malouin, R.J. Bergeron, G.M. Brittenham, Eds, 1994.
[9] D. Hirsova, O. Koldovisk, (1969) Physio Bohemoslov, 281.
[10] Maria, Celina; M.M. Fernandes, Eucler B, Paniago and Sandra Carbalho (1997) J. Braz. Chem. Soc. 85, 537 – 548.
[11] Albert. A. and Sergent E.P. The determination of ionization Constants, 2nd Edition, Chapman and Hall, London Ltd, 1971, 44.
[12] Nwabueze, J.N. Aliyu A.O. Bulletin of Ethiopia Chemical Society, Ethiopia (still in press).
[13] Nwabueze, J.N. Transition met. Chem. (1996) 21,258-261.
[14] Cruickshank R. Medical Microbiology Eds Church and Livingstone U.K. 1965.
[15] Nicholls, D. Complexes and first row transition elements, Macmillian Press Ltd. London 1979, 73 – 79.
[16] R.L. Dutta and S. Lahiri, (1962) J. Indian Chem. Soc. 39, 860.

European Journal of Scientific Research
ISSN 1450-216X Vol.18 No.3 (2007), pp.427-431

http://www.eurojournals.com/ejsr.htm

Study of Zig-Zag Carbon Nanotubes Under an External Electric Field

S. Vasheghani Farahani
Islamic Azad University, Share-Rey Branch, Iran
K.N. Tousi University of Technology Department of physics, Tehran, Iran

A. Sajjadi Senejani
K.N. Tousi University of Technology Department of physics, Tehran, Iran

M. R. Soltani Erde Mosa
Islamic Azad University, Share-Rey Branch, Iran

M. Salehkoutahi
K.N. Tousi University of Technology Department of physics, Tehran, Iran

Abstract

In this Paper We investigate the electronic structure change of semi conducting carbon Nanotubes under an external electric field with the density functional theory (DFT). Here We study the band structure and density of state (DOS) of carbon Nanotubes for this purpose and compare them before and after applying an electric field on the carbon Nanotubes. We show that the band gap of energies levels decrease with applied electric field when the electric field was increased.

Keywords: zig-zag carbon Nanotube, external electric field, DFT, band structure, DOS

Introduction

The field of carbon Nanotubes research is remarked in terms of the unique physical properties of the carbon Nanotubes. In most subfields of condensed matter physics, experimental results have led and theoretical explanations have followed to give the subfield a firm foundation. However, in the case of research on carbon Nanotubes, theoretical predictions have often led experimental investigations. This situation is directly related to the difficulty in synthesis of sufficient quantities of pure and well characterized material for detailed studies, the manipulation of tiny size and the technique for experiment on Nanotubes. One of the most currents in semi conducting single wall carbon Nanotubes (s-SWNT) can be switched by an external electric field, which allows these s- SWNT to be used as a channel of field effect transistors (FET). Several groups have demonstrated such functional FETs successfully [1-4] and encouraged calculation of their electronic structure such as energy band, density of state and band structure and etc. The electronic structure of these s-SWNT under an external electric field have been also calculated theoretically [5-7], so far, the previous theoretical studies focus on electronic structure changes of the s-SWNTs under an external electronic field. However, their atomic displacements generated by the electric field effects will definitely influence their electronic structures. Here, we employ ab initio quantum calculations to model s-SWNT and address some of these issues.

Model and Method of Computation

In this study, the electronic properties of zigzag (7, 0) SWNTs were investigated (fig 1.a). The original unperturbed band structure of the SWNT (7, 0) gives a band gap 0.62 eV at the g point (see figure 2.b) and unperturbed DOS gives a band gap 0.62 eV around the Fermi level (see figure 2.a).

Figure 1: a) zig-zag (7, 0) in the center of a rectangular unit cell and b) apply constant external electric field

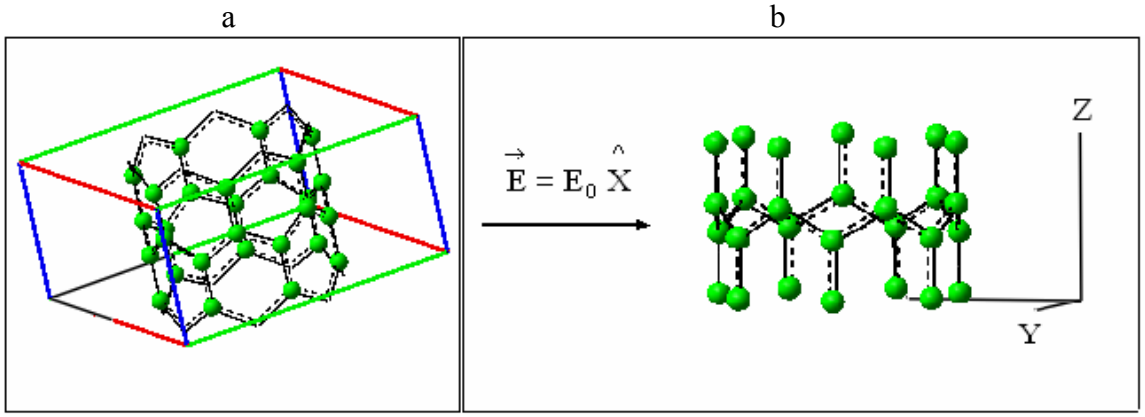

Figure 2: a) Density of state and b) band structure of the (7, 0) Nanotubes unperturbed

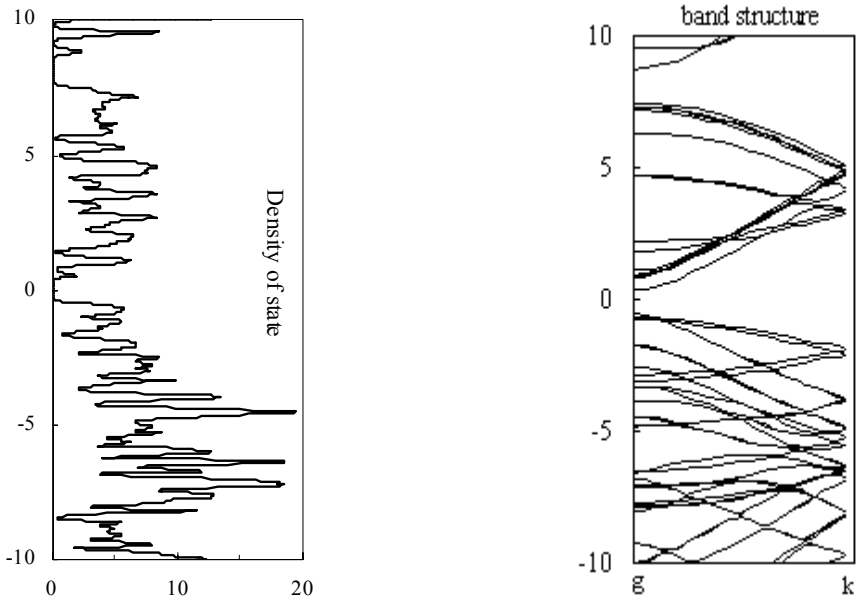

a b

To study the effect of the external electric field on the electronic structure of the Nanotube, we apply a uniform electric field to the unit cell in the Hamiltonian and a electric field magnitude which is linearly from zero to 2 $V/\overset{0}{A}$ with step 0.4 $V/\overset{0}{A}$ in the direction a axis and perpendicular to the a axis (figure 1.b) [8-12]. Under an external electric field 1.2 $V/\overset{0}{A}$ a slight reduction in the band gap with a value of 0.01 eV has been found and the crossed or almost degenerated state are split in both the valence and conduction bands due to the perturbation by an external electric field, which reduces the symmetry of mixing and the splitting of energy levels become more pronounced as the field strength increase (see figures 3&4). The band edge states in both the valence and conduction bands are found to move close to each other and eventually cross over each other. The onset of a semiconductor-metal

transitionFollowed by the band closure occurs as the electric field reaches a value above 0.8 $V/\overset{0}{A}$. Beyond this applied field, the band gap vanishes and the SWNT becomes metallic.

As the external field strengths are enhanced, the modification of the band structures becomes more pronounce in (7, 0) SWNTs. The band gap size decreases rapidly with the increasing electric fields in both cases. The (7,0) SWNTs show a more sensitive semiconductor-metal transition behavior under the electric field compared to the CNT counterparts.

The first principles, total energy and electronic structure calculations were performed using the Openmx 2.3 code [13, 14] which is a plane wave, pseudopotential program based on the density functional theory (DFT) with local density approximation (LDA). We have simulated the lattice constants a, b and c. The lattice constants a and b are equal to avoid the interaction between two adjacent Nanotubes. The lattice constant c along the tube axis is taken to be equal to the one dimensional (1D) lattice parameter of the Nanotubes and for this we have the case $a = b = 8.56\overset{0}{A}$ and $c = 4.27\overset{0}{A}$. A kinetic energy cutoff of 280 eV and 21 special k points are used to ensure the convergence in the calculations.

Figure 3: Band structure for CNT (7, 0) under (a) 0.4 (b) 0.8 (c) 1.2 (d) 1.6 and (e) 2 $V/\overset{0}{A}$ electric field. The zero of band energy indicates the Fermi level

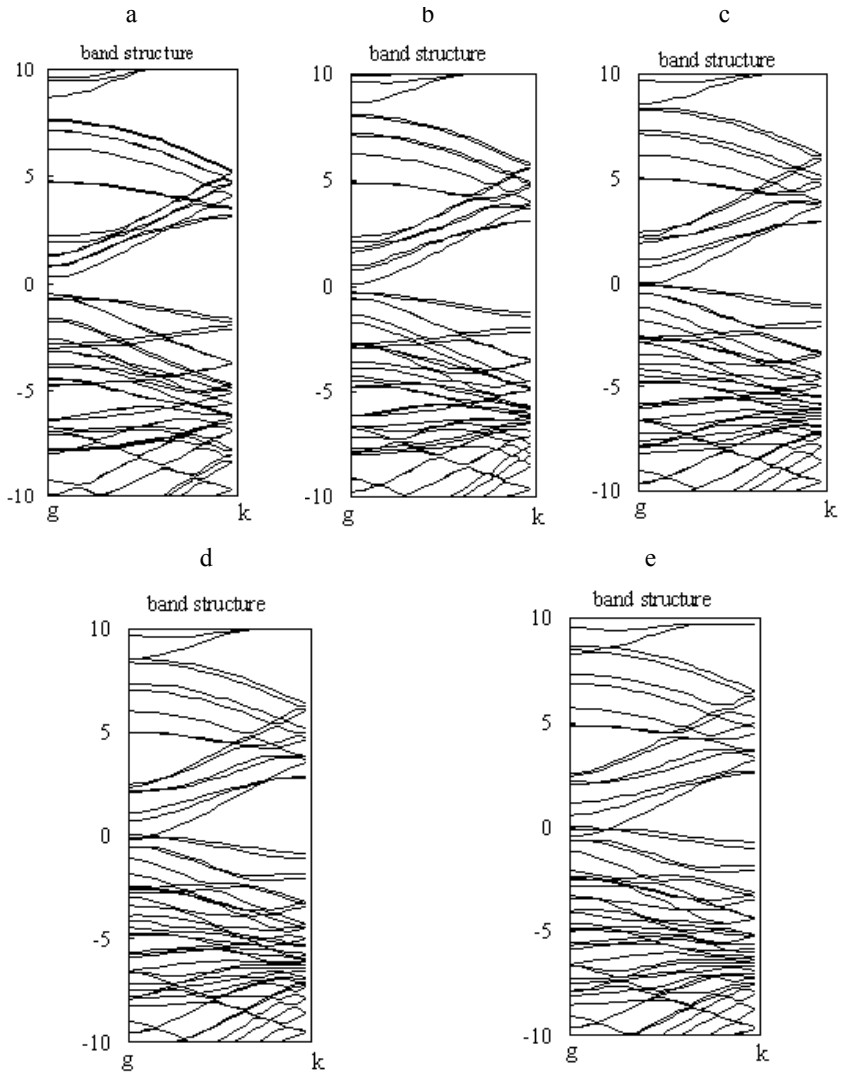

Figure 4: Density of state for CNT (7, 0) under (a) 0.4 (b) 0.8 (c) 1.2 (d) 1.6 and (e) 2 $V/\overset{0}{A}$ electric field. The zero of band energy indicates the Fermi level

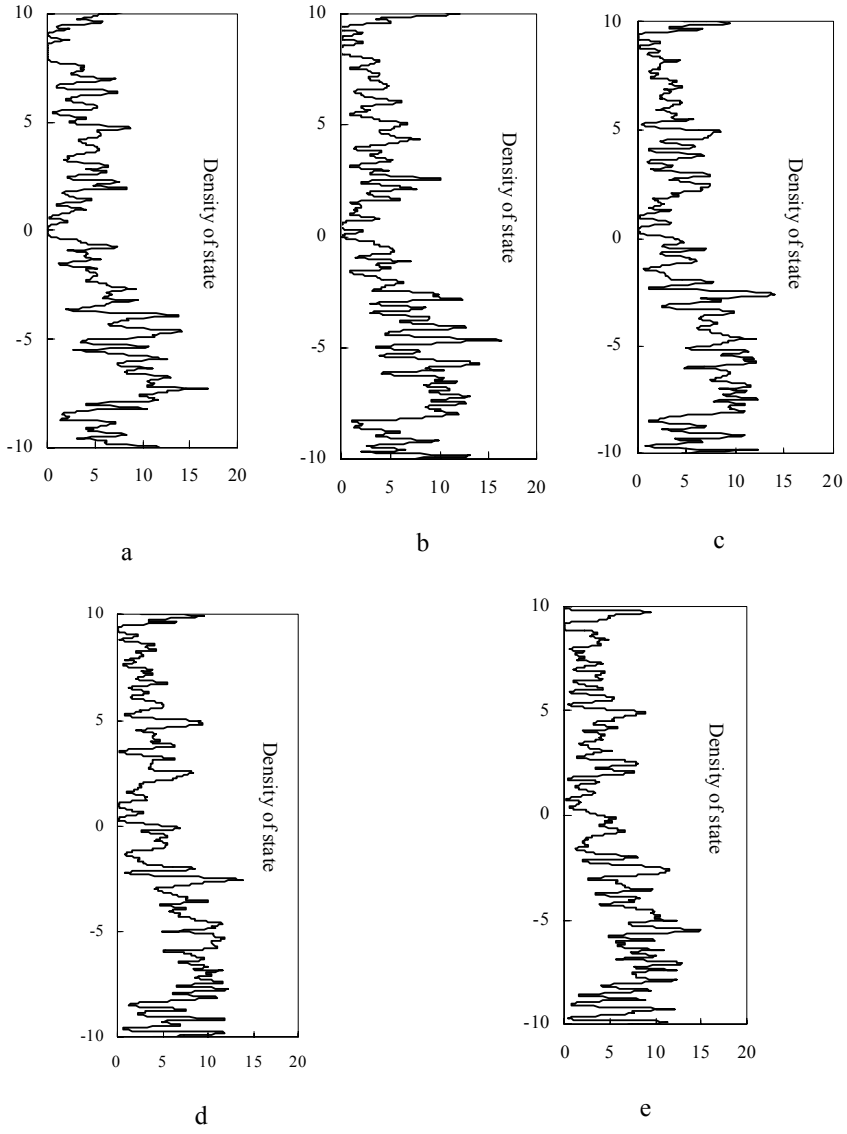

Results

We have analyzed the electronic structure of SWNT (7, 0) and compared the band structure before and after applying an electric field. We found that the energy gap decreases with the increase in the applied electric field (see figure 5). This means that some electrons can be transferred from valence band to conduction band. The states come near to each other indicating that the electrons have obtained the energy to go to the conduction band over Fermi level, so that it causes increase in the electric conduction of the zig-zag carbon Nanotube.

Figure 5: Band gap of energy levels decrease with applied electric field

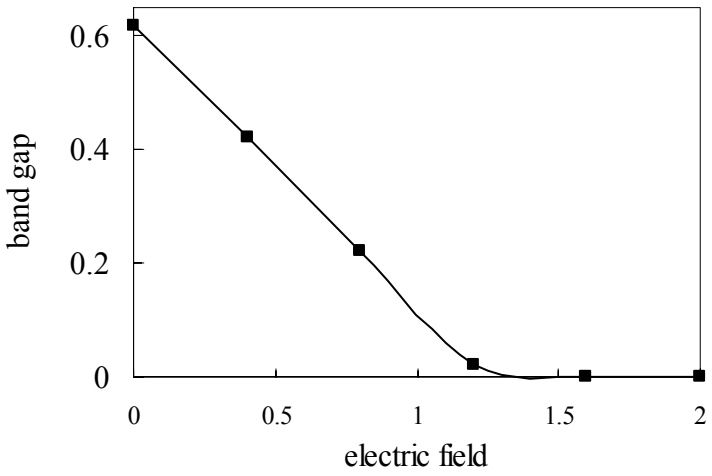

References

[1] Trans S.T, Verschueren R.M, Dekker C, *Nature* , 1998,**393**,49
[2] Martel R,Schemidt T, Shea H, Hertel T ,Avouris Ph, *App.Phys* ,1998,**73**,2447
[3] Zhou C , Kong J, Dai H , *App.Phys.Lett* ,1999, **76** ,1597
[4] Derycke V, Martel R , Appenzeller J, Avouris Ph , *Nano letters* ,2001, **1**,453
[5] Lou L , Nordleander P , Smalley R.E , *Phys.Rev.B* ,1995,**52**,1429
[6] Kim C, Kim B, Lee S.M, Jo C ,Lee Y.H ; *App.Phys.Lett* ,2001,**79**, 1187
[7] Rochefort A , Ventra M.D ,Avouris Ph; *App.Phys.Lett* ,2001,**78**,2521
[8] 8- Changwoof kim, Bongsou kim, Seung Mi Lee Chulsu Jo and Young Hee Lee; *Phys. Rev. B* 2002, **65**, 165418
[9] 9-Yoon-Taek Jang, Jin-Ho Ahn, Byeng – kwon Ju and Yue-Hi Lee ; *solid state communication* ,2003, **126**, 305
[10] 10-A.Latge, C.G.Rocha, L.A.L.Wanderley, M.Pacheco, Z.Barticevic and P.Orellana; *Phys. Rev. B* ,2003, **67**, 155413
[11] C.G.Rocha, M.Pacheco ,Z.Barticevic and A.Latge; *Brazilian Journal of Physics*, 2004, **34**,644
[12] C.G.rocha, M.Pacheo, Z.Barticevic and A.Latge; ; *Phys. Rev.* B ,2004,**70**,233402
[13] Sankey. O. F and Niklewski. D. J, Phys. Rev. B, 1989, **40**, 3979, 1989
[14] Ozaki.T and Kino.H, Phys. Rev. B, 2005, **72**, 045121, 2005

European Journal of Scientific Research
ISSN 1450-216X Vol.18 No.3 (2007), pp.432-444

http://www.eurojournals.com/ejsr.htm

Vegetation Mapping Using Multispectral Aerial Photographs in the Western Mediterranean Coast of Egypt

Hediat M. H. Salama
Botany Department, faculty of Science, Zagazig University, Egypt

Abstract

A representative area of the Western Mediterranean Coast of Egypt was selected for this large scale study. The central issue was to distinguish plant communities and their distribution in relation to micro-environmental conditions. A procedure for automatic mapping of plant communities and their corresponding environmental features by means of statistic modeling and geographic information system (GIS) have been developed. A large scale data from different sources such as a scanned infrared (IR) – aerial photograph, information layers derived a digital elevation model (DEM) and vegetation sampling in the field have been integrated in GIS. Probability model built the links between GIS data layers and plant communities resulting from classification of field data. Based on the probability model maps were produced showing the actual potential distribution of plant communities. The accuracy of the vegetation map was improved by additional information from the DEM. The results indicate that the distribution of seven plant communities dominated by 1- *Limoniastrum monopetalum*, 2 – *Zaygophyllum album*, 3 – *Asphodelus fistulosus*, 4 – *Salsola tetrandra*, 5 – *Anabasis articulata*, 6– *Thymelaea hirsuta*, 7 – *Suaeda vera* are hardly manipulated on the outwash plains closed to the front of wadis. But its high density was on white oolitic limestone, calcareous alluvium, saline calcareous deposits, mixture of calcareous and siliceous deposits and the foot of scraps habitats. The relationship between plant communities and topographical data is weaker with red, green and blue (RGB) components of the images,

Keywords: Plant communities, GIS, DEM, GPS, vegetation, remote sensing, infrared aerial photographs, RGB.

Introduction

Traditional field of vegetation mapping according to the Braun-Blanquet floristic approach (Braun-Blanquet 1965, Täckholm 1974, El-Ghareeb 1990) provide with a possibility to describe vegetation in a large detail but are time/labour intensive and are biased by the subjectivity of the interpreter (Congalton 1991).

Remote sensing can partly eliminate these problems but the nature of resulting information differs (Mosbech and Hansen 1994). Instead of focusing on community structure and floristic composition, remote sensing is based on dominant species, their biomass (i. e. chlorophyll content and leaf area), water content, physiognomy (e. g. height of the plant, width of leaves and their position), canopy structure and its character (e. g. canopy closure – a ratio of bare ground visible through the canopy) and soil conditions (Graetz 1989, Franklin *et al*. 1994).

The relatively high spatial resolution of multispectral aerial photography makes this tool useful for mapping vegetation composed of a mosaic of small units. The remote sensing employed in the present study has several advantages and disadvantages compared to the manual one. Manual vegetation mapping is not only time/labour intensive, hence expensive, but also subjective. Although a higher number of classes (some very small and unique) can be achieved, the classification is not reproductive. Labour intensity of manual interpretation usually limits the special extent of data bases and the manual classification accuracy is not readily assessed (Carmel and Kadmon 1998). Digital remote sensing is more homogeneous and consistent. It often distinguishes fewer classes, but their number increases as the operator gets more experienced.

Remote sensing and GIS have become powerful tools for vegetation mapping, modeling of vegetation distribution (Brown 1994, Goodchild 1994), and ecosystem monitoring in general. Studies have been performed using remote sensing data for vegetation mapping and mainly at intermediate or small scales with a ground resolution of 20 meters or larger (Craighead *et al*. 1988, Ostendorf and Reynolds 1993, Salem *et al*. 2003, Salama and Shehata 2003). Digitized aerial photographs have been applied and compared with satellite data (Frank and Thorn 1985, Masbech and Hansen 1994, Müllerová 2004). Evans *et al*. (1989) and Salama and Shehata (2003) made a large scale studies using GIS, DEM and aerial photographs to analyze relationships between vegetation pattern and terrenes. Some studies have also been performed using remote sensing data monitoring different aspects of vegetation (Elven *et al*. 1990, Brossard and Joly 1994, Spjelkavik, 1995).

The present study examined the application of infrared aerial photographs data to the mapping of the Western Mediterranean Coast of Egypt vegetation that is vulnerable to human-induced disturbances and extremely valuable from the conservation point of view. The aims of this study at following: 1) to distinguish plant communities and their spatial distribution in relation to environmental conditions using classification algorithms on infrared-aerial photographs, 2) to vegetation classification by using additional environmental information. Data of multi-disciplinary sources were integrated in a GIS database. The GIS database make it possible to model, combine and analyze spatial relationships between the data sets for the characterization and mapping of plant communities and their habitats. Two types of data were collected.

1. Field data: These are obtained from punctual recording of vegetation and environmental features along transect covering the study area.
2. Raster data layers : The first layer is a digitized color IR-aerial photograph. The second data layer is precise DEM of the study area, it was made using a ground positioning system (GPS) based on satellite navigation technology.

Additional significant information such as exposure, sloping, rock type, geomorphic features and potential radiation were derived from the DEM. They cover the study area as a continuum in raster format at high resolution.

Study Area

The study area extends along the coastal belt of the Mediterranean Sea and West of the Nile Delta. It lies between Latitudes 30º 00', 31º 00' N, and Longitudes 25º 00', 31º 00' E. It ranges about 50 km from north to south and about 500 km from east to west covering an area of approximately 25000 km^2 (Fig.1). The Mediterranean Coastal Desert of Egypt has a rather special climate, which differs from the inland desert area to the south, which is characterized by comparatively high humidity, frequent dew formation and small diurnal temperature variations. The degree of aridity of the Mediterranean Coastal Desert of Egypt has been discussed by many authors on the regional level (e. g. Sultan *et al*. 1997, lange *et al*. 1999). The seasonally in climate in the northern part of Western Desert of Egypt tends towards Mediterranean distribution of rainfall, ranging between 150-300 mm annually. Summer rainfall does not occur from northwest cloud bands and less frequently from tropical depression. The summer events are typically the most extreme rainfall events. Mean potential evaporation exceeds

rainfall in most months and in all months in the lower rainfall zones. The potential evaporation gradient is the reverse of the rainfall, with 400-600 mm mean annual evaporation near the coastal and over 800 mm in the most inland parts of the catchments (Shehata 2005, Salama and Shehata 2005). This general aridity and lack predictability has major implications for the evolutionary adaptation of Egyptian biota and the productivity of Egyptian ecosystems.

Figure 1: Location map and drainage basins of the Mediterranean Coastal Desert of Egypt.

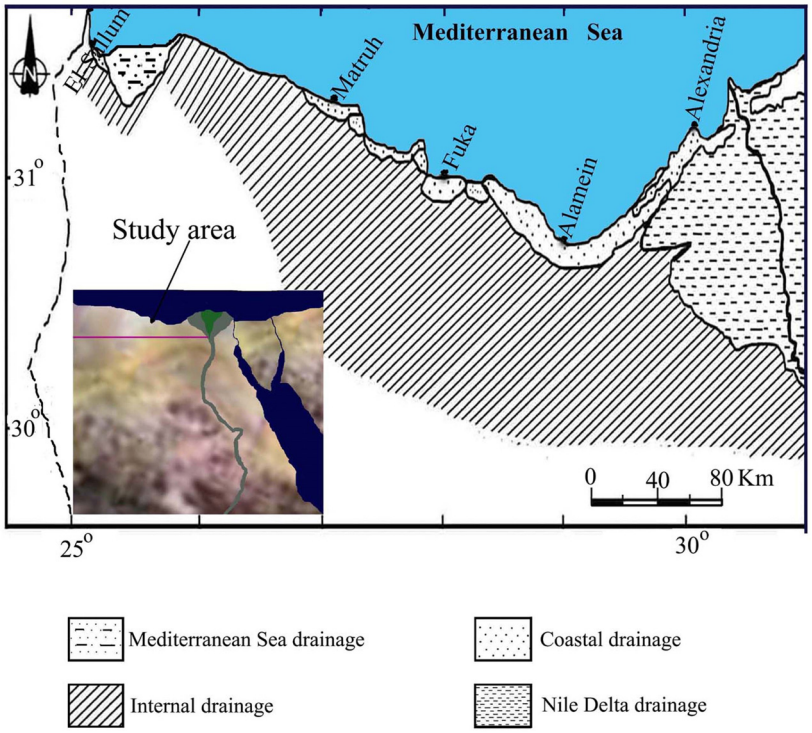

Topographically; the Mediterranean Coastal Desert occupies the northern extremity of the rocky platform of Egypt and is characterized by fairly regular surface relief. The low coastal plain with elevations rarely exceeding 50 m. This plain extending regionally in an east-west direction, shows a number of undulations corresponding to headlands protruding into the sea and to short embayments. Along the coastal plain there are a number of shallow lakes and lagoons. The mild upland area with elevation of about 200 m. The northern edge of this upland is dissected by short drainage lines, which are directed to the sea. The short drainage lines which lake almost the form of gullies going to the sea or to the foreshore depressions. El-Sallum, El-Qasr and Fuka basins offer classical examples of this type of drainage.

Geomorphologically; the Western Mediterranean Coastal Desert of Egypt is differentiated into a northern coastal plain and a southern inland plateau. The coastal plain is characterized by the following physiographic features from the northern Mediterranean coast to the south.

1. Coastal ridge: These mainly composed of snow-white oolitic limestone, overlain by sand dunes.
2. Saline depressions: These are composed of brackish water and saline calcareous sediments. These saline depressions are less saline and the water table is relatively deep more than one meter.
3. Non-saline depressions: Composed of calcareous and siliceous deposits of deep loss soil.
4. Inland ridges: Formed from limestone with a hard crystallized crust, and less calcareous deposits than the coastal ridges.
5. Inland plateau: Characterized by an extensive flat rocky surface and shallow loss soil.

6. Inland siliceous deposits: Sporadically distributed on the inland plateau and occasionally forming sand dunes and alluvial fans, especially in more sites. Occasional formation of alluvial fans of different dimension, particularly at the foot of the escarpment bordering of low coastal plain where formed, namely at El-Sallum , Matruh and Fuka, piedmont plains are developed.

The study area is heterogeneous in terms of vegetation and biotic environmental features such as geomorphology, texture, soils, microclimate and distribution regime. The vegetation cover is generally sparse (as large areas are unstable and disturbed on fluvial sand, around sand dunes, sandy plain, oolitic limestone plain, calcareous alluvium and foot of scarps. Phytosociological and ecological studies in the study area reveal many species (e. g. *Thymelaea hirusta*, *Asphodelus fistulosus*, *Plantago albicans*, *Anabasis articulata*, *Gymnocarpos decandrum*, *Zygophyllum album*, *Pituranthos Turtuosus*, *Helianthemum lippii* and *Noaea mucronta*) are of wide ecological amplitude. This is followed by the other minor associated species. The structure of the communities of the vegetation was analyzed sociologically according to the procedures described by (Braun-Blanquet 1964, Batanouny and Ezzat 1971, Migahed *et al*. 1971, 1974, Ayyad and El-Ghonemy 1976, El-Ghareeb 1990). Major areas are covered by sandy plains and calcareous ridges vegetation, corresponding to the phytosociological alliances. Areas oftentimes devoid of vegetation are confined to seasonally active outwash plain, land use and deposits just in the bottom of the wadis.

Methods

Vegetation data were sampled systematically along transects. The transects were positioned to cover the major geomorphologic features and plant communities in the study area. The dominant perennial species of the communities were listed and counted in 400 randomly distributed quadrates of 25 m^2 for each. Each quadrate was characterized by a reasonable degree of visual physiographic and physiognomic homogeneity. The species-area relationship was deduced. The frequency index, frequency classes and frequency diagram were generated. The importance of component species was determined by computation of density and relative density.

The position of each quadrate was determined using a GIS. This was done in order to ensure that the quadrate could be traced in a very precise and compared to a digital counter part in the scanned IR-aerial photographs. The vegetation data was then classified using a computer program for multivariate data analysis in ecology and systematic; SYN-TAX version 5.1 (Podani 1994).

The detailed vegetation analysis was carried out on the multispectral photographs. From the four channels available (0.54, 0.60, 0.66, 0.84 μm) Red and Infrared channels provide to be most useful. The IR-aerial photograph was transformed into raster format with scanning device. The basic red , green and blue components (RGB) were stored in different image files as usually done with the different channels of satellite images. The DEM of the study area was constructed by mean of a GPS used in differential and kinematics modes. Altogether 9500 points were positioned in the field using GPS. According to control measurements, the accuracy of the system keeps the error within 10 cm. The DEM layer is processed by interpolation between the 9500 points. From the DEM several sub-layers such as gradient, aspect and solar energy can be derived. To minimize the errors caused by miss-registration the final resolution was coarsened to pixel size 1 x 1 m for all raster data and the Universe Transverse Macerator (UTM) projection makes it possible to superimpose the different layers.

The modeling method operates by cross linking field data (i. e. the defined plant communities) and the raster data layers of the GIS. If all the considered layers contained quantitative and pseudo-quantitative values, the criterion of distance can be used for analyzing the relationships between these data and field observation (Brossard and Joly 1994). But, in the present study, the data layers are heterogeneous as they also include non-quantitative values such as the categories, which define the slope aspect. To overcome this problem, the quantitative values were discretised and turned into Boolean items.

The statistic links between vegetation types and GIS data were analyzed in terms of occurrence and frequency vector. This approach rests upon binomial low (Spiegel 1982, Davis 1986) and proceeds to establish empirical probability models (Tom and Miller 1994). Spjelkavik (1995) proposed the term comparison matrix, and Brossard and Joly (1994) have explored in similar way, the statistical links between plant communities and classification of satellite data.

The next step is to use the empirical probability model as an operator the mapping plant communities by means of GIS layers including scanned IR-aerial photograph as well as information derived from the DEM. The presented matrix (Table 1) is the core of the model and indicates how it works. As UTM position of each observation point known, it is possible to extract from the GIS data base the values of pixels corresponding to RGB components of the IR-image. The quantitative values are then into Boolean characters. The occurrence of each positive Boolean item inside the different plant communities is counted up and converted into percentage as done in Table 1. The sum of each row is 100%. According to Boolean value of a given pixel, the probability of ranking in different plant communities is known. As each pixel is characterized by seven Boolean items (one per data layer), the corresponding probability values are to be summed up column by column. The considered pixel is allocated to the plant community for which the probability score is the highest. Thus it is possible to make probability maps showing the actual and potential distribution of plant communities.

Table 1: The probability used as an operator for mapping. The values are expressed as percent probability.

	CL-1	CL-2	CL-3	CL-4	CL-5	CL-6	CL-7		CL-1	CL-2	CL-3	CL-4	CL-5	CL-6	CL-7
IRR- 1	2	1	1	2	2	92	0	**IRB-1**	5	40	50	1	1	2	1
IRR- 2	1	2	2	1	1	89	4	**IRB- 2**	70	18	4	2	2	2	2
IRR- 3	0	1	71	3	1	2	22	**IRB- 3**	24	12	2	45	15	1	1
IRR- 4	42	1	0	1	21	1	34	**IRB- 4**	2	60	2	2	2	2	30
IRR- 5	15	30	1	1	25	1	27	**IRB- 5**	2	2	3	3	72	8	10
IRR- 6	2	12	2	74	0	1	9	**IRB- 6**	1	1	1	35	3	55	4
IRR-7	2	0	1	3	90	2	2	**IRB-7**	1	1	1	1	14	32	45
IRG-1	85	2	0	1	2	7	3	**GR = 0**	2	9	8	17	26	20	18
IRG-2	0	38	52	2	3	5	0	**GR = 1-2**	12	16	13	17	13	15	14
IRG-3	2	2	47	0	8	11	34	**GR = 3-4**	25	19	20	10	7	8	11
IRG-4	1	54	0	2	1	2	40	**GR = 5-6**	30	14	10	6	7	8	25
IRG-5	2	4	1	0	83	6	4	**GR > 7**	25	16	12	17	11	10	9
IRG-6	2	2	2	92	1	1	0	**SO < 3 KW**	15	6	11	8	10	30	20
IRG-7	0	1	2	2	2	48	45	**SO < 4 KW**	21	5	31	13	11	10	9
As=NNE	41	4	21	7	10	2	15	**SO<4.5KW**	30	4	9	25	12	6	14
As = E	43	4	20	11	3	9	10	**SO <5 KW**	15	9	8	14	24	10	20
AS=SSE	2	4	8	12	3	30	41	**SO<5.5KW**	8	7	17	20	14	15	19
AS=SSW	5	65	4	2	2	10	12	**SO < 6 KW**	8	18	20	12	14	13	15
AS = W	4	4	74	2	3	2	11	**SO<6.5KW**	9	17	18	14	15	11	16
AS=NNW	2	2	3	40	25	18	10	**SO < 7 KW**	10	24	12	8	11	20	15
AS = Flat	5	11	4	15	26	21	20	**SO > 7 KW**	25	11	14	10	9	11	20

Abbreviations: **CL** = Clusters and refers to the plant community 1 to 7.
IRR = red, **IRG** = green, and **IRB** = blue components of the infrared aerial photograph.
GR = gradient. **AS** = aspect. **SO** = solar radiation. **KW** = radiation in (kilo watt / m^2).

Results

1. Vegetation Classification

The quadrate plant data were subjected to non-hierarchical clustering (Fuzzy C-mean clustering) as described by Podani (1994). It differs from other non-hierarchical classification by calculating a membership weights expressing the affinity of the quadrate plant data to all the clusters rather than assigning them to a single cluster like deterministic partitioning techniques. Higher number of clusters made their interpretation comparatively difficult. The number of clusters has to be specified in advance and quadrate plant data are assigned to the cluster for which it has the highest membership weights. The Fuzzy clustering was performed specifying 7 clusters or plant communities according to the field verification dominated by;

1. *Limoniastrum monopetalum*
2. *Zygophyllum album*
3. *Asphodelus fistulosus*
4. *Salsola tetrandra*
5. *Anabasis articulata*
6. *Thymelaea hirsuta*
7. *Suaeda vera.*

There are certain restrictions to the choice of number of clusters as there has to be a sufficient number of quadrate plant data inside each cluster to make a reliable statistical model for classification of the raster data.

In order to find a suitable number of clusters (plant communities) from a mathematical point of view, Bezdek's partition coefficient (Bezdek's 1981) were computed and plotted against cluster number (Fig. 2). But Bezdek's cluster coefficient is a rather crude measure of optimal cluster number. Coefficient that was not normalized seems to produce bias towards a small number of clusters, while a normalized coefficient leads to bias in the opposite direction (Equihua 1990).

Figure 2

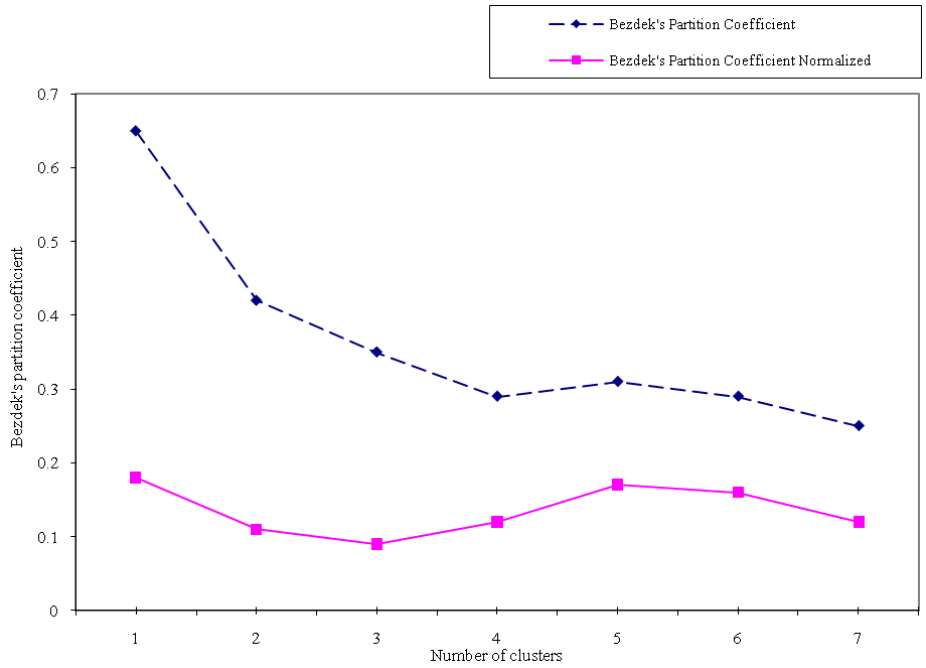

Figure 2 shows that, within the range of clusters 1 to 7 there is slightly better separation (on average) at the 7 clusters level. But a visual inspection of the tabular vegetation data reveals that a similarity of clusters 5 and 6 would result in loss of important floristic information as two plant

communities are combined. A further separation beyond the seven-cluster level resulted in clusters within too few quadrate plant data inside.

Restricted by the above mentioned assumption the vegetation data set seems to support stratification into seven plant communities. Pairwise separation coefficients for the 7 clusters were then calculated indicating which of different plant communities (clusters) that are clearly separated from each other and which are not separated (Table 2).

Table 2: Pairwise separation coefficients of the seven clusters. Clusters that have weakly separated are shown with underline text.

Pairwise separation coefficients for clusters 1 to 7							
Cluster No.	**1**	**2**	**3**	**4**	**5**	**6**	**7**
1	0						
2	36.77	0					
3	49.26	50.12	0				
4	12.85	35.54	48.62	0			
5	**5.63**	33.35	53.62	**3.85**	0		
6	**3.56**	45.81	57.90	**5.27**	16.68	0	
7	**1.22**	53.80	58.61	11.86	22.62	18.65	0

2. Vegetation mapping

Two tests were made in order to estimate the efficiency of the model. The first test (Table 3) was made using only the RGB components of the IR-aerial photograph. The confusion matrix makes it possible the fit between classification of vegetation data and the results obtained from the model leading to the cartography. Most of the values are high (ranging from 76 to 95%) indicating that the IR-aerial photograph makes an efficient discrimination of plant communities as defined by classification of vegetation data.

Table 3: The confusion matrix between vegetation classification (in rows) and the results (in columns) of the mapping procedure. The model is applied to RGB components only.

	PRBIR-1	**PRBIR-2**	**PRBIR-3**	**PRBIR-4**	**PRBIR-5**	**PRBIR-6**	**PRBIR-7**
VEG-1	**95**	1	1	1	0	1	1
VEG-2	3	**92**	0	1	3	1	0
VEG-3	4	1	**89**	2	0	3	1
VEG-4	2	1	3	**85**	4	0	5
VEG-5	0	6	3	2	**81**	5	3
VEG-6	8	3	2	5	4	**78**	0
VEG-7	6	3	8	3	4	1	**75**

The second test was made by adding topographic data for processing. Figure 3 shows a raster map of constructed DEM covering the study area. The confusion matrix (Table 4) emphasizes that residuals are less important than previously. A map generated from the model using only the RGB components of the IR-aerial photograph, and a map (Fig 4) derived from the model applying additional information from the DEM were produced.

Figure 3: Digital elevation model of the study area. The equidistance is 2 m.

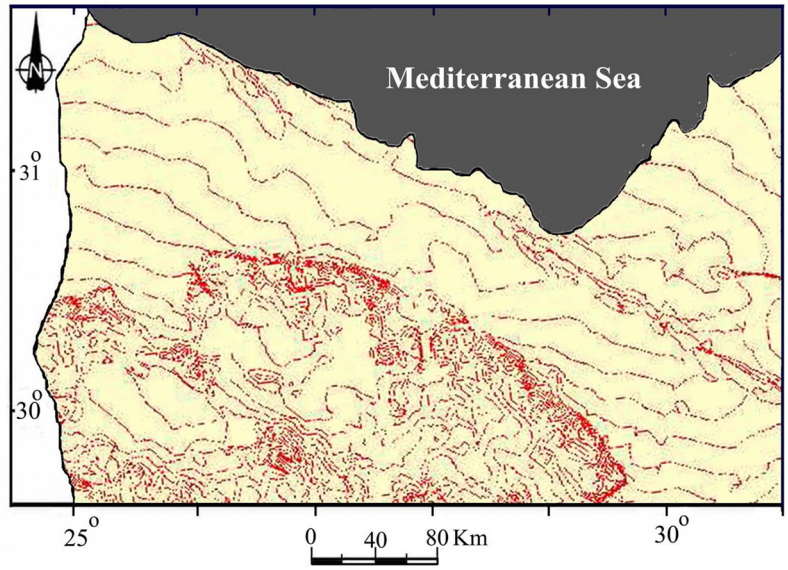

Table 4: The confusion matrix improved by adding into the statistical model topographic data derived from the DEM.

	PRBTO-1	PRBTO-2	PRBTO-3	PRBTO-4	PRBTO-5	PRBTO-6	PRBTO-7
VEG-1	**97**	1	1	0	1	0	0
VEG-2	2	**94**	1	1	1	1	0
VEG-3	1	1	**92**	1	2	2	1
VEG-4	3	2	1	**89**	2	1	2
VEG-5	4	1	3	1	**87**	3	1
VEG-6	6	1	1	2	2	**85**	3
VEG-7	5	2	3	1	2	4	**83**

Discussion

The classification of the vegetation data revealed seven floristically and ecologically different plant communities dominated by:

1. *Limoniastrum monopetalum*
2. *Zygophyllum album*
3. *Asphodelus fistulosus*
4. *Salsola tetrandra*
5. *Anabasis articulata*
6. *Thymelaea hirsuta*
7. *Suaeda vera*

The requirement of sufficient number of field data inside each cluster can force some of the quadrates plant data although they are very different thus making the average cluster somewhat special and heterogeneous regarding plant species composition. The decision of cluster must therefore be carefully inspected looking species that obviously should not occur together by means of their habitat requirement. If this happens it is an indication of an artificial grouping solely resulting from the specified number of clusters. This means a loss of ecological and floristic information.

How well the statistical model for classification of the scanned IR-photo performs, rely on the initial classification of vegetation data. Inaccurate classification of vegetation data (heterogeneous units) is likely to give results that fail to reproduce the spatial distribution of the defined plant communities. Comparing table 2 with table 3 there is an overall agreement between the two tables.

Those plant communities that seem to be clearly separated in the vegetation classification are those who have probability of belonging to more than on probability class in table 3. If the confusion is very large this can be indicate that the obtained plant community is too heterogeneous and a subdivision should be take place in order to make smaller and more homogeneous vegetation units. The results from tables 2 and 3 indicate that plant communities 5, 6 ,and 7 are heterogeneous. And these communities are also those which contain the smallest number of field data.

From figure 4, the main point is that the distribution of plant communities is hardly manipulated on the outwash plains closed to the front of wadi. This can normally be expected as the topographical conditions are more contrasted in these area. The large scale of the DEM makes it possible to model precise differences, which appear when the map is constructed using topographic information. The relationship between plant communities and topographical data is weaker than with RGB components of the image, as shown by the probability matrix in table 1. However, the topographical data are effective and contributes to improving the mapping procedure. For the seven plant communities there is an average improvement of 10.2% in terms of probability using the additional topographic information from the DEM. And for plant communities 1 and 7 the improvement was 38.6% and 32.8% respectively.

Figure 4: The final map derived from the scanned infrared aerial photographs using additional information from the DEM.

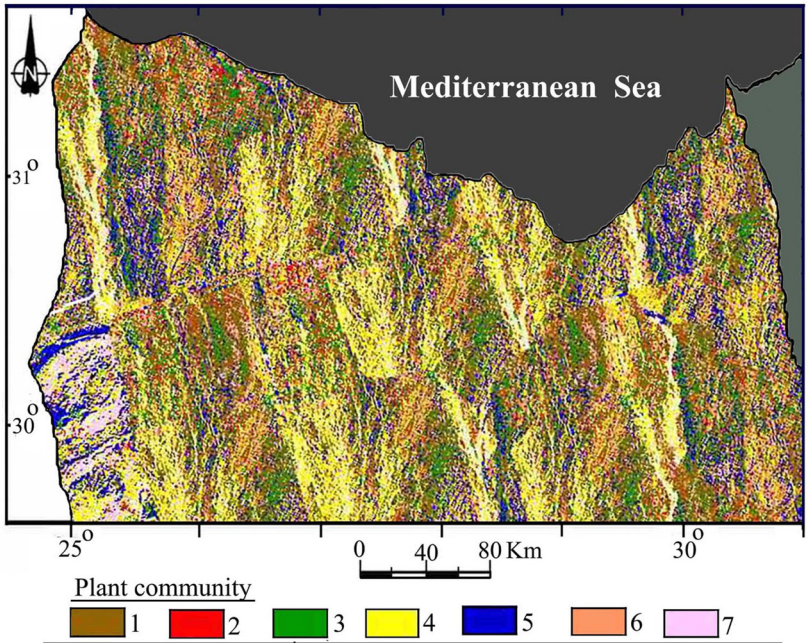

No.	Dominant Species	Habitat Types
1	*Limoniastrum monopetalum*	Saline calcareous, siliceous deposits (30 - 40% cover)
2	*Zaygophyllum album*	Oolitic limestone plains, calcareous alluvium (30-50% cover)
3	*Asphodelus fistulosus*	Coastal plains, saline calcareous deposits (> 25% cover)
4	*Salsola tetrandra*	Sandy plains, foot of the scarps, saline deposits (< 40% cover)
5	*Anabasis articulata*	Alluvium fans, sandy soil plains (< 30% cover)
6	*Thymelaea hirsuta*	Calcareous alluvium, ridges, foot of the scarps (< 30% cover)
7	*Suaeda vera*	Foot of the scarps, alluvium fans, sandy soil (< 25% cover)

Concerning the plains, the difference is more distinct. Plant communities present on the oolitic limestone plains and calcareous alluvium (*Zygophyllum album*), saline calcareous deposits and mixture of calcareous and siliceous deposits (*Limoniastrum monopetalum*), also appear around some small sand dunes on the gradient of the scarps. This may be attributed to the great topographical contrasts in the study area which supply information that make it possible to discriminate new sites.

The classification of the digitized image sometimes fails to distinguish between sparsely vegetated areas and non-vegetated areas. Areas close the front of wadi (outwash deposits) that is obviously devoid of vegetation. In case where the vegetation cover is scattered the soil component will be the primary determinant of color, texture and shade in the IR-image and hence the digital value of the scanned image. In case the map actually show the soil distribution rather than reflecting the plant communities distribution.

Conclusions

The results should that it is possible to produce a vegetation map by classifying a scanned IR-aerial photograph, which aim to reproduce the spatial distribution of the defined plant communities. The IR-aerial photography coupled with the GIS provides the technical resources for making a GIS database when requiring high-resolution data sets. The results showed that using additional information derived from the DEM improved the conformity between classification of vegetation data and the raster RGB-data. The improvement in mapping accuracy that can be gained using this method relies heavily on which environmental factors that are selected to be recorded and included in the model.

The developed probability model is an appropriate method for mapping plant communities based on heterogeneous data layers originating sources. However, when adding the additional information from the DEM the model does not perform satisfactory for areas containing unstable and scattered vegetation such as white oolitic limestone plains and calcareous alluvium. Using data from the present day vegetation in combination with auxiliary environmental data (from GIS and DEM), it is possible to generate maps showing the potential (future) vegetation distribution according to the considered environmental factors. Using quantitative methods the collected field data, is possible to experiment with different floristic and environmental parameters in combinations and adjust and adapt for cartography.

References

[1] **Ayyad, M. A. and El-Ghonemy, A. A., 1976**. Phytosociological and environmental gradients in a sector of the Western Desert of Egypt. Vegetatio **31**: 93 – 102.

[2] **Batanouny, K. H. and Ezzat, N. H., 1971**. Eco-physiological studies on desert plants. I. Autecology of Egyptian *Zygophyllum* species. Oecologia (Berlin) **7**: 70 -83.

[3] **Bezdek, J. C., 1981**. Pattern recognition with fuzzy objective function algorithms. Plenum Press, New York, U. S. A.

[4] **Braun-Blanquet, J., 1965**. Plant sociology. The study of plant communities. Hafner, U.K.

[5] **Brossard, T. and Joly, D., 1994**. Probability models, remote sensing and field observations: test for mapping some plant distributions in the Kongsfjord area (Svalbard). Polar Des. **13**: 153 – 161.

[6] **Brown, D. G., 1994**. Predicting vegetation types at treeline using topography and biophysical disturbance variables. In: **Walsh, S. J., Davis, F. W. and Peet R. K**. (**Eds**). Special feature in vegetation science 6. J. Veg. Sci. **5**: 641 – 656.

[7] **Carmel, Y. and Kadmon, R., 1998**. Computerized classification of Mediterranean vegetation using panchromatic aerial photographs. Journal of Vegetation Science **9**: 445 – 454.

[8] **Congalton, R. G., 1991**. A review of assessing the accuracy of classification of remotely sensed data. Remote Sensing of Environment **37**: 35 – 46.

[9] **Craighead, J. J., Stephen, K. S. and John, M. D., 1988**. Mapping arctic vegetation in northwest Alaska using LANDSAT MSS imagery. Nat. Geogr. Res. **4**: 496 – 527.

[10] **Davis, J. C., 1986**. Statistics and data analysis in geology. Wiley and Sons, New York, NY, U. S. A.

[11] **El-Ghareeb, R., 1990**. A phytosociological study of Zygophyllum album L. in the Western Mediterranean Coast of Egypt. J. Univ. Kuwait Sci. **17**: 143 – 155.

[12] **Elven, R., Harry, M. and Joly, D., 1990**. Gipsdalen, central Svalbard; flora, vegetation and botanical values. In: **Brekke, B. and Hansson, R**. (**Eds**). Environmental atlas Gipsdalen, Svalbard. II. Norsk Polarinst. Rapp. **61**: 27 –66.

[13] **Equihua, M., 1990**. Fuzzy clustering of ecological data. J. Ecol. **78**: 519 – 534.

[14] **Evans, B. M., Walker, D. A., Benson, C. S., Nordstrand, E. A. and Peterson, G. W., 1989**. Special interrelationship between terrain, snow distribution and vegetation patterns at an arctic foothills site in Alaska. Holarc. Ecol. **12**: 270 – 278.

[15] **Frank, T. D. and Thorn, C. E., 1985**. Stratifying alpine tundra for geomorphic studies using digitized aerial imagery. Arc. Alp. Res. **17**: 88 – 188.

[16] **Franklin, S. E., Connery, D. R. and Williams, J. A., 1994**. Classification of alpine vegetation using Landsat Thematic Mapper, SPOT HRV and DEM data. Canadian Journal of Remote Sensing **20**: 49 – 56.

[17] **Goodchild, M. F., 1994**. Integrating GIS and remote sensing for vegetation analysis and modeling: methodological issues. In: **Walsh, S. J., Davis, F. W. and Peet, R. K**. (**Eds**). Special feature in vegetation science 6. J. Veg. Sci. **5**: 615 – 626.

[18] **Graetz, R. D., 1989**. Remote sensing of terrestrial ecosystem structure: an ecologist's pragmatic view. Ecological studies **79**: 5 – 30.

[19] **Lange, J., Leibundgut, C., Greenboum, N. and Schick, A. P., 1992**. A noncalibrated rainfall-runoff model for large arid catchment. Water Resources Research **35**: 1261 – 1272.

[20] **Migahed, A. M., Batanouny, K. H. and Zahi, M. A., 1971**. Phytosociological and ecological studies of a sector in the Mediterranean Coastal region in Egypt. Vegetation, **23**: 113 – 134.

[21] **Migahed, A. M., El-Sharkawy, H. M. Batanouny, K. H. and Shalaby, A. F., 1974**. Phytosociological and ecological studies of Maktila sector of Sidi-Barrani. I-Sociology of the communities. Feddes Repetorium, **84**: 747 – 760.

[22] **Mosbech, A. & Hansen, B. U., 1994**. Comparison of satellite imagery and infrared aerial photography as vegetation mapping methods in an arctic study area; Jameson Land, East Greenland. Polar Res. **13**: 139 – 152.

[23] **Müllerová, J., 2004**. Use of digital aerial photography for sub-alpine vegetation mapping: A case study from the Krkonose Mts., Czech Pepublic. Plant Ecology **175**: 259 – 272.

[24] **Ostendorf, B. and Reynolds, J. F., 1993**. Relationship between a terrain-based hydrologic model and patch-scale vegetation patterns in an arctic tundra landscape. Landsc. Ecol. **8**: 229 – 237.

[25] **Podani, J., 1994**. Multivariate data analysis in ecology and systematic –a methodological guide to the SYN-TAX 5.1 package. Ecol. Comp. Ser. **6**: 1- 316, SPB Academic Publishing.

[26] **Salama, H. M. H. and Shehata, M., 2003**. Vegetation mapping using scanned infrared aerial photographs in Wadi Sudr area, Sinai, Egypt. J. Envi. Sci. **26** (**1**): 139 – 161.

[27] **Salama, H. M. H. and Shehata, M., 2005**. Preclearing hydrology of the Mediterranean coastal desert of Egypt wheatbelt: Target for the features?. European Journal of Scientific Research **2** (**1**): 1 – 26.

[28] **Salem, B. B., Henedy, S. Z. and Awad, M. A., 2003**. Mapping rangelands for sustainable utilization in Wadi El-Natroun area, Egypt. Symposium Taxnomy, Flora, Ecology and Application Aspects. Symposium Abstract.

[29] **Shehata, M., 2005**. Reliability analysis of the Wadi Al-Arish surface water supply system on the Sinai Peninsula, Egypt. Kuwait J. Sci. Eng. **32** (**1**): 175 - 194.

[30] **Spiegle, M. R., 1982**. Theory and problems of statistics. Mc-Graw Hill. New York. U. S. A.

[31] **Spjelkavik, S., 1995**. A satellite based map compared to a traditional vegetation map of arctic vegetation in the Ny-Iesund area, Svalbard. Polar Record. **31**: 257 – 269.

[32] **Sultan, M., Sturchio, N., Hassan, F. A. R., Mohamed, A. M., El-Alfy, Z. and Stein, T., 1997**. Precipitation source inferred from stable isotopic composition of Pleistocene groundwater and carbonate deposits in the Western Desert of Egypt. Quaternary Geology **4**: 29 - 37.

[33] **Täckholm, V., 1974**. Student's flora of Egypt. University of Cairo press, Cairo, 888 pp.

[34] **Tom, C. H. and Miller, L. E., 1994**. An automated land-use mapping comparison of the Bayesian maximum likelihood and linear discriminate analysis algorithms. Photogram. Eng. Remote Sens. **50**: 193 – 207.

European Journal of Scientific Research
ISSN 1450-216X Vol.18 No.3 (2007), pp.445-457

http://www.eurojournals.com/ejsr.htm

Ecophysiological and Chemical Studies on *Limoniastrum Monopetalum (L.) Boiss*

Hediat M. H. Salama
Botany Department, faculty of Science, Zagazig University, Egypt

Abstract

Salt marshes are widely distributed in the north western part of Egypt with their own distinct vegetation. Of these *Limoniastrum monopetalum* is characteristic of two sites; Burg El-Arab and Matruh of the Mediterranean Coastal salt marshes. Soil and plant samples were collected during March 2005. The present investigation deals with ecophysiological and chemical studies of the aerial parts of *Limoniastrum monopetalum* naturally growing at Burg El-Arab and Matruh habitats. These studies including the results of soil and plant analysis; moisture content, ash, minerals, carbohydrates and nitrogen fractions. The soil supporting *Limoniastrum monopetalum* in both habitats are poor in organic matter content. The moisture, ash, minerals of ash and the metabolic content, carbohydrates and nitrogen fractions were higher in plant samples of Matruh habitat than those from Burg El-Arab habitat. Concerning the chemical studies, two new flavonoid glycosides, 6,7 dihydroxy-5-methoxy-flavone 7-O-β-D- gluco pyranoside and 6, 7-dihydroxy-5-methoxy flavanone 7-O-β-D- gluco pyranoside, were isolated from the aerial parts of *Limoniastrum monopetalum*. The structures were established on the basis of acid hydrolysis to aglycone and sugar, UV, ^{1}H and ^{13}CNMR and FAB-mass spectra. The investigated plant have economic value (e. g. medicinal and fuel) and ecological value (e. g. sand accumulation, salt tolerant and windbreak).

Keywords: *Limoniastrum monopetalum*, salt marshes, soils, ecophysiology, carbohydrate, nitrogen, flavonoids

Introduction

Halophytes are highly specialized plants known to overcome the accumulation of salts in their tissues in different ways with or without a regulating mechanism (Chapman 1974). In a previous studies the autecology of *L. monopetalum* was studied by Batanouny and Abo Sitta (1977) as a first part of a series on the ecophysiology of halophytes in arid and semi-arid zones. In this species, they were studied the structure of salt glands, composition of excreted salts and the diurnal march of osmotic potential. The second part in this series, which was dealt with the ecophysiology of the salt excreting halophyt *Limonium delicatulum*, was also conducted by Batanouny *et al*. (1992). El-Shourbagy *et al*. (1989) studied the ecophysiology on the halophytes of the Mediterranean salt marshes, north Egypt. Salama and Ali (2003) demonstrated that variation in mineral ion composition of soil in salt marshes is not likely to be a limiting factor for the plant growth. The concentration of mineral elements in the soil reflects the abundance and distribution of plant species (Ben-Shahar and Coe 1992).

Plumbaginaceae is a moderate-sized group of shrubs, climbers or herbs (rarely) living in saline regions or cool alpine areas world-wide. This family consists of 27 genera and about 650 species.

Many of these are micro taxa of restricted distribution, mostly concentrated in tropical and subtropical Africa and Eurasia. In many saline areas, *Plumbaginaceae* are the dominant plants. *Plumbaginaceae* have plumbagin and proto anthocyanins (Dolores *et al*. 1998). Intensive studies of the flovonoids and related phenols in the *Plumbaginaceae* have been carried (Harborne 1964, 1967a, Thomson 1971).

Many substances that we use in our daily lives are plant products, numerous medicines were first isolated from species of seed plants and in extracts of these plants. Many of the drugs and flavorings that are now synthesized in laboratories were originally discovered from plants (Heneidy and Bidak 2004). *Limoniastrum monopetalum* was medicinal plant (Heneidy and Bidak (2004).

There fore, the objectives of this work were a) to study the ecophysiology of this plant and soils in two different habitats of salt marshes. b) to identify the flavonoid compounds in the aerial parts of this species. c) to point on ecological and economic values of *Limoniastrum monopetalum*.

Materials and Methods

The study area is characterized by a succession of small sand dunes and rocky surface dissected by several wadis toward the Mediterranean Sea (Abu Al-Izz 1971). In Burg El-Arab habitat, the chain of sand dunes is composed of solid oolitic limestone. Between each sand dune and other there are salty lagoons, and sometimes there is cultivable land. The surface of Matruh area is covered by a salty crust of white color. The coastal area of Matruh habitat is characterized by alternate appearance and disappearance of sand dunes and by the lines of saline lagoons. In both habitats, the *Limoniastrum monopetalum* distributed above the sand dunes and in some wadis between them.

Sample materials used in the present investigation were obtained from the aerial parts of *Limoniastrum monopetalum* plant naturally growing in salt marshes of Burg El-Arab and Matruh regions which lies between Latitudes 30º 00', 31º 00' N, and Longitudes 27º 00', 30º 00' E (Fig. 1). From each region, the soil samples were taken from the successive depths of 0 – 20 cm and 20 – 40 cm close to naturally growing plants by using a digging tool. These soil samples were air-dried and shaken in a set of sieves having a different mesh diameter from 2 mm to 0.063 mm, using a hydrometer method according to Day (1965).

Figure 1: Location map of Burg EI-Arab and Matruth habitats.

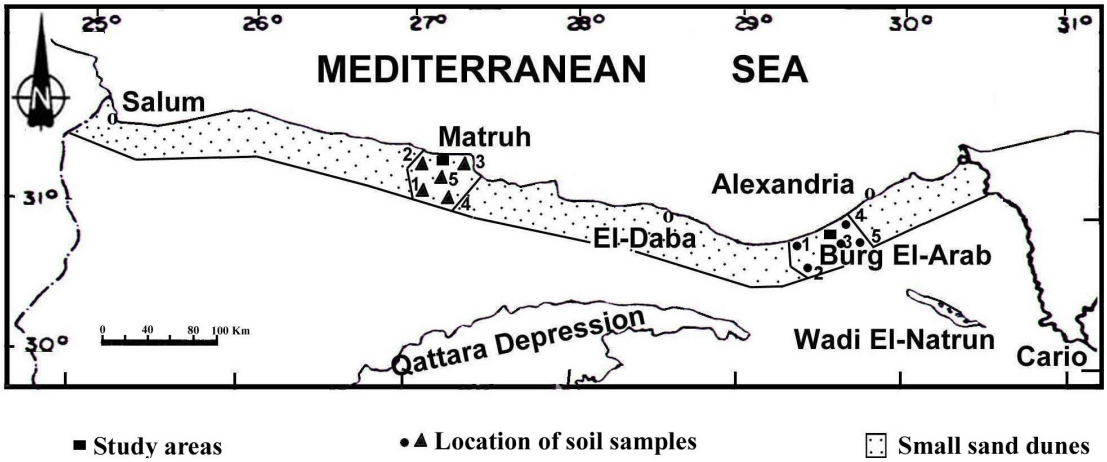

Soil-water extracts (1:5) were prepared. Determination of electrical conductivity (E. C.) was carried out by means of a direct indicating conductivity (mmhos/cm). Soil pH was determined with glass electrode pH-meter (Fresenius *et al*. 1988). The method described by Jackson (1962) was used for determination of the total soluble salts (T. S. S.) and calcium carbonate content. Soil organic matter was determined colorimetrically using the method described by Walinga *et al*. (1992). Chloride determination was carried out by using the $AgNO_3$ method according to Jackson and Thomas (1960). Sulfates were determined gravimetrically using $BaCl_2$, while carbonates and bicarbonates were

determined with 0.1 HCl using Ph. Ph. and methyl orange as indicators respectively. The nitrogen content was determined after Kjeldahl digestion. Soil and plant samples were acid digested (hydrochloric and nitric acids) before determination of cations concentrations by atomic absorption spectrophotometer (De Ruig 1986).

The air-dried aerial parts of *Limoniastrum monopetalum L*. (*Boiss*) were collected in March 2005 from plants growing wild in Burg El-Arab and Matruh of Mediterranean salt marshes. The plant material was subjected to the following analysis. The methods described by Ward and Johnson (1962) plant moisture content, ash content and elemental composition of the ash were analyzed. Analysis of carbohydrate content including extraction and estimation of total carbohydrate content, total and reducing sugars as well as polysaccharides was carried out using the methods described by Dubois *et al*. (1951) and Naguib (1964). The total nitrogen content as well as soluble and insoluble nitrogen were determined according to the methods described by Peach and Tracy (1956). Results obtained were treated statistically simple linear correlation coefficient (*r*). The variance ratio (VR) test and the two-way analysis of variance (ANOVA) were applied to Steel and Torie (1980) and Davis (1986).

TLC of glycosides and aglycones was carried out on silica gel 60 FG 254 aluminum sheets, the spots were visualized under UV light (365 nm) and by spraying with 1% $AlCl_3$ in EtOH. CC, polyamide and sephadex LH-20 were used; 1HNMR: 500, 360 and 250 MHz; ^{13}CNMR: 125, 90 and 62.5 MHz; FAB-mass spectra were obtained in the positive ion mode using lactic acid as solvent.

Extraction and isolation of flavonoids

The air-dried aerial parts (500 g) of *Limoniastrum monopetalum* was extracted with MeOH at room temperature for one week. The combined extracts were evaporated to dryness under reduced pressure, yielding a dark green residue (80 g). The concentrate was applied to a column of polyamide (400 g, 3x60 cm) followed by step wise elution with H_2O, 30% MeOH, 50% methanol, 70% methanol and methanol (250 ml for each). The eluates with 50% and 70% MeOH were combined and evaporated in vacuum to dryness. The residue (5.8 g) was dissolved in a small amount of 60% sephadex MeOH and applied to a CC of (500 g, 3 x 60 cm) and eluted with the same solvent. Four fractions (100 ml for each) were separately obtained and concentrated to a small volume. The compounds present in these fractions were purified by a combination of TLC on silica gell in pyridine – EtOAc – HOAc – H_2O (36 : 36 : 7 : 21v/v), and CC on silica gell (500 ml of 60% MeOH) to afford compound **1** (110 mg) and compound **2** (200 mg). Compound **1** is recrystallized from MeOH as yellow cubes and compound **2** as fine needles.

Acid hydrolysis

Samples were dissolved in a small amount of MeOH and hydrolyzed in 2N - HCl (10 ml) for 30 min. and aglycones liberated were extracted with EtOAc. The water layers were used for sugar analysis on TLC using pyridine-EtOAc-HOAc-H_2O (36 : 36 : 7 : 21 v/v). The nature of sugars was confirmed by comparison with anthentic samples by GC (Markham 1982).

Results

Physical properties of the soil

Soil texture

Results of granulometric analysis of the soil samples associated with the studied plant (Table 1) indicate that, the soil is medium in texture especially in the surface layer (0-20 cm) at Burg El-Arab and the bottom layer (20-40 cm) at Matruh. The main bulk of the soil samples was mixed sand in both habitats. The soils supporting the plant were loamy sand in the surface layer (0-20 cm) at Burg El-Arab and in the bottom layer (20-40 cm) at Matruh, and sandy loam in bottom layer (20-40 cm) at Burg El-

Arab and surface layer (0-20 cm) at Matruh. The granulometric analysis of the soil samples show that, the grain size is medium to fine sands contributed the major part of the soil in both habitats.

Table 1: Granulometric analysis of the soil supporting *Limoniastrum monopetalum* in the Burg El-Arab and Matruh habitats.

Habitats	Soil Depth (cm)	Soil texture	Granulometric analysis of the soil fraction (%)						
			Gravel > 2mm	Very coarse sand 2-1mm	Coarse sand 1-0.5 mm	Medium sand 0.5-0.25 mm	Fine sand 0.25-0.125mm	V.f. Sand 0.125-.063mm	Silt and clay<0.063
Burg El-Arab	0-20	Loamy sand	5.4	3.7	9.4	44.6	21.9	11.2	3.8
	20-40	Sandy loam	19.6	5.1	6.6	21.9	34.6	8.6	3.6
Matruh	0-20	Sandy loam	16.5	5.0	9.2	31.7	21.3	7.4	8.9
	20-40	Loamy sand	4.5	6.2	9.3	46.3	20.7	8.5	4.5

Soil moisture content

The data show that there was a general increase in soil moisture with increasing soil depth. The mean value of moisture content at Matruh is higher than at Burg El-Arab. The mean values of soil moisture content at Burg El-Arab were 13% and 15.1% in surface layer (0-20 cm) and bottom layer (20-40 cm) respectively, while these values were 15.1% and 18% in surface layer (0-20 cm) and bottom layer (20-40 cm) respectively, at Matruh (Table 2).

Table 2: Analysis of soil samples supporting Limoniastrum monopetalum in Burg El-Arab and Matruh habitats.

Habitats	Soil depth (cm)	Moisture content %	pH	E.C.	Organic matter (mg/g)	T.N. (mg/g)	T.S.S (%)	$CaCo_3$ (%)	Soluble anions (g %)				Soluble cations (g %)			
									CO_3^{2-}	HCO_3^-	Cl^-	SO_4^{2-}	Na^+	K^+	Ca^{2+}	Mg^{2+}
Burg El-Arab	0-20	13.0	7.6	2.6	0.16	0.06	0.07	9.7	0.0	0.12	0.14	0.13	0.83	1.40	1.93	2.60
	20-40	15.1	7.9	2.8	0.07	0.04	1.2	10.8	0.0	0.11	0.16	0.15	1.23	1.04	1.33	2.03
Matruh	0-20	15.1	8.0	4.9	0.23	0.14	0.09	13.3	0.0	0.40	0.15	0.16	3.40	3.70	2.04	4.10
	20-40	18.0	8.3	5.1	0.12	0.11	1.4	15.2	0.0	0.30	0.18	o.17	2.30	2.50	2.01	3.60
Correlation coefficient (r) in the Burg El-Arab									No	No	0.687	0.672	0.762	0.932	0.875	0.934
Significant									No	No	*	*	**	***	***	***
Correlation coefficient (r) in the Matruh									No	No	0.735	0.653	0.758	0.971	0.843	0.942
Significant									No	No	**	*	**	***	***	***

N.B.: No, not tested; * significant at P < 0.05; ** significant at P < 0.01; * significant at P < 0.001**

Chemical properties of the soil

Organic matter

The soil supporting *L. monopetalum* in Burg El-Arab and Matruh habitats was poor in organic matter content. It ranged between 0.16% and 0.23% in surface layer (0-20 cm) at Burg El-Arab and Matruh, respectively, and between 0.07% and 0.12% in bottom layer (20-40 cm) at Burg El-Arab and Matruh, respectively, (Table 2). Organic matter content was slightly higher at Matruh than Burg El-Arab. This study revealed that, the vertical distribution of organic matter in the soil profiles tested have shown that the organic matter content usually gradually decreases with depth. Regarding soil reaction, the pH value of soil samples ranged between 7.6 and 7.9 at Burg El-Arab and between 8.0 and 8.3 at Matruh. These results indicate that the soils in the two habitats are moderately alkaline. Electrical conductivity (E. C.) ranged between 2.6 and 2.8 mmhos/cm at Burg El-Arab, while at Matruh, it ranged between 4.9 and 5.1 mmhos/cm (Table 2). The total nitrogen content of the soils was higher in the Matruh habitat than Burg El-Arab habitat. This may be due to the denser vegetation and the incorporation of decomposed plants (Table 2).

Total soluble salts (T. S. S.)

The data in table 2 shows that, the concentration of total soluble salts (T. S. S.) in the soil samples supporting the *L. monopetalum* in the two habitats were relatively low, ranging from 0.07% to 1.2% at Burg El-Arab and between 0.09% and 1.4% at Matruh.

Calcium carbonate

The percentages of calcium carbonate were higher at Matruh than Burg El-Arab (Table 2). Their values ranged from 13.3% to 15.2% in the examined two profiles of Matruh habitat. In Burg El-Arab habitat the value ranged from 9.7% to 10.8%.

Anions content

The anions content of the soil samples collected from the two habitats were relatively low (Table 2). The highest value of HCO_3^- (0.4%) was recorded at Matruh, while the lowest value (0.11%) was recorded at Burg El-Arab. On the other hand, all examined soil samples were free from carbonates. The value of chloride content ranges between 0.14% and 0.16% in the two profiles at Burg El-Arab and between 0.15% and 0.18% in the two profiles at Matruh. The sulfate content of Matruh habitat were higher than those at Burg El-Arab. Their value varied from 0.16% to 0.17% in the two profiles at Matruh and from 0.13% to 0.15% in the two profiles at Burg El-Arab.

Cations content

Magnesium content form the major component of the soil in the two habitats and its ion concentration was relatively high. It ranged between 2.03% and 2.6% at Burg El-Arab and between 3.6% to 4.1% at Matruh habitat (Table 2). Calcium content form the second major component of the soil after Mg^{+2} ion, its ion concentration in soil samples supporting *L. monopetalum* at the two studied areas was relatively high (between 1.33% and 1.93% at Burg El-Arab and between 2.01% and 2.04% at Matruh as shown in table 2. Sodium ion ranges between 0.83% and 1.23% at Burg El-Arab and between 2.3% and 3.4% at Matruh habitat. Potassium ion ranges between 1.04% and 1.4% at Burg El-Arab and between 2.5% and 3.7% at Matruh habitat.

Plant analysis

Moisture content

The moisture content of aerial parts of *L. monopetalum* varies in the two habitats. The highest value (38.8%) was recorded at Matruh, while the lowest value (37%) was recorded at Burg El-Arab (Table 3).

Ash content

From table 3 it is clear that the values of the ash content of *L. monopetalum* varies in the two habitats. The highest value (27.4%) was recorded at Matruh, while the lowest value (26.6%) was recorded at Burg El-Arab.

Elemental composition of ash

Data displayed in table 3 showed remarkable variation in ions content of the aerial parts of L. *monopetalum*. These indicate that, the Ca^{+2} is the prominent cation in the ash content of *L. monopetalum*, its values ranged from 7.6% at Burg El-Arab to 9.1% at Matruh habitat. The least represented cation was potassium, its values varied from 0.9% at Matruh to 1.1% at Burg El-Arab habitat. The values of Na+ ranged from 4.5% for plants collected from Burg El-Arab to 8.8% for plants collected from Matruh habitat. Magnesium reached its maximum value of 1.5% at Matruh and 1.1% at Burg El-Arab habitat.

Table 3: Moisture, ash content and elemental composition of aerial parts of *Limoniastrum monopetalum* naturally growing in Burg El-Arab and Matruh habitats.

Habitats	Moisture (%)	Ash (%)	Elemental composition of ash (g%)			
			Na^{+}	K^{+}	Ca^{+2}	Mg^{+2}
Burg El-Arab	37	26.6	4.5	1.1	7.6	1.1
Matruh	38.8	27.4	8.8	0.9	9.1	1.5
Correlation coefficient (r) in Burg El-Arab	0.687	0.927	0.892	0.946		
Significant	*	***	***	***		
Correlation coefficient (r) in Matruh	0.786	0.932	0.842	0.961		
Significant	**	***	***	***		

N.B.: * significant at P < 0.05; ** significant at P < 0.01; * significant at P < 0.001**

Carbohydrate contents

From the results obtained in table 4 it is apparent that the values of total carbohydrates reached the value of 96.5 mg/g in plants collected from Burg El-Arab, and 106.9 mg/g in plants collected from Matruh habitat.

Direct reducing value (D. R. V.)

The values of reducing sugars ranged from 10.5 mg/g in plants collected from Burg El-Arab to 12.3 mg/g in plants collected from Matruh habitat (Table 4). The total reducing values and polysaccharides in the aerial parts of *L. monopetalum* showed marked variations among the two habitats. The results obtained in table 4 indicated that, the values of total reducing value and polysaccharides were greater in the plant collected from Matruh habitat than those collected from Burg El-Arab habitat. The total sugar content reached its maximum values of 24.4 mg/g at Matruh and 22.1 mg/g at Burg El-Arab habitat. It is evident also that maximum values of polysaccharide content was attained in Matruh being 71.2 mg/g, the lowest values were obtained in Burg El-Arab being 66.4 mg/g.

Table 4: Analysis of carbohydrates of the aerial parts *of limoniastrum monopetalum* naturally growing in Burg El-Arab and Matruh habitats.

Habitats	Carbohydrate contents (mg/g) dry weight			
	Total carbohydrate	D. R. V.	T. R. V.	P. S.
Burg El-Arab	96.5	10.5	22.1	66.4
Matruh	106.9	12.3	24.4	71.2
Correlation coefficient (r) in Burg El-Arab	0.687	0.853	0.902	0.742
Significant	*	***	***	**
Correlation coefficient (r) in Matruh	0.792	0.764	0.831	0.751
Significant	**	**	***	**

N.B.: * significant at P < 0.05; ** significant at P < 0.01; * significant at P < 0.001**

Nitrogen contents

The changes in nitrogen content of aerial parts of *L. monopetalum* growing in the two habitats are presented in table 5. The results obtained show that the total nitrogen, soluble nitrogen and insoluble nitrogen contents reached their maximum values in plants growing in Matruh habitat, being 20.1, 3.75 and 17.1 mg/g respectively. In the plants collected from Burg El-Arab habitat their values are relatively lower, being 15.6, 1.8 and 13.7 mg/g respectively.

Table 5: Analysis of nitrogen contents of the aerial parts of *Limoniastrum monopetalum* naturally growing in Burg El-Arab and Matruh habitats.

Habitats	Nitrogen contents (mg/g) dry weight		
	Total nitrogen	Soluble nitrogen	Insoluble nitrogen
Burg El-Arab	15.6	1.8	13.7
Matruh	20.1	3.75	17.1
Correlation coefficient (r) in Burg El-Arab	0.735	0.932	0.785
Significant	**	***	**
Correlation coefficient (r) in Matruh	0.694	0.872	0.681
Significant	*	***	*

N.B.: * significant at P < 0.05; ** significant at P < 0.01; * significant at P < 0.001**

Identification of flavonoids

6, 7 Dihydroxy -5- methoxyflavone 7-O-β-D- glucopyranoside (**1**). Light yellow cubes, C_{22} H_{22} O_{10} (Fig. 2), mp. 156-158º MeOH. TLC (polyamide): MeOH-H2O (2:1) R_f 0.81. UV λ_{max}^{MeOH} nm (log ε) : 240, (4.02), 270 (4.32), 306 (4.17); + NaOMe: 268, 291, 396; + $AlCl_3$: 240, 270, 306; + $AlCl_3$ + HCl : 240, 270, 306; + NaOAc : 269, 293, 394; + NaOAc + H_3BO_3 : 270, 307. FABMS m/z 447 $(M+1)^+$, 285 $(M+1\text{-Glc})^+$, 270 $(285\text{-Me})^+$.

^{1}HNMR (500 MHz, DMSO-d_6); aglycone moiety, 8.87 (1H, s, OH-6), 8.04 (2H, dd, J = 8.1, 1.6 Hz, H-2$^/$ and H-6$^/$), 7.58 (3H,m, H-3$^/$, H-4$^/$ and H-5$^/$), 7.31 (1H, s, H-8), 6.79 (1H, s, H-3), 3.80 (3H, s, OMe-5); glucosyl moiety, assigned by C-H correlation spectrum, 5.45 (1H, d, J = 4.1 Hz, OH-2$^{//}$), 5.19 (1H, d, J = 4.7 Hz, OH-3$^{//}$), 5.14 (1H, d, J = 5.3 Hz, OH-4$^{//}$), 5.10 (1H, d, J = 7.3 Hz, H-1$^{//}$), 4.71 (1H, t, J = 5.6 Hz, OH-6$^{//}$), 3.78 (1H, m, H-6$^{//}$), 3.53 (2H, m, H-6$^{//}$ and H-3$^{//}$), 3.39 (1H, m, H-2$^{//}$), 3.37 (1H, m, H-5$^{//}$) and 3.24 (1H, m, H-4$^{//}$). ^{13}CNMR (125 Hz, DMSO-d_6) displayed in table 6.

6,7-Dihydroxy-5-methoxyflavanone 7-O-β-D- glucopyranoside (**2**). Fine needles, $C_{22}H_{24}O_{10}$ (Fig. 2), mp. 213-215º. TLC (polyamide): MeOH-H_2O) (2:1), R_f 0.9. UV λ_{max}^{MeOH} nm (Log ε): 236 (4.27), 274 (4.14), 345 (3.71); + NaOMe: 256, 287, 393; +$AlCl_3$: 236, 274, 345; + $AlCl_3$ + HCl : 236, 274, 345; + NaOAc : 257, 277 sh, 352 sh, 398; + NaOAc + H_3BO_3 : 276, 348. FABMS m/z : 449 $[M+1]^+$ (5), 287 $[M+1\text{-Glc}]^+$ (100), 286 (7), 271 (5), 257 (6), 183 (14).

^{1}HNMR (500 MHz, DMSO-d_6) : aglycone moiety 8.27 (1H, s, OH-6), 7.51 (2H, br d, J = 7.2 Hz, H-2$^/$ and H-6$^/$), 7.42 (2H, br t, J = 7.3 Hz, H-3$^/$ and H-5$^/$), 7.37 (1H, br t, J = 7.2 Hz, H-4$^/$), 6.59 (1H, s, H-8), 5.50 (1H, dd, J = 2.9, 12.9 Hz, H-2), 3.73 (3H, s, OMe-5), 3.08 (1H, dd, J = 16.6, 12.9 Hz, H-3) and 2.68 (1H, dd, J = 2.9, 16.6 Hz, H-3); [glucosyl moiety] 5.35 (1H, d, J = 3.5 Hz, OH-2$^{//}$), 5.11 (1H, d, J = 4.5 Hz, OH-3$^{//}$), 5.05 (1H, d, J = 5.3 Hz, OH-4$^{//}$), 4.93 (1H, d, J = 7.2 Hz, H-1$^{//}$), 4.56 (1H, t, J = 5.5 Hz, OH-6$^{//}$), 3.68 (1H, m, H-6$^{//}$), 3.38 – 3.46 (2H, m, H-6$^{//}$ and H-3$^{//}$), 3.27 – 3.34 (2H, m, H-2$^{//}$ and H-5$^{//}$), 3.16 (1H, m, H-4$^{//}$). ^{13}CNMR (62.5 MHz, DMSO –d_6) as shown in table 6.

Figure 2: Structure of compounds 1 and 2.

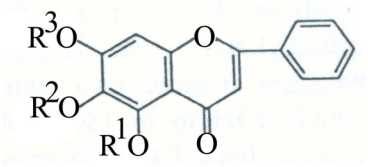

	R^1	R^2	R^3
Compound 1	Me	H	Glc

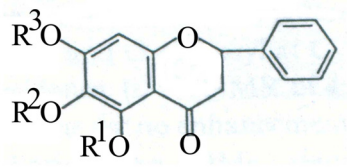

	R^1	R^2	R^3
Compound 2	Me	H	Glc

Table 6: ^{13}CNMR spectral data of compounds 1 and 2 (δ ppm)

C	1	2
2	160.2	78.4
3	107.3	44.9
4	175.9	188.9
5	144.6	147.0
6	137.6	134.6
7	150.3	155.2
8	99.8	99.1
9	150.5	152.0
10	113.0	109.7
$1^{/}$	131.0	139.0
$2^{/}$, $6^{/}$	125.9	126.5
$3^{/}$, $5^{/}$	129.0	128.4
$4^{/}$	131.3	128.4
$1^{//}$	100.5	100.3
$2^{//}$	73.1	73.0
$3^{//}$	75.9	75.7
$4^{//}$	69.6	69.5
$5^{//}$	77.3	77.1
$6^{//}$	60.6	60.5
OMe – 5	61.0	60.2
OMe – 6	--	--
OMe – 7	--	--

Discussion

A large spatial heterogeneity was found in the chemical composition of soils and plant considering the two habitats studied. Soils supporting plant in Matruh habitat showed the highest concentrations for all elements analyzed. The soil associated with the plant is loamy sand at surface layer at Burg El-arab and sandy loam at Matruh, while at bottom layer it was sandy loam in Burg El-Arab and loamy sand in Matruh habitat. It was noticed that in the two habitats, the mean value of soil moisture content increased with increasing depth. Shalaby *et al*. (1981) reported that in desert soils below a certain depth

there was a permanently wet layer so as to supply deep rooted perennials with available water all the year round. These results are also in agreement with Salama and Ali (2003).

The pH values were all alkaline in both habitats with range of 7.6 and 7.9 in the soil from Burg El-Arab region and 8.0 to 8.3 in the soil from Matruh region. The soil pH reflects the calcium carbonate contents. The pH were alkaline in Matruh soils ranging from 8.0 to 8.3 respectively which exhibited the highest concentration of calcium carbonate 13.3% and 15.2% respectively. On the other hand Burg El-Arab soils showed slightly alkaline (pH 7.6 and 7.9) contained the least amount of calcium carbonate 9.7% and 10.8% respectively. These results agree with Al-Falih (2001).

All soil samples in the two habitats contained a low percentage of organic matter (Table 2). The concentration of total soluble salts (T. S. S.) in soil samples supporting *L. monopetalum* in both localities were relatively low and varied within a narrow range, from 0.07% to 1.2% at Burg El-Arab and between 0.09% to 1.4% at Matruh habitat. The sulfate content in soil samples in the two studied areas showed that the lower values were detected in Burg El-Arab habitat. Soluble carbonates were not detected in the two habitats, while bicarbonates content fluctuated within a narrow range, it ranges between 0.3% and 0.4% as maximum values and between 0.11% and 0.12% as its minimum values at Matruh and Burg El-Arab habitat, respectively. Na^{+}, K^{+}, Ca^{+2} and Mg^{+2} concentrations were higher in soil samples of Matruh habitat than in Burg El-Arab habitat. Mg^{+2} is the major element followed by Ca^{+2} in both habitats.

The data obtained from plant analysis show fluctuation in different constituents in response to habitat conditions. The plant moisture content showed that the relatively higher percentage in the Matruh habitat as compared with Burg El-Arab habitat, this may be due to the high soil moisture content of the Matruh habitat and the presence of compact surface layer which minimize the rate of evaporation. The percentage and composition of ash showed a noticeable variation in the two habitats. The present investigation indicated that the highest percentage of ash content was attained in plant samples collected from Matruh being 27.4% and the lowest percentage was attained from plant samples collected from Burg El-Arab being 26.6%. Analysis of the ash content revealed higher concentration of calcium in plants of the two habitats, which may be due to the effect of nature of soil texture on the release and availability of ions. Other elements also showed fluctuation in the two habitats.

Results obtained from investigation of carbohydrate contents indicated changes in carbohydrate fractions in response to habitat conditions. Total carbohydrate content showed higher concentrations in plants of Matruh habitat than those of the plants of Burg El-Arab habitat. The total reducing sugars and polysaccharides recorded in the plants collected from Matruh habitat was much higher than those collected from Burg El-Arab habitat. The values of different nitrogen constituents in the plant samples collected from the two habitats were fluctuated. The higher values of total nitrogen, soluble nitrogen and insoluble nitrogen were reported from plants of Matruh habitat this may be due to the higher percentage of organic carbon as well as calcium contents in the soil of this habitat.

Concerning the flavonoid content, two new flavonoid compounds, 6,7-dihydroxy-5-methoxyflavone 7-O-β-D-glucopyranoside and 6-7-dihydroxy-5-methoxyflavanone 7-O-β-D-glycopyranoside were isolated from aerial parts of *Limoniastrum monopetalum* naturally growing at Matruh and Burg El-Arab habitats. A survey of fifty-five species of genera of the family Plumbaginaceae has been carried out by Harborne (1967a), revealing the presence of flavonoids, e. g. quercetin -3- rhamnoside, myricetin -3- rhamnoside, europetin, annulatin and azaleatin. Other flavonoids, liteolin, apigenin, isoorientin and quercitrin were isolated from *L. bonduelli* (Asen and Plimmer 1972).

Spectral data for compound **1** indicated it to be a flavone with three substituents in the A-ring and none in the B-ring. The three substituents in compound **1** were identified as OMe (δ 3.80), OH (δ 8.87) and OR (R = sugar). The moiety was determined to be β – D – glucose by ^{13}CNMR and by acid hydrolysis. Therefore, the ^{1}HNMR signals at δ 7.31 and δ 6.79 of compound **1** are assigned to H-8 and H-3, respectively. The assignment of substituents to sites 5,6 and 7 was carried out as follows. The hydroxyl group in compound **1** was clearly not sited at C-5 as no $AlCl_3$. HCl shift was observed in the

absorption spectrum. Accordingly, the hydroxyl group is assigned to C-6. The methoxyl is considered to be sited at C-5 rather than C-7 (Mabry *et al*. 1970). The ^{13}CNMR spectrum also supported the presence of a OMe-5 in that the C-4 resonance appeared at δ 175.9, and the methoxyl signal at δ 61.0. Markham *et al*. (1987) together these data define compound **1** as 6,7-dihydroxy-5-methoxy flavone 7-O-β-D-glucopyranoside. FAB mass spectrum of compound **1** gave a $(M + 1)^+$ at m/z 447 which was in accord with a flavone.

Compound **2** exhibited typical ^{1}H and ^{13}CNMR signals for flavanone: an 1HNMR was observed for H-3 and H-2, and ^{13}CNMR signals at δ 78.4 and 44.9 were representative of C-2 and C-3 respectively (Table 6). As with compound **1**, compound **2** was also found to have an unsubstituted B-ring and three A-ring substituents: OMe (δ 3.73), OH (δ 8.27) and O-glucosyl. The FAB mass spectrum of compound **2** gave a $(M + 1)^+$ at m/z 449, which was in accord with a flavanone containing these substituents. Compound **2** has the same substitution pattern as compound **1**, i. e. OMe at C-5, OH at C-6 and O-glucosyl at C-7 on the basis of the following evidence: ^{1}HNMR of compound **2** OH-6 at δ 8.27, the OMe signal (δ 3.73) and ^{13}CNMR of compound **2**: δ 60.2 for a C-5 OMe. Accordingly the structure 6,7 dihydroxy-5-methoxy 7-O-β-D- glucopyranoside is assigned to compound **2** (Markham 1982).

Economic and ecological values

In countries having large area of deserts, like Egypt, the limited number of species, whose habitats are generally at risk, is better reason for enumeration, description and conservation. This is because desert plants are hardly and have developed over millennia adaptational mechanisms, including the production of a host of secondary metabolites, to protect themselves from physical and biotic aggressions. These metabolites are the stuff of the medicinal uses of these plants. Conservation of desert plants for medicinal uses is therefore a must and requires a through knowledge of their morphology, taxonomy, ecology, physiology and biochemistry (Boulos 1995).

The economic values of *Limoniastrum monopetalum* are classified as medicinal, aromatic, forage, edible or as fuel. *L. monopetalum* have a medicinal values as extracted or direct herb. Also, this species are edible by human and birds, are aromatic sources and used as fuel wood in arid and semi-arid region. Alternative sources of fuel or firewood reserves are usually available for the established urban area, but there is need for stronger awareness of the requirements of smaller settlements. On the other hand, the ecological values of *L. monopetalum* include sand accumulation, salty tolerant and windbreak. It also serves as refuge for some plant species. this may be conceive the biodiversity of the species and for water storage.

References

[1] **Abu Al-Izz, M. 1971**. Landforms of Egypt. 1st Eds. The American University in Cairo press, Cairo, Egypt, pp 281.

[2] **Al-Falih, A. M. 2001**. Estimation of available phosphorus in agricultural soils of Saudi Arabia. Kuwait J. Sci. Eng. **28** (**2**): 371 – 380.

[3] **Asen, S. and Plimmer, J. R. 1972**. Flavonoids from *Limoniastrum bonduell*. Phytochemistry, **11**(**2001**).

[4] **Batanouny, K. H. and Abo Sitta, Y. M. 1977**. Ecophysiological studies on halophytes in arid and semi-arid zones. I – Autecology of the salt-secreting halophyte *Limoniastrum monopetalum* (*L*.) Boiss. Acta Bot. Sci. Hung. **23** (**13**).

[5] **Batanouny, K. H., Hasson, A. H. and Fahmy, G. M. 1992**. Eco-physiological studies on halophytes in arid and semi-arid zones. II- Eco-physiology of *Limonium delicatulum* (GIR.) KTZE. Flora, 186(**105**).

[6] **Ben-Shahar, R. and Coe, M. J. 1992**. The relationship between soil factors, grass nutrients and the foraging behaviour of wild-ebeest and Zebra. Oecologia **90** (**3**): 422 – 428.

[7] **Boulos, L. 1995.** Flora of Egypt. Al Hadara Publishing, Cairo, Egypt. PP: 286.

[8] **Chapman, V. J. 1974**. Salt marshes and salt deserts of the world. J. Cramer, Lehr, Germany.

[9] **Davis, J. C., 1986**. Statistics and data analysis in geology. (2nd Ed), Wiley and Sons, New York, NY, U. S. A. pp. 635.

[10] **Day, P. R. 1965**. Particle fractionation and particle size analysis. In: **Black, C. A.** (**Ed**). Methods of soil analysis. American Society of Agronomy, Madison, Wisconsin, U. S. A.

[11] **De Ruig, W. G. 1986**. Atomic absorption spectrometric determination of calcium, copper, iron, magnesium, manganese, potassium, sodium and zinc in animal feeding stuffs: Inter – laboratory collaborative studies. J. Ao. Ac. **69** (**6**): 1009 – 1013.

[12] **Dolores, M., Manuel, B., Kenneth, M. and Michael, F. 1998**. Systematics of plumbaginaceae based upon cladistic analysis of rbcl sequence data. Systematic Botany, **23** (**1**): 21 – 29.

[13] **Dubois, M., Gilles, K. A., Hamilton, J. K., Robers, P. A. and Smith, F. 1951**. Determination of sugars. Nature, **168** (**167**).

[14] **El-Shourbagy, M. N., Ahmed, A. M., Osman, M. E. and Hamada, E. A. 1989**. Ecophysiological studies on the halophytes of the Mediterranean salt marshes, north Egypt. I-Osmotic and mineral patterns in succulent and non succulent species. Desert Inst. Bull., **39**: 449 – 482.

[15] **Fresenius, W., Quentin, K. E. and Schneider, W. 1988**. Water analysis. A practical guide to physico-chemical, chemical and microbiological water examination and quality assurance. Springer Verlag, Berlin, Heidelberg, Germany.

[16] **Harborne, J. B. 1964**. Biochemistry of phenolic compounds. Academic press, London, U. K.

[17] **Harborne, J. B. 1967a**. Comparative biochemistry of the flavonoids. Academic press, London, U. K.

[18] **Heneidy, S. Z. and Bidak, L. M. 2004**. Potential uses of plant species of the coastal Mediterranean region, Egypt. Pakistan Journal of Biological Sciences, **7** (**6**): 1010 – 1023.

[19] **Jackson, M. L. 1962**. Soil and plant analysis, constable , Co. London, U. K.

[20] **Jackson, W. A. and Thomas, G. W. 1960**. Effect of KCl and dolomitic limestone on growth and ion uptake of sweet potato. Soil Sci., **89**: 347 – 352.

[21] **Mabry, T. J., Markham, K. R. and Thomas, M. P. 1970**. The systematic identification of flavonoids. Springer, Berlin. Germany.

[22] **Markham, K. R. 1982**. Techniques of flavonoid identification. Academic press, London, U. K.

[23] **Markham, K. R., White house, L. A. and Webby, R. F. 1987**. Journal of Natural Products, **50** (**660**).

[24] **Naguib, M. I. 1964**. Colourimetric estimation of plant polysaccharides. Zucker, **160**: 15 – 18.

[25] **Peach, K. and Tracey, M. V. 1956**. Modern methods of plant analysis. Vol. **1**, Springer Verlag, Berlin.

[26] **Salama, H. M. and Ali, A. A. 2003**. Variations in mineral ion composition of soil and some halophytes in the Mediterranean coastal north of Egypt. J. of Envi. Sciences, **26** (**1**): 207 – 228.

[27] **Shalaby, A. F., El Monayeri, M. O., Youssef, M. M. and El-Ghamry, A. A. 1981**. Phytochemical studies on two Zygophyllum species grown in the Egyptian desert. J. Fac. Sci., Riyad Univ., **13** (**2**): 175 – 192.

[28] **Steel, R. G. D. and Torie, J. H. 1980**. Principles and procedures of statistics. McGrow-Hill Book Co. Inc., New York, London.

[29] **Thomson, R. H. 1971**. Naturally occurring quinones. (2nd Ed). Academic press, London, U. K.

[30] **Walinga, I., Kithome, M., Novozamsky, L., Houba, V. J. G. and Van Der Lee, J. J. 1992**. Spectrophotometric determination of organic carbon in soil. Community of Soil Science and Plant Analysis, **33** (**16**): 1935 – 1944.

[31] **Ward, G. M. and Johnson, F. B. 1962**. Chemical methods of plant analysis. Canada Dept. Agric., **10**: 1 -59.

European Journal of Scientific Research
ISSN 1450-216X Vol.18 No.3 (2007), pp.458-463

http://www.eurojournals.com/ejsr.htm

Study of the Acute Effects of Different Doses of *Azadiracta Indica* (Neem) Seed Extract on Blood Glucose Levels of Streptozocin – Diabetic Wistar Rats

M.A.M. Okasha
Department of Human Physiology, Faculty of Medicine, A.B.U, Zaria

Y. Tanko
Department of Human Physiology, Faculty of Medicine, A.B.U, Zaria

A. Mohammed
Department of Human Physiology, Faculty of Medicine, A.B.U, Zaria
E-mail: amohd177@hotmail.com

A. Abdul-Mottaleb
Department of Human Physiology, Faculty of Medicine, Al-Azhar University, Cairo

Abstract

The treatment of insulin-dependent diabetes mellitus has been a great challenge, especially in developing countries. Thus the need for plant based substitutes to overcome this problem. The influence of varying doses (500, 1000 and 1500mg/kg B.w.) of petroleum ether extract of *Azadiracta Indica* (Neem) seed on streptozocin - diabetic Wistar rats was studied. The dose of 500mg/kg B.W., when administered to streptozocin – diabetic rats, produced an appreciable hypoglycemic effect similar to that produced by insulin in streptozocin - diabetic group. As regards the other two doses of the extract, the dose of 1000mg/kg B.W. produced a significant reduction of blood glucose level only after 3 and 5 hours of administration, while the last biggest dose (1500mg/kg B.W.) did not show any significant differences as compared to streptozotocin – diabetic group. Thus, it is safer for diabetics to use the smallest dose of the extract as anti-diabetic regimen.

Keywords: *Azadiracta Indica*; Blood glucose; Streptozotocin.

Introduction

Diabetes Mellitus is a syndrome of impaired carbohydrate, fat and protein metabolism caused by either lack of insulin secretion or decreased sensitivity of the tissue to insulin (Guyton and Hall, 2005). Greek and Roman physicians used the term “diabetes” to refer to condition in which the cardinal finding was a large urine volume. Two types were distinguished: “diabetes mellitus”, in which the urine tasted sweet, and “diabetes insipidus”, in which the urine had little taste. Today, the unmodified word “diabetes” is generally used as a synonym for diabetes mellitus. Diabetes is characterized by polyuria, polydipsia, weight loss in spite of polyphagia, hyperglycemia, glucosuria, ketosis, acidosis, and coma (Ganong, 2005). The fundamental defects to which most of the abnormalities can be traced are: (1)

reduced entry of glucose into various" peripheral" tissues and (2) increased liberation of glucose into the circulation from the liver (Kulkarni and Kahn, 2004). Therefore, there is an extracellular glucose excess and, in many cells, an intracellular glucose deficiency - a situation that has been called "starvation in the midst of plenty". Also, the entry of amino acids into the muscle is decreased and lipolysis is increased (Ganong, 2005).

The plant *Azadiracta Indica* belongs to the family Maliaceace.It is commonly referred to in many countries as the "Neem Tree" (Mann, 1990). The tree produces ellipsoidal fruits about 2 cm in length each and are arranged in axillary clusters. The fruits contain kernels that have high concentration of serious metabolites (National Research Council, 1992). *Azadiracta Indica* seed contains many chemical compounds including tannins, alkaloids, flavonoids, glycerin, steroids, cholesterol and terpenoids (Marles and Farnsworth, 1995; Ojewole, 2003). A number of investigators have shown that flavonoids and a host of other secondary plant metabolites including arginine and glutamic acid possess hypoglycemic effect in various animal models (Akah and Okafor, 1992; Ojewole, 2002).

The present study aimed to throw some lights on the acute effects of *Azadiracta Indica* seed extract on blood glucose level of diabetic rats.

Materials and Methods

(A) Plant material

Fresh samples of *Azadiracta Indica* seeds were obtained from the Botanical garden of Ahmadu Bello University, Zaria, Nigeria. Identification of the seeds was done in the herbarium section of the department of Biological Sciences, ABU, Zaria by the herbarium keeper (Mallam Musa Mohammed) and was given a batch voucher number 900151. The seeds were washed thoroughly by running clean water, dried by air, then pilled from the covering shell and kernels were exposed .Then the kernels were ground and transferred to the Pharmacognosy laboratory for extraction of the neem seed oil. The extraction was carried out by the aid of a soxhlet extractor machine (Electromantle, EX5/ 75, Quickfit, England) using petroleum ether under temperature ranging between 60-80ºC to help removing oil from the pounded seed kernel. Then, the components of the mixture of petroleum ether and neem oil were separated by separating funnel since they were immiscible (Harborne, 1998).

(B) Chemicals

Streptozotocin (Sigma).

Biphasic isophane insulin as mixtard (Novo Nordisk, Denmark)

(C) Animals

Wistar albino rats of both sexes weighing between 120 and 150 grams were used in this study. The animals were housed under similar conditions in standard cages in environmentally controlled room at 25 ± 2ºC, 12-h light/dark cycle in the animal house, Department of Human Physiology, Ahmadu Bello University, Zaria. The animals were allowed commercial food with tap water *ad libitum*. The animals were deprived of food for 12 hours before the commencement of the experiment but allowed free access to water (Rao and Rao, 2001).

(D) Experimental design

The experimental animals were divided into the following categories:

(1) Control group:

It consisted of 5 rats which received only saline.

(2) Normoglycemic extract – treated group:

It included 15 rats which received extract in doses of 500, 1000 and 1500 mg/kg B.W. intraperitoneal, five rats for each dose.

(3) Normoglycemic insulin – treated group:

Five rats which received biphasic isophane insulin 6 i.u. /kg B.W.subcutaneously (Stanley *et al*., 1997).

(4) Streptozotocin – diabetic group:

25 rats received streptozotocin 60 mg/kg B.W. in 0.1 M citrate buffer (pH 4.5) in a volume of 1 ml/kg as a single intraperitoneal (i.p.) dose. The animals were subdivided into:

- 5 rats as streptozotocin – diabetics.
- 5 rats received biphasic isophane insulin 6 i.u. / kg B.W. subcutaneously.
- 15 rats received extract in a dose of 500, 1000 and 1500 mg/kg B.W.i.p., 5 rats for each dose.

(E) Induction of Diabetes

Diabetes was induced in the experimental animals by injecting streptozotocin 60mg/kg B.W. in 0.1 M citrate buffer (pH 4.5) in a volume of 1 ml/kg as a single intraperitoneal dose. Three days later, the rats showed a blood glucose level range of 150-230 mg/dl which was considered to be diabetic (Stanely and Venugopal, 2001). Blood samples for estimation of blood glucose level were collected by the end of the 12 hours fasting as zero(0) hour level then after 1, 3, 5 and 7 hours of administration of the test drugs (Rao and Rao, 2001).

(F) Statistical analysis

The mean and standard error of mean (SEM) of blood glucose levels for all test groups at each point in time were obtained and statistical significance between the treated groups and the control group was determined using ANOVA. Data were considered significant by different at $p< 0.05$.

Results

Acute toxicity studies of the extract of *Azadiracta Indica* seed revealed that the LD_{50}, according to the method of Lorke (1983), was 3000mg/kg .B.W. i.p.

The influence of *Azadiracta Indica* seed extract in three different doses (500, 1000 and 1500mg/kg B.W.) on blood glucose level was studied in normoglycemic and streptozotocin diabetic rats. The first two doses of the extract (500 and 1000mg/kg B.W.) produced marked decrease in blood glucose level of normoglycemic rats after 3,5 and 7 hours and after 5 and 7 hours respectively compared to control group as shown in table (1).

Table 1: Showing the blood glucose levels (mg/dl) of control group and *Azadiracta Indica* seed extract – treated normoglycemic rats.

Groups / Time (Hours)	Control group	*Azadiracta Indica* seed extract – treated normoglycemic rats		
		(500mg/kg)	(1000mg/kg)	¬(1500mg/kg)
0	47.0±2.50	49.4±6.32	56.0±4.82	48.8±3.91
1	49.8±2.70	45.4 ± 6.32^{ns}	56.2 ± 5.13^{ns}	46.2 ± 5.87^{ns}
3	47.4±1.88	38.6 ± 4.16^{a}	38.8 ± 1.49^{ns}	45.0 ± 2.16^{ns}
5	46.4±2.56	38.6 ± 2.48^{a}	36.4 ± 3.44^{a}	45.2 ± 2.67^{ns}
7	49.2±3.20	33.6 ± 2.88^{a}	34.2 ± 2.88^{a}	42.0 ± 2.91^{ns}

-Values are expressed as mean ± standard mean of error.

- ^{a} = $P < 0.05$
- ^{ns} = non significant.

As regards the normoglycemic rats, their blood glucose level showed significant decrease after administration of insulin as compared to the effect of the different doses of the extract specially after 3,5 and 7 hours from the administration as shown in table (2). This means that both of insulin and the extract had produced a significant decrease of blood glucose level as compared to control group but that produced by insulin even showed marked decrease in blood glucose level as compared to that produced by the extract.

Table 2: Showing the blood glucose levels (mg/dl) of biphasic insulin – treated normoglycemic group and *Azadiracta Indica* seed extract – treated normoglycemic rats.

Groups / Time (Hours)	Insulin – treated Normoglycemic group	*Azadiracta Indica* seed extract – treated normoglycemic rats		
		(500mg/kg)	(1000mg/kg)	(1500mg/kg)
0	44.2±0.86	49.4±6.32	56.0±4.82	48.8±3.91
1	30.2±2.26	45.4±6.32^{ns}	56.2±5.13^{a}	46.2±5.87^{ns}
3	28.6±3.56	38.6±4.16 ^{a}	38.8±1.49^{ns}	45.0±2.16^{a}
5	24.4±2.98	38.6±2.48 ^{b}	36.4±3.44 ^{b}	45.2±2.67^{b}
7	22.0±3.07	33.6±2.88 ^{b}	34.2±2.88^{b}	42.0±2.91^{b}

- Values are expressed as mean ± standard error of mean.
- ^{a} = P < 0.05
- ^{b} = P < 0.001
- ^{ns} = non significant.

Besides, the first two doses of the extract (500 and 1000mg/kg B.W.) produced an appreciable decrease in blood glucose level when administered to streptozotocin- diabetic group as compared to streptozotocin – diabetic group specially after 3,5 and 7 hours and after 3 and 5 hours of administration successively as clarified in table (3).

Table 3: Showing the blood glucose levels (mg/dl) of streptozotocin – diabetic group and streptozotocin – diabetic groups plus *Azadiracta Indica* seed extract rats.

Groups / Time (Hours)	Streptozotocin – diabetic group	Streptozotocin – diabetic plus *Azadiracta Indica* seed extract rats		
		(500mg/kg)	(1000mg/kg)	(1500mg/kg)
0	189.4±7.60	188.0±14.9	186.0±7.01	190.2±10.4
1	192.4±7.22	169.2±9.48^{ns}	168.4±23.3^{ns}	193.6±12.5^{ns}
3	192.6±9.16	142.2±14.9^{a}	132.0±20.3 ^{a}	'185.2±9.17^{ns}
5	191.8±8.77	134.0±16.7 ^{a}	134.0±18.9 ^{a}	174.8±8.15^{ns}
7	191.6±7.74	127.6±14.5 ^{a}	148.0±7.51^{ns}	163.0±11.5^{ns}

- Values are expressed as mean ± standard error of mean.
- ^{a} = P < 0.05
- ^{ns} = non significant.

Also, the first dose of the extract (500mg/kg B.W.) produced a decrease in blood glucose level which is similar to that produced by insulin in streptozotocin- diabetic group after 1,3,5 and 7 hours. The doses of 1000 and 1500mg/kg of the extract decreased the blood glucose level in streptozotocin – diabetic group after 1,3 and 5 hours and after 1 and 3 hours respectively as compared to insulin – treated diabetic rats as shown in table (4).

Table 4: Showing the blood glucose levels (mg/dl) of insulin – treated diabetic group and streptozotocin – diabetic plus *Azadiracta Indica* seed extract rats.

Groups / Time (Hours)	Insulin-treated Diabetic rats	Streptozotocin – diabetic plus *Azadiracta Indica* seed extract-treated rats		
		(500mg/kg)	(1000mg/kg)	(1500mg/kg)
0	192.6±11.9	188.0±14.9	186.0±7.01	190.2±10.4
1	165.6±11.5	169.2±9.48^{ns}	168.4±23.3^{ns}	193.6±12.5^{ns}
3	140.0±9.35	142.2±14.9^{ns}	132.0±20.3^{ns}	185.2±9.17^{ns}
5	112.2±6.23	134.0±16.7^{ns}	134.0±18.9^{ns}	174.8±8.15^{a}
7	99.6±5.80	127.6±14.5^{ns}	148.0±7.51^{a}	163.0±11.5^{a}

- Values are expressed as mean ± standard error of mean.
- ^{a} = $P < 0.05$
- ^{ns} = non significant.

Discussion and conclusion

The growing interest in herbal medicine currently witnessed globally in most scientific circles is viewed as a welcome development. In many African countries today, a place of prominence is being given to herbal medicine both for curative and nutritional purposes (Akah, 1994). Also the World Health Organization (1980) has recommended that medical and scientific examination of such plants should be undertaken.

The results of the present work revealed that *Azadiracta Indica* seed extract produced hypoglycemic activity in normoglycemic and streptozotocin - diabetic rats. As regards the dose of 500mg/kg B.W. of *Azadiracta Indica* seed extract, it showed a significant hypoglycemic activity when compared to control normoglycemic group and streptozotocin-diabetic rats specially after 3,5 and 7 hours of administration. As compared to insulin- treated streptozotocin diabetic group, the hypoglycemic activity was similar to that produced by insulin. In the meantime, insulin showed an appreciable decrease in blood glucose level of normoglycemic rats as compared to the effect produced by this dose of the extract.

In relation to the dose of 1000mg/kg B.W. of the extract, it showed a significant reduction in blood glucose level of normoglycemic rats after 5 and 7 hours from administration as compared to control group. As regards the effect on diabetic rats, it showed a marked decrease in blood glucose level after 3 and 5 hours only. In the meanwhile, it produced a hypoglycemic activity similar to that produced by insulin in diabetic rats especially after 1, 3 and 5 hours of administration.

In regard to the last dose of the extract (1500mg/kg B.W.), it showed no change in blood glucose level as compared to control group or streptozotocin – diabetic rats.

The results of the present work are consistent with the results of Khosla and his colleagues (2000) who reported in their study that *Azadiracta Indica* leaves extract produced hypoglycemic activity in normal and alloxan – diabetic rats. Also, our results are in agreement with the study of Gupta et al. (2004) who reported that chronic oral administration of 2 gm/ kg B.W. of *Azadiracta Indica* seed extract for 28 days produced hypoglycemic activity in normal and streptozotocin – diabetic rats.

In conclusion, the present study demonstrated that the smallest dose of *Azadiracta Indica* seed extract (500mg/kg B.W.) showed the best hypoglycemic activity. While this dose did not produce marked decrease in blood glucose level of normoglycemic rats as compared to that produced by insulin (in normoglycemic rats), it produced an appreciable hypoglycemic activity similar to that produced by insulin in streptozotocin – diabetic rats. Thus, it becomes safer for the diabetics to use the extract in its smallest dose because it has the advantage of not producing the marked hypoglycemic effect which is produced by insulin at normoglycemic levels.

References

[1] Akah, P.A. and Okafor, C.L : Blood sugar lowering effect of *Vernonia amygdalina* (Del) in an experimental rabbit model. Phytother. Res., 6: 171-173.1992

[2] Ganong, W.F: Endocrine functions of the pancreas and regulation of carbohydrate metabolism. In: Review of Medical Physiology. 22nd ed., McGraw – Hill Companies, Lange Medical Publication, U.S.A., 19: 333-355.2005

[3] Gupta, S., Kataria, M., Gupta P.K., Murganandan, S., Yashroy, R.C: Protective role of extracts of neem seeds in diabetes caused by streptozotocin in rats.J.Ethnopharmacol., 90 (2-3): 185-189. 2004

[4] Guyton, A.C and Hall, J.E: Insulin,glucagon and diabetes mellitus. In: Textbook of Human Physiology. 11th ed., W.B.Saunders Company, U.S.A., pp: 961-977. 2005

[5] Harborne, J.B: Methods of plant analysis. In: Phytochemical Method, A guide to modern techniques of plant analysis. 3rd ed., Chapman and Hall, an imprint of Thomson science, 2-6 Boundary Row, London, U.K., pp: 1-39.1988

[6] Khosla, P., Bhanwra, S., Singh, J.S and Srivastava, R.K: A study of hypoglycemic effect of *Azadiracta Indica* (Neem) in normal and alloxan-induced diabetes. Indian Journal Physiology and Pharmacology, 44 (1): 69-74.2000

[7] Kulkarni, R.N. and Kahn, C.R: HNF_S – linking the liver and pancreatic islets in diabetes. Science, 303: 1311. 2004

[8] Lorke, D: A new approach to practical acute toxicity testing. Arch. Toxicology, 4: 275-287.1983

[9] Mann, J.J: USDA interest in the neem research. In: Proceeding of workshop on neem potentials in the pest management programmes. Locke, J.C .and Lawson, R.H. (eds), USDA-ARS-86, pp: 1-3. 1990

[10] Marles, R.J. and Farnsworth, N.R: Antidiabetic plant and their active constituents. Phytomedicine, 2: 137-189. 1995

[11] National Research Council: Neem, a tree for solving global problems. National academic press, Washington D.C., 90: 21-24.1992

[12] Ojewole, J.O.A: Hypoglycemic effect of *Clausena anisata* (willd) Hook methanolic root extract in rats. J. Ethnopharmacol., 81: 231-237.2002

[13] Ojewole, J.O.A: Hypoglycemic effects of *Sclerocarya birrea* stem bark aqueous extract in rats.Phytomedicine, 10: 675-681.2003

[14] Rao, B.K. and Rao, Ch.A: Hypoglycemic and anti-hypoglycemic activity of *Syzygium alternifolium* (wt.) walp. Seed extracts in normal and diabetic rats. Phytomedicine, 8 (2): 88-93.2001

[15] Stanely, P.M.P., Mainzen, P., and Venugopal, M.P:Anti-oxidant action of *Tinospora cordifolia* root extract in alloxan-induced diabetic rats.Phytother. Res.15: 213-218.2001

[16] Stanely, P.M.P., Menon, V.P. and Pari, L: Effect of *Syzygium cumini* extracts on hepatic hexokinase and glucose-6-phosphatase in experimental diabetes. Phytother. Res., 2: 529-531.1997

[17] World Health Organization: Expert Committee on Diabetes mellitus: Second Report. Technical Report Series, World Health Organization, Geneva, Number 646, pp: 61.1980

European Journal of Scientific Research
ISSN 1450-216X Vol.18 No.3 (2007), pp.464-478

http://www.eurojournals.com/ejsr.htm

Hydrologie et Évolution Spatio-Temporelle des Charges Solides en Suspension Dans Le Lac du Barrage Hydroélectrique de Taabo (Côte D'Ivoire)

Kouassi Kouakou Lazare
Laboratoire de Géologie Marine, Sédimentologie et Environnement, Centre de Recherche en Ecologie
Université d'Abobo-Adjamé, 01 BP 10588 Abidjan 01 (Côte d'Ivoire)
E-mail: k_lazare@yahoo.fr
Tel: (225) 21257336/05612306; Fax: (225)21240191

Gone Droh Lanciné
Laboratoire Géosciences et Environnement ; UFR-Sciences et Gestion de l'Environnement
Université d'Abobo-Adjamé, 02 BP 801 Abidjan 02 (Côte d'Ivoire)
E-mail: dialou25_9@yahoo.fr
Tel: (225)20378100/05043337; Fax: (225)20378118

Meledje N'Diaye Hermann
Laboratoire de Géologie Marine, Sédimentologie et Environnement, Centre de Recherche en Ecologie
Université d'Abobo-Adjamé, 01 BP 10588 Abidjan 01 (Côte d'Ivoire)
E-mail: meledjendiay@yahoo.fr
Tel: (225)21257336/939617; Fax: (225)21240191

Wognin Ama Valérie Irma
Laboratoire de Géologie Marine et Sédimentologie
UFR-Sciences de la Terre et des Ressources Minières, Université de Cocody
22 BP 582 Abidjan 22 (Côte d'Ivoire)
E-mail: ama_valerie@yahoo.fr
Tel: (225)22483802/904962

Aka Kouamé
Laboratoire de Géologie Marine et Sédimentologie
UFR-Sciences de la Terre et des Ressources Minières
Université de Cocody, 22 BP 582 Abidjan 22 (Côte d'Ivoire)
E-mail: akaraphael@yahoo.fr
Tel: (225)22483802/08873097

Abstract

The measurements taken on the lake of the hydroelectric dam of Taabo, during the campaigns work, achieved on a hydrologic cycle between october 2004 and august 2005 were used for the physicochemical characterization of Taabo lake. In addition, the hydrological data of the hydrometric station of Kimoukro, located upstream Taabo's dam, permitted to quantify the solid transport in suspension in Taabo Lake. This work is a preparatory study for the setting up of a sedimentation model in Taabo Lake.

This study revealed that the variations of the suspended matters fluxes are closely bound to the hydrologic seasons. During the rain seasons, the suspended matters are higher than during the dry seasons. The distribution of suspended matters from upstream to downstream describes a negative gradient. But the gradient from the surface to the bottom of the lake is positive.

The suspended particles of Taabo Lake have an annual average of 12 $mg.L^{-1}$ with a standard deviation of 5.4 $mg.L^{-1}$ and the middle turbidity is about 19.85 NTU with a standard deviation of 6.1 NTU. Taabo dam stopped yearly about 8812 tons of suspended particles. These suspended matters are composed of an inorganic fraction and an organic fraction. The inorganic fraction is mostly composed of detritus quartzes and various clays. The organic fraction is formed of plant fibres and the remnants of organisms.

Keywords: dam's lake, suspended matters, solid loads, Bandama, Taabo, Côte d'Ivoire

1. Introduction

La Côte d'Ivoire possède un vaste réseau hydrographique avec six (6) importantes retenues d'eau (Ayamé 1 et 2, Kossou, Taabo, Buyo et Fayé) qui ont fait l'objet de plusieurs études (Reizer, 1967 ; Kassoum, 1979 ; Galy-Lacaux *et al.*, 1999 ; Ouattara, 2000 ; Diomandé, 2001 ; Yapo, 2002). Ces travaux traitent essentiellement des caractéristiques physico-chimiques et biologiques des eaux. Cependant, les problèmes hydrosédimentaires auxquels ces lacs peuvent être confrontés restent peu étudiés. Selon Okacha *et al.* (2002), l'alluvionnement des retenues d'eau conduisant à la réduction de leur durée de vie, constitue une des conséquences les plus néfastes de l'érosion hydrique. Ce comblement des lacs s'opère au fur et à mesure qu'ils vieillissent car, les particules transportées par les courants fluviatiles s'accumulent dans les lacs de barrages qui constituent des barrières potentielles à leur migration et réduisent ainsi leur capacité de stockage (Ramade, 1993).

Le lac de Taabo pourrait subir ces phénomènes de comblement avec célérité eu égard aux pressions anthropiques auxquelles son bassin versant est de plus en plus confronté. En effet, un recensement effectué par la Direction des Grands Travaux en 1996 a permis d'apprécier l'importance des activités menées sur le bassin du Bandama. Environ 184 retenues d'eau y sont construites, soit 32,18% de l'ensemble des retenues d'eau de la Côte d'Ivoire. Aussi, l'exploitation de la mine de diamant de Tortiya, les activités agricoles, l'urbanisation et les activés qui s'en suivent, ont-elles laissé dans le paysage d'énormes terrains stériles érodés par les eaux de pluies.

Les études N'go (2000) et Kouassi *et al.* (2007) portant sur la granulométrie et la nature des sédiments des fonds des lacs de Buyo et Taabo ont révélé un probable comblement des retenues d'eau de la Côte d'Ivoire. Toutefois, la quantification des apports solides susceptibles de combler la retenue d'eau de Taabo n'a pas été abordée 26 ans après sa mise en eau. Or, la compréhension de la dynamique de tout milieu alluvial réside dans les interactions entre l'écoulement et le transport des sédiments (Boyer, 1996). La prédiction des phénomènes d'envasement est primordiale afin de cerner leur intensité et définir les actions nécessaires à leur réduction (Bessenassé *et al.*, 2003).

Cette étude a pour objectif de connaître la dynamique spatio-temporelle et le bilan global annuel des charges solides en suspension dans le lac du barrage hydroélectrique de Taabo. Ce travail s'inscrit dans un programme d'étude de l'hydrologie, du transport solide et de la sédimentation dans les lacs des barrages hydroélectriques de Côte d'Ivoire.

2. Site et Méthodes

2.1. Site d'étude

L'aménagement hydroélectrique de Taabo est implanté sur le bras principal du fleuve Bandama à environ 110 km en aval du confluent du Bandama blanc et du Bandama rouge et à environ 120 km en aval du barrage de Kossou. Il est situé entre 5°07' et 5°33' de longitude Ouest et 6°25' et 6°56' de latitude Nord (Figure 1).

Construit entre 1975 et 1979, le barrage de Taabo a été mis en service en 1979 (Kaisers Engineers and Constructors, 1980). Ce barrage ne dispose pas d'organe de vidange de fond. Le lac de Taabo a une superficie de 69 km² et un volume de 625.10^6 m^3 à la cote de retenue normale (124 m). La profondeur maximale est d'environ 30 m.

Le principal type de roche rencontré sur le site du barrage est le complexe de base granite/gneiss granitique avec différents types de roches allant des gabbros et péridotites basiques aux schistes quartzeux et granites fins (Avenard, 1971 ; Aka, 1991).

La superficie approximative du bassin versant drainé dans le cadre de l'aménagement hydroélectrique de Taabo est de 58700 km^2. Dans l'ensemble, le relief du bassin du Bandama est peu accentué ; seuls émergent un peu au Nord-Ouest quelques reliefs dépassant 800 m d'altitude (Camus, 1972).

Figure 1: Présentation du site d'étude

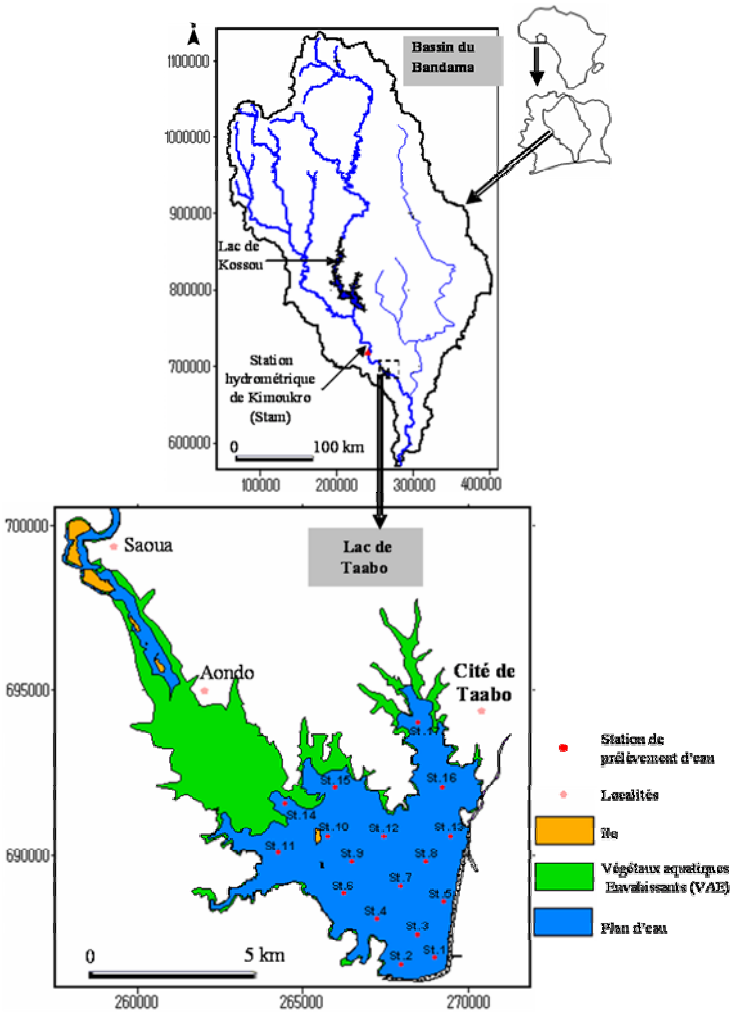

Du point de vue climatique, au regard des travaux de Eldin (1971) et Girard *et al.* (1971), le Nord du bassin est sous l'influence du régime tropical de transition. Le lac de Taabo subit directement l'influence des régimes tropical de transition atténué et équatorial de transition. On distingue deux saisons des pluies (la grande saison se déroule entre avril et juin et la petite entre septembre et novembre) et deux saisons sèches (la grande saison s'étale de décembre à mars et la plus petite de juillet à septembre). Les données hydrologiques recueillies auprès de la Direction de l'Hydraulique Humaine (DHH) et la Direction des Mouvements d'Energie de la Compagnie Ivoirienne d'Electricité (DME-CIE) permettent d'apprécier ces différentes saisons (Figure 2).

Figure 2: Variations des valeurs moyennes mensuelles des précipitations et des apports à Taabo et à Kossou de 1980 à 2005 (Source : DME-CIE et DHH)

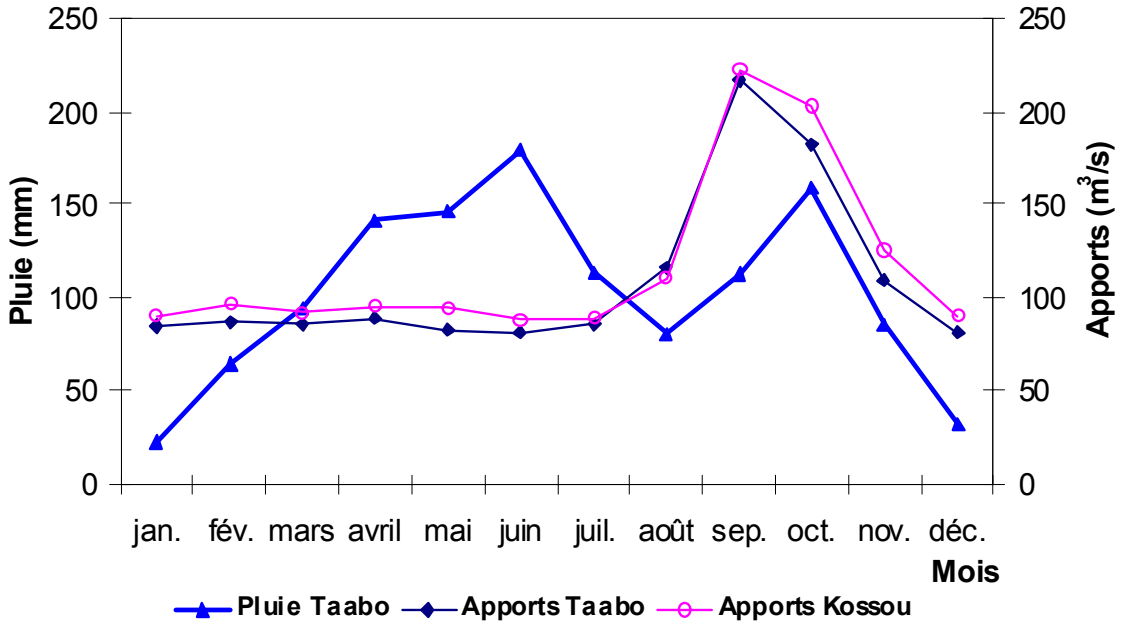

Les écoulements observés dans les parties centrale et inférieure du bassin du Bandama sont fortement influencés par le régime tropical de transition du Nord du bassin. Ce régime comporte généralement une seule période de hautes eaux (août-septembre-octobre), suivie d'un tarissement rapide de novembre à décembre.

Les apports les plus importants sont enregistrés dans la période septembre-octobre au moment où se produisent généralement les petites saisons des pluies. Toutefois, Girard *et al* (1971) soulignent que sur les sous bassins, les deux saisons des pluies provoquent des crues en juin-juillet et semptembre-octobre qui sont d'inégale importance suivant la prédominance de l'une ou l'autre saison des pluies.

Au niveau du couvert végétal, la région de Taabo appartient au secteur mésophile caractérisé par une végétation semi décidue (Guillaumet et Adjanohoun, 1971). On distingue dans cette formation végétale une zone de savane préforestière au Nord, opposée à une zone forestière à savanes incluses au Sud. Cette végétation a subi d'importantes modifications à cause de l'intensification des activités agricoles et la forte pression démographique.

Les travaux réalisés sur l'occupation du sol par Véi (2005) et une analyse des images Landsat 196-56-Q4-1b de 1990 et 196-56-Q4-1b de 2001 obtenues au Centre de Cartographie et de Télédétection montrent que le lac de Taabo est confronté à un problème d'eutrophisation qui se

manifeste par une colonisation permanente et progressive de la surface du plan d'eau par les végétaux aquatiques envahissants (Voir figure 1).

2.2. Méthode

Les prélèvements ont été effectués sur quatre saisons hydrologiques : octobre 2004, février, juin et août 2005 correspondant respectivement à la petite saison des pluies, la grande saison sèche, la grande saison des pluies et la petite saison sèche. Pour déterminer les concentrations moyennes en matières en suspension (MES) des eaux du lac de Taabo, 50 échantillons d'eau en moyenne, ont été prélevés par saison. Au total, 204 prélèvements ont été effectués sur 18 stations de mesure reparties sur l'ensemble de la retenue, non couverte par les VAE (Voir figure 1). Les échantillons d'eau ont été prélevés à différentes profondeurs dans le lac (0,5 ; 2 ; 5 ; 10 et 15 m). Des prélèvements ont également eu lieu en amont du barrage, à la station hydrométrique de Kimoukro, pour apprécier les variations des paramètres physico-chimiques du milieu fluviatile au milieu lacustre. Les mesures de température, de pH, et de conductivité ont été effectuées *in situ* au moyen d'un pH-mètre-conductimètre portatif modèle W.T.W. 82362. La teneur en oxygène dissous et la turbidité ont également été mesurées sur le terrain respectivement avec un oxymètre portatif, modèle CRISON OXi 330 et un turbidimètre de marque HANNA, modèle LP 2000.

La position des stations de mesure a été repérée à l'aide d'un GPS modèle GARMIN GPS 40. Les déplacements sur le lac ont été effectués au moyen d'un hors-bord de la Compagnie Ivoirienne d'Electricité.

La quantification des MES a été effectuée au laboratoire de Géologie Marine, Sédimentologie et Environnement du Centre de Recherche en Ecologie. Les échantillons d'eau ont été filtrés sur une rampe de filtration millipore à l'aide de filtres WHATMAN circulaires de 47 mm de diamètre et de porosité 0,45 µm préalablement pesés. Après séchage à l'étuve à 105°C pendant deux heures, les filtres sont soigneusement récupérés et repesés afin de déterminer les concentrations totales de matières en suspension exprimées en $mg.L^{-1}$ (Afnor, 1996). Après filtration, l'observation des différents filtres à la loupe binoculaire a permis d'examiner et d'identifier la nature des éléments recueillis.

Les résultats obtenus ont été appréciés selon un gradient longitudinal (amont-aval) et un gradient vertical (surface-profondeur). D'amont en aval, le comportement des différents paramètres a été observé sur un transect au niveau des stations St1, St3, St7, St9, St10, St14 et St_{am} situées respectivement à 200, 1000, 1500, 3000, 3700 et 5000 m de la prise d'eau et à la station de Kimoukro.

La charge solide annuelle du lac de Taabo a été obtenue à partir de la moyenne des concentrations des échantillonnages saisonniers. Le débit solide est calculé à partir des concentrations moyennes des MES pondérées par les débits liquides comme suit (Bricquet *et al.*, 1997 ; Bouanani, 2004) :

$$Q_{SS} = Q_L.C \quad (1)$$

Avec :

Q_{SS} : Débit solide en suspension ($kg.s^{-1}$),
QL : Débit liquide ($m^3.s^{-1}$),
C : Concentration moyenne de matières en suspension ($g.L^{-1}$).

Pendant un intervalle de temps δt correspondant à la durée totale de la saison, on déduit les apports solides saisonniers (A_S en kg) en posant :

$$A_S = Q_{SS}.\ \delta t \quad (2)$$

Le flux annuel des matières solides en suspension transportées par le fleuve dans la retenue de Taabo est finalement obtenu en additionnant les apports solides des quatre saisons.

3. Résultats et Discussion

3.1. Caractéristiques physico-chimiques du lac de Taabo

Le tableau I présente les valeurs moyennes des paramètres physico-chimiques du lac de Taabo en fonction des différentes saisons hydrologiques.

Table 1: Variations des moyennes saisonnières des paramètres physico-chimiques dans le lac de Taabo

Saison	pH		Temp. (°C)		Cond. ($\mu S.cm^{-1}$)		Turb. (NTU)		MES ($mg.L^{-1}$)		O_2 ($mg.L^{-1}$)	
	Moy.	**σ**	**Moy.**	**σ**	**Moy.**	**σ**	**Moy.**	**σ**	**Moy.**	**σ**	**Moy.**	**σ**
Petite saison des pluies (octobre 04)	7,72	0,21	29,03	0,98	81,40	1,83	26,66	3,33	17,76	2,26	3,55	0,45
Grande saison sèche (février 05)	7,45	0,41	29,74	1,08	92,84	3,53	14,63	0,45	5,47	0,33	5,02	0,99
Grande saison des pluies (juin 05)	6,88	0,02	28,77	0,49	82,98	1,81	23,25	1,22	14,85	1,57	2,92	0,32
Petite saison sèche (août 05)	7,51	0,07	25,95	0,09	88,67	2,54	15,78	0,46	9,91	0,46	3,91	0,78
Moy.	**7,39**		**28,37**		**86,47**		**19,85**		**12**		**3,85**	
σ (inter-saisonnier)	**0,36**		**1,66**		**5,27**		**6,07**		**5,38**		**1,08**	

Moy. : Moyenne ; σ : Ecart-type

L'examen du tableau 1 montre que les variations inter-saisonnières des paramètres physico-chimiques sont plus significatives que les variations intra-saisonnières. Les MES et la turbidité présentent les plus fortes variations intra-saisonnières pendant les saisons pluvieuses. En revanche, pendant les saisons sèches les valeurs de la conductivité subissent les plus fortes fluctuations (écart-type intra-saisonnier plus élevé). Par ailleurs, les MES, la turbidité, la conductivité, le taux d'oxygène dissous connaissent des fluctuations saisonnières bien marquées. Ainsi, les MES et la turbidité enregistrent leurs plus fortes valeurs en saisons pluvieuses contrairement à la conductivité et au taux d'oxygène dissous dont les valeurs les plus élevées s'observent en saisons sèches.
Les eaux du lac sont faiblement minéralisées avec des valeurs de pH proches de la neutralité. Le milieu est faiblement oxygéné sur toutes les saisons.

3.2. Evolution spatio-temporelle des paramètres physico-chimiques du lac de Taabo

3.2.1. Evolution saisonnière amont-aval

La figure 3 (a, b, c, d, e et f) montre la variation des moyennes saisonnières des paramètres physico-chimiques de la retenue d'eau de l'amont vers la prise d'eau du barrage.

Figure 3: Variations des moyennes saisonnières des paramètres physico-chimiques de l'amont vers la prise d'eau du barrage de Taabo

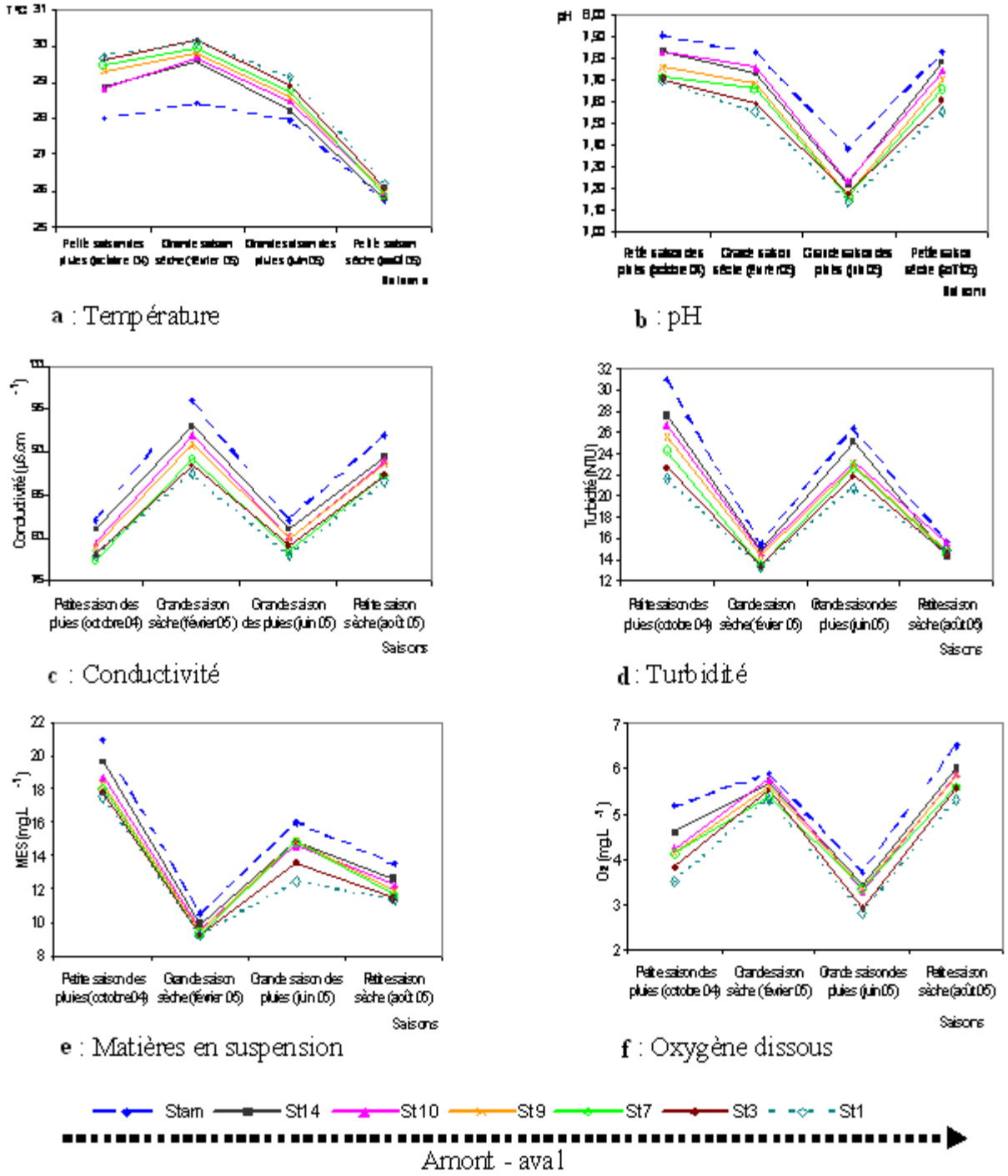

La figure 3-a permet de constater que la température de la retenue d'eau augmente légèrement de l'amont vers l'aval sur toutes les saisons. On remarque par ailleurs que, dans le cours d'eau (Stam) les températures sont plus faibles que dans le lac (St1) si bien que l'écart entre la température dans le fleuve et celle du lac atteint 1,6°C. Cet écart est plus faible (0,5°C) au cours de la petite saison sèche où la température reste quasi constante sur toutes les stations. Les variations saisonnières de la température atteignent des amplitudes de 1,6°C.

Contrairement à l'évolution de la température, le pH, la conductivité, la turbidité, les MES et l'oxygène dissous présentent globalement des gradients amont-aval négatifs (Figure 3 b, c, d, e et f) pendant toutes les saisons.

L'oxygène dissous subit une légère diminution de l'amont vers l'aval (Figure 3-f). L'écart moyen entre les valeurs en amont et celles en aval est de 1 $mg.L^{-1}$. Le pH de la retenue d'eau diminue globalement de l'amont vers l'aval sur toutes les saisons (Figure 3-b). Il varie de 7,6 dans le cours d'eau (Stam) à 7,4 dans le lac. L'écart maximal est observé pendant la grande saison des pluies.

La turbidité et les MES présentent une distribution similaire. Globalement, leurs teneurs diminuent de l'amont vers l'aval et présentent respectivement des écarts moyens de 2,8 $mg.L^{-1}$ pour les MES et 4,7 NTU pour la turbidité. Les écarts entre les valeurs au niveau des stations sont plus significatifs pendant les saisons pluvieuses que pendant les saisons sèches.

La conductivité du lac subit une baisse de l'amont vers l'aval. L'écart entre la conductivité du fleuve et celle du lac est de 5,8 $\mu S.cm^{-1}$.

3.2.2. Evolution saisonnière verticale

L'analyse de la figure 4 (a, b, c, d, e et f) permet de suivre l'évolution saisonnière des valeurs moyennes des paramètres physico-chimiques en fonction de la profondeur dans le lac de Taabo. Pour chaque saison, la valeur moyenne de chaque paramètre a été calculée respectivement à 0,5 ; 2 ; 5; 10 et 15 m de la surface de la retenue.

Figure 4: Variations des valeurs moyennes saisonnières des paramètres physico-chimiques en fonction de la profondeur dans le lac de Taabo

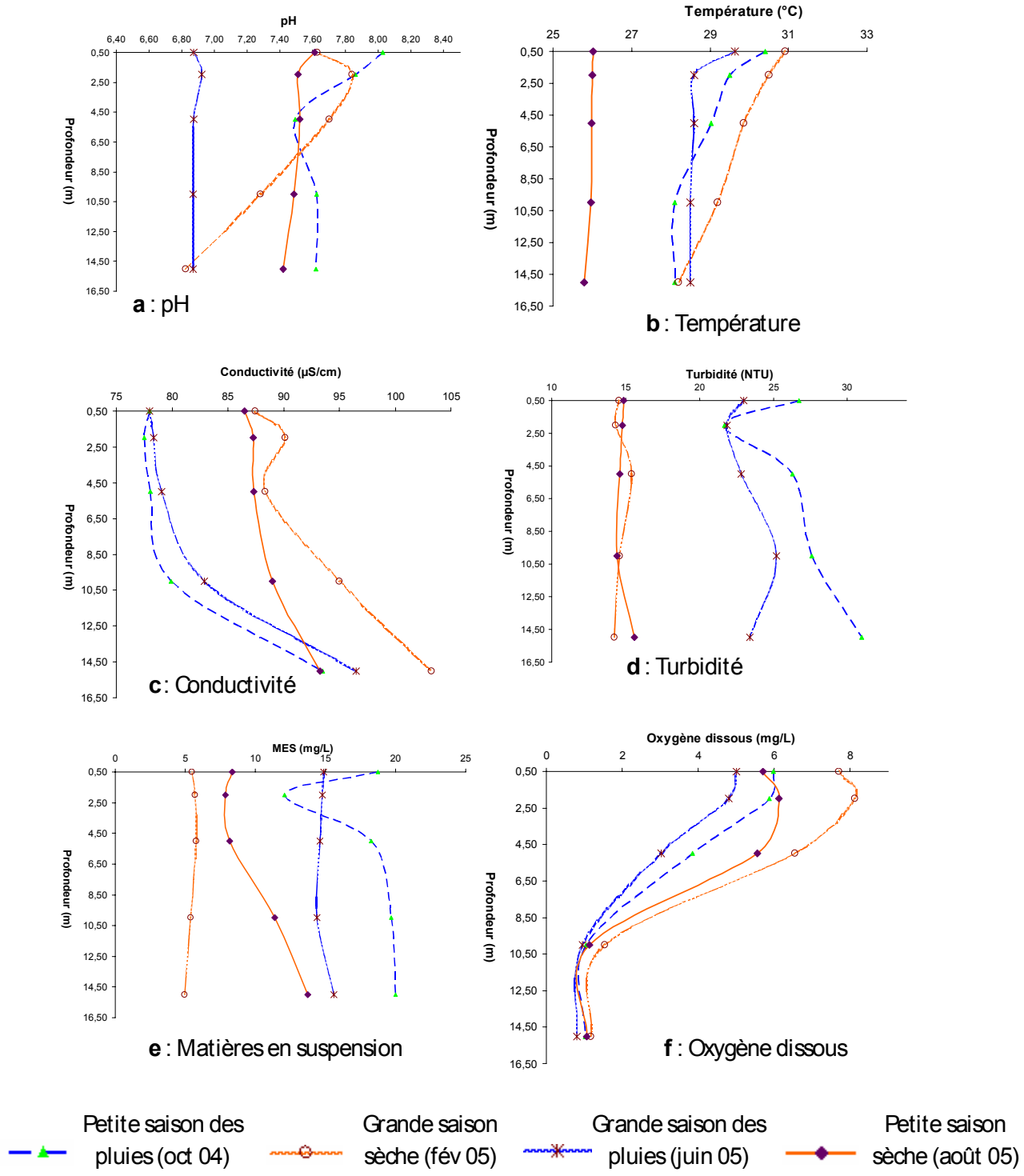

Dans l'ensemble, le pH, la température et l'oxygène dissous diminuent de la surface vers le fond sur toutes les saisons (Figure 4 a, b et f).

La variation du taux d'oxygène dans la colonne d'eau présente trois tendances durant toutes les saisons. De la surface à 3 m de profondeur, la teneur en oxygène dissous augmente légèrement et les valeurs oscillent entre 6,1 et 6,2 mg.L^{-1}. A partir de 3 m, elle diminue brusquement pour atteindre 1,2

$mg.L^{-1}$ autour de 10 m et reste quasiment constante. De façon générale, les amplitudes entre les teneurs en oxygène dissous de la surface et celles du fond sont de 4,1 $mg.L^{-1}$.

En comparant les valeurs de l'oxygène dissous au cours des deux différentes saisons, on constate que les teneurs les plus élevées s'obtiennent pendant les saisons sèches où elles varient, en moyenne, de 6,9 $mg.L^{-1}$ en surface à 1,1 $mg.L^{-1}$ au fond. La valeur moyenne est de 4,5 $mg.L^{-1}$ avec un écart type de 2,9 $mg.L^{-1}$. Pendant les saisons pluvieuses, les teneurs en oxygène dissous oscillent entre 5,5 et 0,9 $mg.L^{-1}$ avec une moyenne de 3,2 $mg.L^{-1}$ et un écart type de 2,2 $mg.L^{-1}$.

La diminution du pH avec la profondeur est plus remarquable au cours de la grande saison sèche où l'amplitude entre le pH à la surface et le pH au fond est de 0,8. Pendant les autres saisons, les amplitudes entre les valeurs à la surface et celles du fond sont de l'ordre de 0,2. Les valeurs les plus élevées (7,5) s'observent autour de 3 m de profondeur. Le pH prend ses plus faibles valeurs (6,9) pendant la grande saison des pluies où il reste quasiment constant dans la colonne d'eau.

Concernant la température, les amplitudes entre les valeurs à la surface et celles du fond sont en moyenne de 1,6°C. Les plus fortes valeurs (32,9°C) s'obtiennent pendant la grande saison sèche alors que les valeurs les plus faibles (25,8°C) sont enregistrées pendant la petite saison sèche où la température est quasiment constante.

Contrairement à l'évolution du pH, de la température et de l'oxygène dissous, la distribution verticale de la conductivité, la turbidité et des MES présente un gradient vertical positif (Figure 4 c, d et e). Cette augmentation est plus perceptible au niveau de la conductivité où l'amplitude entre la conductivité des eaux du fond et celles de surface est en moyenne de 14,2 $\mu S.cm^{-1}$ par saison. En général, la conductivité présente une évolution à deux tendances. De la surface à 3 m de profondeur, elle augmente lentement et oscille entre 82,5 et 83,3 $\mu S.cm^{-1}$. A partir de 3 m, on observe une rapide augmentation avec des valeurs qui varient entre 83,3 et 96,6 $\mu S.cm^{-1}$.

Les variations de la turbidité et des MES en fonction de la profondeur présentent globalement deux tendances. De la surface à 3 m de profondeur, la turbidité diminue et les valeurs oscillent, en moyenne, entre 19,8 et 18,2 NTU. De même, la concentration en MES connaît une diminution et les valeurs varient, en moyenne, entre 11,8 et 10,1 $mg.L^{-1}$.

Au-delà de 3 m, la turbidité augmente progressivement avec la profondeur et atteint 21,1 NTU à 15 m. La concentration des MES augmente également pour atteindre 13,6 $mg.L^{-1}$ à 15 m de profondeur.

Ces deux paramètres enregistrent leurs plus fortes valeurs pendant les saisons pluvieuses où la turbidité est, en moyenne, de 24,9 NTU et la concentration moyenne des MES est de 16,3 $mg.L^{-1}$. Pendant les saisons sèches notamment, au cours de la grande saison, la turbidité et la concentration des MES restent faibles et quasiment constantes dans la colonne d'eau.

3.3. Nature des Matières en suspension (MES)

L'observation à la loupe binoculaire des particules recueillies sur les filtres montre que les matières en suspension sont composées de constituants organiques et inorganiques. Sur le plan granulométrique, la charge solide correspond à des matériaux allant de la taille des colloïdes à celle des argiles et même parfois des sables. Les constituants organiques renferment des débris végétaux, des insectes, etc. La fraction inorganique, la plus abondante, est majoritairement formée d'argiles et de quartz détritiques.

3.4. Bilan des flux de matières solides en suspension

Le tableau 2 présente les flux entrant et sortant des MES en fonction des saisons hydrologiques.

Table 2: Bilan des flux de MES dans le lac de Taabo

	Grande saison sèche (février)	Grande saison des pluies (juin)	Petite saison sèche (août)	Petite saison des pluies (octobre)	Moyenne Annuelle
Débits entrants (m^3/s)	114	90	140	203	129
Débits sortants (m^3/s)	80	108	117	211	117
Concentration en MES (mg/L) amont	6	16	13	20	14
Concentration en MES (mg/L) aval	5	14	9	17	11
Concentration moyenne en MES (mg/L)	5	15	10	18	12
Flux particulaires entrants (t)	7268	15091	9679	21991	54029
Flux particulaires sortants (t)	4207	15887	5739	19385	45217
Bilan global entrées-sorties (t)	3062	-796	3940	2606	**8812**

Les séries hydrologiques mensuelles fournies par la DHH ont permis d'estimer, au cours de ces vingt dernières années, les apports liquides saisonniers et les apports moyens annuels dans le lac de Taabo à environ 129 $m^3.s^{-1}$. Ce qui permet par ailleurs, d'évaluer les flux particulaires en suspension qui sont plus élevés au cours des saisons pluvieuses. En effet, le lac reçoit 15091 t de sédiments pendant la grande saison des pluies et 21991 t pendant la petite saison. Les flux particulaires sont plus élevés pendant la petite saison des pluies à cause des débits entrants qui sont plus importants pendant la petite saison (181 m^3/s) que pendant la grande saison (80 $m^3.s^{-1}$). Les flux particulaires restent relativement faibles (7268 t) pendant la grande saison sèche.

Durant le cycle hydrologique, le lac a reçu, en moyenne, 54029 t de matières en suspension dont 45217 t en sont sorties vers l'aval. Le bilan global annuel des flux de MES entrant et sortant montre que le lac a retenu environ 8812 t soit 16% des MES transportées par les eaux de ruissellement vers le lac.

3.5. Discussion

Des différents paramètres physico-chimiques étudiés, il ressort, concernant la température qu'il n'apparaît aucune stratification thermique notable entre la surface et le fond durant toutes les saisons. Rysing et Rast (1994) rapportent que cela est caractéristique des lacs tropicaux. Toutefois, les eaux du lac sont plus chaudes que celles du fleuve. Cette augmentation de la température du milieu lotique au milieu lentique peut s'expliquer par la forte exposition de la retenue d'eau au rayonnement solaire. Par ailleurs, le refroidissement général du lac pendant la grande saison des pluies et la petite saison sèche est due à la présence quasi permanente des nuages qui atténuent l'ensoleillement pendant ces deux périodes. Les températures du lac de Taabo sont du même ordre de grandeur que celles des lacs de Kossou, Buyo et Ayamé. Au niveau du lac de Kossou, Brunel et Bouron (1992) trouvent une température moyenne de 28, 62°C. A Buyo, Yapo (2002) rapporte que la température moyenne du lac varie entre 26 et 32°C. Au niveau de la retenue d'eau d'Ayamé, Diomandé (2001) trouve des températures qui varient entre 26,45 et 29,45°C.

Les valeurs de l'oxygène dissous montrent que les eaux du fleuve sont plus oxygénées que celles du lac. Cette diminution de l'oxygène dissous, du cours d'eau à la retenue, peut être liée aux mouvements de convexion provoqués par les courants qui favorisent une bonne oxygénation du cours d'eau. Le profil vertical de l'oxygène dans le lac montre une stratification quasi générale de la retenue d'eau. Les eaux superficielles sont plus oxygénées (6,1 $mg.L^{-1}$) que celles du fond (1 $mg.L^{-1}$). Les fortes teneurs en oxygène, enregistrées dans les zones superficielles, sont dues aux activités photosynthétiques qui se déroulent généralement avec une plus grande intensité dans ces zones du fait de la forte pénétration de la lumière. Ces mêmes observations ont été faites par Galy-Laucaux *et al.* (1999) sur les lacs d'Ayamé 1 et 2 où ils obtiennent des teneurs moyennes de 2,5 $mg.L^{-1}$. Selon Dufour *et al.* (1994), l'oxygénation par échange avec l'atmosphère et l'oxygénation par photosynthèse sont à l'origine des fortes teneurs en oxygène dissous dans la partie superficielle. En revanche, dans les zones

profondes, l'oxydation de la matière organique entraîne une désoxygénation des eaux. Par ailleurs, la minéralisation des charges organiques qui se traduit par une augmentation de la conductivité mobilise l'oxygène dissous qui est consommé par les micro-organismes intervenant dans ce processus. Ainsi, après les deux saisons pluvieuses, les saisons sèches qui suivent constituent les périodes pendant lesquelles la minéralisation des charges apportées en saison pluvieuse atteint son maximum. Ce qui se traduit par des valeurs élevées de conductivité (figure 4c).

Le bilan annuel des entrées et sorties des flux de matières en suspension dans le lac de Taabo met en évidence un piégeage d'environ 8812,17 t soit 16,31% des MES transportées par les eaux de ruissellement vers le lac. Les flux particulaires dans le lac sont dépendants des variations des paramètres hydroclimatiques (pluies et apports). Pendant les saisons sèches, les eaux sont faiblement chargées ; la concentration moyenne en MES est de 7,89 $mg.L^{-1}$. En revanche, pendant les saisons pluvieuses, les MES deviennent relativement importantes et la concentration moyenne se situe autour de 16,30 $mg.L^{-1}$. Cette augmentation est sans doute liée aux apports des eaux de ruissellement, assez chargées en sédiments, dans le lac. Picouet (1999), Zhongyuan *et al.* (2001), Orfeo et Stevaux (2002), Benedetti (2003), Andrew *et al.* (2004), Sarma (2005), Kaiqin *et al.* (2005) rapportent qu'il existe une forte corrélation entre les charges solides en suspension et les variations des apports liquides. Les travaux de ces auteurs révèlent que les pics de concentration en MES se produisent généralement avant ceux des apports liquides. C'est pourquoi des mesures continues s'avèrent nécessaires, notamment lors des crues, pour une bonne évaluation des charges solides en suspension. La diminution de la turbidité et des MES d'amont en aval peut être liée aux phénomènes de décantation qui se traduisent par des dépôts progressifs des charges solides dans la retenue d'eau. Par ailleurs, l'augmentation de ces deux paramètres de la surface vers le fond est due à la décantation qui provoque un déplacement des particules vers le fond. En surface, les fortes turbidités sont dues au maintien en suspension des particules moins denses que l'eau. Aussi, les phytoplanctons qui se développent dans la colonne proche de la surface contribuent-ils à l'augmentation de la turbidité. Cependant, près du fond, les courants déterminent fréquemment des reprises sédimentaires, qui conduisent à l'augmentation de ces deux paramètres.

Les concentrations en MES obtenues au cours de cette étude sont inférieures à celles enregistrées par Yapo (2002) dans le lac de Buyo qui sont de l'ordre de 20,6 $mg.L^{-1}$. Cette différence de concentration pourrait s'expliquer par la dégradation du couvert végétal et l'inclinaison régulière de la pente qui augmentent la vulnérabilité des sols à l'érosion sur le bassin du lac de Buyo (N'go, 2000). De même, le transport solide en suspension dans le lac de Taabo est relativement faible comparativement aux valeurs obtenues par Bricquet *et al.* (1997), Picouet (1999), Okacha *et al.* (2002), Shaw (2003), Bessenassé *et al.* (2003) et Bessenassé (2004) sur le bassin du Niger et dans les retenues d'eau en Tunisie et en Algérie où le piégeage dans les retenues d'eau varie souvent entre 200 et 800 milliers de tonnes par an. Selon Monnet (1972) et Lenoir (1972), les faibles concentrations de MES enregistrées sur le Bandama peuvent s'expliquer par le fait que ce fleuve dont le bassin versant présente un relief pénéplané exporte peu de matériel détritique. De plus, le nombre important de retenue d'eau (183) situé en amont de celle de Taabo, notamment le barrage de Kossou constitue un obstacle majeur à la migration des sédiments vers le lac de Taabo.

4. Conclusion

Ce travail qui est une étude préparatoire pour la mise en place du modèle de sédimentation a permis de déterminer les caractéristiques des paramètres physico-chimiques et de quantifier les flux particulaires en suspension dans le lac de Taabo.

Les eaux du lac sont faiblement minéralisées et présentent une stratification de l'oxygène dissous suivant le profil vertical.

Les variations des apports particulaires sont étroitement liées aux saisons hydrologiques. Pendant les saisons de pluie, les eaux sont plus chargées que pendant les saisons sèches. La distribution

spatiale des MES présente un gradient amont-aval négatif alors que de la surface vers le fond le gradient est positif. Les charges solides en suspension, dont la concentration moyenne annuelle est de 12 $mg.L^{-1}$, sont composées d'une fraction inorganique et d'une fraction organique. La fraction inorganique est essentiellement constituée de quartz détritiques et d'argiles diverses. La fraction organique est formée de fibres végétales et de débris d'organismes. Le bilan annuel des entrées et sorties des flux particulaires montre un comblement du lac de Taabo par 8812,17 t de MES par an.

Les études sédimentologiques en cours permettront de déterminer le transport particulaire total et d'évaluer l'ampleur et l'impact des phénomènes de sédimentation sur le lac du barrage hydroélectrique de Taabo.

5. Remerciements

Cette recherche a fait l'objet d'un soutien financier et logistique de la Fondation Internationale pour la Science (IFS, Suède) et la Compagnie Ivoirienne d'Electricité (CIE). Nous leur adressons nos sincères remerciements pour leur contribution à nos travaux.

References

[1] Afnor (1996). Qualité de l'eau. 6ème édition, Tome 2. Analyses organoleptiques, mesures physico-chimiques, paramètres globaux, composés organiques. 629p.

[2] Aka K. (1991). La sédimentation quaternaire sur la marge de la Côte d'Ivoire: Essai de modélisation. Thèse de doctorat d'Etat ès Sc. Nat., université d'Abidjan (Côte d'Ivoire), n°146, 320p.

[3] Andrew S., Wendy D., Amanda H. (2004). Suspended-sediment transport rates at the 1.5-year recurrence interval for ecoregions of the United States: transport conditions at the bankfull and effective discharge? *Geomorphology* 58 : 243-262.

[4] Avenard J.M. (1971). Aspect de la géomorphologie. in : "Le milieu naturel de Côte d'Ivoire", mém. ORSTOM, Paris, n° 50 : 1-72.

[5] Benedetti M. M. (2003). Controls on overbank deposition in the Upper Mississippi River. *Geomorphology* 56 : 271–290.

[6] Bessenassé M. (2004). Problématique de l'envasement des barrages algériens. *Tribune de l'eau* n°631/5-632/6 : 39-43.

[7] Bessenassé M., KETTAB A., PAQUIER A., RAMEZ P., GALEA G. (2003). Simulation numérique de la sédimentation dans les retenues de barrages : cas de Zardezas, Algérie. *Rev. Sci. Eau* (16) : 103-122.

[8] Bouanani A. (2004). Hydrologie, transport solide et modélisation : étude de quelques sous bassins de la Tafna (NW –Algérie). Thèse de doctorat d'Etat, université de Abou Bekr Belkaid Tlemcen, 249p.

[9] Boyer C. (1996). Turbulence, transport des sédiments en charge de fond et forme du lit d'un confluent de cours d'eau naturels. Thèse de doctorat, université de Montréal, Faculté des études supérieures, 340p.

[10] Bricquet J.P, Mahé G., Bamba F., Diara M., Mahieux A., Des Tureaux T., Orange D., Picouet C., Olivry J. C. (1997). Erosion et transport particulaire par le Niger : du bassin supérieur à l'exutoire du delta inférieur (bilan de cinq années d'observation). *IAHS*, n°246 : 335-346.

[11] Brunel J.P. et Bouron B. (1992). Evaporation des nappes d'eau libre en Afrique sahélienne et tropicale. CIEH, Cahiers de l'ORSTORM, Sér. Hydrologie, 410p.

[12] Camus H. (1972). Hydrologie du Bandama, tome 1: le Bandama blanc. Mém. ORSTOM, Service Hydrologique, Adiopodoumé, 96p.

[13] Diomandé D. (2001). Macrofaune bentique et stratégies alimentaires de Synodontis batiani et S. schall en milieu fluvio-lagunaire (bassins bia et agnébi ; Côte d'Ivoire). Thèse de doctorat, université d'Abobo-Adjamé, 250p.

[14] Dufour P., Durand J-R, Guiral D., Zabi G. S. (1994). Environnement et ressources aquatiques de Côte d'Ivoire, Tome II : Les milieux lagunaires. Ed. ORSTOM, 546p.

[15] Eldin M. (1971). Le climat. in : "Le milieu naturel de Côte d'Ivoire", mém. ORSTOM, Paris, n°50 : 73-108.

[16] Galy-Lacaux C., Delmas R., Kouadio G., Richard S., Gossé P. (1999). Long-terme greenhouse gas emissions from hydroelectric reservoirs in tropical forest regions. *Global Biogeochemical Cycles*, 13(2) : 503-517.

[17] Girard G., Sircoulon J., Touchebouef P. (1971). Aperçu sur les régimes hydrologiques. in :"Le milieu naturel de Côte d'Ivoire", mém. ORSTOM, Paris, n°50 : 109-155.

[18] Guillaumet J. L., Adjanohoun E. (1971). La végétation. in : "Le milieu naturel de Côte d'Ivoire", mém. ORSTOM, Paris, n°50 : 161-262.

[19] Kaiqin X., Zhongyuan C., Yiwen Z., Zhanghua W., Jiqun Z., Seiji H., Shogo M., Masataka W. (2005). Simulated sediment flux during 1998 big-flood of the Yangtze (Changjiang) River, China. *Journal of Hydrology* 313 : 221-233.

[20] Kaiser engineers and Constructors, INC-USA (1980). Aménagement hydroélectrique de Taabo: Rapport final de l'aménagement, AFFAIRE N°73118, vol. 2, 263p.

[21] Kassoum T. (1979). Caractéristiques limnologiques du lac de Kossou (Côte d'Ivoire). Ann. université Abidjan, *série E (Ecologie),* Tome XII : 30-69.

[22] Kouassi K. L., Wognin A. V-I., Gnagne T., N'go Y. A., Courivaud J-R., Kassy P., Demé M., Aka K. (2007). Caractérisation des sables et morphologie du fond du lac du barrage hydroélectrique de Taabo. *Sci. Nat.* 4(1) : 93-104.

[23] Lenoir F. (1972). Exportation chimique d'un bassin intertropical (Le Bandama, Côte d'Ivoire) influence des conditions hydrologiques. Thèse de doctorat d'Etat ès Sc. Nat. n° CNRS, A.O.7845, 375p.

[24] Monnet C. (1972). Contribution à l'étude de la dynamique et de la nature des suspensions d'un fleuve intertropical, le Bandama, Côte d'Ivoire : évolution des éléments chimiques des eaux de son estuaire. Thèse de doctorat d'Etat ès Sc. Nat, université de Nice, n° CNRS, A.O.7826, 427p.

[25] N'go A. (2000). Etude de l'érosion des sols de la région de Buyo: analyse des facteurs et essai d'évaluation des risques par la télédétection et les systèmes d'information géographique. Thèse de 3ème cycle, université d'Abobo-Adjamé, 155p.

[26] Okacha T., Abdelkader M., Med A. T. (2002). Mise en place d'un système d'information géographique pour le suivi et la quantification de l'érosion hydrique: application au basin versant de l'Isser (Tlemcen). *Sécheresse,* 13(3) : 9-175.

[27] Orfeo O., Stevaux J. (2002). Hydraulic and morphological characteristics of middle and upper reaches of the Parana´ River (Argentina and Brazil). *Geomorphology* 44 : 309-322.

[28] Ouattara A. (2000). Premières données systématiques et écologiques du phytoplancton du lac d'Ayamé (Côte d'Ivoire). Thèse de doctorat, Leuven, Belgique, 226p.

[29] Picouet C. (1999). Géodynamique d'un hydrosystème tropical peu anthropisé : le bassin supérieur du Niger et son delta intérieur. Thèse de doctorat, université de Montpellier II, Sciences et Technologie de Languedoc, France, 386p.

[30] Ramade F. (1993). Dictionnaire encyclopédique de l'Ecologie et des Sciences de l'environnement Ediscience international, Paris : 334-355.

[31] Reizer C. (1967) Aménagement piscicole du lac artificiel d'Ayamé. Centre technique Forestier Tropical, 108p.

[32] Ryding S. O., RAST W. (1994). Le contrôle de l'eutrophisation des lacs et réservoirs. Science de l'environnement 9, édition Masson, 294p.

[33] Sarma J. N. (2005). Fluvial process and morphology of the Brahmaputra River in Assam, India. *Geomorphology* 70 : 226-256.

[34] Shaw O. (2003). Quantification de l'envasement des lacs collinaires dans les petits bassins de la dorsale tunisienne. Mém. de DEA, université 7 Novembre à Carthage, 90p.

[35] Véi K. N. (2005). Suivi et évaluation de l'impact socio-temporel d'un projet d'aménagement du territoire en Afrique de l'Ouest. L'exemple du barrage de Taabo en Côte d'Ivoire. Apport de la télédétection et des SIG. Thèse de doctorat unique, université de Cocody, Côte d'Ivoire. 155p.

[36] Yapo O. (2002). Evaluation de l'état trophique du lac de Buyo (côte d'Ivoire), aspects physico-chimiques et biologiques. Thèse de doctorat, université d'Abobo-Adjamé, 328p.

[37] Zhongyuan C., Jiufa LI, Huanting S., Wang Z. (2001). Yangtze River of China: historical analysis of discharge variability and sediment flux. *Geomorphology* 41 : 77-91.

European Journal of Scientific Research
ISSN 1450-216X Vol.18 No.3 (2007), pp.479-482

http://www.eurojournals.com/ejsr.htm

Development of a Novel Spreading Code Generator for WCDMA Rake Receiver

Fazida Hanim Hashim
Department of Electric, Electronics and System, Faculty of Engineering
Universiti Kebangsaan Malaysia, Selangor, Malaysia
E-mail: fazida@vlsi.eng.ukm.my
Tel: (603) 89216009

Masuri Othman
Department of Electric, Electronics and System, Faculty of Engineering
Universiti Kebangsaan Malaysia, Selangor, Malaysia
E-mail: masuri@vlsi.eng.ukm.my
Tel: (603) 89216011

Mahamod Ismail
Department of Electric, Electronics and System, Faculty of Engineering
Universiti Kebangsaan Malaysia, Selangor, Malaysia
E-mail: mahamod@vlsi.eng.ukm.my
Tel: (603) 89216326

Abstract

This paper describes a proposed spreading method to improve the Bit Error Rate (BER) and user capacity in WCDMA system using Rake receiver. The method is applied to the WCDMA system up-link. The spreading process includes a new proposed random matrix constructed using the Walsh code generator, called randmat spreading code generator. Conventionally, the selection of seed is highly dependable on the Spreading Factor (SF) of the system. This spreading factor has to be in the power of 2. However, by carefully selecting a variable *n*, to result in SF-*n* for the input seed to the Walsh code, the simulation results show that the BER can improve dramatically. The proposed multi-level modulation method could also increase the data rate and user capacity of the WCDMA system. In terms of hardware implementation, a Walsh-based code generator has an advantage of being able to be implemented using look-up table (LUT) cascade. The main advantages of LUT cascades are its short design time, easy implementation, little memory requirements and fast operational time.

Keywords: Rake receiver, spreading code, Walsh Code, WCDMA.

Simulation Model

To test the functionality of the proposed spreading method, a simulation model using MATLAB that is close to the behavior of a mobile station as specified in the WCDMA standards is being used. The simulation model is depicted in Figure 1. To test the BER performance of the design, the simulation is

compared against the conventional WCDMA system using Orthogonal Variable Spreading Factor (OVSF) spreading code with all other parameters remaining the same.

At the first stage, MATLAB will generate the scrambling code, the initial signals for Mutual Access Interference (MAI), the spreading code (OVSF or randmat) and the multipath channels. The signals will then be multiplied by the scrambling code, followed by the spreading code. Then noise will be added to the modulated signals before being detected by the Rake receiver. The output signals are then being compared with the original input signals, and from here the BER and error counts can be formulated.

Figure 1: MATLAB simulation flowchart of an up-link WCDMA system.

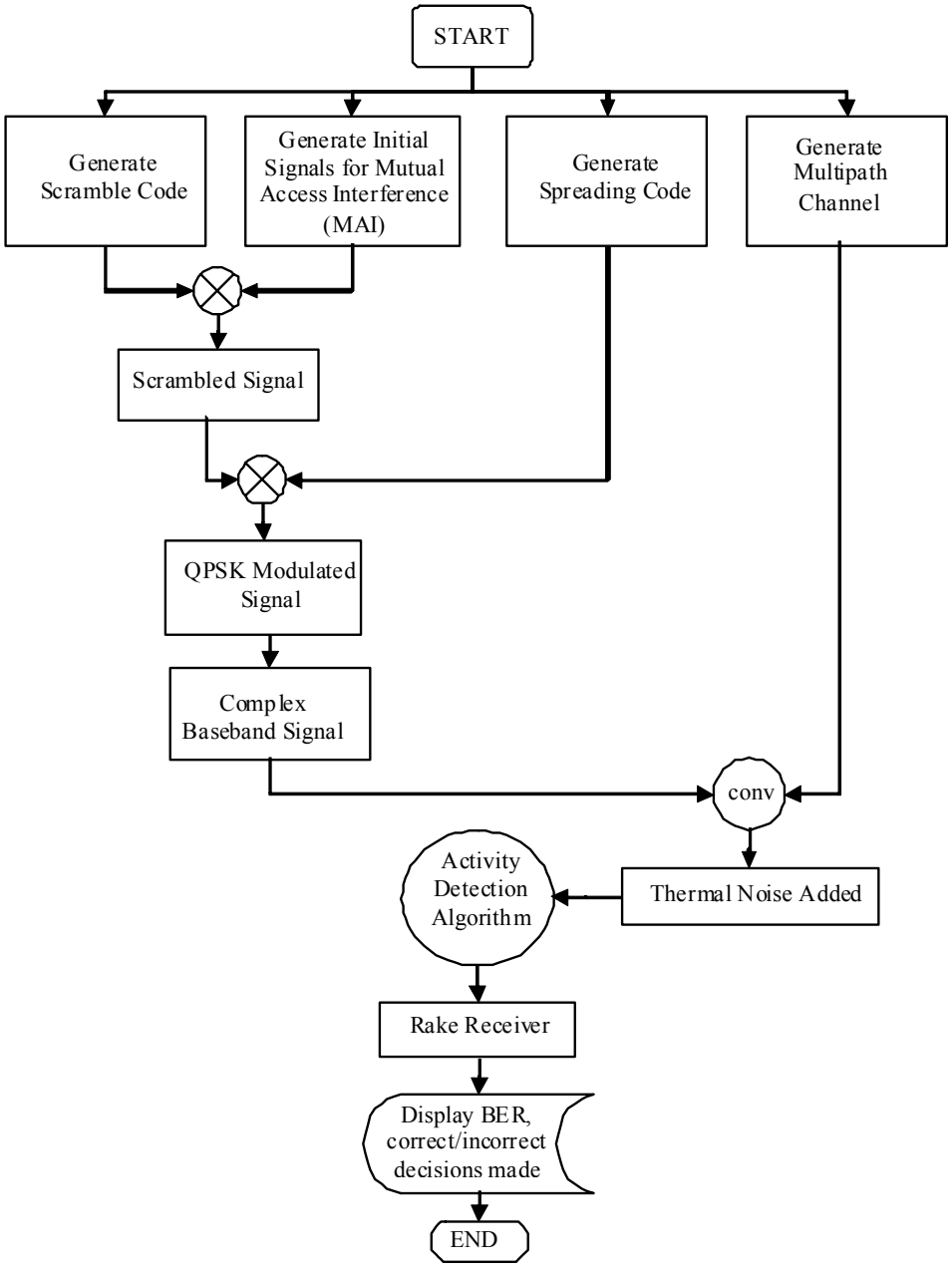

The design is tested for improved BER versus signal to noise ratio, Eb/No. A set of Eb/No values in the range of -20 to 20 are chosen and the corresponding BERs are calculated. Negative values for Eb/No are included because in simulation, negative values of Eb/No are the closest imitation to the real world environment. In addition, the simulation assumes 10 interfering mobile stations, with each

moving at 60 km/hr. These parameter values are purposely chosen to create a worst-case scenario environment. Table 1 shows some of the simulation parameters. The BER can be defined in terms of Probability of Error (POE):

$$POE = \frac{1}{2}(1 - erf)\sqrt{Eb/No} \quad (1)$$

where *erf* is the error function, *Eb* is the energy in one bit and *No* is the noise power spectral density (noise power in the one Hertz bandwidth). Eb has a unit of joules, No is in power (joules per second) per Hz (seconds). Therefore, Eb/No is a dimensionless term. On a more simplified note, BER can also be defined as:

$$BER = \frac{Errors}{TotalNumberofBits} \quad (2)$$

This formula is used to calculate the BER for each value of Eb/No and plot the graphs for both WCDMA system using OVSF spreading code and our proposed randmat spreading code. Figure 2 shows the MATLAB simulation environment. The prompt window displays the BER value, the maximum consecutive correct decisions made in a row and the maximum consecutive errors made in a row. The plots show the sequence of correct decisions and incorrect decisions. From the plot of incorrect decisions, the system can identify where and when it makes the most errors.

Table 1: Simulation parameters.

Parameter	Value
Spreading Factor	8
Oversampling rate	5
Velocity of mobile in km/hr	60
Number of interfering mobile stations	10
Number of pilot symbols per frame in DPCCH	8
Multipath delay profile	0
Weight gain for DPCCH *	5
Weight gain for DPDCH **	15

*DPCCH: Dedicated Physical Control Channel
**DPDCH: Dedicated Physical Data Channels

Figure 2: MATLAB simulation environment.

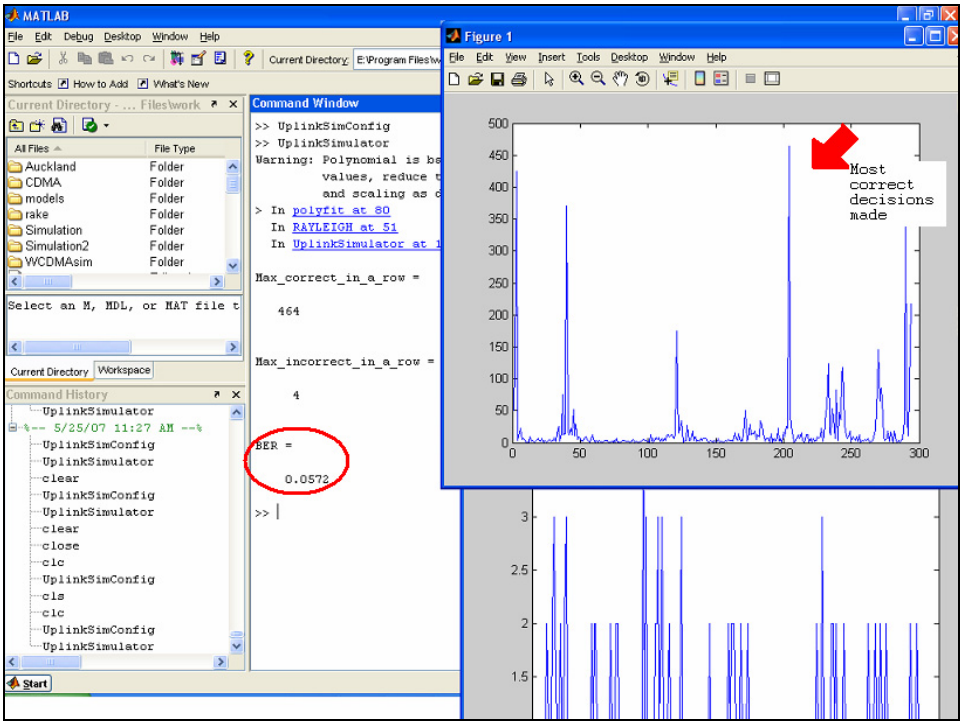

Results & Discussion

In theory, as signal over noise ratio, Eb/No increases, BER decreases. The simulation results in Figure 2 show exactly this. From the simulation using the conventional OVSF spreading code, excluding the negative values of Eb/No, the BER average is 0.2223. While simulation with our proposed randmat spreading code, the BER is improved to the average of 0.0546, an improvement of 75% in BER. There is also an improvement in maximum consecutive correct decisions made and a decrease in maximum consecutive errors made. These consistent simulation results show that the proposed randmat Walsh-based spreading code generator minimizes the error made when converting the data received at the Rake receiver.

Figure 3: BER versus Eb/No performance for OVSF code and randmat code.

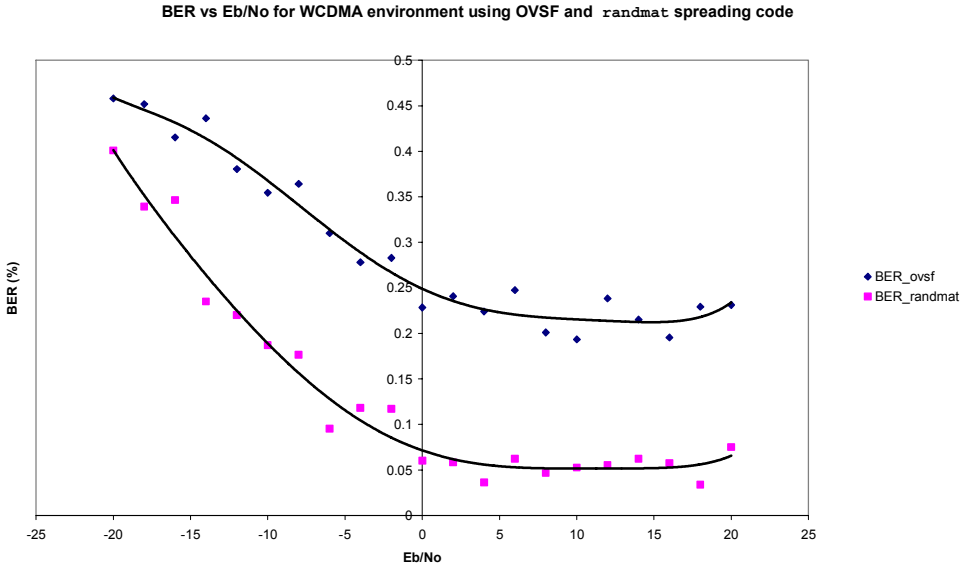

Conclusion

The simulation results are consistent with the results from a conventional simulation for WCDMA environment. It is proven that the design produces better BER values in comparison to a conventional OVSF spreading code. A Walsh-based spreading code generator is chosen because its hardware implementation can be simplified later in the FPGA and more importantly in the ASIC design. By using an LUT cascade for the Walsh-based spreading code generator, not only the usage of memory can be minimized, but a faster working system can be produced.

References

[1] Sklar, Bernard (2001). Digital Communication: Fundamental and Applications. 2nd Edition. New Jersey: Prentice Hall.

[2] Falkowsky, B.J., Yan, Shixing, (23-26 May 2005). Fixed Sign Walsh Transform and Its Iterative Hardware Architecture. IEEE International Symposium on Circuits and Systems, 2005. ISCAS 2005.

[3] The Mobile and Portable Radio Research Group, Virginia Technology University, Virginia, USA (26 February 2007). http://www.mprg.org/introduction/index.php.

[4] Breed,G., (January 2003). High Frequency Electronics, Bit Error Rate: Fundamental Concepts and Measurement Issues, Copyright 2003 Summit Technical Media.

European Journal of Scientific Research
ISSN 1450-216X Vol.18 No.3 (2007), pp.483-490

http://www.eurojournals.com/ejsr.htm

Effects of Magnesium Sulfate Applications on Magnesium Retention and Calcium Release in Calcareous Soil

El-Garawany, M. M
Agricl. & Vet. Training and Research Station, KFU. P. O. Box 420, Al-Hassa. 31982 Hofof, KSA
E-mail: mgarawany2000@yahoo.com

I. A. Al-Hawas
College of Agricultural and Food Sciences, King Faisal University
P. O. Box 420 & Al-Hassa. 31982 Al-Hofof, Kingdom of Saudi Arabia

A. M. Almadini
Agricl. & Vet. Training and Research Station, KFU. P. O. Box 55036Al-Hassa. 31982 Hofof, KSA
E-mail: aalmadini@kfu.edu.sa

Abstract

A surface calcareous soil sample was shacked with $MgSO_4$ solutions containing 0 to 9000 *mg* Mg l^{-1} for 48 hours at room temperature to study Mg retention and Ca release in the calcareous soil. $MgSO_4$ solutions were divided into three groups (group 1 of 25 treatments containing 0 to 100 *mg* Mg l^{-1}, group 2 of 10 treatments from 100 to 1000 *mg* Mg l^{-1} and group 3 of 9 treatments from 1000 to 9000 *mg* Mg l^{-1}). Recorded pH was 8.2 at 0 *mg* l^{-1} and 7.6 for all other concentrations. The amount of released Ca^{2+} was nearly stable for the three groups. Positive high correlations were found between the released Ca^{2+} and added Mg^{2+} for the first two groups of solutions. The Ca^{2+} or Mg^{2+} sulfate ion pairs were higher than the bicarbonate ion pairs with both ions. Ion pairs of Mg^{2+} were higher than those of Ca^{2+} with sulfate and bicarbonate ions. The ion pairs of $CaSO_4^\circ$, $MgSO_4^\circ$ and $MgHCO_3^+$ increased with increasing solution concentrations. The saturation index of gypsum increased with increasing concentration. The molar percentages of $MgCO_3$ in the total carbonate were 2.44, 31.11, 45.68, 292.4 and 1624.4% at 0, 50, 100, 1000 and 9000 *mg* Mg l^{-1}, respectively. Dolomite system appeared after the soil treatment with 100 *mg* Mg l^{-1} where molar% of $MgCO_3$ became 345.68%. Further increase of added Mg formed a system that becomes undersaturated with magnesite. The Mg^{2+} retention was curvilinear for all the ranges of added Mg^{2+}. Langmuir equation failed to explain the adsorption of Mg^{2+} on calcareous soil under the conditions of the current study. However, Freundlich extended equation showed two stages for Mg^{2+} retention by calcareous soil.

Keywords: Calcareous Soils, Calorthids, $MgSO_4$, Ca release, Mg^{2+} retention, Ion pairs, carbonate, saturation index

Introduction

The calcareous (i.e., calcisol) soils have a worldwide total extent of about 800 million hectares, being mainly located in the arid and semiarid regions. They are distinguished by the presence of calcium

carbonate ($CaCO_3$) in the parent materials with a calcic horizon, which is characterized with secondary accumulation of carbonates (usually Ca or Mg) in excess of 15% $CaCO_3$ equivalent and at least 5% more CO_3 than the underlying layer (FAO, 2000). The presence of high $CaCO_3$ contents in the soils shows various constraints for plant growth and production. They greatly influence the soil physical and chemical properties (McFadden et al., 1991). In general, calcareous soils are low in organic matter (OM) and available nitrogen (N). Their high pH levels reduce the availability of phosphate (due to the formation of unavailable calcium phosphates as apatite) and sometimes reduced micronutrient availability (e.g. zinc and iron inducing lime chlorosis). They may also possess nutritional problems of potassium (K) and magnesium (Mg), resulting from the nutritional imbalance between these elements with calcium (Ca) (Cho, 1991; FAO, 2000). Overall, many properties of the calcareous soils principally depend on the presence of $CaCO_3$ in aqueous solution. However, calcite is a low soluble salt with a solubility value of 0.15 $mmol\ L^{-1}$ (Amrhein and Suarez, 1990). On the other hand, it was shown that the additions of Mg^{2+} or SO_4^{2-} to synthetic and natural solutions of $CaCO_3$ enhance its solubility according to Akin and Lagerwerff (1965), who also devised a model based on Langmuir adsorption of all the ions on a crystal surface. This increase in solubility of $CaCO_3$ by applying Mg^{2+} salts was also implied by Marion and Babcock (1977). Moreover, Inskeep and Bloom (1986) added that the applications of Mg^{2+} at high concentrations will inhibit Ca^{2+} precipitation. Such effects of Mg^{2+} on the solubility of $CaCO_3$ are attributed to the surface reaction with Mg^{2+} and/or SO_4^{2-} during precipitation that can be explained by the formation of the dissolved ion-pairs of $MgCO_3$ and $CaSO_4$ (Berner, 1967). It was also proved that both Mg^{2+} and SO_4^{2-} ions inhibit Ca^{2+} precipitation as a result of adsorption onto calcite surface (Reddy and Wang, 1980). Mg^{2+} and Ca^{2+} are equally subjected to the adsorption on calcite surface (Akin and Lagerwerff, 1965). Mg^{2+} may also alter the formation of calcium phosphate precipitates and apatite formation through substituting Mg^{2+} for Ca^{2+} in such precipitates, which leads to disruption of mineral crystal structure by highly hydrated Mg^{2+} (Martens and Harriss, 1970). The increase in the adsorption of $H_2PO_4^{2-}$ and SO_4^{2-} anions in the presence of Ca^{2+} and/or Mg^{2+} relates to the formation of a surface complex between these anions and Ca^{2+} and Mg^{2+} ions (Shariatmadari and Mermut, 1999).

Thus, this investigation aims to study the effects of $MgSO_4$ applications on the Mg^{2+} retention and Ca^{2+} release in calcareous soil. The retention process of Mg^{2+} was also evaluated by the by Langmuir and Freundlich extended equation.

Materials and Methods

A bulk soil sample of Ap horizon from calcareous soil (calorthids) was collected from the Agricultural and Veterinary for Training and Research Station, King Faisal University, Al-Hassa, Saudi Arabia. The main physical and chemical properties of this soil are summarized in table 1. These properties were analyzed following the proper methods described in Klute et al. (1982) for physical and Page, et al. (1982) for chemical properties.

A duplicate of 2 g soil samples were shaken with a series of 50 ml of $MgSO_4$ solutions containing different concentrations of Mg^{2+} as $MgSO_4$ (i.e., from 0 to 9000 $mg\ Mg^{2+}\ l^{-1}$) for 48 hours at a constant speed of 40 rpm. The shaking process was completed under room temperature using polyethylene centrifuge tubes. The treatments of Mg^{2+} concentrations were divided into three groups as followings: 25 treatments represented group 1 from 0-4 to 96-100; 10 treatments represented group 2 from 100-200 to 900-1000 and 9 treatments represented group 3 from 1000-2000 to 8000-9000 $mg\ l^{-1}$ of Mg^{2+}. After competing the centrifuge steps, all filtrates were then analyzed for pH, Na^+, K^+, Ca^{2+}, Mg^{2+}, HCO^{-3}, CO_3^{2-}, SO_4^{2-} and Cl^{-1}. the analyses were completed following the proper procedures described in Page, et al. (1982). The total calcium carbonate ($CaCO_3$) content in the soil sample was determined according to Nelson (1982).

The ion activity (a_i) was calculated from the corresponding concentrations (c_i) using the following equation:

$$a_i = \delta_i C_i \quad (1)$$

where δ refer to the activity coefficients that were calculated from Davis's equation:

$$-\log \delta_i = 0.509\ Z_i^2\ \{[(\sqrt{\mu} / (1+ \sqrt{\mu}))] - 0.3\mu\} \quad (2)$$

Where Z_i is the ion's charge.

And μ is the ionic strength that was calculated from EC by equation described by Ponnamperuma et al. (1966) after being modified by El-Garawany and El-Fayoumy (2001) for the calciorthids soils.

$$\mu = 0.0168\ EC - 0.0044\ (R^2 = 0.989) \quad (3)$$

Langmuir fraction parameters (m = ABC/(1+BC)) were used to describe Mg^{2+} retention and the comparison of the maximum Mg^{2+} retention with the CEC of the soil under conditions of the current study. Also, Freundlich equation and extended Freundlich equation (Fitter and Sutton, 1975) were used to describe the Mg^{2+} retention. SAS program (SAS, 2001) was used to calculate the correlation coefficients and the linear equations between Mg^{2+} retention on the soil and Mg^{2+} concentrations of equilibrium solution after being shaked with $MgSO_4$.

Results

The physical and chemical properties of the soil sample were summarized in Table 1. The analyses indicated that the sample was high in $CaCO_3$ content (29.1%) and very low in OM (0.31) while CEC was 7.4 *cmol* kg^{-1}soil and exchangeable Ca^{2+} was (3.3 cmol kg^{-1}) higher than exchangeable Mg^{2+} (2.3 *cmol* kg^{-1}).

Table 2 shows the reduction in pH values of the supernatant after equilibrium time as a result of increased applied $MgSO_4$. The recorded pH was 8.2 at 0 $MgSO_4$ concentrations and become 7.6 for all other concentrations. The gradually addition of Mg^{2+} (Table 2) increased the released stable Ca^{2+} for every stage of Mg addition. The amounts of calcium were 0.45-0.95, 1.55-1.85 and 2-3 *mmol* l^{-1} for 0-4, 8-41 and 41-375 *mmol* l^{-1} of added Mg^{2+}, respectively. The release rates (*mmol* Ca^{2+} / *mmol* of added Mg^{2+}) were 0.10, 0.001 and 0 for the three added Mg stages, respectively. The differences in the release rates indicated that the Mg^{2+} ion might replace exchangeable Ca^{2+}, replace some of the structural Ca^{2+} of carbonate, react with non-carbonate substances or / and form some type of complex with other soil constituents. Alva et al. (1991) reported that a mechanism involving ion pair ($MgSO_4°$ and $CaSO_4°$) adsorption on mineral surface in which the presence of one ion in high concentration facilitates the formation of anion pair and increases the adsorption of other ion.

Positive high correlations were found between the released Ca and the added Mg for the first two stages of added Mg^{2+} (r = 0.797 and 0.921, respectively). However, the Ca^{2+} released at high Mg^{2+} concentrations (> 1000 *mg* Mg^{2+} l^{-1}) became constant. This might be explained by the following reasons: (1) The Mg^{2+} ions at this stage of high concentrations is not able to attack another source of Ca in the soil; (2) The available Ca^{2+} in the system might be precipitated as $CaSO_4$ or (3) The Mg^{2+} ions is involved in some types of complex reactions with other soil constituents.

The ion-pairs (Table 3) of sulphate with Ca^{+2} and Mg^{+2} were higher than the ion-pairs of bicarbonate with both ions. Also, the ion-pairs of Mg^{+2} were higher than of Ca^{+2} with sulphate and bicarbonate ions. This implies that the sulphate ion was the main ion in the system. The results showed that the $MgSO_4°$, $CaSO_4°$ and $MgHCO_4^+$ increased with the increases of the $MgSO_4$ concentration in irrigation water. The results in the table also showed that the gypsum precipitated at concentration of Mg^{+2} higher more than 700 *mg* l^{-1} where the saturation index (SI) of gypsum increased with the increase of $MgSO_4$ added in the solutions. However, the SI became less than 1 at the 700 mg Mg^{+2} l^{-1} and then increased to more than 1. This means that the gypsum precipitated at Mg^{+2} concentrations higher than 700 *mg* l^{-1} as $MgSO_4$.

The Mg^{2+} retention by soil was curvilinear for all the Mg^{+2} ranges from zero to 9000 *mg* l^{-1} (Table 4 and Fig.1). The results show that the retention of Mg^{+2} can be subdivided to: 0-0.4, 0.4-3, 3-19, 19-29, 29-125, 125-250 and 250-375 *mg* l^{-1} Mg^{+2}. For every part of the curve, the maximum

absorption (A) according to Langmuir equation was calculated (Table 5). The maximum A values were 2.07, 3.97, 3.55, 7.1, 27.97, 26.04, 47.25 and 67.42 *mmol* Mg^{+2} / 100g soil, respectively.

The calculated values of retained Mg^{+2} clearly indicated that the surface retention reached its maximum in a range varies between 72 and 450 *mg* l^{-1} of added Mg^{+2}. The maximum retention of this stage represented 95.95% of CEC of the soil sample. The Mg^{+2} bonding energy values decreased to about 0.5 of its initial value with the increased Mg^{+2} adsorption representing 53.7% of the CEC. Additional decreases in the Mg^{+2} bonding energy to 0.1 of its initial value at maximum surface retention was observed. Also, the bonding energy of retained Mg^{+2} continued to drop 100 times when surface retention seemed to be covered. These large drops in the bonding energy might indicate other retention mechanisms and/or precipitation perhaps occurred. The Mg^{+2} ions react with other soil components as carbonates, hydroxides, silicates and may be chelated by soil organic matter (Salmon, 1963). Carbonates containing appreciable Mg showed a decrease in solubility with increasing Mg^{2+} ion. Whereas, carbonates with low or no Mg showed an increase in solubility (Hassett and Jurinak, 1971).

The maximum retention increased with Mg concentration treatments. These could be due to heterogeneity of soil constituents' surfaces especially of carbonate in soil. Akin and Lagerwerff (1965) showed that the failure of Langmuir equation to explain the adsorption of Mg^{+2} in calcareous soil may be attributed to the impurity and partial crystalline of carbonate in soil. In addition, the soils mostly possess a degree of complexity with surfaces of unknown heterogeneity. The equation however requires well-defined conditions regarding the absorbed ions. Therefore, it is suggested that the equation is best treated as empirical equation describing actual sorption processes

The maximum amount of Mg^{2+} retention and the proportion of the total CEC are shown in Table 5. The percentages of maximum amount (A%) from CEC were 27.9, 53.7, 96, 377.9, 352, 638.5, and 911% for 0-0.4, 0.4-3, 3-19, 19-29, 29-125, 125-250, and 250-375 *mmol* l^{-1} treatments, respectively.

The Freundlich equation was used to describe the Mg retention data for all $Mg_{\neg\neg}{}^{\neg\neg 2+}$ concentrations. Fitter and Sutton (1975) extended the Freundlich equation by including a constant D which account for ions already present in the soil

$m = A\ C^{B}$-D (where A and B are the maximum retention and bonding energy, respectively)

The Freundlich extended equation (Fig. 2) showed two stages for $Mg_{\neg\neg}{}^{\neg\neg 2+}$ retention by calcareous soil. The first stage (I) represents the saturation steps of exchangeable sites in the soil. The second stage (II) describes the retention of $Mg_{\neg\neg}{}^{\neg\neg 2+}$ with other soil compounds or processes. The critical value of refraction point between the two stages is the value of CEC without the exchangeable $Mg_{\neg\neg}{}^{\neg\neg 2+}$ value.

Discussion

From above results, it could be concluded that the decline of the pH values could be attributed to the exchange of Mg^{2+} for H^{2+} ions in Mg-soil system. Available exchangeable sites or complexes with organic matter do not limit the Mg^{2+} retention. On the other hand, carbonate compounds, iron and aluminum amorphous materials and precipitation might be considered. The fact that Mg^{2+} retention is not limited by available exchangeable sites could be explained by the linear nature of the curve for all Mg^{2+} concentrations. Other explanations to such fact are that the precipitation reaction, the Mg^{2+} sorption after occupying the exchangeable sites and lime formation with $MgCO_3$ continued up-to 24 mole $MgCO_3$ %. Mg^{2+} ions can be replaced by the Ca^{2+} ions and precipitated with other anions in the soil system that is particularly accompanied with Mg^{2+} ion. Mg^{2+} salts (i.e., $MgSO_4$) can be used to improve the calcareous soil. The addition of Mg^{2+} ion elevates the ratio of Mg to Ca, which may help in releasing Ca ions from $CaCO_3$ and causes distortion of the $CaCO_3$ crystallize.

Table 1: The physical and chemical analyses of soil –water extract (1:2.5)

Type	item	The property	unit	Value
Physical Properties	Soil moistures	Field capacity	%	26
		Saturation percentage	%	40
	Particle size distribution	Clay	%	14.5
		Silt	%	55.2
		Sand	%	30.3
Chemical Properties	pH	-	-	8.1
	EC	-	($dS\ m^{-1}$)	2.1
	Soluble cations	Ca^{2+}	($mmol\ l^{-1}$)	5. 6
		Mg^{2+}		3.1
		Na^{+}		3.9
		K^{+}		1.5
	Soluble anions	CO_3^{2-}		Nil
		HCO_3^{-}		1.7
		Cl^{-}		14.0
		SO_4^{2-}		2.7
		$CaCO_3$	%	29.1
		Organic Matter	($g\ kg^{-1}$)	3.0
		CEC	($cmol\ kg^{-1}$)	7.4
	Exchangeable cations	Ca^{2+}	($cmol\ kg^{-1}$)	3.3
		Mg^{2+}		2.3
		$NaHCO_3$- P	($mg\ l^{-1}$)	7.0

Table 2: The pH, EC, soluble ions, Ca/Mg molar ratio and mole% Mg CO_3 in soil extract after addition of Mg SO_4 to calcareous soil and shaking for 48 hours.

added Mg as $MgSO_4$ (*mg* Mg l^{-1})	pH	Article I. EC *dS* cm^{-1}	*Article II.* Concentration *mmol liter-1*				Activity# *mmol* $liter^{-1}$		Ca/Mg (Molar ratio)	$MgCO_3$ (mole %)
			Mg^{2+}	Ca^{2+}	SO_4^{2-}	HCO_3^{-}	Mg^{2+}	Ca^{2+}		
0	8.2	0.15	0.05	0.30	-	-	-	-	6.06	2.44
10	7.7	0.19	0.33	0.53	0.25	0.18	0.27	0.43	1.58	9.27
72	7.6	0.54	2.18	0.97	2.91	0.19	1.52	0.68	0.44	33.27
450	7.6	2.30	18.70	1.70	17.32	0.50	9.77	0.89	0.09	
700	7.6	2.90	26.37	1.75	23.70	0.37	12.97	0.86	0.067	
3000	7.6	8.00	112.25	2.75	105.50	3.00	41.40	1.02	0.024	
6000	7.6	14.50	234.25	2.75	200.00	3.01	73.80	0.87	0.012	
9000	7.6	19.50	350.00	3.00	318.00	3.50	104.00	0.84	0.009	

Table 3: Ions pairs and saturation index of gypsum in soil extract after addition of $MgSO_4$ to calcareous soil and shaking for 48 hours

Added Mg (*mg* l^{-1}) as $MgSO_4$	Ions pairs (*mmol* l^{-1})				Saturation index (SI) of gypsum
	$CaSO_4^{\circ}$	$MgSO_4^{\circ}$	$CaHCO_3^{+}$	$MgHCO_3^{+}$	
10	0.016	0.053	0.007	0.001	0.0036
72	0.262	0.530	0.002	0.041	0.058
450	1.531	15.042	0.007	0.062	0.340
700	1.910	2.570	0.004	40.190	0.420
3000	7.520	273.887	0.043	1.404	1.660
6000	10.456	791.969	0.036	2.147	2.299
9000	15.118	1671.25	0.040	3.888	3.330

Table 4: Liner equations between the Mg concentration (C) of equilibrium solution and Mg retention (x/m) by calcareous soil after shaking with $MgSO_4$ for 48 hours.

Added Mg (*mg l*$^{-1}$) as $MgSO_4$	Linear equation	Correlation coefficient
0-10	X/m = 1.93 + 12.18 C*	0.999
10-72	X/m = 198.7 + 3.48 C	0.940
72-450	X/m = 453.1+ 2.04 C	0.973
450-700	X/m = 344.6 + 2.15 C	0.970
700-3000	X/m = -516.5 + 2.90 C	0.999
3000-6000	X/m = 6177 + 0.57 C	0.993
6000-9000	X/m = -9089 + 2.87 C	

* Where x/m is *mg* adsorbed Mg *kg*$^{-1}$ soil and C is *mg* Mg *l* $^{-1}$ of equilibrium solution.

Table 5: Langmuir fraction parameters (m = ABC/(1+BC)) used to describe Mg^{2+} retention and comparison of the maximum Mg^{2+} retention and CEC of soil under study.

Added Mg (*mg l*$^{-1}$) as $MgSO_4$	Parameter *		A% of total CEC**
	A	B	
	(*cmole*$_c$ *kg*$^{-1}$)		
0-10	2.07	5.3 x 10^{-2}	27.91
10-72	3.97	2.1 x 10^{-2}	53.56
72-450	7.10	5.6 x 10^{-3}	95.95
450-700	27.97	5.4 x 10^{-4}	377.91
700-3000	26.04	5.5 x 10^{-4}	351.89
3000-6000	47.25	7.81 x 10^{-4}	638.51
6000-9000	67.42	5.75 x 10^{-5}	911.08

* A and B are the maximum retention and bonding energy, respectively.
** CEC of soil was 7.4 *cmolec kg*$^{-1}$.

Figure 1: Magnesium retention by calcareous soil (Mg, *mg kg*$^{-1}$), after shaking with $MgSO_4$ for 48 hours (*Mg, mg l*$^{-1}$).

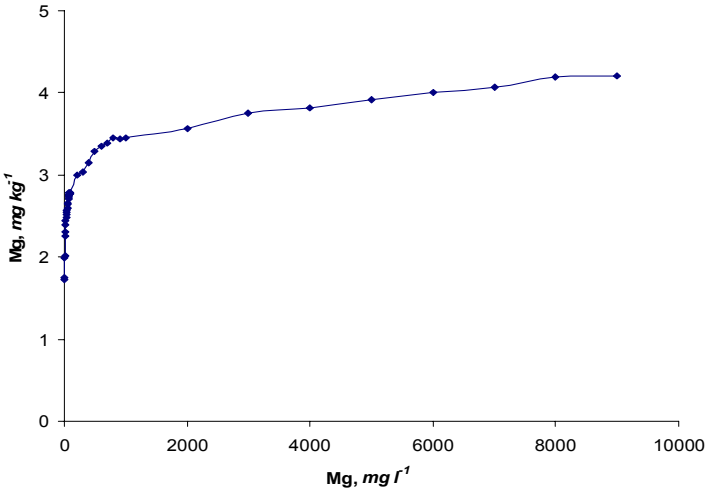

Figure 2: The relationship, using Freundlich and extended Freundlich eqs., between the log Mg conc. (Log C, (C, *mg* l^{-1})) of equil. solution and log Mg retention, x/m (Log m, (m, kg^{-1}) by calcareous soil after shaking with $MgSO_4$ for 48 hours.

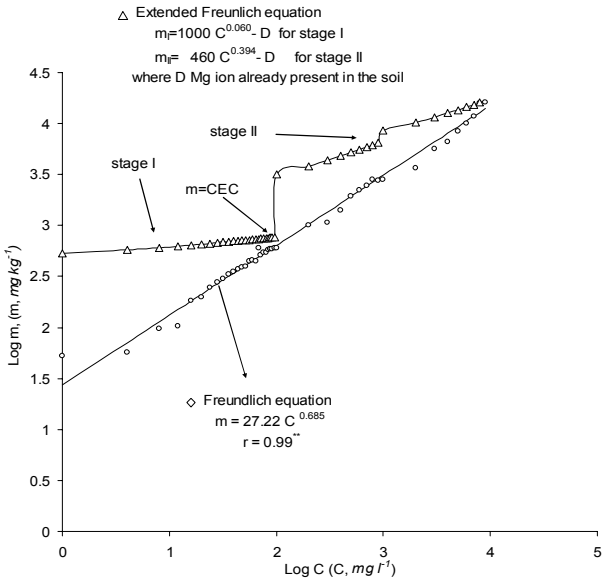

References

[1] Akin, G. W. and Lagerwerff. J. V. (1965) Calcium carbonate equilibria in solutions open to the air. II. Enhanced solubility of $CaCO_3$ in the presence of Mg^{2+} and SO_4^{2-}. Geochim. Cosmochim. Acta, 29: 353-360.

[2] Alva, A. K., Sumner M. E. and Miller. W. P. (1991) Relationship between ionic strength and electrical conductivity for soil solutions. Soil Science 152: 239-241.

[3] Amrhein, C. and Suarez, D. L. (1990) Determining sodium-calcium selectivity in calcareous and gypsiferous soils. Soil Sci. Soc. Amer. J., 54, 999-1007.

[4] Berner, R. A. (1967) Comprative dissolution characteristics of carbonate minerals in the presence and absence of aqueous magnesium ion. Amer. J. Sci., 265: 45-70.

[5] Cho, C. M. (1991) Phosphate transport in calcium – saturated system: I. Theory, Soil Sci. Soc. Amer. J., 55, 1275-1281.

[6] 6. El-Garawany, M. M. and El-Fayoumy. M. E.) 2001(The relationship between ionic strength and electrical conductivity and prediction of Ca-Mg- carbonate in some great groups of Aridisols and Entisols. Egypt. J. Appl. Sci. 16: (16) 374-389.

[7] FAO (2000). Calcareous Soils. United Nation, Rome, Italy, http://www.fao.org/WAICENT/ FaoInfo/Agricult/agl/ agll/prosoil/calc.htm

[8] Fitter, A. H. and. Sutton. C. D. (1975) The use of the Freundlich isotherm for phosphate sorption data. J. Soil Sci. 26:241-246.

[9] Hassett, J. and Jurinak J. J. (1971) Effect of Mg^{2+} ion on the solubility of solid carbonates. Soil Sci. Soc. Am. Proc. 35: 403-406.

[10] Inskeep, W. P. and Bloom P. R. (1986) Calcium carbonate saturation in solution of calciaquous. Soil Sci. Soc. Am. J. 50: 1431-1437.

[11] Kulte, A. (ed) (1986). Methods of soil analysis, Part 1-Physical and mineralogical methods, Agronomy, 2nd ed.,No. 9, Part 1, 53-82.

[12] Marion, G. M. and Babcock K. L. (1977) The solubility of calcium carbonate and phosphate in calcareous soils suspensions. Soil Sci. Soc. Am. J. 41: 724-728.

[13] Martens, C. S. and Harriss R. C. (1970) Inhibition or apatite precipitation in the marine environment by magnesium ion. Geochim. Cosmochim. Acta. 37: 621-625.

[14] McFadden, L. C., Amundson R. C. and Chadwick O. A. (1991) Numurical modeling, chemical and isotopic studies of carbonate accumulation in soil arid regions. In Occurrence, characterstics and genesis of carbonate, gypsum and silica accumulation in soils. Soil Sci. Soc. of Amer. Madison, WI, USA.

[15] Nelson, R. E. (1982) Carbonate and gypsum. in: Methods of Soil Analysis, part 2 p. 181-196, (ed) A. L. Page, Monograph No 9. Am. Soc. of Agronomy, Madison, WI, USA.

[16] Ponnamperuma, F. N., Tianco E. M. and Loy T. A. (1966) Ionic strength of solutions of flooded soils and other natural aqueous solutions from specific conductance. Soil Science 92: 408-410.

[17] Reddy, M. M. and Wang K. K. (1980) Crystallization of calcium carbonate in the presence of metal ion at ph 8.8-and 25° C. J. Crystal Growth 50: 470-480.

[18] Rhoades, J. D. (1982) "Soluble salts" in: Methods of Soil Analysis, part 2 p. 167-178, (ed) A. L. Page, Monograph No 9. Am. Soc. of Agronomy, Madison, WI, USA.

[19] SAS, Institute (2001) SAS procedures guide, Version 6, 3rd edition. SAS institute, Cary.

[20] Salmon, R. C. (1963) Magnesium relationships in soils and plants. J. Sci. Food Agric. 14: 505-610.

[21] Shariatmadari, H. and A. R. Mermut. (1999) Magnesium and silicon phosphate desorption in semectite-, palygorskite-, and sepiolite-calcite systems. Soil Sci. Soc. Am. J. 63: 1167-1173.

[22] Welcher, F. J. (1957) The analytical uses of EDTA. D. Van. Nostrand Company, Inc. Princeton. N. J. USA. P. 258-259.

European Journal of Scientific Research
ISSN 1450-216X Vol.18 No.3 (2007), pp.491-499

http://www.eurojournals.com/ejsr.htm

Malicious Objects Dynamics in the Presence of Anti Malicious Software

Hemraj Saini
Computer Science and Information System Group, Practice School Division
Birla Institute of Technology and Science, Pilani
Rajasthan (India) – 333031
E-mail: hemraj@bits-pilani.ac.in

Dinesh Saini
Computer Science and Information System Group, Information Processing Unit
Birla Institute of Technology and Science, Pilani
Rajasthan (India) – 333031
E-mail: dsaini@bits-pilani.ac.in

Abstract

To understand the behavior of malicious objects and to know the population dynamics at some instance (t), modeling plays an important role. In this paper we discuss a general model of malicious object dynamics which tells the spreading behavior and the population of malicious objects at a particular instance. Malicious objects first find out the target node for attack, from the existing domain of uninfected target nodes. Thereafter, the uninfected target node converts in either one of productively active infectious node, mysterious infectious node, long-lived infectious node, or latently infectious node. Further the non-infectious malicious object may convert into the infectious malicious object and help to spread the malicious object by attacking the remaining target nodes. The attack may occur in the presence of anti malicious software (AMS). The population dynamics depends on the efficacy of AMS, the rate of production of infected nodes and the rate of decay of malicious object. The model shows, how the uninfected target nodes converts to the infected nodes and due to the users awareness and AMS how the infected nodes converts back into the uninfected target nodes. The model is discrete one and is helpful to present the behavior of various fast spreading worms such as Red Code.

Keywords: Malicious Object, Anti Malicious Object, Mathematical Model.

1. Introduction

In the present era of Internet, security of information is the major concern. A large number of malicious objects are infecting the interconnected computers. A report according to (A. Mukhopadhyay et al., 2007) adds that, during the period May 2004 to May 2005, about 73 million consumers have received malicious attack. Another research mentioned in (A. Mukhopadhyay et al., 2007), says that, 0.6 million Internet banking customers turned away from online financial transactions due to fear of keystroke logging Trojans and phishing mails. Fast spreading worms such as Morris worm arose in 1988 and infected thousands of computers and cost millions of dollars to both public and private sectors (C. C.

Zou, 2003). By taking a specific example, we can feel the threat of malicious attacks such as, the Code Red worm and Nimda worm also influence a huge amount of valuable information stored at thousands of computers within a very sort period i.e. in some hours (C. C. Zou et al., 2002; Z. Chen et al., 2003; D. Moore et al., 2002)

A lot of work has been carried out for the virtual vaccination of malicious objects infection. Ten to fifteen years ago epidemiological or biological based nonlinear differential models were developed to understand the malicious objects propagation (C. C. Zou et al., 2005; V. Capasoo, 1993; J. W. Mickens et al., 2005; P. Liu et al., 2005; J. O. Khephart et al., 1998). In the case, where malicious objects spread slowly in the global prevalence, these epidemiological models are not perfect to predict the virtual behavior (Khephart et al., 1998). Therefore to understand the propagation of malicious objects is still a challenge due to the discrete nature of the attacks (Z. Chen et al., 2003). Also a large number of constraints such as distinct nature of each malicious object, distinct mode of propagation, less visibility of malicious objects to the user, etc. play an important roll in making it difficult to understand their behavior.

Figure 1: Malicious objects attack and conversion of different types of nodes.

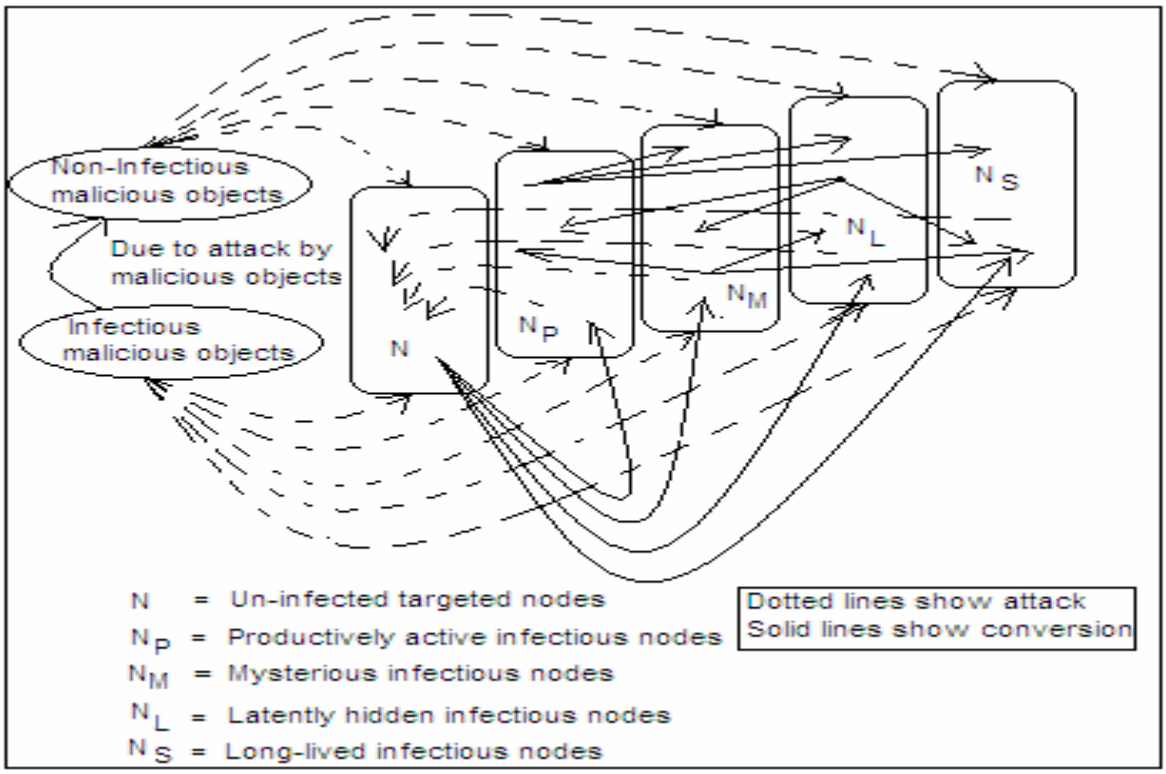

We are providing a better explanation of the malicious object propagation and proposing a discrete model for malicious object dynamics. In our model, we fixed certain parameters to predict the behavior of malicious objects. The paper is organized as under:

- Theoretical modeling the dynamics of transmission
- Nomenclature
- Mathematical model and its analysis
- Summary and discussion

2. Theoretical Modeling the Dynamics of Transmission

Figure-1 shows the attack of the infectious and non-infectious malicious objects, conversion of uninfected target nodes to productively active infectious nodes (which are actively propagating malicious objects), mysterious infectious nodes (whose behavior is unknown), latently infectious nodes (which contain pro-malicious objects but don't produce malicious objects till they become active), or long-lived infectious nodes (those are infected and long-lived), and vice versa.

3. Nomenclature

In discrete-event simulation paradigm, the dynamics of a complex system are captured by discrete (temporal) state variables, where an event is a combined process of large number of state transitions between a set of state variables accomplished within the event execution time (L. W. Schruben, 2000; J. Misra et al., 1986), the key idea is to segregate the complete state-space into a disjoint set of independent events that can be executed simultaneously without any interaction (Fishman, S. et al., 1993). The application of discrete-event based system modeling techniques in large-scale computer and communication networks has demonstrated the accuracy of this approach for higher order system dynamics within the limits of input data, state partitioning algorithms, uncertainty of information propagation and highly mobile entities (M. Pidd, 1995).

In malicious object attack, it is difficult to predict the time of next attack. The attack is totally discrete event. So, we are opting discrete modeling for our work. Malicious object dynamics model provides a good scene of the malicious object elimination, replication, and propagation during anti malicious object treatment. Thus for evaluating the efficacy of anti malicious object software and understanding the dynamics of propagation, it is of great interest to estimate dynamics parameters for the whole population and for individual computer. We proposed a mathematical model for mathematical dynamics by considering following computers or nodes and malicious object parameters:

N: Uninfected target nodes (vulnerable nodes).
N_M: Mysterious infectious nodes with unknown behavior.
N_L: Latently or hidden infectious nodes.
N_P: Productively (Actively propagating malicious object) infectious nodes.
N_S: Long-lived infectious nodes.
V_I: Infectious malicious objects.
V_{NI}: Non-infectious malicious objects.
$\Theta_L(t)$: Conversion rate (per unit time) of N to N_L at instance t.
$\Theta_M(t)$: Conversion rate (per unit time) of N to N_M at instance t.
$\Theta_S(t)$: Conversion rate (per unit time) of N to N_S at instance t.
$\delta_L(t)$: Conversion rate (per unit time) of N_L to N_P at instance t.
$\delta_M(t)$: Death rate (per unit time) of N_M after producing new infections at instance t.
$\delta_S(t)$: Death rate (per unit time) of N_S after producing new infections at instance t.
$\delta_P(t)$: Death rate (per unit time) of N_P after producing new infections at instance t.
$\mu_M(t)$: Death rate (per unit time) of N_M without producing new infections at instance t.
$\mu_L(t)$: Death rate (per unit time) of N_L without producing new infections at instance t.
$\mu_S(t)$: Death rate (per unit time) of N_S without producing new infections at instance t.
$\mu_P(t)$: Death rate (per unit time) of N_P without producing new infections at instance t.
$C_1(t)$: Death rate (per unit time) of infectious malicious objects at instance t.
$C_2(t)$: Death rate (per unit time) of non infectious malicious objects at instance t.
γ: Efficacy of anti malicious software.
Z: Total number of infections produced by infectious nodes before death during their life time.
η: Proportion of noninfectious malicious objects produced by infectious nodes.
$P(t)$: Additional average malicious object production rate at instance t.
x: Total number of IP addresses available in the network

s: Scanning rate of IP table

4. Mathematical Model and its Analysis

Without the intervention of anti malicious treatment, uninfected target nodes (N) may either decrease due to malicious object infection due to proliferation of new users and malicious object infection. Some uninfected target nodes (N) are infected by infectious malicious objects (V_I) and may become mysterious infectious nodes (N_M), latently or hidden infectious nodes (N_L), long-lived infectious nodes (N_S), or productively infectious nodes (N_P) as shown in figure-1.

Latently infectious nodes (N_L) may be stimulated to become productively infectious nodes (NP) with a rate $\delta_L(t)$. Infectious nodes N_M , N_S , and N_P can die (recovered from the infection and converted back to the uninfected targeted node) at the rates say $\delta_M(t)$, $\delta_S(t)$, and $\delta_P(t)$, respectively after producing or replicating malicious object an average of total Z infections during their life time. Infectious nodes N_M, N_S, and N_P can also be totally jammed (killed) at the rates $\mu_M(t)$, $\mu_S(t)$, and $\mu_L(t)$ respectively, without replicating or producing malicious objects.

We assume the proportion of noninfectious malicious objects propagated by infected nodes (due to user's cautiousness) is η without the intervention of AMS. The elimination rates (nodes are no further targeted nodes due to some means such as patching to remove the vulnerability) of infectious malicious objects and noninfectious malicious object are, say $C_1(t)$ and $C_2(t)$ respectively.

Now we assume that the anti malicious treatment is having more than one AMS. Here we model the effect of AMS by reducing the infection rate 1 to (1- γ), where γ is AMS efficacy and 0≤ γ≤1. If γ = 0, then AMS is totally ineffective and γ=1, then AMS is absolutely effective. We assume that AMS will not block the malicious objects perfectly and x is the size of IP address space such as 16, 32, 64 etc. Therefore the probability to choose a node will be $1/2^x$. The probability not to choose a node from the IP table is $(1-1/2^x)$. If scanning rate of an IP table is S, then the rate of not choosing a node is $(1-1/2^x)^S$. Therefore the possibility to choose a target node is $(1-(1-1/2^x)^S)$.

We describe the population of infectious malicious nodes as a function of time, with starting time as t=0; the only infectious malicious objects to be considered should be those in the interval [t, t+h], h is the length of time interval.

Dividing this interval into n equal parts, so that $\Delta\tau = (t+h)/n$ and defining $\tau_1 = t, \tau_2 = t+\Delta\tau, ...\tau_{n+1} = n\Delta\tau$ i.e. τ j=t + (j-1) $\Delta\tau$, j=1, 2, …, n+1, we should state, for $\Delta\tau$ small enough, that the number of mysterious infectious nodes in the interval [τ j, τ j+1]=[τ j, τ j+$\Delta\tau$] is given approximately as

(Aggregate production rate for Mysterious malicious node at instance τ j)((τ j+1 - τ j) =$\Delta\tau$)

Then, the number of mysterious infectious nodes in the interval remain infectious at t is approximately,

$Q_M + (1-\gamma)(N_t - N_{M_t})(1-(1-1/2^x)^S\theta_M(\tau_j)\Delta\tau - \delta_M(\tau_j)\Delta\tau - \mu_M(\tau_j)\Delta\tau$, j=1, 2, … n, and therefore, the total number of mysterious malicious nodes at t may be written, as $N_{M_{t+\Delta\tau}} = \sum[Q_M + (1-\gamma)(N_t - N_{M_t})(1-(1-1/2^x)^S)\theta_M(\tau_j)\Delta\tau - \mu_M(\tau_j)\Delta\tau]$, where, $Q_M = \dfrac{Z_t\delta_M(t)}{(\delta_M(t)+\delta_P(t)+\delta_S(t)+\delta_L(t))}$ is the number of infections produced by mysterious malicious nodes before they died at an instance t.

Where, in the limit $\Delta\tau \to 0$, gives

$$N_{M_{t+h}} = \int_t^{t+h}[Q_M + (1-\gamma)(N_t - N_{M_t})(1-(1-1/2^x)^S)\theta_M(\tau) - \delta_M(M) - \mu_M(\tau)]d\tau\,,\ t \geq 0 \qquad (1)$$

Here N_t, N_{M_t} represents the vulnerable nodes and mysterious infectious nodes respectively at some time tick t. $N_{M_{t+h}}$ represents the mysterious infectious nodes after the interval h. So the value

$(N_t - N_{M_t})$ represents the actual targeted nodes because there is no sense of considering the attack on already mysterious infectious nodes.

$$N_{S_{t+h}} = \int_t^{t+h} [Q_S + (1-\gamma)(N_t - N_{S_t})(1-(1-1/2^x)^S)\theta_S(\tau) - \delta_S(\tau) - \mu_S(\tau)]d\tau \text{ , } t \geq 0 \quad (2)$$

Here N_t, N_{S_t} represents the vulnerable nodes and Long-lived infectious nodes respectively at some time tick t. $N_{S_{t+h}}$ represents the Long-lived infectious nodes after the interval h. So the value $(N_t - N_{S_t})$ represents the actual targeted nodes because there is no sense of considering the attack on already Long-lived infectious nodes and $Q_S = \frac{Z_t \delta_S(t)}{(\delta_M(t) + \delta_P(t) + \delta_S(t) + \delta_L(t))}$ is the number of infections produced by long-lived malicious nodes before they died at an instance t.

$$N_{L_{t+h}} = \int_t^{t+h} [Q_L + (1-\gamma)(N_t - N_{L_t})(1-(1-1/2^x)^S)\theta_L(\tau) - \delta_L(\tau) - \mu_L(\tau)]d\tau \text{ , } t \geq 0 \quad (3)$$

Here N_t, N_{L_t} represents the vulnerable nodes and latently hidden infectious nodes respectively at some time tick t. $N_{L_{t+h}}$ represents the latently hidden infectious nodes after the interval h. So the value $(N_t - N_{L_t})$ represents the actual targeted nodes because there is no sense of considering the attack on already latently hidden infectious nodes and $Q_L = \frac{Z_t \delta_L(t)}{(\delta_M(t) + \delta_P(t) + \delta_S(t) + \delta_L(t))}$ is the number of infections produced by latently hidden malicious nodes before they died at an instance t.

$$N_{P_{t+h}} = \int_t^{t+h} [Q_P + (1-\gamma)(N_t - N_{P_t})(1-(1-1/2^x)^S)\theta_L(\tau) + \delta_L(\tau) - \delta_P(\tau) - \mu_P(\tau)]d\tau \text{ , } t \geq 0 \quad (4)$$

Here N_t, N_{P_t} represents the vulnerable nodes and productively active infectious nodes respectively at some time tick t. $N_{P_{t+h}}$ represents the productively active infectious nodes after the interval h. So the value $(N_t - N_{P_t})$ represents the actual targeted nodes because there is no sense of considering the attack on already productively active infectious nodes and $Q_P = \frac{Z_t \delta_P(t)}{(\delta_M(t) + \delta_P(t) + \delta_S(t) + \delta_L(t))}$ is the number of infections produced by mysterious malicious nodes before they died at an instance t.

$$V_{I_{t+h}} = V_{I_t} + \int_t^{t+h} [(1-\eta)P(\tau)(V_t - V_{I_t}) - c_1(\tau)]d\tau \quad (5)$$

Where, $P(\tau)$ is additional production rate of malicious objects i.e. number of malicious objects outbreak per second and $c_1(\tau)$ is the elimination rate of infectious malicious objects that is proportional to the AMS efficacy.

$$V_{NI_{t+h}} = V_{NI_t} + \int_t^{t+h} [\eta(1-P(\tau))V_{I_t} + \delta_M(\tau) + \delta_S(\tau) + \delta_P(\tau) - c_2(\tau)]d\tau \quad (6)$$

$$V_{t+h} = V_{I_{t+h}} + V_{NI_{t+h}} \quad (7)$$

The conversion rate (per unit time) of N to N_M at instance t, $\Theta M_{(t)}$, is a time function. To find it we assume that the infection can be propagated by nodes through sending messages in an average time, say t_0. Also, each node transmits the infection when, used by the first time in an infected node, it is used by second time in a targeted one.

Another assumption is that once the Network is built, the numbers of total nodes are rarely changed within a short span of time. So, we can say that the proportions of infected and targeted nodes should follow,

$(I_{(t)} = (M_{(t)} + P_{(t)} + S_{(t)} + L_{(t)})) + T_{(t)} = 1$, where, $M_{(t)}$, $P_{(t)}$, $S_{(t)}$, $L_{(t)}$, and $T_{(t)}$ are the proportions of mysterious infectious, productively infected active infectious, Long-lived infectious, latently hidden infectious, and target nodes, respectively, at any instant t.

The event conversion of mysterious infectious nodes into the targeted nodes due to the effect of AMS increases the domain of attack to convert the attacked node into mysterious infectious one with the probability, as

$M_{(t)}(P_{(t+t_0)} + S_{(t+t_0)} + L_{(t+t_0)} + T_{(t+t_0)} = M_{(t)}(1 - M_{(t+t_0)})$ In case of nodes interacting with each other, there is a characteristic frequency of submission of electronic messages, say $N_r(t)$. Then for a time interval Δt small enough, we may write the number of new mysterious nodes which are increased to those already existing at $t+ t_0$, approximately, as

$$\Delta N_{M_{t+t_0}} = N_r(t) M_{(t)}(1 - M_{(t+t_0)})\Delta t$$

Now taking the limit $\Delta t \to 0$, we have

$$\theta_M(t) = \frac{N_r(t-t_0)}{N} M_{(t-t_0)}(1 - M_{(t)}) \tag{8}$$

Similarly, we can get the expressions for other conversion rates, as follows

$$\theta_L(t) = \frac{N_r(t-t_0)}{N} L_{(t-t_0)}(1 - L_{(t)}) \tag{9}$$

$$\theta_S(t) = \frac{N_r(t-t_0)}{N} S_{(t-t_0)}(1 - S_{(t)}) \tag{10}$$

$$\theta_P(t) = \frac{N_r(t-t_0)}{N} P_{(t-t_0)}(1 - P_{(t)}) \tag{11}$$

Second parameter we have considered in our modeling is death rates of different types of infectious nodes. Death rates of different types of infectious nodes are of two types, deaths per unit of time without producing any new infections and deaths per unit of time after producing new infections. For every category of infectious nodes,

Death rate α Number of infectious nodes or

Death rate = d *Number of infectious nodes,

Where d is the proportional constant and depends on the efficacy of the AMS and probability to detect and remove the infections before it spreads, P'(t), i.e. $d = \gamma * P'(t)$. In other words P'(t)is the function of time elapsed between the detection of infection and its eradication by erasing the hard disk and it will be monotone decreasing with time. Therefore different death rates are as follows

$$\delta_M(t) = \gamma(1 - P'(t))N_M \tag{12}$$

Figure 2: Nature of the solution for the equation (1) with the values set:

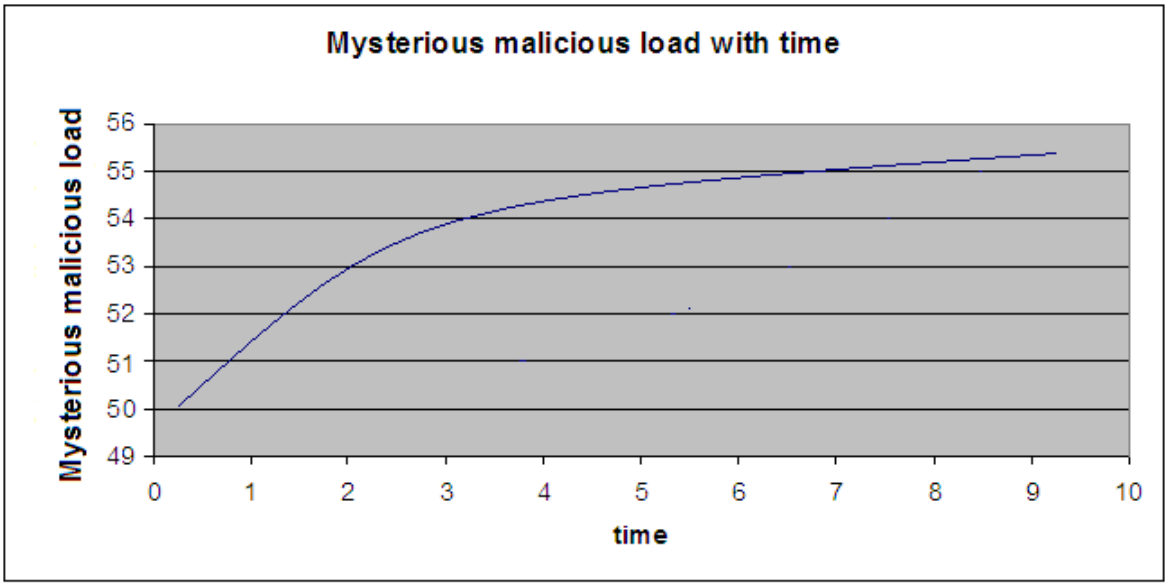

$\gamma = 0.5, N_t = 100, N_{M_t} = 10, x = 32, s = 0.3, N_r = 100, t_0 = 10, N = 200$ and proportions of mysterious, latently hidden, long-lived infectious nodes in the total produced infectious malicious nodes before the death of various infectious nodes at an instance are 0.3, 0.3, 0.2 and 0.2 respectively.

$$\delta_S(t) = \gamma(1 - P'(t))N_S \quad (13)$$

$$\delta_P(t) = \gamma(1 - P'(t))N_P \quad (14)$$

$$\delta_L(t) = \gamma(1 - P'(t))N_L \quad (15)$$

$$\mu_M(t) = \gamma P'(t)N_M \quad (16)$$

$$\mu_L(t) = \gamma P'(t)N_L \quad (17)$$

$$\mu_S(t) = \gamma P'(t)N_S \quad (18)$$

$$\mu_P(t) = \gamma P'(t)N_P \quad (19)$$

Figure-2 shows the nature of solution of Equation (1). In the figure the malicious object increase with the time, although the AMS is present and restricting the malicious object spread. As soon as the number of mysterious nodes reaches towards the maximum value it becomes almost constant with time. Similar solutions can be found for the other malicious infectious nodes mentioned in the paper. They also reach towards an almost constant value after some time.

This discrete model can behave like the curve in figure-3. This behavior of proposed model is similar to the code red (crv 2) propagation dynamics developed by R. Russell et al. (R. Russell et al., 2001).

Figure 3: Infectious malicious load with time for the values set:

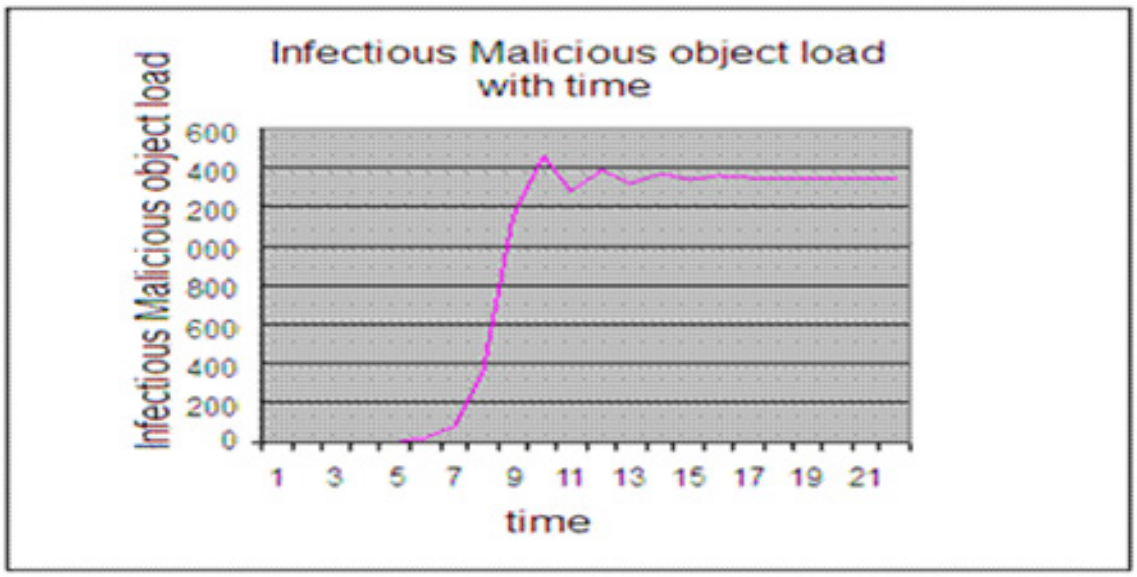

$\gamma = 0, \eta = 0.8, N_t = 100, N_r = 100, t_0 = 10, N = 200, P(t) \cong 10,$ and proportions of mysterious, latently hidden, long-lived infectious nodes in the total produced infectious malicious nodes before the death of various infectious nodes at an instance are 0.3, 0.3, 0.2 and 0.2 respectively.

Figure-3 represents the dynamics of infectious malicious objects with respect to time and assuming the efficacy of AMS as zero means AMS is disabled. We can see that in starting there are many numbers of targeted nodes to be converted into the infectious malicious nodes. After approaching towards the number equivalent to the targeted nodes, infection becomes constant because system is not having non-infected nodes.

Figure 4: AMS effects on malicious object load with time. Infectious malicious load with time for the values set:

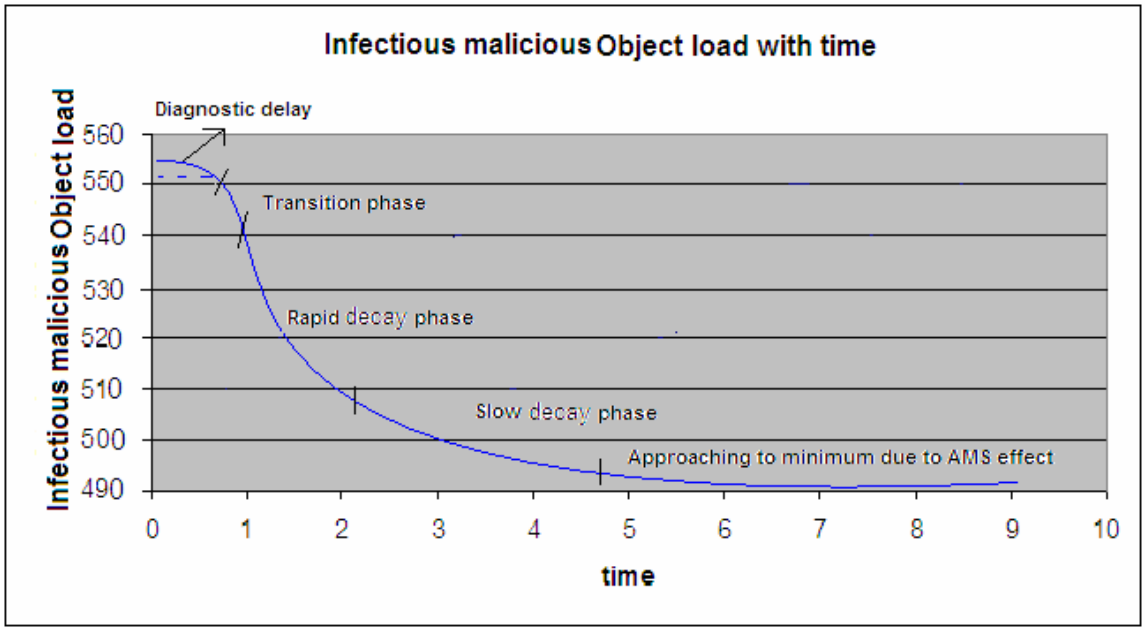

$\gamma = 0, \eta = 0.8, N_t = 100, N_r = 100, t_0 = 10, N = 200, P(t) \cong 10,$ and proportions of mysterious, latently hidden, long-lived infectious nodes in the total produced infectious malicious nodes before the death of various infectious nodes at an instance are 0.3, 0.3, 0,2 and 0.2 respectively.

Figure-4 shows the effect of the AMS, user's consciousness and five different phases after starting of the treatment by AMS. In the starting there may be some diagnostic delay to identifying the malicious object. Second phase is the transition phase which reflects the decay of productively active infectious nodes. Third phase is Rapid decay phase which reflects the productively active infectious, long-lived infectious, mysterious infectious nodes, and latently infectious nodes. Fourth phase is slow decay phase and reflects the decay of long-lived infectious nodes, mysterious infectious nodes, and latently infectious nodes. Now after the fourth phase the system gradually approaches to the minimum.

5. Summary and Discussion

The proposed model is a complex mathematical model based on compartmentalization approach. It works well for fast spreading worms such as code red-2 as shown in the figure-2. It presents all the possibilities of the conversion of the unaffected targeted nodes into different infectious and noninfectious nodes. In the particular time interval, model gives the dynamics of different types of nodes. This dynamics helps to predict the state of the system. Apart from this, the model also represents the behavior of the AMS. Simplification of the model is also possible; one can explore any of the phases mentioned in the graph (figure-4) after ignoring the other phases for the statistical analysis.

We assumed growth rates and death rates for all types of compartments so that we can explain the propagation of malicious object and to represent the characteristics of propagation media. The assumption regarding the additional growth rate of infectious malicious object and non-infectious malicious object (i.e. same) does not fit well in the real sense. We also assumed that at any instances of time the proportions of different compartments are remained constant because the nodes in the network rarely changes after initial setup. This assumption also does not exactly fit into the right sense.

References

[1] Mukhopadhyay, S. Chatterjee, R. Roy, D. Saha, A. Mahanti, S. K. Sadhukhan (2007) 'Insuring Big Losses Due to Security Breaches through Insurance: A Business Model', hicss, p. 158a, 40th Annual Hawaii International Conference on System Sciences (HICSS'07).

[2] C. Zou, W. Gong, D. Towsley (2002) 'Code Red Worm Propagation Modeling and Analysis', *CCS'02,* Washington, DC, USA.

[3] C. Zou, W. Gong, D. Towsley (2003) 'Formation and simulation: Worm propagation modeling and analysis under dynamic quarantine defense', proceedings of the 2003 ACM workshop on Rapid malcode, Washington, DC, USA, pp. 51 – 60.

[4] C. Zou, W. Gong, D. Towsley and L. Gao (2005) 'The Monitoring and Early Detection of Internet Worms', IEEE/ACM Transactions on networking, Vol. 13, Issue-5, pp. 961-974.

[5] Moore, C. Shannon, K. Claffy (2002) 'Code-Red: a case study on the spread and victims of an Internet worm', ACM Internet Measurement Workshop.

[6] Fishman, S. George (1973) 'Concepts and methods in discrete event digital simulation' 2nd Ed., Wiley, New York.

[7] J. Misra, T. Blank (1986) 'Distributed Discrete-Event Simulation', Computing survey, Vol. 18, Issue-1, pp. 39-65.

[8] J. O. Kephart, S. R. White (1998) 'Open problem in computer virus research', Presented at virus bulletin conference.

[9] J. W. Mickens, B. D. Noble (2005) 'Modeling Epidemic Spreading in Mobile Environments' *WiSE'05,* Cologne, Germany.

[10] L. W. Schruben (2000) 'Mathematical Programming Models of Discrete Event System Dynamics', Simulation Conference Proceedings, Orlando, USA, Vol.1, pp. 381-385.

[11] M. Pidd (1995) 'Object-orientation, discrete simulation and the three-phase approach', Journal of the Operational Research Society, Vol. 46, pp. 362-374.

[12] P. Liu, W. Zang, M. Yu (2005) 'Incentive-Based Modeling and Inference of Attacker Intent, Objectives, and Strategies', ACM Transactions on Information and System Security, Vol. 8, Issue 1, pp. 78-118.

[13] R. Russell, A. Machie (2001) 'Code Red II Worm', Tech. Rep., Incident Analysis, Security Force.

[14] V. Capasoo (1993) 'Mathematical Structure of Epidemic Systems', Springer – Verlag.

[15] Z. Chen, L. Gao, and K. Kwiat (2003) 'Modeling the Spread of Active Worms', Proceedings of 22nd Annual Joint Conference of the IEEE Computer and Communications Societies (INFOCOM'03), San Francisco, California, USA.

European Journal of Scientific Research
ISSN 1450-216X Vol.18 No.3 (2007), pp.500-513

http://www.eurojournals.com/ejsr.htm

Evaluation et Cartographie de la Vulnérabilité à la Pollution en Aquifère Confiné Selon La Méthode DRASTIC: Cas de La Région d'Aboisso, Sud-Est de La Côte d'Ivoire

Dibi Brou
Laboratoire des Sciences et Techniques de l'Eau et de l'Environnement (LSTEE) – UFR des Sciences de la Terre et des Ressources Minières – Université d'Abidjan – Cocody
22 BP 526 Abidjan 22 – Côte d'Ivoire

Doumouya Inza
Laboratoire Géosciences et Environnement (LGE) – UFR des Sciences et Gestion de l'Environnement – Université d'Abobo-Adjamé., 02 BP 802 Abidjan 02 – Côte d'Ivoire

Koffi Kouadio
Laboratoire Géosciences et Environnement (LGE) – UFR des Sciences et Gestion de l'Environnement – Université d'Abobo-Adjamé., 02 BP 802 Abidjan 02 – Côte d'Ivoire

Soro Nagnin
Laboratoire des Sciences et Techniques de l'Eau et de l'Environnement (LSTEE) – UFR des Sciences de la Terre et des Ressources Minières – Université d'Abidjan – Cocody
22 BP 526 Abidjan 22 – Côte d'Ivoire

Kouame K. Jean
Laboratoire des Sciences et Techniques de l'Eau et de l'Environnement (LSTEE) – UFR des Sciences de la Terre et des Ressources Minières – Université d'Abidjan – Cocody
22 BP 526 Abidjan 22 – Côte d'Ivoire

Savane Issiaka
Laboratoire Géosciences et Environnement (LGE) – UFR des Sciences et Gestion de l'Environnement – Université d'Abobo-Adjamé., 02 BP 802 Abidjan 02 – Côte d'Ivoire

Abstract

The Aboisso area is characterised by important surfaces of agro industrial plantations. Streams and lakes favourable for fishing as well as mining fields are also abundant. Agricultural, fishing and morning activities pose a serious pollution threat in the region. This is mainly due to the use of pesticides even in low quantities. In order to prevent pollution risk to ground water, map of affected areas was drawn using a numerical quotation method: DRASTIC. It is based on the combination of 7 parameters: depth and recharge of aquifer, soil, topographic, the impact of the valdose zone and the hydraulic conductivity. Vulnerability indices obtained using this method was grouped into 3 classes (weak, moderate and high). Results show that the region fell within the moderate vulnerability class (77 %) followed by the high vulnerability class (18 %) these show the areas, mainly concentrated in the east, that are under pollution threat. Finally the weak

vulnerability class (5 %) is located in Centre-West and South of the area, where granitoids are generally found. Areas with higher concentrations of nitrates are even associated with polluted areas, showing the importance of the vulnerabilities map. Nonetheless, a land use map prove to be more useful for a better idenfication of pollution sources

Keywords: Cartography, Vulnerability, DRASTIC, pollution, aquifer confined, Aboisso

Introduction

La région d'Aboisso est une zone forestière est une zone à forte densité de population (67 habitants/km^2) du fait de ces potentialités sur le plan de l'agriculture et de la pèche (Aké, 2001). En effet, cette région regroupe d'énormes plantations agro-industrielles telles que le palmier à huile, l'ananas, l'hévéa, la banane, et autres. A cela, il faut ajouter, l'ancien site de la mine d'Afema. Malgré l'arrêt de l'exploitation, ce site minier a laissé sur place d'énormes dépôts stériles responsables des phénomènes de drainage minier acide (DMA). Bien que la pollution ne soit pas alarmante comme l'indiquent les teneurs généralement faibles des polluants d'origines diffuses (NO_3^-, NO_2^-, NH_4^+, etc…), les risques de pollution sont réels. Pour prévenir ces risques surtout, au niveau des eaux souterraines, une des approches est la connaissance des zones spécialement vulnérables (Jourda et *al*, 2005).

Pour atteindre cet objectif qui vise à évaluer la vulnérabilité surtout intrinsèque, la méthode DRASTIC a été adoptée. Il s'agit d'une méthode développée par Aller et *al* (1987), qui est une méthode qui prend en compte les processus physiques, chimiques et biologiques dans la zone noyée. C'est une méthode de pondération entre différents critères affectant la vulnérabilité (Gogu et Dessargues, 1998). Elle a donné des résultats satisfaisants en milieux fissurés dans les régions du Québec au Canada (Murat et *al*, 2003) et de Korhogo (Jourda, 2005) en Côte d'Ivoire comme c'est le cas d'Aboisso. Aussi, permettra t-elle aux décideurs une prise de décision adéquate dans l'intérêt des populations (Savané et *al*., 2006).

Generalite Sur La Zone D'etude

La région d'Aboisso est située dans l'extrême Sud-est de la Côte d'Ivoire entre les latitudes 5°05 et 6°15 Nord et les longitudes 2°40 et 3°25 Ouest et appartient à la Région du Sud-Comoé dont elle est le chef lieu (Figure 1). Elle couvre une superficie d'environ 4563 Km^2. Cette étude couvre les sous-préfectures d'Aboisso, Ayamé, Bianouan et Maferé. Elle englobe en son sein les deux barrages d'Ayamé I et II.

Figure 1: Localisation de la zone d'étude

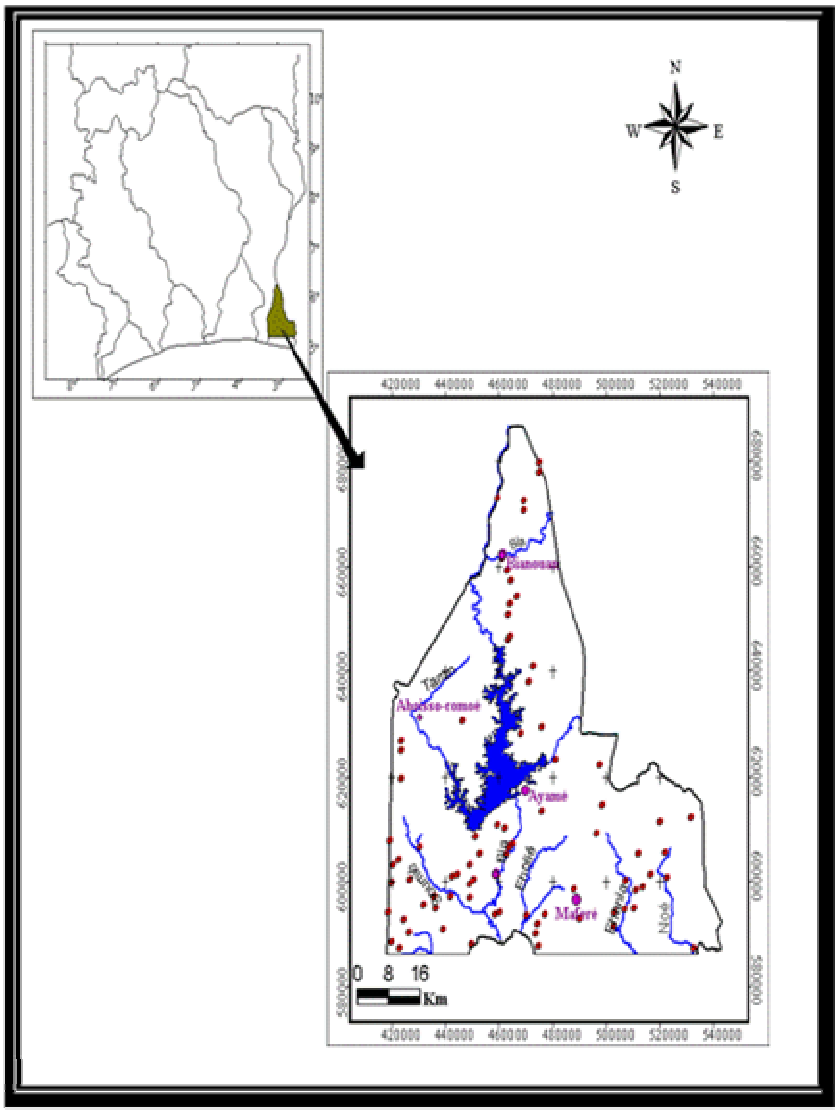

La région d'Aboisso est une zone très peuplée à l'instar des autres régions forestières du pays du fait non seulement de l'existence d'énormes plantations agro-industrielles mais aussi des nombreux plans et cours d'eau. La population totale de la zone est estimée à 322 498 habitants (INS, 1998).

Les sols de la région appartiennent généralement au groupe des sols ferrallitiques fortement lessivés sous une forte pluviométrie qui couvre la quasi-totalité de la zone d'étude. Il faut aussi signaler l'apparition en lambeau surtout dans le Nord des sols ferrallitiques moyennement lessivés et l'existence des cuirasses sommitiques bauxitiques sous forme d'intrusion (Tricart, 1971).

Le relief est monotone dans son ensemble. Il s'agit d'un paysage relativement peu élevé. Il est fait de surfaces d'aplatissements dont l'altitude moyenne varie entre 150 et 200 m (Kindo, 1998).

Sur le plan hydrographique, la région d'Aboisso est l'une des régions les mieux irriguées du pays. Les principaux cours d'eau sont : la Comoé, la Tanoé qui constitue dans la partie sud la frontière naturelle avec le Ghana et la Bia qui traverse la zone d'étude du Nord au Sud. A côté des principaux cours d'eau, nous avons Eholié, Timin et Soumié qui se déversent dans la Bia ainsi que Noé et Ehania qui se jette dans le Tanoé.

Le climat est caractérisé par une masse d'air chaud et sec (harmattan) qui souffle du Nord-Est vers le Sud et une masse d'air froid et humide (mousson) provenant de l'atlantique au Sud et circulant vers le Nord. Il comprend quatre saisons dont deux sèches et deux humides.

Au niveau géologique, plusieurs unités géologiques se côtoient. Toutes ces formations se regroupent en trois grandes entités que sont les schistes, les granites et les formations sédimentaires (Figure 2).

Figure 2: Esquisse géologique de la région d'Aboisso (Delor et *al*, 1992)

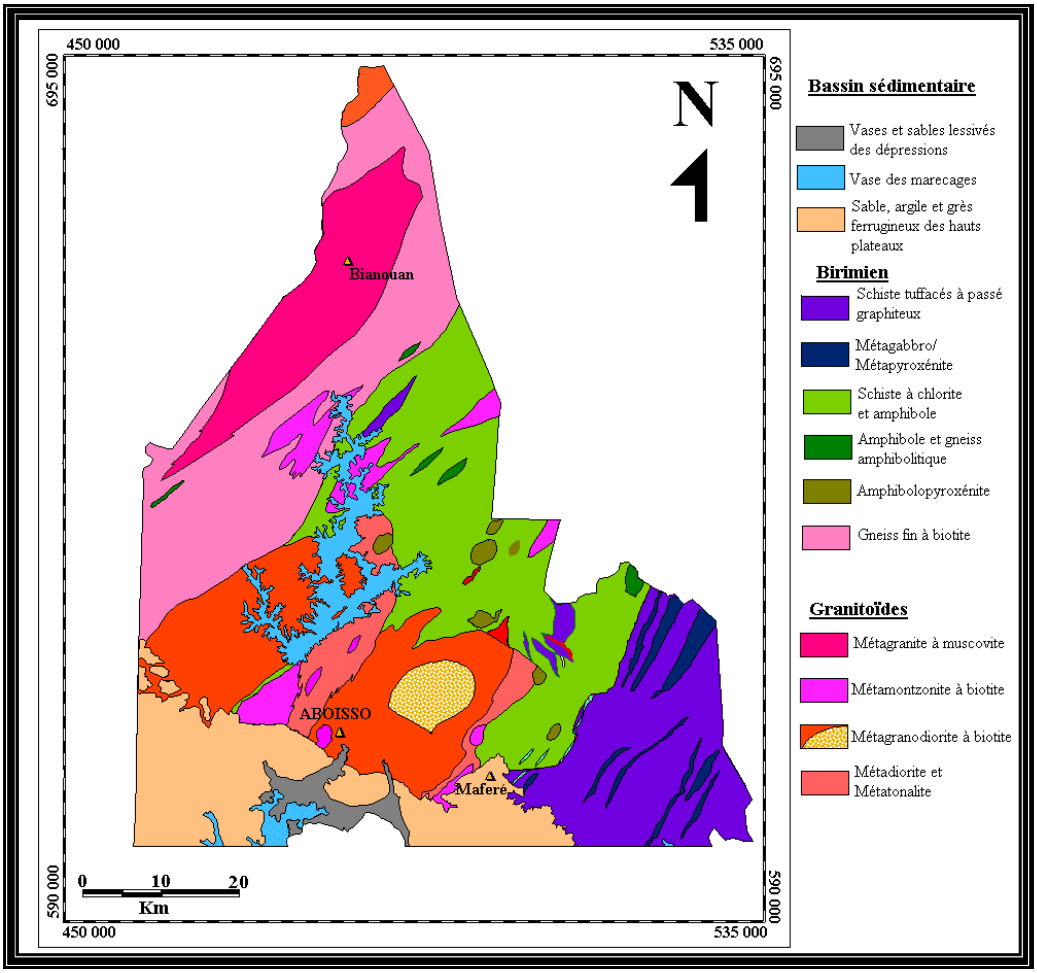

2. Materiel Et Methodes

2.1. Données et matériel

Les données utilisées pour cette étude sont constituées de données cartographiques, d'image satellitaire et d'une base de données de sources diverses. Ce sont :

- les données images landsat ETM+ : scène 196-55 de février 2000 et SRTM utilisées respectivement pour la détermination de la conductivité hydraulique en milieu fissuré et l'élaboration de la carte topographique ;
- les données de forages pour la détermination de la profondeur de nappe, la texture du sol et analyse des paramètres physico-chimiques acquis avec l'antenne hydraulique villageoise de Bietry.

- les données hydroclimatiques et de débits pour l'évaluation de la recharge ont été obtenues à la SODEXAM ;
- les cartes géologiques au 1/200 000 pour la caractérisation de la zone saturée et de la zone vadose.

Le matériel utilisé est composé de logiciels qui sont : MapInfo® 6.0 et Envi 3.6. Pour le traitement des images ainsi la réalisation des cartes et ArcView® 3.3 pour la combinaison des différentes couches ou critère pour la réalisation de la carte de vulnérabilité.

2.2. Méthodologie

2.2.1. Détermination de l'indice Drastic (Id)

L'évaluation de la vulnérabilité a été faite par la méthode DRASTIC. La méthode DRASTIC utilisée a été développée par l'Agence Américaine de Protection de l'Environnement (E.P.A) (Aller et *al*., 1987). Elle est basée sur l'estimation de sept (7) paramètres relatifs à la recharge, au sol, à la zone non saturée et à la zone saturée de l'aquifère. Ce sont la profondeur de la surface de la nappe, l'infiltration efficace, la nature lithologique de l'aquifère, le type de sol, la topographie des terrains, l'impact de la zone non saturée et la conductivité hydraulique.

A l'issue de l'évaluation paramétrique, l'indice de vulnérabilité DRASTIC (Id) est déterminé. Celui-ci permet de caractériser le degré de vulnérabilité d'un secteur donné de la nappe. Cet indice est défini de la manière suivante :

Id = DnDp + RnRp + AnAp + SnSp + TnTp + InIp + CnCp

avec D, R, A, S, T, I, C, les paramètres cités plus haut

n : notation accordée à chaque paramètre ; p : facteur de pondération accordé à chaque paramètre.

2.2.2. Elaboration de la carte de vulnérabilité

Pour l'élaboration de la carte de vulnérabilité, nous avons opté pour les classifications adoptées par Lobo et *al*. (2003) et Menani (2001) indiquées dans le tableau I et tenant compte des résultats obtenus de la zone d'étude.

Table 1: Classes d'indice Drastic selon Lobo et *al*. (2003) et Menani (2001)

Classe de Vulnérabilité Lobo et *al.* (2003)	Appréciation des Classes	Classe de Vulnérabilité Menani (2001)
Id < 120	Faible vulnérabilité	Id < 100
120 < Id < 160	Moyenne vulnérabilité	100 < Id < 150
160 < Id < 199	Vulnérabilité élevée	Id > 150
Id > 199	Vulnérabilité très élevée	

2.2.3. Origine des données DRASTIC

Il s'agit ici de présenter les différentes données utilisées pour l'évaluation des différents paramètres. Ces données seront classifiées et classe se verra attribuée une note qui variera selon son importance dans l'évaluation de la vulnérabilité verticale.

La profondeur de la nappe

Elle est représentée par les niveaux statiques qui indiquent le niveau d'eau dans les aquifères. Ces données proviennent de l'antenne de l'hydraulique villageoise d'Abidjan Biétry. Elles ont été triées en vue de retenir celles qui couvrent de façon rationnelle la zone d'étude. Nous avons seulement retenu six classes car la profondeur comprise entre 0 et 1,5 m n'existe pas dans la zone car le niveau statique le plus faible est de 2 m. Ces données (Tableau II) ont été interpolées sous ArcView.

Table 2: Notation des classes de la profondeur de la nappe

Profondeur de la nappe (m)	Notation
2 – 4,4	9
4,4 – 9,1	7
9,1 - 16,1	5
16,1 - 23,2	3
23,2 - 30,2	2
> 30,2	1

Infiltration efficace (Recharge)

L'infiltration efficace représente la frange d'eau qui va effectivement alimenter les aquifères. C'est la quantité d'eau disponible pour la recharge de la nappe postérieurement à toutes les influences subies par l'eau des précipitations (Kouadio, 2005). Cette recharge est déterminée à partir du bilan hydrologique (Menani, 2001). Dans le cadre de cette étude nous disposons, pour l'ensemble de la zone d'étude, d'une seule station synoptique pour laquelle nous avons pu évalué l'infiltration efficace. Ce critère sera considéré comme homogène sur l'ensemble de cette zone. Elle a été déterminée à partir du modèle pluie débit GR2M et cette valeur est de 416,8 mm. A cette classe, nous avons attribué la note 10.

Nature de la zone saturée

Elle représente le type d'aquifère. La zone saturée dans la région d'Aboisso est représentée par les formations cristallines et cristallophylliennes, les schistes et une couche sédimentaire très réduite. Nous pouvons donc regrouper les formations en trois grands groupes : Les formations roches métamorphiques et ignées, les schistes et enfin les formations sédimentaires dominées représentées par les sables et graviers. Le tableau III indique les notations attribuées à ces différentes formations.

Table 3: Notation de la nature de la zone saturée

Nature de la zone saturée	Notation
Roches métamorphiques et ignées	4
Schistes	6
Sable et gravier	8

Type de sol

Le type de sol fait allusion à la nature de la couche de terre végétale qui est la première formation traversée par les polluants. De leur nature dépendra la diffusion de ces polluants. Dans la région d'Aboisso, son épaisseur varie généralement entre 0 et 1 m. Il est constitué de sable et d'argile. Il correspond dans le tableau de classification au limon sableux auquel on va attribuer la note 6.

Nature de la zone vadose

Elle conditionne le temps de transfert des polluants. Dans la région d'Aboisso la plupart des arrivées exploitées se rencontrent dans le socle. Cette zone sera donc constituée en plus des couches d'altérites qui forment le premier lieu de transit, des formations cristallines et cristallophylliennes sous-jacentes. Elle sera à ce titre, représentée par les mêmes formations Les notations de cette formation sont indiquées dans le tableau IV

Table 4: Notation attribuée à la nature de la zone non saturée

Zone non saturée	Notation
Sable et gravier	8
Roches métamorphiques et ignées	4
Schiste	6

La topographie

Elle est caractérisée par la pente qui a été obtenue à partir des images SRTM à partir desquelles, nous avons généré la carte des pentes. Dans la région d'Aboisso, le relief est généralement monotone. Toutefois, quelques sommets élevés apparaissent dans l'extrême est dans la région d'Ayamé et dans la partie nord de Maféré où quelques sommets atteignent les 400 m. La pente varie de 0 à près de 30 %. Les notations attribuées aux différentes classes sont indiquées dans le tableau 5.

Table 5: Topographie

Pente	Notation
0 - 2	10
2 - 6	9
6 - 12	5
12 - 18	3
> 18	1

Conductivité hydraulique

Elle a été déterminée à partir de la carte de fracturation obtenue à partir d'image satellitaire ETM+. La carte de réseau linéamentaire a été maillée selon la taille de 5 km x 5 km et les perméabilités ont été calculées par la méthode de Francis. Les valeurs moyennes obtenues varient entre $1{,}77.10^{-7}$ à $8{,}06.10^{-6}$ m/s. Cette tranche appartient à la classe de conductivité hydraulique qui varie de $4{,}7.10^{-7}$ m/s à $4{,}7.10^{-5}$ m/s. La notation attribuée à cette classe est 1

2.2.4. Pondération des paramètres

La méthode DRASTIC propose deux systèmes de pondération suivant les conditions d'occupation du sol: occupation "normale" ou avec une occupation par une activité agricole intensive utilisant par exemple des produits phytosanitaires (Bézèlgues et *al*, 2002). Dans la zone d'étude, qui est certes une région agricole mais où les cultures pratiquées n'utilisent pas suffisamment les produits phytosanitaires. Nous adopterons donc au cours de cette étude, les facteurs de pondérations dits « normaux ». Le tableau 6 présente les facteurs de pondération en fonction des sept critères de la méthode DRASTIC.

Table 6: Facteurs de pondération des différents critères de la méthode DRASTIC (Lallemand-Barrès, 1994).

Critères	Facteurs de pondération	
	« Normal »	« Produits phyto »
Profondeur	5	5
Recharge	4	4
Zone saturée	3	3
Type de sol	2	5
Topographie	1	3
Nature de la zone non saturée	5	4
Conductivité hydraulique	3	2

2.2.5. Evaluation des différents paramètres

Pour l'évaluation de la zone saturée, du type de sol et de la zone non saturée, nous avons procédé à un regroupement des unités géologiques selon le schéma de classification propre à cette méthode. En ce qui concerne la profondeur de la nappe, elle a été évaluée par interpolation des données du niveau d'eau. Il en est de même pour la recharge et la conductivité hydraulique (Murat et *al*., 2003).

Toute la méthodologie utilisée est résumée dans l'organigramme de la figure 3.

Figure 3: Organigramme de la méthode DRASTIC (Murat et *al*, 2003)
(1): Calcul des valeurs de vulnérabilité pixel par pixel selon la formule de l'indice DRASTIC
(2): Classification des pixels en fonction des classes DRASTIC.

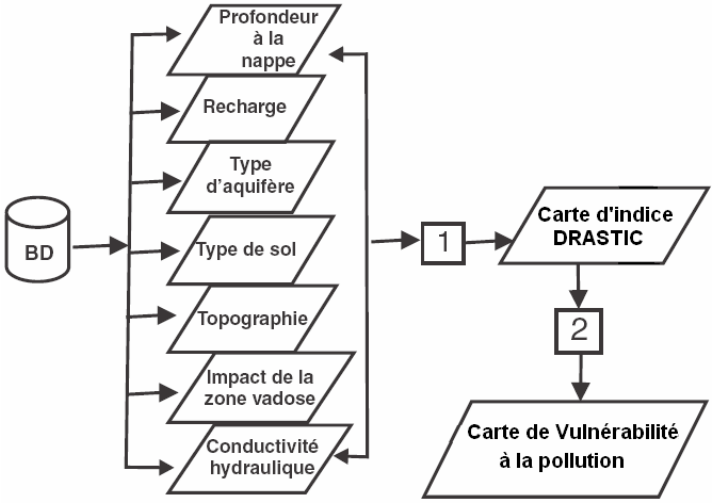

3. Resultats Et Analyse

La combinaison des différents paramètres évalués a permis d'élaborer la carte des indices DRASTIC (Figure 3). Les différents indices ont été classifiés selon les plages adoptées par Lobo et *al*. (2003) et Menani (2001) en tenant compte des caractéristiques de la zone d'étude. En effet, bien que les indices soient souvent du même ordre que ceux déterminés au cours des études des auteurs précités, les formations géologiques diffèrent. Dans la région d'Aboisso, nous sommes en milieu fissuré contre des aquifères continus pour ces derniers. Les trois (3) classes ainsi obtenues sont indiquées dans le tableau (Tableau 7).

Figure 4: Carte d'indice Drastic

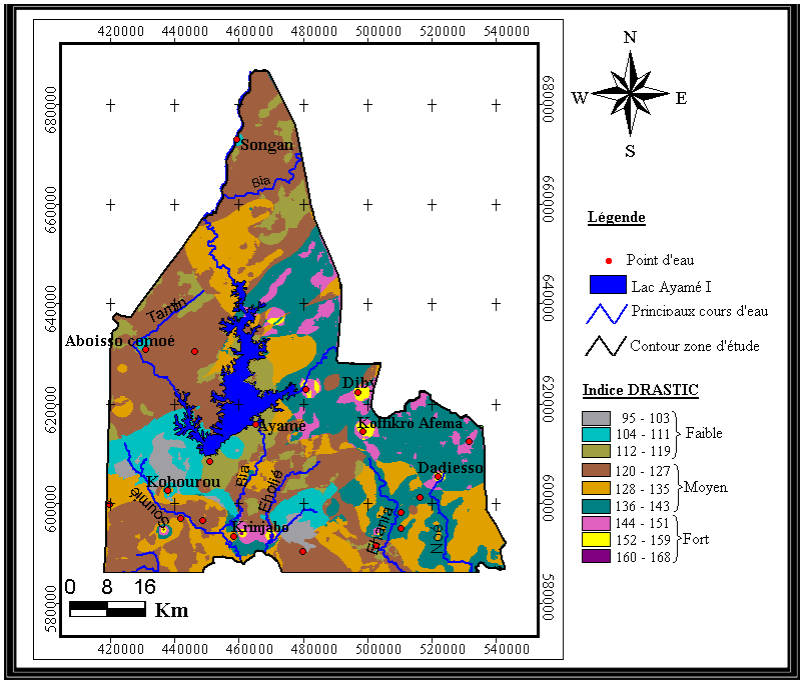

Table 7: Résumé statistique des indices DRASTIC

	Classes	Valeurs	Ecart type
Faible	95 - 119	95	
Moyenne	120 - 143	131,5	20,83
Forte	144 - 168	168	

A partir des différentes, nous avons élaboré la carte de vulnérabilité intrinsèque à la pollution illustrée par la figure 4.

Figure 5: Carte de vulnérabilité à la pollution

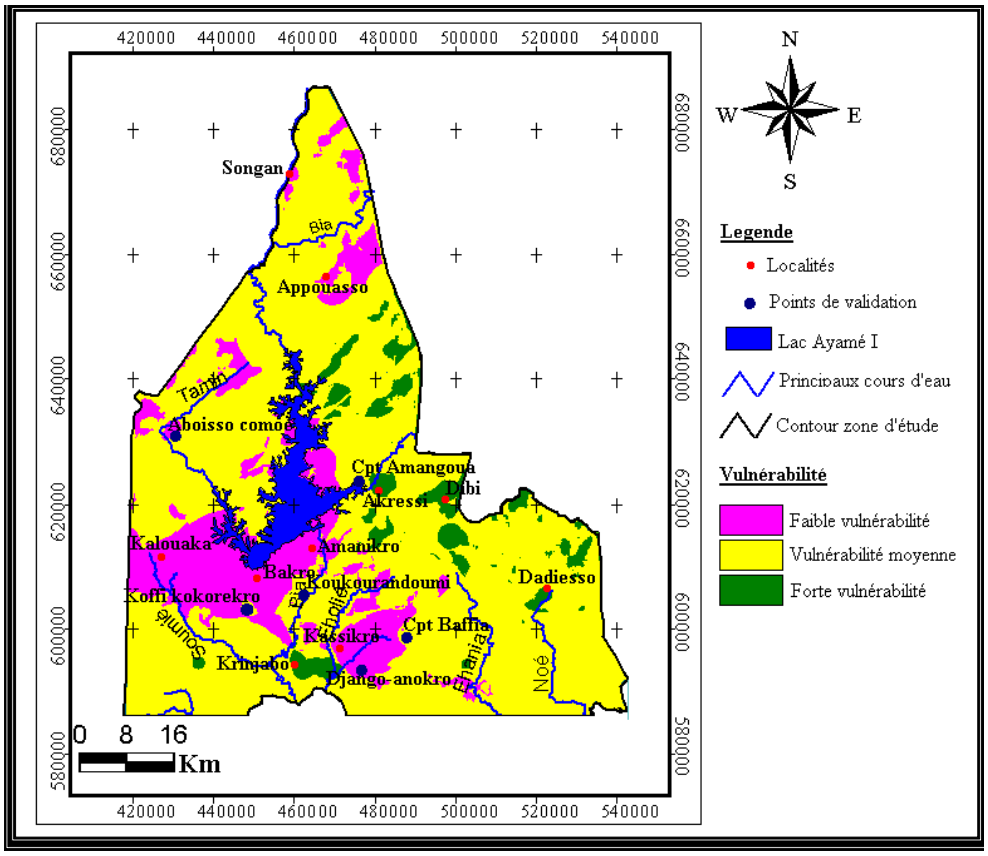

Sur la base des surfaces occupées par chaque classe, nous avons déterminé les différentes proportions à partir du nombre de pixels qui sont indiquées dans le tableau 8.

Table 8: Proportions des différentes classes thématiques des sites potentiels

Classes thématiques	Proportion en %
Vulnérabilité forte	5
Vulnérabilité moyenne	77
Vulnérabilité faible	18

3.1. Analyse de la carte de vulnérabilité

La carte de vulnérabilité comprend trois classes que sont les classes de faible, moyenne et forte vulnérabilité. D'une manière générale, la région reste dominée par la vulnérabilité moyenne. L'analyse détaillée de ces différentes classes se présente comme suit :

- la classe de faible vulnérabilité reste moins présente dans la zone d'étude par rapport à la zone de vulnérabilité moyenne. Elle occupe environ 18 % de la superficie totale de la zone d'étude et couvre généralement les granitoïdes. L'observation de la carte permet de constater qu'elle est beaucoup plus aperçue au Centre- Ouest dans les localités de Bakro, Kalouaka ainsi qu'Amanikro. Elle forme pratiquement une ceinture autour des lacs d'Ayamé. Quelques poches un peu plus réduites se retrouvent dans le Sud au niveau de Django-anokro et dans les environs de Kassikro de même que dans le Nord du coté d'Appouasso et Songan.
- la classe de moyenne vulnérabilité est de loin la classe la plus importante de la zone étude. Elle couvre 77 % de cette zone. Elle est présente sur la quasi-totalité de la zone d'étude. Cette présence est assez renforcée dans le Sud. Elle est aussi signalée dans tous les secteurs où coexistent des schistes tuffacés et des profondeurs de nappes moyennes variant entre 9 et 23 m.
- la classe de forte vulnérabilité se rencontre dans la zone est surtout, sur les formations schisteuses à Dibi, Campement Amangoua ainsi qu'une poche un peu plus représentative au Sud dans les localités de Krinjabo Elle couvre seulement 5 % de la zone d'étude.

3.2. Validation de la carte de vulnérabilité

Pour la validation de cette carte, nous avons utilisé les nitrates qui constituent l'une des principales sources de pollution d'origine superficielle. En effet, dans la région, les polluants tels que les nitrites (NO_2^-) et l'ammonium (NH_4^+) sont pratiquement inexistants dans les eaux souterraines analysées. Le tableau 9 présente les localités où les teneurs sont supérieures ou égales à 10 mg/L. Les teneurs les plus élevées ont été obtenues à Krinjabo (88 mg/L) et Django-anokro (30 mg/L). La teneur observée à Krinjabo qui reste supérieure à la norme OMS est récente (2007) contrairement à celle obtenue à Django-anokro qui fait partir de la tranche (1999 – 2000) utilisées pour la réalisation de la carte des nitrates (figure 6). Elle montre la faiblesse généralisée de la teneur en NO_3^- qui couvre plus de 90 % de la région contre 9 % pour les teneurs allant de 12 à 30 mg/l. Cette tranche (9 %) se retrouvent sur des zones de moyenne à forte vulnérabilité comme c'est le cas dans les localités de Campement Amangoua, Koukourandoumi et Campement Baffia. De plus, la teneur de 88 mg/L obtenue à Krinjabo se situe au niveau d'une zone de forte vulnérabilité.

Table 9: Données de validation de la carte de vulnérabilité

Localités	**NO_3^- (mg/L)**
Cpt Baffia	10
Aboisso comoé	10
Koukourandoumi	20
Cpt Amangoua	25
Django-anokro	30
Krinjabo	88

Figure 6: Carte des teneurs en nitrates (NO_3^-)

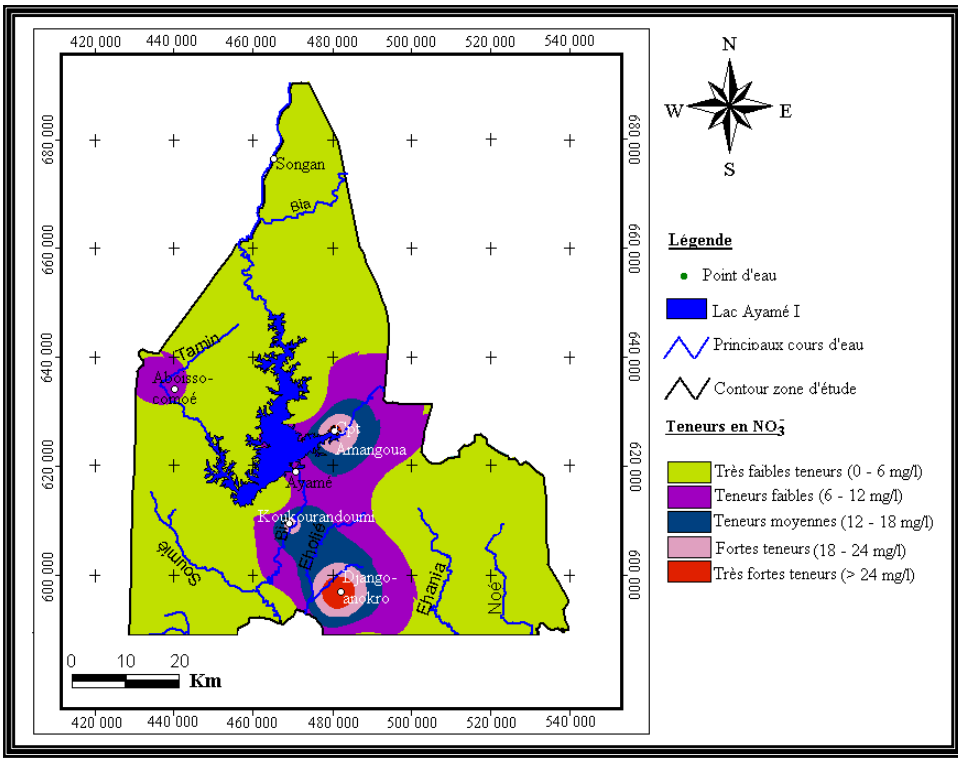

4. Discussion Des Resultats

Pour la cartographie des zones vulnérables, nous avons choisi la méthode de pondération dite normale bien que nous soyons dans une zone où se trouvent d'énormes plantations agro-industrielles. En effet, malgré l'existence de ces plantations, les teneurs des polluants restent très faibles, généralement inférieures aux normes OMS. Toutefois, l'observation de quelques valeurs élevées (88 mg/L à Krinjabo) emmène à rester vigilant et donc à identifier les zones menacées en vue de prendre les dispositions utiles en cas de besoins.

La vulnérabilité évaluée bien qu'ayant une tendance moyenne reste assez élevée en tenant compte de l'indice DRASTIC qui varie de 95 à 168. Ce qui donne une moyenne de 131,5. Cette valeur reste largement supérieure à celles déterminées dans la région de Korhogo qui est de 117 et à Central Oklahoma qui est 124 (Jourda, 2005) sur généralement des formations magmatiques et métamorphiques ou des gneiss. Cette tranche reste cependant sensiblement identique à celle déterminée par Murat et *al* (2003) dans le Nord-Ouest de Montréal au Canada sur des aquifères confinés où des poches d'indices supérieurs à 160 ont été obtenues. Les différences souvent observées pourraient être attribuées aux paramètres très importants dans l'évaluation de cette vulnérabilité que sont la recharge et la profondeur de la nappe. En effet, dans la région d'Aboisso, la recharge est très importante du fait des précipitations qui sont de l'ordre de 2000 mm/an. Quant à la profondeur de la nappe, elle reste dominée par la classe de faible à très faible profondeur qui couvre près de 80 % de la zone d'étude. Ces classes constituent les zones les plus exposées à la pollution du fait de la faible distance parcourue par le polluant pour atteindre la nappe.

Pour ce qui concerne l'évaluation de la vulnérabilité à la pollution en milieu fissuré surtout la vulnérabilité intrinsèque, la méthode DRASTIC est l'une des techniques les plus adaptées du fait du nombre important de paramètres considérés (Murat *et al*, 2003). En plus, c'est une méthode standardisée d'évaluation et de cartographie de la vulnérabilité des eaux souterraines indépendamment du type de polluant et qui prend en compte la majeure partie des facteurs hydrogéologiques qui

affectent et contrôlent l'écoulement des eaux souterraines (Menani, 2001). Selon Jourda et *al* (2005), la carte de vulnérabilité intrinsèque en milieu fissuré selon la méthode DRASTIC est fiable et permet d'avoir une idée sur les zones sensibles qu'il va falloir prendre en compte lors de l'aménagement des différentes régions.

Toutefois, cette étude possède des limites car la continuité des aquifères en zone de socle reste une simple vue de l'esprit. Selon les travaux de Jourda (2005), plus les intervalles des isobathes de niveau de la nappe sont larges moins l'estimation de cette profondeur est précise et de plus les conductivités hydrauliques déterminées restent discutables surtout en zone de socle.

Ces résultats sont confirmés par les teneurs élevées de nitrates qui se superposent globalement aux zones de moyennes et fortes vulnérabilités. La teneur la plus élevée a été obtenue récemment à Krinjabo (88 mg/L) qui se localise au niveau d'une zone de forte vulnérabilité. Ces fortes teneurs qui s'observent aussi à Django-anokro mais à un degré moindre (30 mg/L) peuvent s'expliquer par la présence du contact socle – sédimentaire. En effet, ces endroits sont considérés comme des zones de forte recharge (Murat et *al*., 2003) et par conséquent de forte intrusion de polluants qui proviennent des plantations agro-industrielles (banane, ananas et palmier à huile). Ces plantations qui se situent dans les environs de ces localités utilisent très souvent les produits phytosanitaires qui sont de véritables libérateurs de polluants dans la nature.

Conclusion

Cette étude s'est fixée comme objectif, la cartographie des zones vulnérables à la pollution en vue de prévoir dans la mesure du possible les périmètres de protection. Les principaux résultats obtenus sont :

- une classe à vulnérabilité faible couvrant 18 % de la région et essentiellement située dans le secteur centre-ouest, au Sud avec quelques poches isolées dans le nord ;
- une classe à vulnérabilité moyenne, de loin la plus importante, couvrant 77 % de la superficie du territoire;
- une classe à vulnérabilité forte couvrant 5 % de la zone d'étude qui occupe de petites poches dans la partie est.

A terme, cette étude a donc permis d'identifier les zones plus exposées comme c'est le cas de Krinjabo où une teneur de 88 mg/L vient d'être observée. Cependant, il convient d'intégrer à cette étude, la carte d'occupation des sols pour mieux cibler les sources de ces polluants.

References

[1] AKE G. E. (2001) : Evaluation des ressources en eau souterraine de la région de Bonoua. *Mémoire de DEA des sciences de la terre, Université de Cocody, 72 p.*

[2] ALLER L., BENNETT T., LEHR J.H., PETTY R., ET HACKETT G. (1987): DRASTIC: a standardized system for evaluating groundwater pollution in potential using hydrogeological settings: *U.S. Environmental Protection Agency Report 600 2-87 035, 622 p.*

[3] BEZELGUES S. ET DES GARETS E. MARDHEL V. ET DÖRFLIGER N. (2002). Cartographie de la vulnérabilité des nappes de Grande-Terre et de Marie-Galante (Guadeloupe). *Phase 1 : méthodologie de détermination de la vulnérabilité, BRGM/RP-51783-FR, 44 p.*

[4] DELOR C., DIABY Y., SIMEON Y., TASTET J.-P., VIDAL M., CHIRON J.- C. et DOMMANGET A. (1992) : Notice explicative de la Carte géologique de la Côte d'Ivoire à 1/200 000, *Feuille Grand – Bassam. Mémoire de la direction de la Géologie mémoire N°4.*

[5] DELOR C., DIABY Y., SIMEON Y., TASTET J.-P., VIDAL M., CHIRON J.- C. et DOMMANGET A. (1992) : Notice explicative de la Carte géologique de la Côte d'Ivoire à 1/200 000, *Feuille Abengourou. Mémoire de la direction de la Géologie, mémoire N°4.*

[6] INS. (1998) : Recensement Général de la Population et de l'Habitation (RGPH). *Données sociodémographiques et économiques des localités, résultats définitifs par localités, région du Sud comoé, vol.III, tome 1, 2001, 43 p.*

[7] JOURDA J. P., SALEY M. B., KOUAME K. J., KOUADIO B. H. ET RAZACK M. (2005) : Gestion et protection des ressources en eaux souterraines : contribution d'un SIG à la réalisation de la carte de vulnérabilité à la pollution des aquifères fissures de Korhogo (Nord de la Côte d'Ivoire) selon la méthode DRASTIC. *Communication scientifique, Eau – Environnement ; 21p.*

[8] JOURDA J.P. (2005): Méthodologie d'application des techniques de télédétection et des systèmes d'information géographique à l'étude des aquifères fissurés d'Afrique de l'Ouest.concept de l'hydrotechniquespatiale : cas des zones tests de la cote d'ivoire. *Thèse doct. ès sc. nat., Univ. de Cocody à Abidjan, 429 p.*

[9] KINDO B. (1978) : Dynamisme économique et organisation de l'espace rural chez l'Agni du N'Dénéan et du Djuablin (Côte d'Ivoire). *Thèse de Doctorat 3ème cycle, Université nationale de Côte d'Ivoire, Faculté des Lettres et des Sciences Humaines, Institut de Géographie Tropicale, Abidjan, 328 p.*

[10] KOUADIO K. E. (2005) : Stratégie de prospection des nappes de fissures par analyse spatiale du potentiel de productivité et optimisation de la profondeur des forages. Cas du Denguelé (Nord-ouest de la Côte d'Ivoire). *Thèse de Doctorat unique, Université de Cocody, 181p.*

[11] LALLEMAND-BARRES A. (1994) : Normalisation des critères d'établissement des cartes de vulnérabilité aux pollutions. *Etude documentaire préliminaire. Rapport BRGM R 37928.*

[12] LOBO P.; NOVO E.; OLIVEIRA M. (2003): Groundwater vulnérability mapping: application to the the Minho watershed in northern Portugal's celtic Region; *7 p*

[13] MENANI M. (2001) : Evaluation et cartographie de la vulnérabilité à la pollution de l'aquifère alluvionnaire de la plaine d'El Madher, Nord-Est algérien, selon la méthode Drastic. *SECHERESSE, vol 11, n°2, pp 95-101.*

[14] MURAT, V., PARADIS, D., SAVARD, M.M., NASTEV, M., BOURQUE, E., HAMEL, A., LEFEBVRE, R. AND MARTEL, R. (2003) : Vulnérabilité à la nappe des aquifères fracturés du sud-ouest du Québec- Évaluation par les méthodes DRASTIC et GOD. *Current Research, no. 2003-D3; 14 p.*

[15] SALEY M.B. (2003) : Système d'informations hydrogéologiques à référence spatiale, discontinuités pseudo-images et cartographies théma-tiques des ressources en eau de la région semi- montagneuse de Man (Ouest de la Cote d'Ivoire).*Thèse de Doct. unique, Univ. de Cocody-Abidjan, 209 p.*

[16] SAVANE I., GOULA B. T., DOUA G. A. ET KOUAME K. I (2006) : Vulnérability assessment of the Abidjan Quaternary Aquifer using the DRASTIC method. *Ground water pollution in Africa, pp 115 – 124.*

[17] TRICART J. (1974) : De la géomorphologie à l'étude écographique intégrée. *L'Agr. Trop., XXIX, 2/3, pp 122-132.*

European Journal of Scientific Research
ISSN 1450-216X Vol.18 No.3 (2007), pp.514-531

http://www.eurojournals.com/ejsr.htm

PWM-IGBT Inverter Based Power Flow Control at the Load Bus in the Presence of Utility Supply

Aamir Hanif
Member IEEE and M.A. Choudhry Senior Member IEEE
Department of Electrical Engineering
University of Engineering and Technology Taxila, 47050 Pakistan
E-mail: aamirhanif@uettaxila.edu.pk
Tel: +92-51-9047550

Abstract

This research work presents an innovative strategy for power flow control in the primary distribution network working in parallel with a DC source as distributed energy resource. The paper proposes the application of static device, battery as DC source, PWM-IGBT inverter based power flow control at the load bus in the presence of utility supply. The power flow control from utility supply and distributed energy resource (DER) to common load bus is such that power flows to the load without facing any power quality problem. Simulations were carried out using SimPower Systems toolbox of MATLAB® and Simulink®. The results show that a reliable, effective and efficient operation of battery as DER in coordination with main utility network can be achieved. Hence the power quality of the supply may be significantly enhanced for the critical industrial processes and loads through the proposed innovative strategy for power flow control.

Introduction

Integration of distributed energy resources (DER) into distribution systems is a new concept for improving system capacity and stability, feeder voltage, and supply quality and reliability. Distributed energy resources (DER) are usually installed at the distribution level, close to the place of utilization, and generate power typically in the range of a few kW to a few MW. DER is capable of injecting different proportions of real and reactive power to the grid and load. It is observed that the peak demand loads are increasing all over the world and the load factor is decreasing year after year. A huge amount of capital investment is required for construction and enhancement of generation or transmission systems. One of the solutions to this problem is installation of distributed energy resources. Electricity generation by distributed energy resources with lower emission technologies contribute, to loss reduction and greenhouse effects through reducing environmental pollution and global warming. Through utilizing DER, network augmentation/new construction can be deferred, system losses can be reduced and customer's demands may be satisfied instantaneously.

The area of distributed energy resources is a topical area of research and interest has been rapidly growing worldwide in this field. Utilities have recognized the DER as an imperative tool that can partially replace the need to erect new generating stations as a reinforcement strategy, in order to meet the increasing load demand. The Distributed Generation (DG) option is enjoying a global popularity to offset the future load growth [1]. The Discos or end-users can install DER or DG units within their service area. Due to the availability of such a flexible option at the distribution voltage level, the distribution network is now being transformed from passive network to an active one.

Following the trend of deregulating electric power industry, the demand for flexible power flow control is becoming a technical need feasibly achievable by the innovative power electronics technology. The mechanical switched or control equipment simply can not match with the trend of fast on-line decision making as required in Energy Management Systems (EMS). Power electronic interfaces are used to connect renewable energy sources which produce DC (e.g. photovoltaic, fuel cells or battery storage etc) to common A.C. load bus at 50 or 60 Hz. In this regard the use of power electronics based inverters or converters helps to control power flows as required from DER, working standalone or in parallel with utility supply at the A.C load bus. This is achieved by controlling modulation index through PWM control of inverter along with phase angle at the load bus either of PWM-IGBT inverter output voltage or DER output voltage and DC source voltage.

In this paper, first a brief introduction underlining importance of application of distributed generation and the use of power electronics technology for flexible power flow control is discussed. Existing power flow control strategies at the load bus with utility supply and DER are presented with one line diagrams in section II. Section III of this paper provides brief description of power flow control using Battery as DER with PWM-IGBT Inverter. Section IV describes proposed innovative power flow control strategy.

Section V provides detail about the test system to be used for our analysis along with its modeling and simulation. MATLAB®, Simulink® [2] setup using SimPower Systems tool box is first developed for a standalone static DER which is able to take three phase load at 11KV and then is connected in parallel to utility supply at 11KV common load bus.

Simulation studies were carried out to examine, active powers flows from DER to three phase load along with A.C load bus voltage by controlling suitable parameters of PWM control of IGBT inverter and results are presented both in tabulated and graphical forms.

After accomplishing above results we then proceed forward for the development of MATLAB®, Simulink® setup using SimPower Systems tool box for the primary distribution network working in parallel with a DC source as distributed energy resource. We used 3-bus test system with 3-phase 11KV primary radial distribution feeder to analyze power sharing from utility supply and static DER at the common load bus. Sinusoidal PWM technique was utilized for the IGBT inverter, to control active power flow from DER and voltage at the load bus. PWM inverters need high power high frequency components such as GTO thyristors, IGBTs, and/or power transistors for proper operation. IGBTs have the advantage of high speed, high power switching, so they are the preferred components for building PWM inverters [3] and that is why they are used in our work. Simulation studies for the active power flow control are performed with DER connected in parallel with utility supply at the common load bus and results are examined to indicate that the static DER power flow control approach at the distribution side is reliable, effective and efficient.

Existing power flow control strategies

There are two existing strategies of sharing DER power in coordination with utility supply at the load bus.

- *Strategy 1:* DER can be used as a stand-alone service to meet customers demand.
- *Strategy 2:* DER can also be used in conjunction with traditional utility service.

In stand-alone applications, DER can serve as remote or isolated area load supply as shown in Figure 1.

Figure 1: Standby DER supplying isolated or remote area load when utility can't supply isolated area load due to geographical obstacles

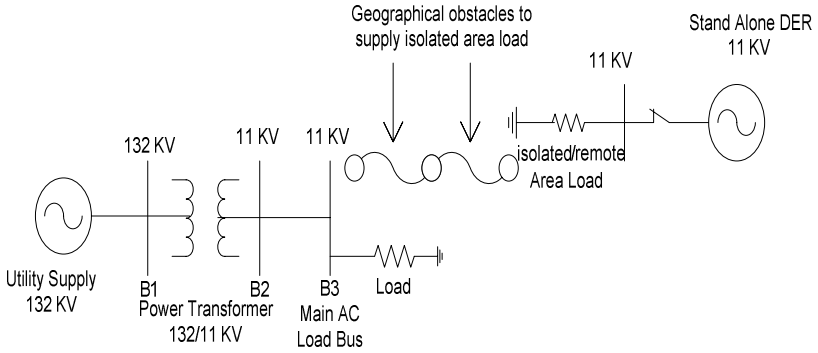

In strategy-2, we have further 3 ways of operating DER, connected with utility supply at the load bus to supply load demand.

- Peak load shaving switched mode of operation
- Standby switched or rollover mode of operation
- Parallel operation of DER with utility supply

In Peak load shaving switched mode operation of DER in conjunction with the utility supply, load bus is bifurcated into two buses such that some load is shifted to the bifurcated load bus while remaining load is supplied by utility connected with main A.C load bus.

The process of shifting some part of load from main A.C load bus to bifurcated load bus is done either manually through a human being (slow) or automatically through sensor switching (fast). This existing load sharing strategy at the main A.C load bus in the presence of utility supply as main source and DER is explained in Figure 2.

Figure 2: DER supplying load while utility supply is isolated from bifurcated bus

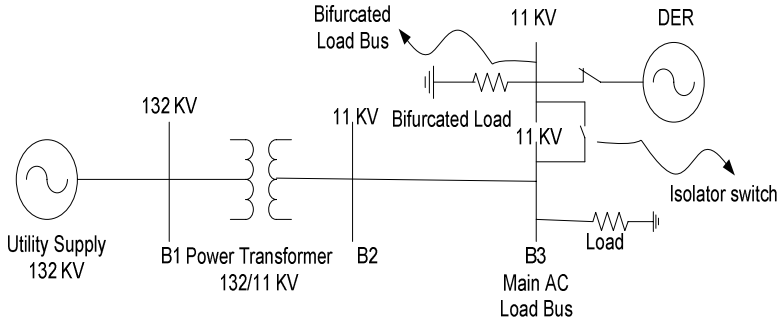

In standby switched or rollover mode as shown in Figure 3, only one of the two sources i.e., the DER is connected to the load at any one time, while the other, the utility supply/grid is disconnected but available at "the flip of a switch." Operating like this, if the DER fails while it is supplying the load, then either a human being (slow) or an automatic sensor (fast) operates two switches, the first to disconnect the DER from the load and the second to "roll" the load over to the utility supply by connecting the load to it. The opposite switching sequence occurs if the utility supply is connected to the load and DER is on standby.

Figure 3: DER standby switched mode operation in conjunction with the utility supply

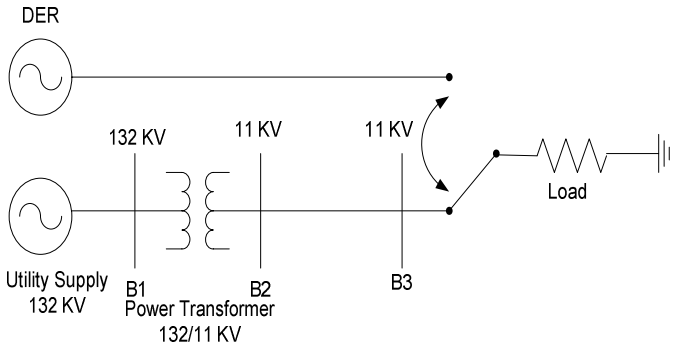

Thus, in switched or rollover mode, a brief interruption of service occurs each time the main source fails, that time being whatever it takes to switch the load to the alternate source.

Operation of the DER and utility supply connection in rollover mode generally reduces only the duration of the time during which the load can be expected to be without power. It does not improve the frequency of "outages" that can be expected. Parallel operation reduces both expected frequency and expected duration of power supply outages. No interruption occurs except when both supplies fail.

In parallel operation, the DER and the utility supply are both always connected to the load, and hence to each other as shown in Figure 4. If DER is supplying power but fails, the utility is there to instantaneously make up the difference, and no interruption of power flow to the load occurs because of sudden failure. Similarly, if the utility is serving the load but the DER is connected and ready, the DER picks up the load instantly if the utility suddenly fails and again there is no interruption of power. The point is: With the parallel operation of sources, an outage of the primary supply causes no interruption of service i.e. the frequency of interruption is reduced.

Figure 4: Parallel operation of DER with the utility supply

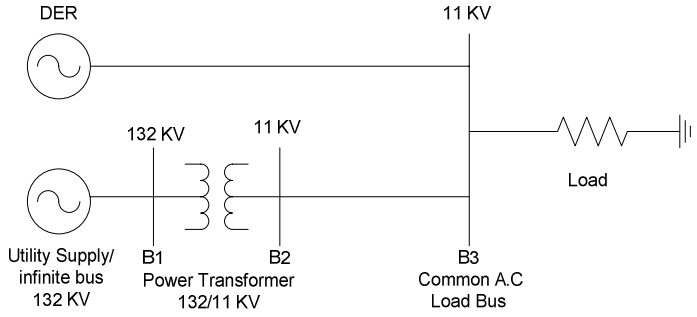

When a DER is connected to a power system/infinite bus, the power system is often so large that it will not have much of an effect on the power system. An infinite bus is a power system so large that its voltage and frequency do not vary regardless of how much real and reactive power is drawn from or supplied to it. There are different advantages and disadvantages of DER-utility supply interconnection but considering pros and cons, when managed properly, two sources of power supply will always provide more reliable power and maintain load voltage than either could alone.

Battery as DER with PWM-IGBT Inverter

A battery system as DC source can be designed for a distribution feeder to support the utility by feeding its all available power during peak time of the day or as and when required. This static DER can be used to inject energy into the network for power flow control and voltage improvement. Connection of DC source as DER to the AC load bus is made through a PWM-IGBT inverter along with LC filter as shown in Figure 5. PWM-IGBT inverter converts DC to AC when battery is discharging.

The size of the battery as DER depends on the energy injection to achieve a specific voltage for desired power flow for a distribution system, which can be determined from off-line simulation for daily energy requirement from a DER. The inverter system will be designed accordingly to regulate voltage of the connection point and hence control power flow from DER.

Figure 5: Schematic diagram of battery as DC source with PWM-IGBT inverter to serve AC bus load

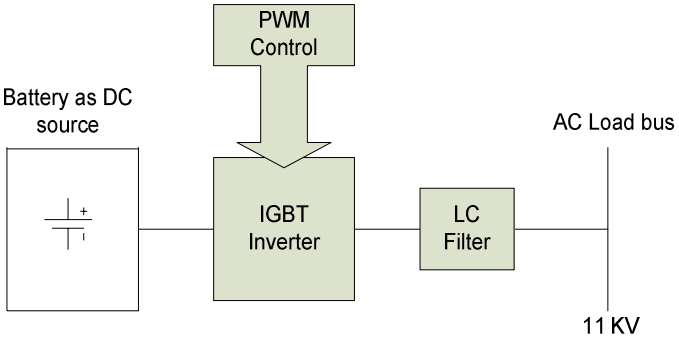

The inverters are available commercially in the market. The connection of inverter to the distribution grids has been already developed [4, 5]. Rules for inverter connection have been proposed by standard Australia [6].

The inverter system of the DER has to be synchronized with the grid so that it can serve load demand as and when required [7]. As, the static DER is synchronized with the utility supply and connected to load bus, the power injection by DER starts by controlling dynamic parameters of PWM-IGBT inverter with static DER. In this way, static DER shares load with utility supply.

There are different modulating schemes that can be used to create the variable-frequency, variable-voltage AC wave forms in PWM-IGBT inverter [8]. The sinusoidal pulse-width modulation (SPWM) technique is commonly used in industrial applications. In it, the width of each pulse in gating or switching signal is varied in proportion to the amplitude of sine wave. The SPWM compares a high frequency triangular carrier with three sinusoidal reference signals, known as the modulating signals, to generate the gating signals for the inverter switches. The frequency of the reference signal (f_r) determines the inverter output frequency and its peak amplitude A_r controls the modulation index 'm' and then in turn the rms output voltage. The ratio of peak amplitude of reference signal A_r to peak amplitude of carrier signal A_c is called modulation index and is written in equation form as

$$m = \frac{A_r}{A_c} \tag{1}$$

A PWM signal generator based on SPWM technique, shown in Figure 6, is used to generate switching signals for the power switches (IGBTs) in the inverter.

The control system of the PWM-IGBT inverter will control real power injection from the static DER as well as from utility. The power flow from standalone static DER and voltage at the A.C load bus is controlled by controlling modulating index 'm' through PWM control of IGBT inverter and DC source voltage. Whereas power flow from static DER working in parallel with utility supply to serve common bus load is controlled by controlling the phase angle (δ_2) at the load bus [9] either of PWM-

IGBT inverter output voltage or DER output voltage along with modulation index through PWM control of IGBT inverter and DC source voltage.

Figure 6: PWM Generator for the IGBT inverter from MATLAB®, SimPower Systems tool box

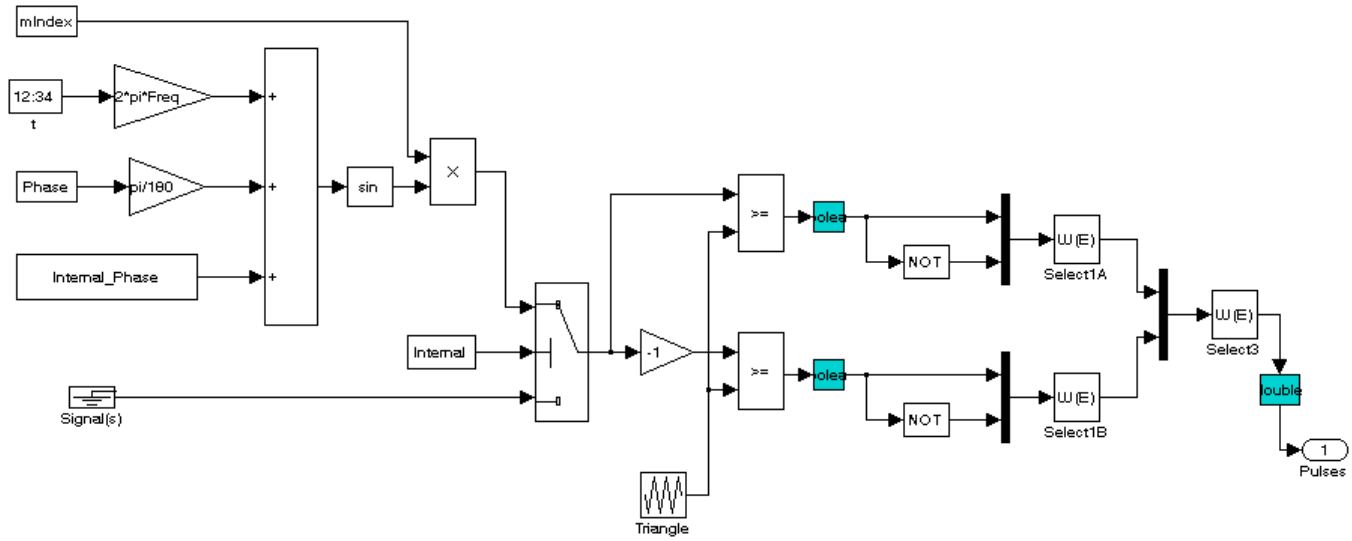

Proposed Innovative Strategy for Power Flow Control

In our proposed strategy of power flow control for the test system of Figure 7, we used a control circuit called PWM generator such that there are three sinusoidal reference signals each shifted by 120º. A bidirectional triangular carrier wave is compared with the sinusoidal reference signal corresponding to each phase to generate the gating signals for the six power switches used in 3-arm PWM-IGBT inverter with an appropriate switching signal generation topology to produce AC output at 50 Hz. Inverter output is further filtered with an LC filter to reduce harmonics and obtain 50 Hz sinusoidal AC output voltage with rms value of around 11KV.

To generate gating signals, we used discrete pulse generator block available in SimPower Systems tool box of MATLAB® that generates pulses for carrier based PWM-IGBT device. The output pulses are a vector (with values =0 or 1). Depending on the selected mode "Generator Mode", the output vector contains six pulses for 3-arm bridge. Pulses 1, 3 and 5 are respectively for upper switches of the first, second and third arm. Pulses 2, 4 and 6 are for the lower switches. By selecting "internal generation of modulating signals" in the discrete PWM generator block parameters, we controlled the modulation index m, frequency and phase of the output voltage of PWM-IGBT inverter. The switches Q1, Q3 and Q5 are turned on/off simultaneously using sinusoidal pulse width modulation technique to generate the first half cycle of AC output voltage for the 3 phases. The length of conduction is controlled proportionally to the sine wave magnitude. For the next half cycle of the three phases, switches Q2, Q4 and Q6 are modulated in the same pattern.

Because of our switching signal generation topology, the DER maximum amplitude of the fundamental phase voltage in the linear region ($m \leq 1$) is $V_s/2$ or $V_{dc}/2$ and the maximum amplitude of the DER fundamental AC output line voltage is $\hat{v}_{ab1} = \sqrt{3}\frac{V_s}{2}$ Therefore, we can write the peak amplitude as

$$\hat{v}_{ab1} = m\sqrt{3}\frac{V_s}{2} \text{ for } 0 < m \leq 1 \quad (2)$$

Hence, the line to line RMS output voltage is

$$V_{LLrms} = \frac{V_{peak}}{\sqrt{2}} = \frac{\hat{V}_{ab1}}{\sqrt{2}} \tag{3}$$

$$V_{LLrms} = \frac{m}{2} \times \frac{\sqrt{3}}{\sqrt{2}} V_{dc} \tag{4}$$

When static DER is connected to utility supply then the load bus voltage is varied and set at/near to 11KV by proper setting of modulation index. By varying modulation index, we can control inverter output voltage and hence load bus voltage along with power sharing by static DER.

To further increase the load voltage and hence power sharing from static DER, the amplitude of the modulating or reference signal can be made higher than the amplitude of the carrier signal, which leads to over modulation. The relationship between the amplitude of the fundamental AC output line voltage and the DC source voltage V_s becomes nonlinear. Thus, in the over modulation region, the line peak amplitude voltage ranges in,

$$\sqrt{3}\frac{V_s}{2} \langle \hat{v}_{ab1} = \hat{v}_{bc1} = \hat{v}_{ca1} \langle \frac{4}{\Pi}\sqrt{3}\frac{V_s}{2} \tag{5}$$

Large values of 'm' in the sinusoidal pulse width modulation technique lead to full modulation. This case is known as square wave operation, where the power devices are on for 180º. In this mode, the inverter cannot vary the load voltage (and hence its power sharing) except by varying the supply voltage ($V_{d.c} / V_s$). In this case, peak amplitude of the fundamental AC line voltage is given by

$$\hat{v}_{ab1} = \frac{4}{\Pi}\sqrt{3}\frac{V_s}{2} \tag{6}$$

The power flow from utility or grid working in parallel with static DER to serve common bus load is also controlled by regulating the phase difference ($\delta = \delta_1 - \delta_2$) between the utility supply voltage, $V_{utility}$ phase angle (δ_1) and PWM-IGBT inverter output voltage, V_{DER_L} phase angle (δ_2) at the load bus. This means that by controlling phase angle (δ_2) at the load bus either of PWM-IGBT inverter output voltage or DER output voltage, V_{DER_L} along with modulation index value, we can control active power supplied by DER and hence active power supplied by utility to common bus load.

Considering Figure 7 the power flow through 11 KV primary distribution feeder, given in complex, $S_{utility}$ is as follows:

$$S_{utility} = P_{utility} + jQ_{utility} \tag{7}$$

This equation can be rewritten in active power ($P_{utility}$) and reactive power ($Q_{utility}$) as follows;

$$P_{utility} = \frac{V_{utility} V_{DER_L}}{X_{feeder}} \sin\delta \tag{8}$$

$$Q_{utility} = \frac{V_{utility}}{X_{feeder}} (V_{utility} - V_{DER_L} \cos\delta) \tag{9}$$

The phase difference (δ) between the phase angle of utility voltage, $V_{utility}$ and phase angle of PWM-IGBT inverter output voltage at the load bus, V_{DER_L} can be calculated from the following equation.

$$\delta = \sin^{-1}\left(\frac{X_{feeder} P_{Load}}{V_{utility} V_{DER_L}}\right) \tag{10}$$

We can use this equation to control phase difference (δ), between the phase angle (δ_1) of utility voltage, $V_{utility}$ and phase angle (δ_2) of PWM-IGBT inverter output voltage at the load bus, V_{DER_L} and hence the power flow from utility and DER to load. But instead in simulation analysis, we set different values of phase angle (δ_2), of PWM-IGBT inverter output voltage at the load bus, V_{DER_L} These values of (δ_2) are set in the parametric window of PWM control of IGBT inverter, using internal generation mode of discrete PWM generator which enables us to control power flow instantly

from static DER side as directed by control circuit (PWM generator) of IGBT inverter in coordination with utility supply.

Detail analysis is carried out in two case studies.

Case 1: presents simulation results at different values of modulation index 'm' of PWM control of IGBT inverter and phase angle (δ_2) of PWM-IGBT inverter output voltage at the load bus, V_{DER_L} to examine active power sharing by the standalone static DER to serve three phase load and load bus voltage.

Case 2: presents simulation results at different values of modulation index 'm' of PWM control of IGBT inverter and phase angle (δ_2), of the PWM-IGBT inverter output voltage at the load bus, V_{DER_L} to examine active power sharing from both utility supply and DER, working in parallel, to serve three phase load and load bus voltage.

Modeling and Simulation of Test System

Test System

Figure 7 shows one line diagram of the test system with main source and static DER supplying common bus load for proposed innovative power flow control strategy.

Test system consists of the upper transmission system of 132 KV and the distribution system of 11KV. B3 is load bus at 11 KV, which consumes the active power of 10 MW. DER source is installed at bus B3 such that DC source rating is set at 19.5 KV so that 11KV rms output voltage at load bus is obtained after supplying a load of 3.25 MW. We assume that DER is a static source, battery as DC source with PWM-IGBT inverter at common load bus. Overhead distribution line is 11 KV feeder, single circuit, 5 Km in length having R= 0.01293 ((Ω/Km), L=0.9337 (mH/Km) and C=0.0121 (μF/Km). Utility side also includes a step down power transformer (T/F) having a rating of 12 MVA, 132/11KV with delta-wye grounded winding configuration.

Six pulse 3 arms PWM-IGBT inverter is used to convert DC source output to AC. LC filter is used to restrict harmonic currents passed into the network and to obtain sinusoidal AC output [10]. Discrete PWM generator with its internal control is used to supply switching signals for the six power switches in the 3-arm PWM-IGBT inverter. Triangular Carrier wave is used and its switching frequency is set at 2000 Hz. This high frequency carrier, to switch IGBTs in the inverter is used to synthesize a sine wave and hence eliminates the low order harmonics. The carrier frequency (f_c) determines the number of pulses per half cycle of reference signal and is found from

$$p = \frac{f_c}{2f_o} = \frac{m_f}{2} \tag{11}$$

where (f_o) is reference or output signal frequency and $m_f = f_c/f_o$ is defined as the frequency modulation ratio.

The reference signal chosen is sine wave with 50 Hz frequency. This frequency of reference signal determines the fundamental frequency of the inverter output voltage. Modulation index is varied (0<m<1) to control inverter output voltage or DER voltage at the A.C load bus.

In our case, static DER (battery as DC source) will be connected in parallel to utility at common load bus when its output is available especially during peak hours of the day to reduce electricity bill. This means that the static DER is not always connected to grid.

Figure 7: One line diagram of the test system with static DER working in parallel with utility supply to serve common bus load

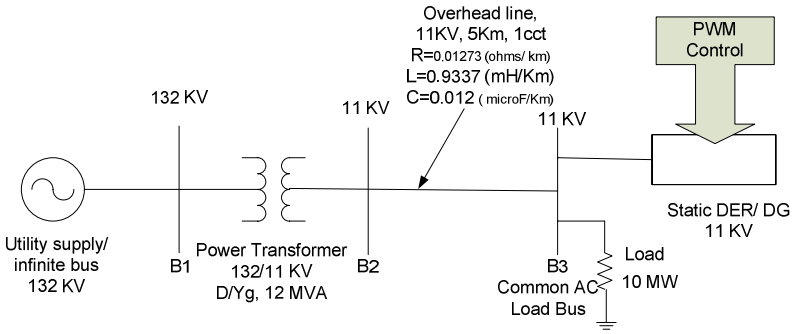

The Matlab®, Simulink® Set up Using SimPower Systems Toolbox for the Test System

The MATLAB® based Simulink® set up using SimPower Systems toolbox for the standalone case of static DER supplying three phase resistive load is developed using Simulink and SimPower Systems libraries and is shown in Figure 8. This setup consists of battery as DC source, PWM-IGBT inverter with discrete PWM generator and LC filter to obtain A.C output at 50 Hz to serve three phase resistive load of 3.25MW at 11KV. We have used power electronics library of SimPower Systems to capture non-ideal behavior of power electronics components such as diodes and IGBTs.

The Simulink setup of Figure 8 is developed using readymade components from the SimPower Systems library, which includes DC voltage source, semiconductor devices, inductors, capacitors and resistors etc. For semiconductor devices, a universal bridge is used to allow discretizing of the model. The Universal Bridge block implements a universal three-phase power converter or inverter that consists of up to six power switches connected in a bridge configuration. The types of power switch and converter configuration are selectable from the dialog box, in the parametric window of Universal Bridge block. The Universal Bridge block allows simulation of converters or inverters using either naturally commutated (or line-commutated) power electronic devices (diodes or thyristors) or forced-commutated devices (GTO, IGBT and MOSFET). The Universal Bridge block is also the basic block for building two-level voltage-sourced converters (VSC).

MATLAB® based Simulink® set up using SimPower Systems toolbox for the test system of Figure 7, involving static DER with PWM-IGBT inverter at the load bus is then developed using Simulink and SimPower Systems libraries as shown in the Figure 15. Ode 5 [Dormand-Prince] fixed step frequency solver is used to simulate developed test system circuit model. The speed of simulation in the Simulink environment is increased significantly by discritizing the model using the PowerGUI tool and fixed step frequency solvers.

Discussion of Key Simulation Results

Case 1. Power Flow Control with Standalone Static DER Connected to the Load Bus

The purpose of developing the MATLAB®, Simulink® setup in the SimPower Systems toolbox using Simulink and SimPower Systems libraries for the standalone case of static DER supplying three phase resistive load, is to study and analyze which one of the following two controls for controlling standalone DER active power flow to load is better.

- Control of DER active power flow to load by controlling modulation index through PWM control of IGBT-PWM.
- Control of DER active power flow to load through phase angle control at the load bus either of DER output voltage or PWM-IGBT inverter output voltage.

We simulated the Figure 8 Simulink setup without and with isolation transformer (T/F) using Ode 5 [Dormand-Prince] fixed step frequency solver as we have discretize the model using the

PowerGUI tool to increase the simulation speed. Because of using a user friendly Graphical User Interface (GUI) based Simulink environment, simulation is faster and is more like system level simulation while at the same time the simulation is able to provide greater details of the dynamics in PWM-IGBT inverters. We used isolation transformer at the output side of IGBT inverter after LC filter to minimize problem of DC injection into utility network as well as to load in the case of any fault on static DER side.

Simulation results without isolation transformer are shown in Figure 9 to Figure 13. Wave forms for the DC source output, inverter output voltage without filtering, in depth view of inverter output voltage without filtering, inverter output voltage after filtering and active power drawn by the load from static DER are shown in Figure 9, 10, 11, 12 and 13 respectively. Simulation stop time is set at 100 ms to completely analyze the settling time of the active power supplied by the standalone DER to serve the load. After a transient period of approximately 25 ms, the active power supplied by DER to serve the load reaches a steady state as shown in Figure 13.

Figure 9 to Figure 13 waveforms are obtained using discrete PWM generator with its internal mode of generating gating signals for the six IGBT switches in the IGBT inverter for the case, when values of parameters, modulation index (m), phase angle of output voltage (δ_2), carrier frequency (f_c) and output frequency (f_o) are set at 0.99, 0° , 2000 Hz and 50Hz respectively. These parameter values are so managed that, static DER can take its full load i.e. 3.25MW at 11KV with appropriate values of L and C in LC filter. Other simulation results at different values of modulation index for both without and with isolation transformer (used between LC filter and three phase load) can be shown but for simplicity results are accumulated in tabulated form as shown in table 1 and table 2.

Figure 8: MATLAB based Simulink and SimPower Systems circuit model showing battery with PWM-IGBT inverter to supply three phase load

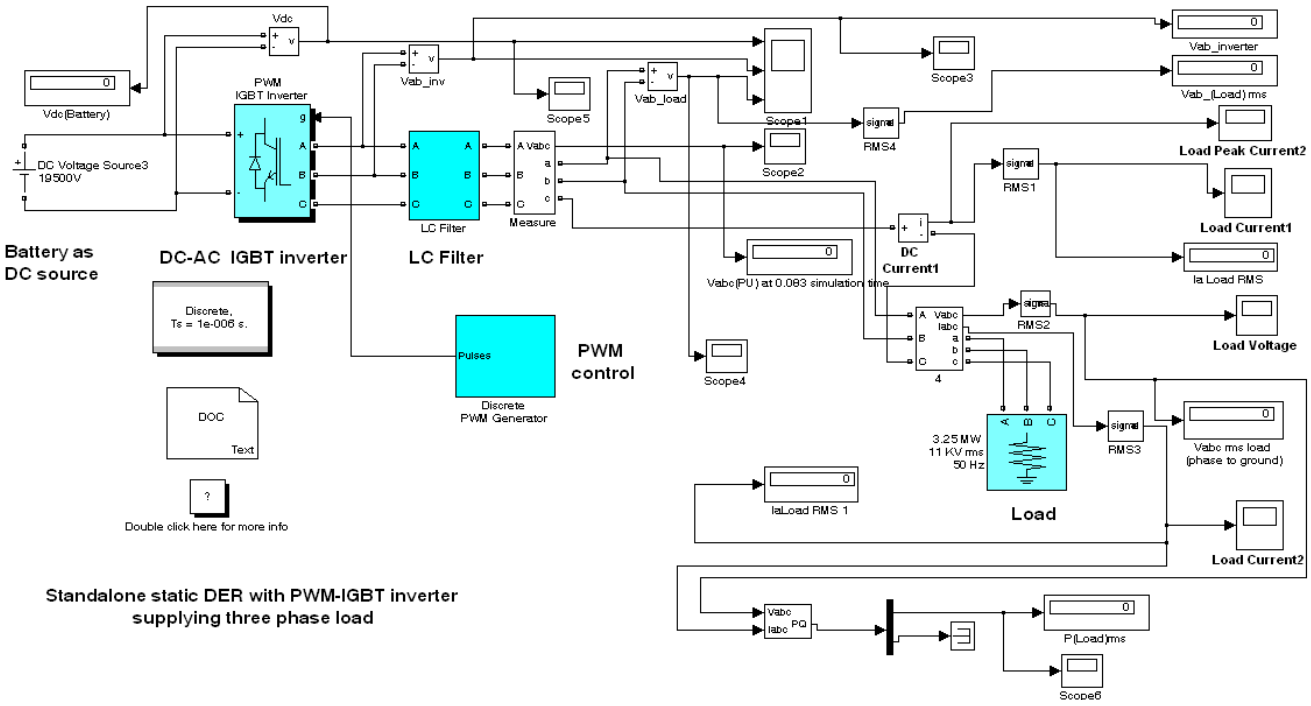

Table 1 and 2 shows, that the variation of modulation index through PWM control considerably affects both the DER output voltage at the load bus as well as DER active power contribution to load in standalone DER case. Whereas table 3 shows that there is no effect of varying phase of DER output voltage at the load bus on the active power flow and DER output voltage at the load bus. This is because; power drawn by the load is already nearly at maximum level at 11 KV when phase angle at

the load bus either of DER output voltage or PWM-IGBT inverter output voltage is at 0°. It is to be noted that equation (9) of active power flow is applicable when two sources working in parallel are supplying load with one source as utility supply. Hence in standalone static DER case, it is not applicable. The power flow will increase from DER by increasing phase angle of PWM-IGBT inverter output voltage at the load bus as and when we connect static DER of Figure 8 in parallel with utility supply to serve common bus load. This is case-b and its results are accumulated in tables 4 and 5.

Figure 9: DC source output voltage

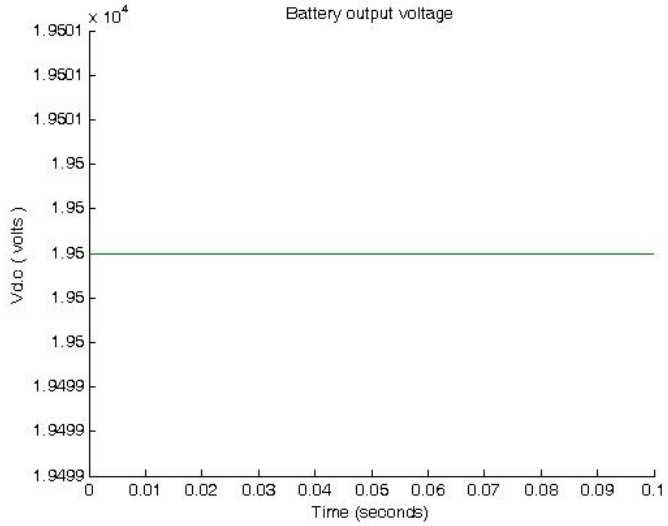

Figure 10: PWM-IGBT inverter output voltage before filtering

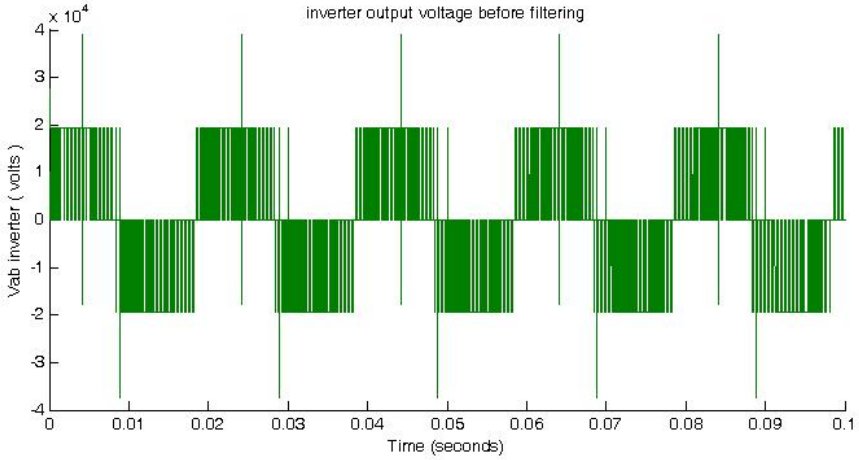

Figure 11: PWM-IGBT inverter output voltage in volts before filtering (in depth view for two cycles)

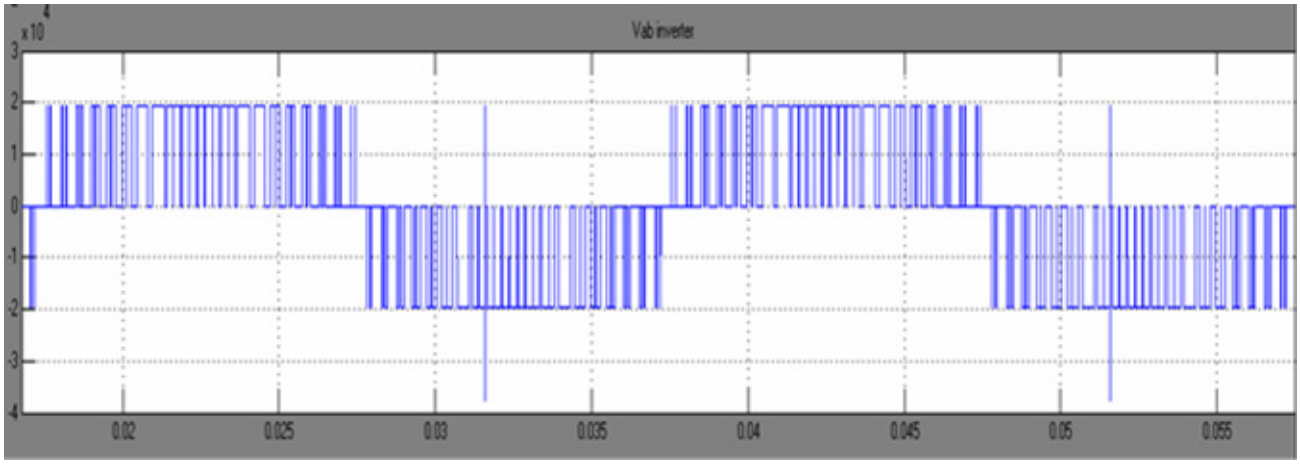

Figure 12: PWM-IGBT inverter output voltage (after filtering) applied to load

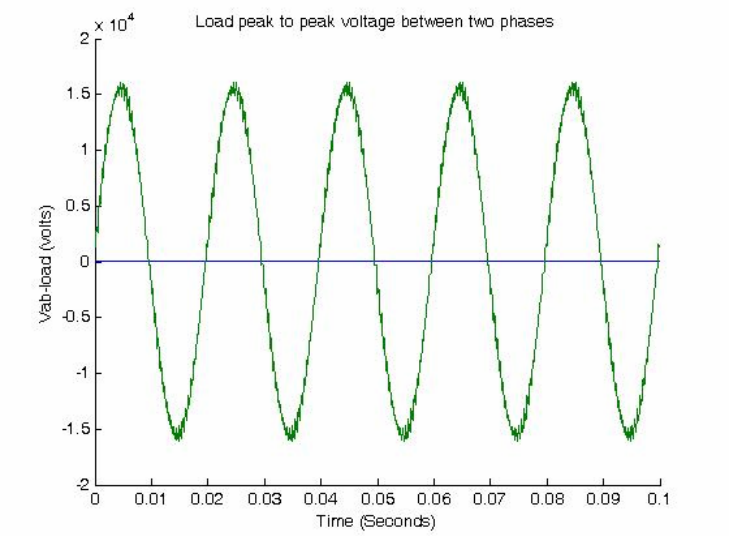

Figure 13: Active power supplied by DER to load when m=0.999 and $\delta_2 = 0°$

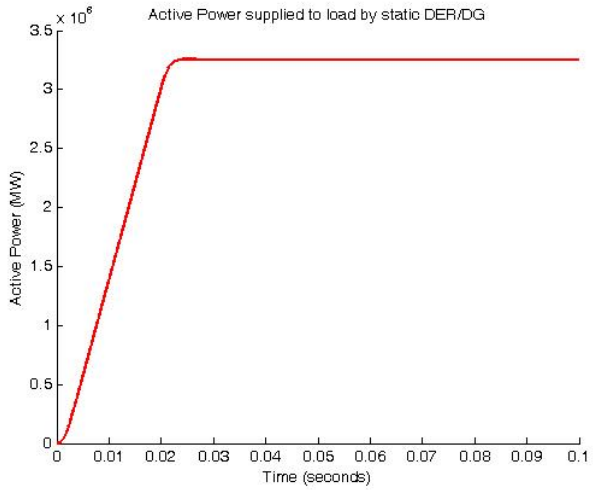

Case 2. Power Flow Control with Static DER Working in Parallel with Utility Supply at the Load Bus

Developed MATLAB®, Simulink® set up using SimPower Systems toolbox for the standalone case of static DER feeding load is now connected in parallel with utility supply at the common load bus according to the test system block diagram of Figure 14 and is shown in Figure 15. Simulation results shown in Figure 16, 17, 18 and 20 are obtained after simulating the developed test system circuit model for the case, when 'm' is set at 0.999 and phase angle of DER output voltage at the load bus is kept 0º.

Figure 14: Block diagram showing, a static DER working in parallel with utility supply/ infinite bus to serve common AC bus load

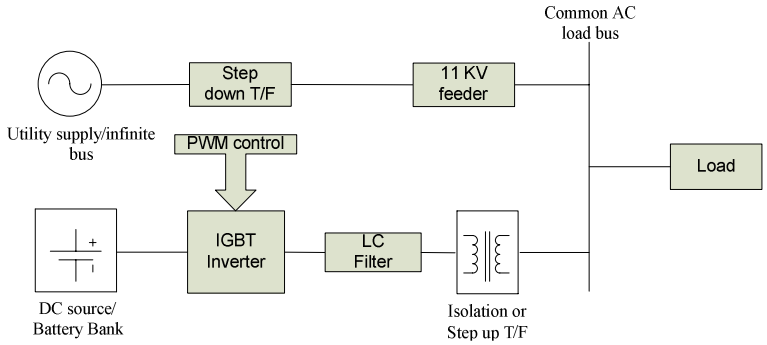

The active power shared by the utility supply and static DER to serve the load is shown in Figure 16 whereas phase to phase voltage of utility, DER and load are shown in Figure 17. Utility side power transformer HT side phase to ground voltage is plotted in Figure 18. Waveforms for the current supplied by utility and DER to common bus load are also shown in Figure 19. Other simulation results at different values of modulation index by keeping phase angle of DER output voltage at the load bus at 0º can be shown but for simplicity results are accumulated in tabulated form as given in table 4.

Table 1: DER output voltage at the load bus and active power contribution by the standalone static DER to load at different values of "modulation index" without isolation transformer.

Sr. No.	Synchronizing Frequency (Hz)	Modulation index with $\delta_2 = 0$	$I_{DER\ rms}$ (A)	V_{rms} Load/DER_L (KV)	P_{rms} load (MW)
1	50	0.99	170.8	11.01	3.25
2	50	0.888	153.4	09.88	2.62
3	50	0.777	134.0	08.63	2.00
4	50	0.555	095.8	06.17	1.02

Table 2: DER output voltage before isolation transformer, Load /DER output voltage at the load bus and active power contribution by the standalone static DER to load with isolation T/F at different values of "modulation index".

Sr. No.	Synchronizing Frequency (Hz)	Modulation index	Phase angle δ_2	I*DER rms* (A)	Vrms DER (KV) (Before isolation T/F)	Vrms Load/DERL (KV) (after isolation T/F)	Prms load (MW)
1	50	0.999	0°	169.0	11.09	10.90	3.19
2	50	0.888	0°	150.2	09.91	09.68	2.52
3	50	0.777	0°	131.2	08.68	08.46	1.92
4	50	0.555	0°	93.85	06.20	06.05	0.98

Table 3: DER output voltage before isolation transformer, Load/ DER output voltage at the load bus and active power contribution by the standalone static DER to load with isolation T/F at different values of "phase angle of DER output voltage at the load bus".

Sr. No.	Synchronizing Frequency (Hz)	Modulation index	Phase angle δ_2	$I_{DER\ rms}$ (A)	V_{rms} DER (KV) (Before isolation T/F)	V_{rms} Load/DER_L (KV) (after isolation T/F)	P_{rms} load (MW)
1	50	0.999	0°	169.0	11.09	10.90	3.190
2	50	0.999	5°	168.7	11.07	10.89	3.187
3	50	0.999	10°	168.9	11.08	10.90	3.186
4	50	0.999	15°	168.9	11.08	10.90	3.191

Table 4: Load voltage, DER voltage, utility voltage and active power contribution by utility and static DER to serve common bus load at various values of modulation index.

Sr. No.	Synchronizing Frequency (Hz)	Modulation index	DER Active Power (MW)	*V_{rms} DER_L (KV)	P_{rms} utility (MW)	P_{rms} load (MW)
1	50	0.999	2.28	10.96	8.22	9.93
2	50	0.888	2.16	10.72	7.80	9.50
3	50	0.777	1.83	10.48	7.67	9.08
4	50	0.666	1.47	10.24	7.49	8.67

* Vrms DER_L = Vrms Utility = Vrms Load

Table 5: Load voltage, DER voltage, utility voltage and active power contribution by utility and static DER to serve common bus load at various values of "phase angle (δ_2) of DER output voltage at the load bus".

Sr. No.	Synchronizing Frequency (Hz)	Modulation index	Phase angle δ_2	I_{DERrms} (A)	*V_{rms} DER_L (KV)	P_{rms} utility (MW)	P_{rms} DER (MW)	P_{rms} load (MW)
1	50	0.999	0°	115.7	10.96	8.22	2.28	9.936
2	50	0.999	5°	155.1	10.96	7.10	3.21	9.932
3	50	0.999	10°	197.5	10.95	6.23	4.18	9.908
4	50	0.999	14°	232.1	10.93	5.51	4.90	9.871
5	50	0.999	16°	250.2	10.91	5.17	5.28	9.847

* Vrms DERL = Vrms Utility = Vrms Load

Figure 15: MATLAB based Simulink and SimPower Systems circuit model showing utility and Static DER working in parallel to supply common bus load for power flow control

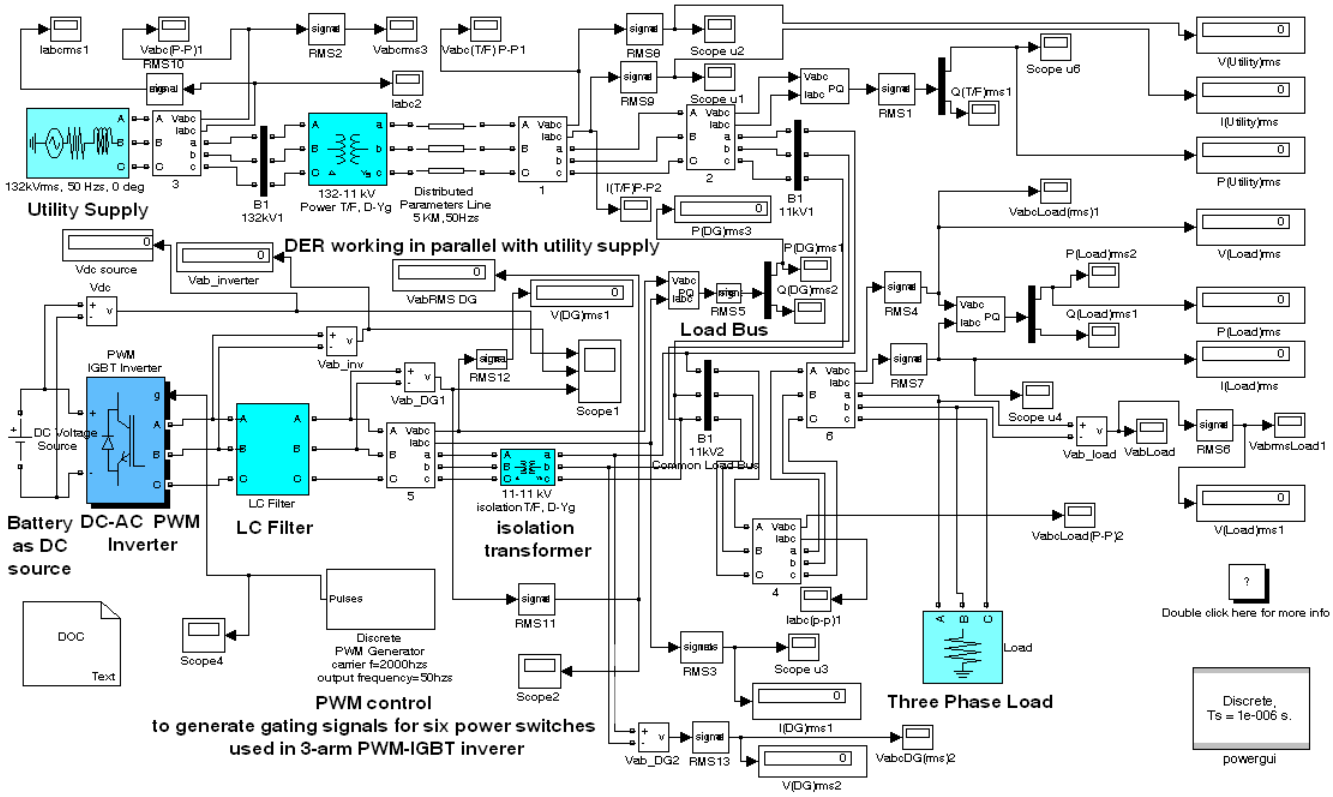

Figure 16: Simulation results showing, active power shared by utility and DER to serve common bus load, when m = 0.999 and = δ_2 0°

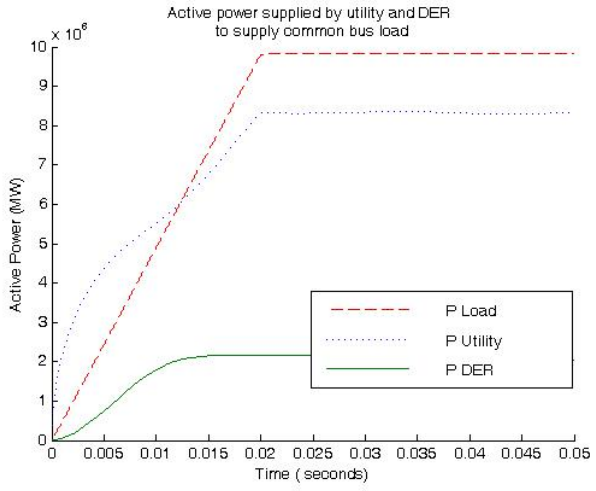

Figure 17: Simulation results showing, phase to phase utility voltage (after power T/F), DER voltage (after isolation T/F) and load voltage in accumulated form, when m = 0.999 and $\delta_2 = 0°$

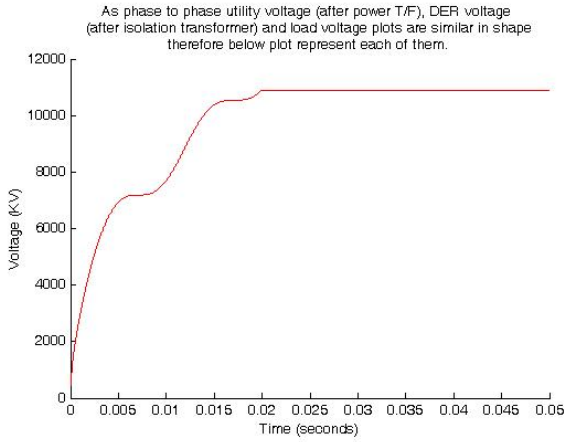

Figure 18: Simulation results showing, utility power transformer HT side phase to ground voltage, when m = 0.999 and $\delta_2 = 0°$

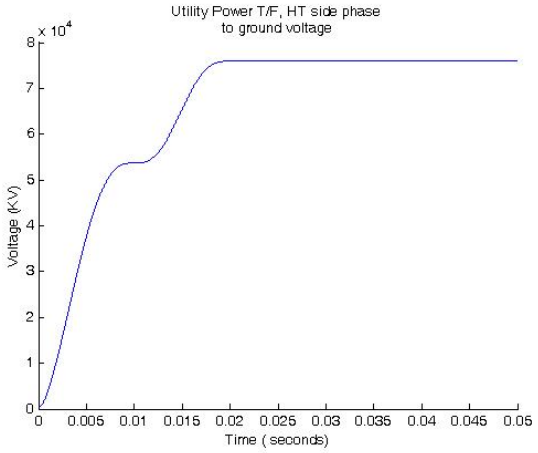

Figure 19: Simulation results showing, current supplied by utility and static DER to common bus load, when m=0.999 and $\delta_2 = 0°$

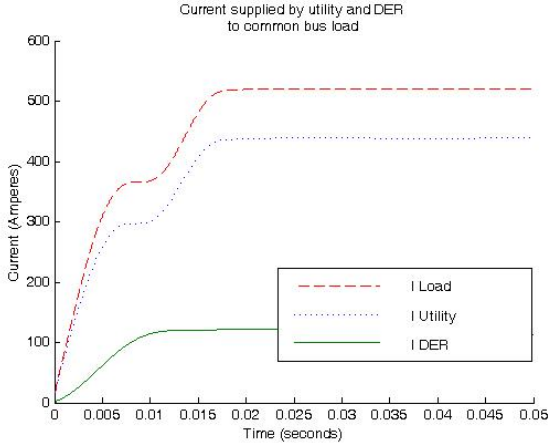

Table 4 shows that by increasing modulation index through PWM control of inverter, active power contribution from both static DER as well as from utility supply increases and at m=0.99 maximum power contributed by DER is 2.28 MW. Although DER in standalone case with isolation transformer took 3.19 MW load at 11KV with m=0.999. This shows that, when DER is connected in parallel with utility supply to share load then for the same value of m i.e. 0.999, DER active power contribution to load is reduced i.e. from 3.19 MW to 2.28 MW and it will increase only when we increase phase angle (δ_2) of DER output voltage at the load bus. Thus the power flow to the load is controlled by regulating the phase difference (δ) between the utility supply voltage and PWM-IGBT inverter output voltage at the load bus or DER output voltage at the load bus according to equation (8). For design purposes, it is assumed that the maximum phase angle $\delta_{2\max}$ is 20º.

Simulation results for the case, when m is fixed at 0.999 and phase angle of DER output voltage at the load bus is increased can be also plotted but again for simplicity results are accumulated in tabulated form as shown in table 5. Table 5 shows that by increasing phase angle of DER output voltage at the load bus, DER active power contribution starts increasing from 2.28 MW and corresponding utility active power contribution to load starts decreasing according to equation (8). This shows that control of active power by controlling phase angle of DER output voltage at the load bus is better then the control of active power by controlling modulation index of inverter. However, it is obvious from table 4 and 5 that, by controlling modulation index through PWM control of IGBT inverter, we can control the common bus load voltage near to a desired constant value.

Simulation stop time in case-b analysis is set at 50 ms to completely analyze the settling time for the active power supplied by the DER to serve the load. Simulation plot of Figure 16 also shows that after a transient period of 20 ms, the active power drawn by load and active power supplied by utility reaches a steady state in one cycle (20 ms). This plot also shows that active power supplied by DER to share load is settled at 15 ms (less than one cycle) whereas settling time for the active power supplied by DER to load in case-a is 25 ms. This shows that settling time for the active power supplied by DER to load in case-b is improved and system quickly attains steady state.

Conclusions

The PWM-IGBT inverter with battery as DC source for power flow control is used on the analogy of the series controller of unified power flow controller (UPFC) called static synchronous series compensator (SSSC). SSSC also involves DC link capacitor or battery as DC source and inverter. The simulation studies with static DER working in parallel with utility supply at the common load bus shows that active power flow to load from utility and static DER is realized by controlling, phase angle (δ_2) at the load bus either of PWM-IGBT inverter output voltage or DER output voltage at the load bus. Whereas DER output voltage or the load bus voltage is controlled by varying modulation index through PWM control of IGBT inverter. SSSC also controls power flow in the line by controlling either the phase angle and (or) magnitude of injected voltage. This shows that static DER with inverter will work as series part of UPFC (i.e. SSSC with storage) at the load bus in the presence of utility supply to control active power flow from static DER and utility supply.

We observed that when power sharing from DER is made to supply some part of load then correspondingly power sharing from utility supply is reduced. This reduction in power sharing by utility helps to reduce utility losses and improve its performance. This also improves load bus voltage and postpones network expansion as load demand is locally met. Reliability of power supply especially during the peak hours of the day is also improved. This shows that the use of DER at common load bus with utility supply saves large investment on constructing new power houses to meet increased peak load demand. Also if load demand is increased and it is to be met by the old power distribution network then either new feeders are to be installed or feeder re-conductoring is done.

Implementation cost of the DC source battery storage DER can be justified from postponement of new capacity, reduction in losses and load bus voltage enhancement.

References

[1] Thomos Ackermanm, Goran Andersosn, Lennart Soder, "Distributed generation: a definition" *Elsevier Electric Power Systems Research* Vol. 57, 2001, pp. 195-204.

[2] The Mathworks Inc. < http://www.mathworks.com/>

[3] Stephen J. Chapman, Electric Machinery fundamentals, 3rd edition, McGraw-HILL International Co. Singapore, 1999.

[4] D. Georgakis, S. Papathanassiou, N. Hatziargyriou, A. Engler, Ch. Hardt, Operation of a micro grid system based on micro-sources equipped with fast-acting power electronics interfaces, in: Proceedings of the 35th Annual IEEE Power Electronics Specialists Conference, Aachen, Germany, 2004, pp. 2521-2526.

[5] A. Ghosh, G. Ledwich, Power Quality Enhancement Using Custom Power Devices, Kluwer Academic Publishers, 2002.

[6] DR 01212-01214: Draft Australian Standard, Grid Connection of Energy Systems via Inverters, Parts 1–3.

[7] C.V. Nayar, M. Ashari, W.W.L. Keerthipala, A grid-interactive photovoltaic uninterruptible power supply system using battery storage and a back up diesel generator, IEEE Trans. Energy Conver. 15 (3) (2000) 348–353.

[8] Muhammad H. Rashid, Power Electronics Circuits, Devices, and Applications, 3rd edition, Pearson Education Pte. Ltd., Singapore, 2004.

[9] M. Ashari,W.W. L. Keerthipala, and C. V. Nayar, "A single phase parallely connected uninterruptible power supply/demand side management system," *IEEE Trans. on Energy Conversion*, vol. PE-275–EC (08-99).

[10] Nick Jenkin, Ron Allen, Peter Crossley, David Kirschen and Goran Strbac, Embeded Generation, The Institution of Electrical Engineers, London, U.K, 2000.

European Journal of Scientific Research
ISSN 1450-216X Vol.18 No.3 (2007), pp.532-540

http://www.eurojournals.com/ejsr.htm

Effect of Insulin on ^{3}H-Deoxy-Glucose Uptake into Brain Slices and Synaptosomal Preparations from Different Brain Regions

Rula Abdul-Ghani
Laboratory of Molecular Tumor Pathology, Humboldt University, Berlin
E-mail: abdalsalam@med.alquds.edu
Fax: 00972-2-2796110

Munir Qazzaz
Biology and Biochemistry Department
Birzeit University, Palestine

Abdul Salam Abdul-Ghani
Physiology & Pharmacology Department, Faculty of Medicine
Al-Quds University, Palestine

Abstract

In the present work we have tested the effect of Insulin in increasing ^{3}H-deoxy glucose uptake into different brain regions, using brain slices and synaptosomal preparations.

In-Vitro studies has shown that addition of Insulin 2 ng/ml has increased ^{3}H-deoxy glucose uptake into brain slices from the hypothalamus by 22% ($P<0.01$) compared to control samples which were treated with the same volume of Krebs Ringer Buffer. With 10 ng Insulin the effect was increased to 48% ($P<0.005$) and higher doses did not show a dose response effect.

In brain slices from cervical spinal cord, Insulin 2 ng/ml was not effective while 10 ng has produced a significant increase of 20% ($P<0.01$), higher doses of 20 ng/ml Insulin has increased ^{3}H-deoxy glucose uptake by 46% ($P<0.005$).

With brain slices from the cortex, medulla-oblongata and cerebellum, insulin has no effect on ^{3}H-deoxy glucose uptake. Similar results were achieved when we used brain synaptosomal preparations. The minimum effective dose was 10 ng/ml and did not show a dose dependent manner.

In Conclusion: Insulin is effective in increasing ^{3}H-deoxy glucose uptake into brain slices and synaptosomes from cervical spinal cord and hypothalamus, and no effect whatsoever on ^{3}H-deoxy glucose uptake into other brain areas. It seems that whole brain tissues are insulin independent except hypothalamus and cervical spinal cord.

Keywords: Insulin, ^{3}H-Deoxy-Glucose, Hypothalamus, Synaptosomes; Brain Slices

Introduction

The brain depends absolutely for its ability to function normally on a constant glucose and oxygen supply from the blood stream. Any interruption in their delivery leads within seconds to

unconsciousness and within minutes to irreversible cell death. The importance of the constant blood supply can be readily appreciated if we remember that this organ, only 3% of the total adult body weight, consumes some 20% of the glucose required by the whole body. The brain has a high metabolic rate and is the most sensitive part of the body to failure in oxygen or glucose (Nelson et al, 1968; Watanabe and passoneau, 1973).

Insulin has been known since 1922, but in spite of intense research activity, the biochemical function of this hormone is not fully understood. Insulin acts in at least two different ways: by increasing transport of some sugars and other metabolites and by influencing the rate of synthesis of some enzymes. The most pronounced effect of an insulin injection is a rapid fall of glucose and free fatty acid concentration of blood. Insulin increases glucose uptake of several body tissues, especially muscle and adipose tissue. Besides the direct insulin effects on various tissues, there are indirect effects caused by the fall in blood sugar. This means that it may be difficult to decide whether the local effects seen after insulin administration are due to the fact that insulin has reached the tissue in question and has acted there on, or whether the changes observed are conditioned by the hypoglycemia. These problems are of special importance for the CNS because this organ is the first to signal important consequences of a general hypoglycemia.

The CNS has been considered for many years as an insulin independent organ. The role of insulin has been postulated as a brain growth factor and/or neuroregulator. The influence of insulin on glucose transport into brain cells is more controversial.

Within the CNS, studies on insulin's effect on glucose uptake have yielded conflicting results. Some of these results have shown the absence of insulin stimulated glucose uptake in brain slices (Rafaelson, 1961; Betz et al, 1973; Philips and Coxon, 1976; Goodner and Berrie. 1977) suggesting that brain tissue would be unresponsive to insulin. Over the past decade, the wide spread of radioligand binding methods (Roth, 1973; Kahn, 1976; Ginsperg, 1977) has demonstrated chemically specific binding sites for insulin in a number of diverse tissues including brain, kidney, placenta and the blood cells (erythrocytes, lymphocytes, macrophages) from many species. The wide special nature of specific insulin binding suggests that insulin may play a much more complicated and fundamental biological role than may have been originally.

Several groups of workers have failed to obtain evidence that insulin enhances transport of hexoses from blood to brain (Crone 1965; Buschiazzo et al, 1970; Sloviter and Yamada, 1971; Daniel et al, 1975). When insulin was given to un-anaesthetized mice it increased both the tissue glycogen concentration and the tissue/serum glucose concentration ratio (Nelson et al, 1968). Insulin added in vitro or injected in vivo increased glucose uptake. The increase in isolated rat spinal cord was 40-80% (Rafaelson, 1960). Experiments with rat brain slices showed only a slight increase in glucose uptake and only in first brain slices (with only one cut surface) the increase was only 10-15% in isolated cerebellum (Rafaelson, 1961). When slices of calf and rat anterior pituitary gland were incubated, insulin increased glucose uptake by 25 % both when the hormone was added to the medium or injected into diabetic rats before sacrifice (Goodner and Freinkel, 1961). It has also been shown that anaerobic glycolysis rises up to 30% after pre-incubation of brain slices with insulin. Insulin gave time and dose dependent stimulation of 2-DG uptake into C6 glioma cultures, which have the properties of glial cells (Wei and Yeh, 1990). Studies done on the retina showed increase in 2-DG uptake by the normal retina, while the retina of diabetic rats showed lower levels of 2-DG accumulation (Vilchis and Salceda, 1996). On the other hand, several experiments gave different results, insulin gave no effect on 2-DG uptake in Hypothalamus and in slices of the anterior, posterior and cortical grey matter, while diaphragm muscle from the same rats responded to insulin under identical conditions (Goodner and Berrie, 1977).

Other experiments showed that insulin failed to influence the pattern of 2-DG uptake in vivo (Goodner et al ,1980). The only published results reported on synaptosomal uptake of 2-DG showed high affinity uptake of 2-DG (Diamond and Fishman, 1973).

Materials and Methods

Animal Dissection:

The animals used in these experiments were Sprague-Dawley rats weighing (250-350g) they were scarified by decapitation. The brain was rapidly removed onto a cooled (0°C) dissecting block. The following regions of the brain were separated for either slicing or synaptosomal preparation: [Whole brain, Cerebrum, Cerebellum, Cortex, Medulla Oblongata, Thalamus, Hypothalamus and Spinal cord].

Preparation of Synaptosomes:

Synaptosomes were prepared using a modified version of the method by Hughes et al., 1993. After decapitation, the whole brain was removed, placed on an ice block 0°C and separated into the following region; Cortex, Hippocampus, Thalamus, Hypothalamus, Pons, Medulla Oblongata, and Spinal Cord. Each region was placed in 9 ml ice cold 0.32M sucrose and homogenized by 12 ups and down strokes in a glass perspex homogenizer. The homogenization leaves the nerve endings intact, allows the pinching off of nerve terminals and breaks up cell bodies but spares the synaptosomes which are much more smaller (0.5-1 μm) in diameter. The homogenate was carefully layered on top of a sucrose gradient [10ml of 0.8 M sucrose / 5ml of 1.2 M sucrose]. The gradient was balanced then centrifuged in 55.2 Ti Rotor at 50000 rpm for 70min at 4°C using Beckman L8-70M ultracentrifuge.

After centrifugation three fractions were obtained, lower pellet consisting of red blood cells, mitochondria and nuclear material. Upper fraction which consists of myelin and middle layer between the 0.8M/1.2M sucrose interfaces which consists of synaptosomes. The synaptosomal layer was removed carefully with a Pasteur pipette and the same volume of Krebs Ringer Buffer (KRB) was added which contain (mM): NaCl 140, KCl 4.9. NaOH 3.25, $MgSO_4$ $7H_2O$ 1.22, KH_2PO_4 1.25, $CaCl_2$ 1.2, glucose 5.6; pH 7.4. in some experiments glucose 1 mM was used instead of 5.6 mM. The buffer was oxygenated with O_2/CO_2 95/5 %. The synaptosomal solution formed was termed the mother fraction and was divided into 1ml appendorf tubes, centrifuged with microcentrifuge for 20 sec at 14000 rpm, after washing for three times with KRB. The synaptosomes were ready for uptake experiments.

Preparation of Slices:

Slices from different brain regions using the Mcilwain mechanical chopper slices of (400 μm) thickness were used. Single slices were then transfered into appendorf tubes containing 1ml oxygenated buffer. The tissue was ready for uptake experiments.

Uptake Experiments:

The synaptosomes or slices were pre-incubated with KRB for 15 min. In a shaking water bath at 37°C, ^{3}H-deoxy-D-glucose (2-DG); 26.2 Ci/mmol) was added for all tubes and incubated for 10 min . insulin (28.1 USP) was added in different concentrations (10-50 ng/ml). After incubation the samples were centrifuged for 2 min .the supernatant was decantated to appendorf tubes (extra-cellular fraction), the pellet was extracted with 1ml of 10% trichloroacetic acid (TCA) and micro-centrifuged at 14000 rpm for 8 min. The supernatant of the TCA fraction is the intracellular (uptaked) fraction and the pellet was kept frozen for protein assay.

Radiolabel Counting:

For radiolabel counting we used liquid scintillant [toluene,! 1; methoxyethanol ,800ml ;2(4-biphenyl) 1,3,4- oxodiazol ,6g] 5ml of the liquid scintillant was added to 100 μ1 of TCA fraction and extra-cellular fraction. All counting vials were mixed well before counting the dpm in Packard Tricarb 1900 scintillation counter.

Protein Assay:

Protein content of the dissolved samples was determined using Bradford method ;1993 ,400 µl of KRB buffer and 600µl dye reagent were added to the samples, whirly mixed, after nearly 5 min the absorbance was read at 595 nm. Standard curve was performed using bovine serum albumin at different concentrations (0-12µg /ml). The absorbance was read for the standard BSA solutions and for the samples

Calculations:

Uptake of 2-DG was measured as dpm/min/mg protein or as an uptake fraction which is equal to dpm in TCA fraction divided by the whole radioactivity in TCA fraction and extra-cellular fraction .Statistical analysis was made for measuring the mean values ± standard error and the significancy of the results was calculated using student t-test.

Results and Discussion

Uptake into Synaptosomes:

Table 1- shows that Insulin in concentrations of 2 ng/ml, 10ng/ml , 20 ng/ml added to the medium was unable to produce any significant effect on ^{3}H-deoxy glucose uptake into synaptosomal preparations from the cortex, thalamus, hippocampus, pons and medulla oblongata. In synaptosomes from the hypothalamus insulin 2 ng/ml was not effective while higher dose of 10 ng/ml has increased ^{3}H-deoxy-glucose uptake by 41% ($P \leq 0.01$), similar increase was achieved with higher dose of 20 ng/ml. In synaptosomal preparations from the cervical spinal cord, insulin 2 ng/ml was not effective while higher concentrations of 10 ng/ml and 20 ng/ml has produced a significant increase of 33 % ($P \leq 0.05$) and 32 % ($P \leq 0.05$) respectively.

The effect of insulin on ^{3}H-deoxy-glucose uptake into synaptosomal preparations from the hypothalamus and cervical spinal cord is not a dose dependent.

Table 1: Effect of Insulin on ^{3}H-Deoxy Glucose uptake into Synaptosomal Preparations

Brain Region	Control	Insulin (2 ng/ml)	Insulin (10 ng/ml)	Insulin (20 ng/ml)
Spinal Cord	1.09 ± 0.08 (10)	1.14 ± 0.09 (12)	1.45 ± 0.10 (12) ↑ 33 % **($P \leq 0.05$)**	1.44 ± 0.10 (9) ↑ 32 % **($P \leq 0.05$)**
Hypothalamus	1.50 ± 0.12 (8)	1.74 ± 0.07 (8)	2.12 ± 0.13 (8) ↑ 41 % **($P \leq 0.01$)**	1.84 ± 0.10 (5) ↑ 23 % **($P \leq 0.05$)**
Cortex	1.80 ± 0.12 (16)	2.10 ± 0.10 (16)	2.20 ± 0.15 (16)	1.40 ± 0.10 (6)
Thalamus	1.90 ± 0.13 (9)	1.80 ± 0.13 (9)	2.00 ± 0.28 (8)	1.70 ± 0.22 (6)
Hippocampus	1.60 ± 0.23 (8)	1.80 ± 0.15 (9)	1.40 ± 0.19 (9)	1.60 ± 0.21 (6)
Pons	1.20 ± 0.09 (8)	1.10 ±0.09 (10)	1.10 ± 0.09 (10)	0.90 ± 0.09 (6)
Medulla Oblongata	2.60 ± 0.18 (6)	2.70 ± 0.27 (9)	2.50 ± 0.17 (9)	2.10 ± 0.32 (3)

Values are mean of uptake fraction of 2-DG ± SEM for the number of experiments indicated in parentheses.

Uptake into Brain Slices:

In brain slices from the hypothalamus, insulin 2 ng/ml was effective in increasing ^{3}H-deoxy-glucose uptake by 22 % ($P \leq 0.01$), concentration of 10 ng/ml has elevated the effect to 48 % ($P \leq 0.005$) while higher concentration of 20 ng/ml has increased glucose uptake by 23 % ($P \leq 0.025$) only Figure 1.

Figure 1: Percentage Change in ^{3}H-Deoxy Glucose uptake into Spinal cord and Hypothalamic Brain Slices Following Treatment with Different Concentrations of Insulin

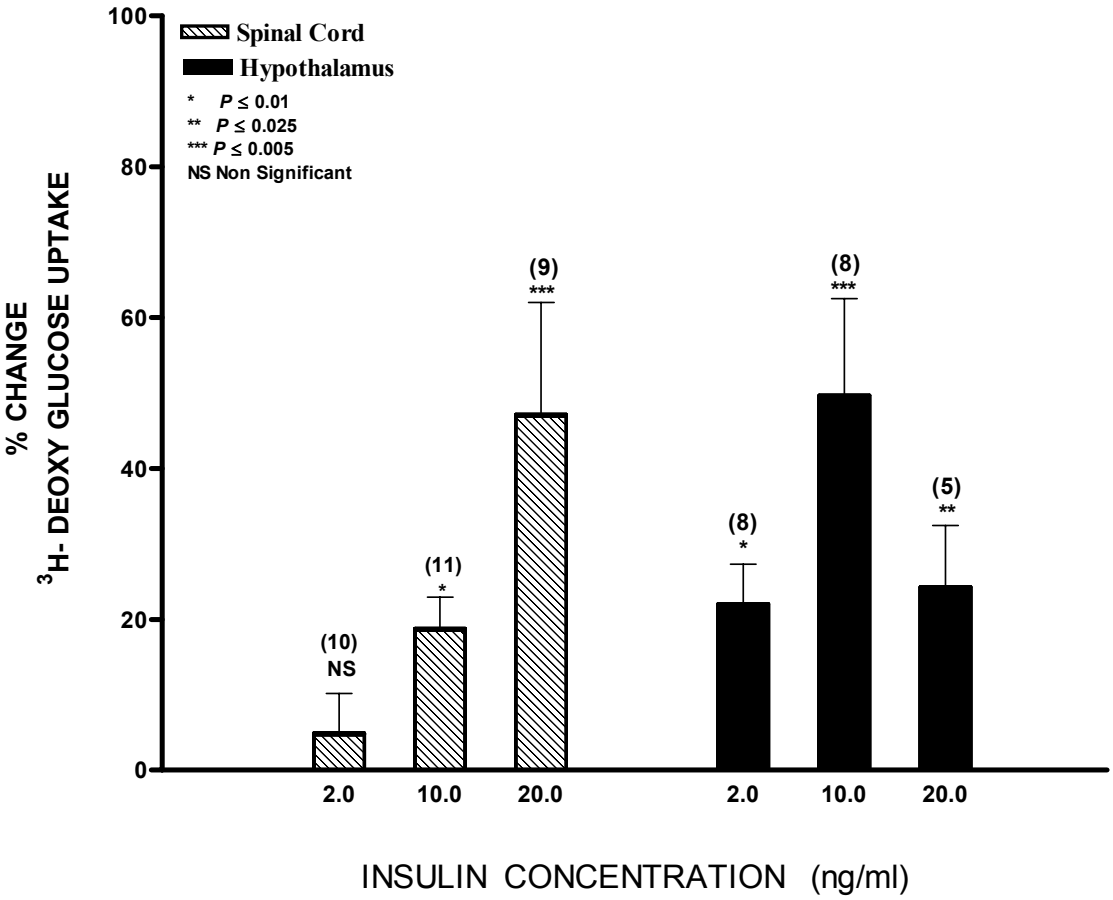

Values are Mean SEM for the percentage change in 2-DG uptake in Insulin treated samples compared to control with krebs ringer buffer solution.
The number of experiments indicated in parentheses.

In slices from cervical spinal cord, insulin 2 ng/ml has no significant effect on ^{3}H-deoxy-glucose uptake, while higher concentrations of insulin 10 ng/ml and 20 ng/ml has increased ^{3}H-deoxy-glucose uptake by 19 % ($P \leq 0.01$) and 48 % ($P \leq 0.005$) respectively.

The effect of insulin on ^{3}H-deoxy-glucose uptake into cervical spinal cord slices was dose dependent between 10 and 20 ng/ml, while in brain slices from the hypothalamus insulin effect was dose dependent in concentrations from 2 to 10 ng/ml. Figure 1.

Insulin was not effective in producing any effect on brain slices from the cerebral cortex, medulla-oblongata or cerebellum Figure 2.

Figure 2: Effect of Insulin on ^{3}H-Deoxy Glucose up take into Cerebellum, Medulla Oblengata and Cortical Slices

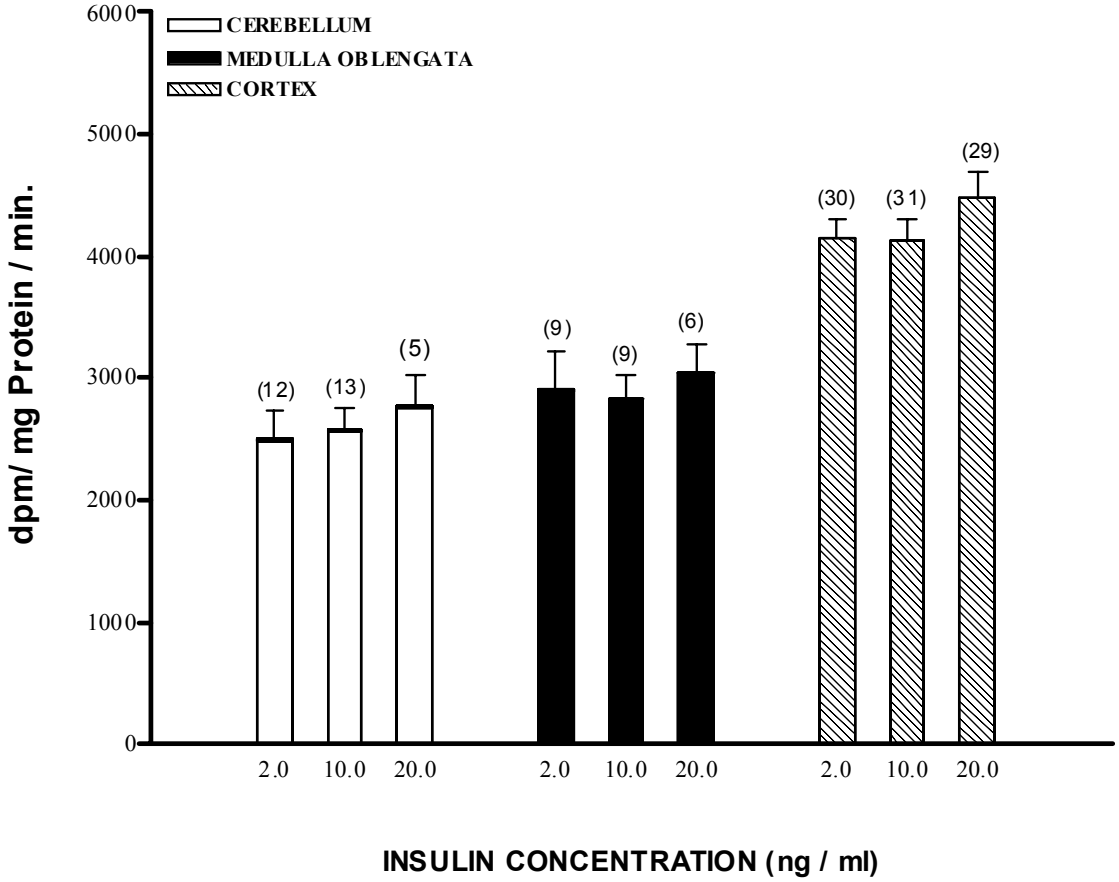

Our recent in-vitro results using both synaptosomal preparations which contains nerve endings and synapses, and brain slices which contains nerve cells and glial cells, proves that most of the areas in the brain are insulin independent, including the cerebral cortex, cerebellum, thalamus, hippocampus, pons and medulla-oblongata. Similar results were reported earlier by (Rafaelson, 1961; Betz et al, 1973; Philips and Coxon, 1976; Goodner and Berrie,1977).

From our results it seems that the hypothalamus and cervical spinal cord are insulin dependent, since insulin was effective in increasing significantly ^{3}H-deoxy-glucose uptake into brain slices and synaptosomal preparations in both tissues. Previous results were contradictory, it have shown a dose dependent stimulation of 2-DG uptake into C6 glioma cultures, which have the properties of glial cells (Wei and Yeh, 1990) and from the retina (Vilchis and Salceda, 1966), and increased glucose uptake in isolated rat spinal cord (Rafaelson, 1960), Insulin was found to bind to specific receptors and stimulates 2-deoxy-glucose uptake in cultured glial cells from rat brain (Clarke et al 1984). The presence of insulin sensitive glucose carrier in ventricular ependymal cells was reported by (Mackawa et al 2000) and their possible role as glucose sensing cells was found in ependymal cell culture model (Prothmann et al 2005), and the effect of insulin in increasing deoxy-glucose uptake into ependymal cells was much less than the insulin like growth factor (IGF-1) (Verleysdonk et al 2004). On the other hand insulin gave no effects on DG uptake in hypothalamus (Goodner and Berrie, 1977). and no effect of insulin on 2-DG uptake into astroglial cultures from rat brain (Hara et al 1989; Hamai et al 1999). In vivo experiments failed to show any effect of insulin on 2-DG uptake (Goodner et al, 1980). Sloviter and Yamada in 1970 concluded that insulin either don't act directly on the brain or that its action is very small in comparison with other tissue. The only published results reported on synaptosomal

uptake of 2-DG showed high affinity uptake of 2-DG (Diamond and Fishman, 1973). This transport of 2-DG was reported to be facilitated process rather than diffusion (Bachelard, 1971).

The recent results showing a significant effect of insulin on ^{3}H-deoxy-glucose uptake into brain slices and synaptosomal preparations from the hypothalamus and cervical spinal cord, together with other results which has demonstrated chemically specific binding sites for insulin in the brain (Kahn, 1976; Ginsperg, 1977) and previous results published in our lab. by (Nahas and Abdul-Ghani, 1989) showing ordered distribution of glycogen across various areas of the brain, and the reduced glycogen concentration in the hypothalamus of diabetic rats which was corrected by insulin treatment indicating that glycogen metabolism in this area is insulin dependent. Whether the effect of insulin on the brain tissue is direct or due to hypoglycemia or due to its effect as a growth factor or as a metabolic regulator (Raizada et al, 1980; Sauter et al. 1983) is not clear yet and needs further investigations to illustrate the exact mechanism of action.

In Conclusion:

Our results show that cervical spinal cord and hypothalamus are insulin dependent, while brain cortex, thalamus, hippocampus, pons and medulla oblongata are insulin independent. In cervical spinal cord slices the uptake of ^{3}H-deoxy glucose is dose dependent. The differences in ^{3}H-DG uptake between brain slices and synaptosomal preparations shows that the effect is more related to glial cells. The Mechanism of action is not clear yet, and needs further investigations.

References

[1] **Bachelard, H. S. (1971)** Specifity and kinetic properties of monosaccharide uptake into guinea pig cerebral cortex in vitro. ***J. Neurochem., 18 (2) 213 – 222.***

[2] **Betz A.L., Gilboe, D.D., Yudilevich, D.L., Drewes, L.R. (1973)** Kinetics of unidirectional glucose transport into the isolated dog brain. ***Am. J. Physiol., 225(3):586–592.***

[3] **Buschiazzo, P. M., E. B. Terrell and D. M. Regen. (1970).** Sugar transport across the Blood-Brain barrier. ***Am. J. physiol. 219: 1505 – 1513.***

[4] **Crone, C. (1965)** Facilitated transfer of glucose from blood into brain tissue. ***J. physiol 181: 103-118.***

[5] **Clarke, D.W., Boyd, F.T. Jr, Kappy, M.S. and Raizada, M.K. (1984)** Insulin binds to specific receptors and stimulates 2-deoxyglucose uptake in cultured glial cells from rat brain. ***Brain. J. Biol. Chem. 259; 11672-11675.***

[6] **Daniel, P.M., Love, E.R., Pratt, O.E. (1975)** Insulin and the way the brain handles glucose. ***J. Neurochem.,*** *25(4):471–476.*

[7] **Diamond, I. and Fishman, R. A. (1973)** High-affinity transport and phosphorylation of 2-deoxy-glucose in synaptosomes. ***Journal of Neurochemistry. 20 (6): 1953.***

[8] **Ginsberg, B.H. (1977)** The insulin receptor: properties and regulation. In *Biochemical. Actions of hormones.* G. Litwack, editor. Academic Press, Inc., New York. 4: 313-349.

[9] **Goodner, C.J., Freinkel, N. (1960)** Carbohydrate metabolism in pregnancy: the turnover of 1-131-insulin in the pregnant rat. ***Endocrinology. 67:862–872.***

[10] **Goodner, C.J. and Berrie, M.A. (1977)** The failure of rat hypothalamic tissues to take up labeled insulin *in vivo* and to respond to insulin *in vitro.* ***Endocrinology 101: 605-612.***

[11] **Goodner, C.T., Hom, F.C. and Berrie, M.A. (1980).** Investigation of the effect of insulin upon regional brain glucose metabolism in the rat in vivo. ***Endocrinology 107: 1827-1832.***

[12] **Hamai, M., Minokoshi, Y. and Shimazu, T. (1999)** L-Glutamate and insulin enhance glycogen synthesis in cultured astrocytes from the rat brain through different intracellular mechanisms. ***J. Neurochem. 73: 400 – 407.***

[13] **Hara, M., Matsuda. Y., Hirai, K. Okumura, N. and Nakagawa, H. (1989)** Characteristics of glucose transport in neuronal cells and astrocytes from rat brain in primary culture. ***J. Neurochem. 52 902 – 908.***

[14] **Hughes, P.D., Foley, P., Bradford, H.F., Chatei, M., Khandanian, N., Bloom, S.R. and Wu, J.Y. (1993).** The differential release of amino acids and neuropeptides from purified subpopulations of mammalian GABAergic and cholinergic cerebrocortical synaptosomes. ***Neurochem. Research ., 18, 393 – 400.***

[15] **Kahn, C.R. (1976).** Membrane receptors for hormones and neurotransmitters ***J Cell Biol. 70(2): 261–286***

[16] **Mackawa, F., Toyoda, Y., Torii, N., Miwa, I., Thompson, R.C., Foster, D.L., Tsukahara, S., Tsukamura, H. and Maeda, K. (2000)** Localization of glucokinase-like immunoreactivity in the rat lower brain stem: For possible location of brain glucose sensing mechanisms. ***Endocrinology 141: 375 – 384.***

[17] **Nahas, N. and Abdul-Ghani, A-S. (1989)** Species-directed variation and non-uniform distribution of glycogen in mammalian brains during starvation, diabetes and anesthesia. ***Neurochemistry International. 14, 19-24.***

[18] **Nelson, S.R., Schulz, D.W., Passonneau, J.V., Lowry, O.H. (1968)** Control of glycogen levels in brain. ***J Neurochem,*** 15**(11):1271–1279.**

[19] **Phillips, M.E., , R.V. (1976)** Effect of insulin and phenobarbital on uptake of 2-deoxyglucose by brain slices and hemidiaphragms. ***J Neurochem. 27(2):643–645.***

[20] **Prothmann, C., Wellard, J., Berger, J., Hamprecht, B. and Verleysdonk, S. (2001)** Primary cultures as a model for studying ependymal functions: Glycogen metabolism in ependymal cells. ***Brain Research 920: 74 – 83.***

[21] **Rafaelson, M. E. (1960)** Studies on the metabolism of virus-infected tissues. III. The effect of influenza virus on ribonucleic acid fractions of chick chorio-allantoic membranes. ***Archives of Biochemistry and Biophysics, 90, 68 – 72.***

[22] **Rafaelson O. J. (1961)** Action of insulin on glucose uptake of rat brain slices and isolated rat cerebellum. ***J Neurochem***., **7:45–51.**

[23] **Raizada, M.K., Yang, W.Y. and Fellows, R.E. (1980)** Binding of [125] insulin to specific receptors and stimulation of nucleotide incorporation in cells cultured from rat brain. ***Brain Research, 200: 389 – 400.***

[24] **Roth, J. (1973)** Peptide hormone binding to receptors: a review of direct studies In-vitro. ***Metabolism (Clin. Exp.), 22:1059-1073.***

[25] **Santer, U.V., Glick, M.C., van Halbeek, H. and Vliegenthart, J.F. (1983)** Characterization of the neutral glycopeptides containing the structure alpha-L-fucopyranosyl-(1 leads to 3)-2-acetamido-2-deoxy-D-glucose from human neuroblastoma cells. ***Carbohydrate Res. 120, 197-213.***

[26] **Sloviter, H.A. and Yamada, H. (1971)** Absence of direct action of insulin on metabolism of the isolated perfused rat brain. ***J. Neurochem. 18, 1269-1274.***

[27] **Watanabe, J. and Passonneau, J.V. (1973)** Factors affecting the turnover of cerebral glycogen and limit dextrin *in vivo*; ***J. Neurochem. 20 1543–1554.***

[28] **Wei, J.W. and Yeh, S.R. (1991)** Effects of insulin on glucose uptake in cultured cells from the central nervous system of rodent. ***Int J Biochem. 23 (9):851–856.***

[29] **Verleysdonk, S., Hirschner, W., Wellard, J., Rapp, M., Garcia, M.A., Nualart, F. and Hamprecht (2004)** Regulation by insulin and insulin-like growth factor of 2- deoxy-glucose uptake in primary ependymal cell cultures. ***Neurochemical Research 29 (1) 123 – 134.***

[30] **Vilchis, C. and Salceda, R. (1996)** Characterization of [2-3H]deoxy-D-glucose uptake in retina and retinal pigment epithelium of normal and diabetic rats. ***Neurochem Int., 28(2):213-9.***

European Journal of Scientific Research
ISSN 1450-216X Vol.18 No.3 (2007), pp.541-550

http://www.eurojournals.com/ejsr.htm

The Effect of L-2-Amino-4-Phosphonobutyrate, A Presynaptic Glutamate Receptor Aganist on Motor Disorders Induced by 6-Hydroxy-Dopamine

Munir Qazzaz
Biology and Biochemistry Department, Birzeit University, West-Bank, Palestine
E-mail: mqazzaz@birzeit.edu
Fax: + 972-2-2982086

Rateb M. Husein
Biology and Biochemistry Department, Birzeit University
West-Bank, Palestine

Munther Metani
Biology and Biochemistry Department, Birzeit University
West-Bank, Palestine

Abdul-Salam
Physiology Department, Faculty of Medicine, Al-Quds University
Jerusalem, Palestine

Abdul-Ghani
Physiology Department, Faculty of Medicine, Al-Quds University
Jerusalem, Palestine

Abstract

The effect of L-2-amino-4-phosphonobutyrate (L-AP4) A Glutamate metabotropic agonist sub-type III was tested in-vivo on rats with motor disorders induced by intra-cerebral micro-injection of 6-OH-DA (16 µ grams in 2 µL buffer phosphate)

Male Sprague Dawley rats intra-cerebrally micro-injected with 6-OH-DA (16 µ grams in 2 µ l buffer phosphate) into the nigrostriatal bundle, coordinates: (AP = -1.8 mm; L = 1.8 mm; V= - 6.1 mm) has produced a Parkinsonian animals with motor disorders characterized by a significant decrease of 44% in locomotion, 36% in eating behaviour and 55% in positive forward pushing reflex, and significant increase in rotational movements, rearing and head bobbing. The changes in locomotion were increased gradually reaching its maximum point after 4 weeks.

Sham control animals which were exposed to the same surgical procedure and cerebrally micro-injected with the same volume of buffer phosphate have shown no significant changes in locomotion rotations or rearing.

Pre-treatment with the glutamate pre-synaptic agonist L-AP4 (40 n gram / 2µl BP) which was focally micro-injected into the nigrostriatal bundle, coordinates: (AP = -1.8 mm; L = 1.8 mm; V = -6.1 mm) for 15 min before injection of 6-OH-DA (16 µ grams in 2 µL BPS) has reduced significantly the motor disorders. Locomotion was reversed to normal

values, from 8.5 ± 0.51 (138) to 11.54 ± 0.78 (63) ($P \leq 0.05$), Percentage change in body weight was reversed from 2% to 39% and positive response to forward pushing was changed from 21% to 78%. On the other side rotations, head bobbing and rearing were reduced significantly by 29% ($P \leq 0.02$), 38 % ($P \leq 0.001$) and 65 % ($P \leq 0.01$) respectively.

These results suggests that agonists of glutamate metabotropic receptors which decrease glutamate release by decreasing Ca^{++} uptake into pre-synaptic membranes in glutamatergic neurons in basal ganglia circuits, could be used in the prevention of the development of Parkinson's disease.

Keywords: Parkinson; 6-OH-DA; L-AP4, Glutamate, Metabotropic Receptors, Rotations, Rearing, Locomotion.

Introduction

The subcortical nuclei of basal ganglia are of great importance in initiation of the normal body motor activities. However, the degeneration of nigrostriatal dopaminergic neurons in the substantia nigra pars compacta was found to be the main cause for Parkinson's disease (PD), a chronic motor disorder (Phillips and Brown, 1999; Phillips et al., 2006; and Truong et al., 2006).

Degeneration of dopaminergic neurons by the neurotoxin 6-Hydroxy Dopamine (6-OH-DA) within the nigrostriatal pathway has widely been accepted as a good model of PD (Wichmann et al., 2002; Osborne, et al., 2002; Willis and Kennedy, 2004; Vernon, et al., 2005; Troung, et al., 2006; Chaturvedi, et al., 2006; Phillips et al., 2006).

The key role of glutamate in basic mechanisms generating epilepsy is well established, review article (Bradford 1995). Thus limbic seizure can be kindled by repeated micro-injection of glutamate or aspartate (Mori and Wada, 1987, Mori et al, 1989; and Croucher and Bradford, 1989) or by the injection of the selective glutamate receptor agonist N-methyl –D-aspartate (NMDA) (Vezzani et al 1988; Croucher et al 1995; Abdul-Ghani et al 1996).

Antagonists of post-synaptic NMDA receptors show clear anti-convulsant and anti-epileptogenic activity (Coutinho-Netto et al; Croucher et al 1982; 1988; Peterson et al 1983; 1984; Meldrum et al 1983; Patel et al 1991; Chapman et al 1990; Kaura et al 1993; Attwell et al 1995). Agonists of pre-synaptic glutamate receptors are effective anti-epileptogenic agents. (1S,3S)-1-aminocyclo-pentane-1,3-dicarboxylic acid (1S,3S)-ACPD and 2R,4R-4-aminopyrrolidine-2,4-dicarboxylate (2R,4R-APDC) the potent agonists at group II receptors has increased generalized seizure thresholds in fully kindled animals, and in reversibly inhibiting kindled epileptogenesis (Attwell et al 1995; Attwell et al 1998a). L-2-amino-4-phosphonobutyrate (L-AP4) the selective agonist of group III receptors, showed strong anti-epileptic effects on cobalt induced epilepsy (Coutinho-Netto et al 1981) and antiepileptogenic and anti-seizure activity against amygdale-kindled seizures (Abdul-Ghani et al 1997a)

Excitatory amino acids play an important role, not only during epilepsy as shown before but during other neurodegenerative diseases (Wilkinski and Acosta 1995). Excitation of sub-thalamic nucleus neurons in vitro was achieved by activation of a group I metabotropic glutamate receptors (S,R)-dihydroxy-phenylglycine (DHPG), and was blocked by the receptor antagonist (+)-alpha-methyl-4-carboxyphenylglycine (MCPG). No effects were obtained with the selective agonists of group II and group III metabotropic receptors like L-AP4 and DCG-IV (Abbott et al 1997). Intra-sub-thalamic injection of (1S,3R)-ACPD produced marked contra-lateral rotation, similar to that seen after intra-striatal injection, of (1S,3S)-ACPD , suggesting correlation between metabotropic glutamate receptors and the treatment of Parkinson's disease (Sacaan et al, 1991: 1992; Kaatz and Albin, 1995 and Vernon et al., 2005). In vitro study, using electrophysiological technique, it was found that the degeneration of

dopaminergic neurons within the substantia nigra results in excessive activity of glutamatergic neurons of the subthalamic nucleus (Meshul, et al., 1999)

In these experiments we have tested the effect of pretreatment with glutamate metabotrobic receptor agonists on Parkinsonian animals induced by intra-cerebral microinjection of 6-OH-DA as described by Willis and Kennedy 2004.

Materials and Methods

Drugs and Chemicals

The drugs 6-Hydroxy-Dopamine hydrobromide (6-OH-DA) and L-2-amino-4-phosphonobutyrate (L-AP4) were obtained from Sigma chemical Co. drugs were dissolved in Phosphate buffer saline solution (PBS).

Animals and Surgery

Sprague-Dawley rats weighing 170 to 250 g were used in all experiments. The animals were anaesthetized with ether and continuous supply of oxygen (O_2/CO_2) (95/5 %) and the animals were kept in light anaesthesia characterized with loss of movement and pain sensation and with positive corneal reflex to avoid any change in autonomic functions such as: heart rate, blood pressure or respiratory rate. Rats were placed on stereotaxic table. The scalp was then incised to expose the parietal bone for drilling. A special stainless-steel cannulae was implanted into the right basal ganglia using stereotaxic apparatus, coordinates from bregma (AP= -1.8 mm; L= ± 1.8 mm; V = - 6.1 mm) as described by Willis and Armstrong, 1999. After insertion of the cannulae it was fixed to the skull with cyanoacrylate cement and zinc powder with the help of stainless steel screws. The animals were kept individually in large plastic cages fitted with Perspex lids, and the animals were left for 24 hours recovery with free access to food and water.

The drugs were dissolved in phosphate buffer solution (PBS, pH = 7.4) injected through the implanted cannulae using a 10 µl Hamilton syringe. 2 µl of the drugs or BPS were injected in a rate of 1 µl per minute and the syringe was left for 1 min before removal to insure good diffusion. 6-OH-DA was dissolved with buffer phosphate in a concentration of 8 µg/µl with 0.1% of ascorbic acid to prevent rapid oxidation of the drug. L-AP4 was dissolved with buffer phosphate prior to injection. Fresh solutions of drugs were prepared immediately prior to injection with stock solutions kept refrigerated or on ice until used. All solutions were kept shielded from light and then discarded by the end of each experiment.

The Measurement of Motor Activities

Rats were left to move freely over squared floor. Locomotion (spontaneous movement) was measured daily by counting the number of squares crossed and calculated as cm/second. The number of rearing, rotations and head bobbing were measured daily by counting the events within 10 minutes, then averages were calculated per one minute. Body weight which indicates changes in eating behaviour was measured weekly and calculated as percentage change per month. Forward pushing reflex was calculated by measuring the number and percentage of rats which responded positively for hitting the back of the rat.

Statistical Treatment of Data

Values were expressed as mean ± standard error of the mean (SEM) for the number of experiments indicated in parentheses, and results were compared by unpaired two-tailed student *t*-test where appropriate and differences were considered statistically significant at $P < 0.05$. All statistical analysis was performed using Microsoft Excel and Graph Pad Prism v3.03.

Results

The Action of 6-Hhdroxy-Dopamine:

Table 1 shows that in control animals without any surgical procedure or treatment, the average of spontaneous movement of rats was 15.71 ± 1.21 (13) cm/sec. The rats body weight was increased during one month by 42%, and forward pushing reflex was positive in 100% of the cases. During the same period rats showed no significant rotation, rearing or head bobbing.

Table 1: Effect Of Intra-Cerebral Microinjection Of 6-Oh-Dopamine On Rats Motor Activity

	LOCOMOTION (cm / sec)	ROTATION (No /min)	REARING (No /min)	HEAD BOBBING (No / min)	% CHANGE BW	FORWARD PUSHING % (Positive Response)
Control	15.71±1.21(7)	0.29±0.18(7)	0.14±0.14(7)	1.00±0.38(7)	**42 %**	8 / 8 **(100 %)**
Sham Control (2µL BPS)	15.15±0.61(13)	0.31±0.24(13)	0.15±0.10(13)	0.23±0.12(13)	**38 %**	12/13 **(92 %)**
6-OH-DA (16µg/2µL)	8.50±0.51(138) *	2.67±0.15(138) **	1.12±0.12(147) *	3.20±0.14(147) **	**2 %**	41 / 201 **(21 %)**

Sham control: The animals were dissected and implanted with special cannulae over the Nigrostriatal bundle, coordinates (AP = -1.8; L = 1.8; V = - 6.1) and injected intra-cerebrally with 2 µl buffer phosphate solution (BPS). Treated animals were injected intra-cerebrally with 2 µl 6-OH-DA.
Percentage change in body weight (BW) was recorded during 1 month treatment.
Values are Mean ± SEM for the number of experiments indicated in brackets.
* $P \leq 0.01$: ** $P \leq 0.001$ compared to control animals .

Sham control animals which passed the same surgical treatment and injected with 2µL phosphate buffer saline has shown no significant change in any of the motor activities measured.

Intra-cerebral microinjection of rats with 6-OH-DA (16µg/2µL) into the nigrostriatal bundle has induced significant changes in most motor activities. Locomotion was significantly reduced from 15.15 ± 0.61 (13) cm / sec. to 8.50 ± 0.51 (138) cm/sec ($P \leq 0.01$). Percentage change in body weight was reduced from 38% to 2%. Similarly, positive forward pushing was reduced from 92% to 21%.

On the other hand, animals have demonstrated clear motor activities disorders. The measured motor disorders are: Rotation 2.67 ± 0.15 (138) per minute ($P \leq 0.001$), rearing 1.12 ± 0.12 (147) per minute ($P \leq 0.01$) and head bobbing 3.20 ± 0.14 (147) per minute ($P \leq 0.001$).

The Action of L-AP4

When animals were pre-treated with LAP4 (40 ng/2µl) 15 minutes before the microinjection of 6-OH-DA into the nigrostriatal bundle, it has significantly reduced the effects of 6-OH-DA. Figure 1 shows that locomotion was significantly increased from 8.50 ± 0.51 (138) to 11.54 ± 0.78 (63) cm/sec ($P \leq 0.05$). Percentage change in body weight was reversed to 39% and the positive forward pushing was increased from 21% to 78% as seen in table 2.

Table 2: Effect Of Pre-Treatment With L-2-Amino-4-Phosphono-Butyrate (Lap 4) On Percentage Change Of Body Weight And Positive Forward Pushing

PRE-TREATMENT	BPS (2µL)	BPS (2µL)	LAP4 (40 ng/2µl)
Treatment	BPS (2µL)	6-OH-DA (16µg/2µL)	6-OH-DA (16µg/2µL)
Positive Forward Pushing REFLEX	12 / 13 (92 %)	41 / 201 (21 %)	28/36 (78 %)
% Change Body Weight	↑ 38 %	↑ 2 %	↑ 39 %

LAP4 (40ng/2µl) was injected intra-cerebrally into the rats nigrostriatal bundle coordinates: (AP = - 1.8; L = 1.8; V = - 6.1). LAP4 was injected 15 min. before injection of 6-hydroxy dopamine (16 µg / 2µl BPS). % change in body weight was measured during 1 month treatment.

Figure 1: Effect of Pretreatment with LAP4 on the Development of Parkins onian animals

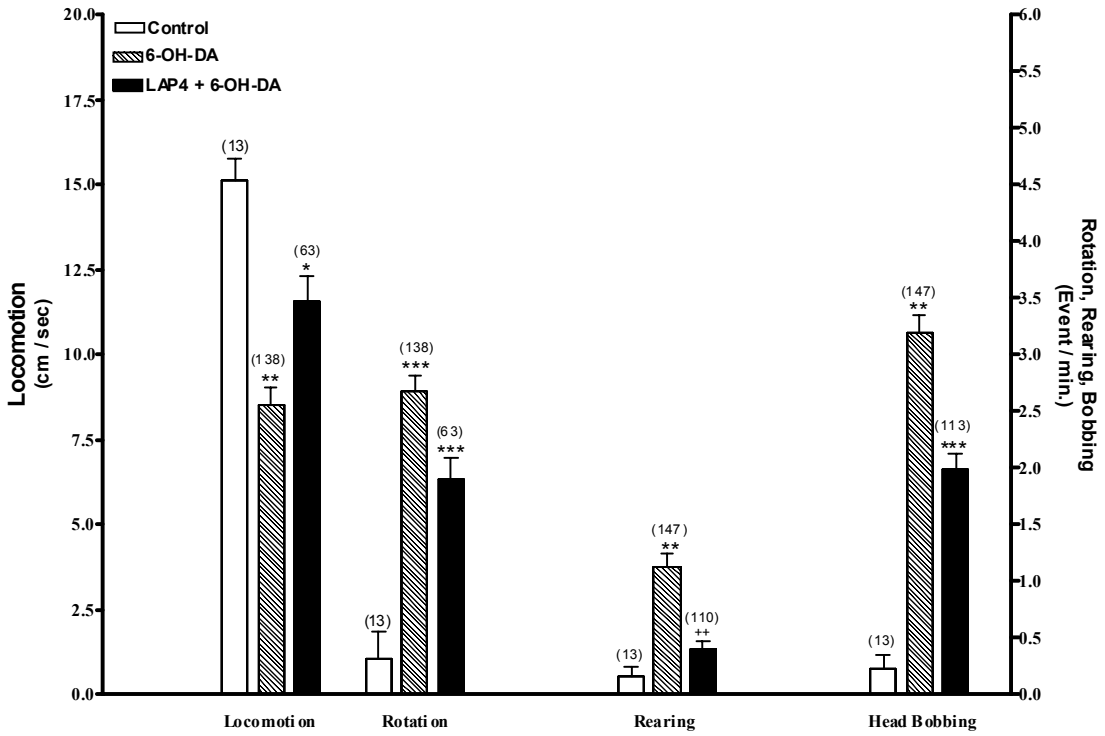

LAP4 (40ng/2µl) was injected intra-cerebrally into the rats nigrostriatal bundle coordinates: (AP = - 1.8; L = 1.8; V = - 6.1). LAP4 was injected 15 min. before injection of 6-hydroxy dopamine (16 µg / 2µl BPS).
Values are Mean ± SEM for the number of experiments indicated in brackets.
* $P \leq 0.05$: ** $P \leq 0.01$: *** $P \leq 0.001$ Compared to control treated animals
$^{+}$ $P \leq 0.05$; $^{++}$ $P \leq 0.01$ $^{+++}$ $P \leq 0.001$ Compared to 6-OH-DA treated animals

On the other hand, the developed motor disorders; rotation was decreased from 2.67 ± 0.15 (138) to 1.89 ± 0.19 (63) rotation / minute ($P \leq 0.05$); rearing was reduced from 1.12 ± 0.12 (147) to 0.39 ± 0.08 (110) rearing/minute ($P \leq 0.01$) and the head bobbing was reversed from 3.20 ± 0.14 (147) to 1.98 ± 0.15 (113) bobbing / minute ($P \leq 0.001$) (see figure 1).

Figure 2 demonstrates the progressive effect of pre-treatment of L-AP4 on rat spontaneous movement disorders induced by the intra-cerebral micro-injection of 6-OH-DA into the nigrostriatal bundle. 6-OH-DA was found to reduce locomotion gradually and significantly. During the first week, locomotion was reduced from 15.15 ± 0.61 (13) cm/sec to 10.61 ± 0.76 (78) cm/sec. a 30% reduction ($P \leq 0.01$). and maximum reduction of 76% ($P \leq 0.0005$) after 4 weeks, from 15.15 ± 0.61(13) to 3.57 ± 0.68 (14) cm/sec.

Figure 2: Effect of Pretreatment with LAP4 on Locomotion Disorders Induced by 6-OH-Dopamine

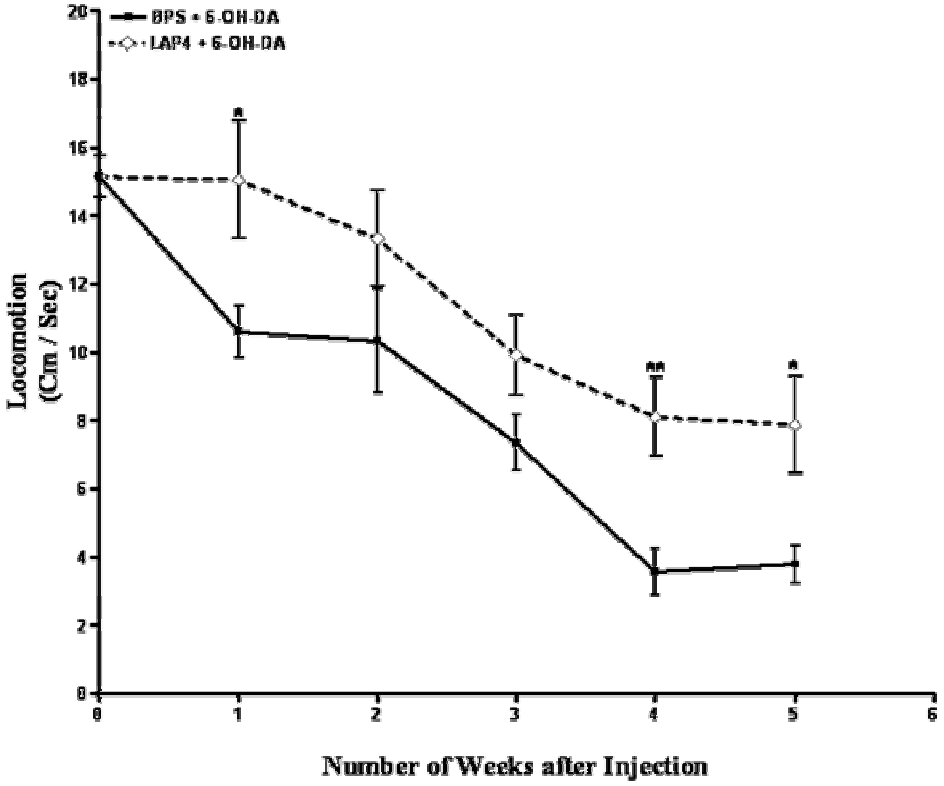

LAP4 (40ng/2µl) was injected intra-cerebrally into the rats nigrostriatal bundle coordinates (AP = - 1.8; L = 1.8; V = - 6.1). LAP4 was injected 15 min. before injection of 6-OH-DA (16 µg / 2µl BPS).
Values are Mean ± SEM for the number of experiments indicated in brackets. And compared to sham control values of locomotion 15.15 ± 1.61 (13) cm/sec.
* $P \leq 0.05$; ** $P \leq 0.02$

LAP4 was found to reduce significantly the effect of 6-OH-dopamine on locomotion. The maximum effect on locomotion was reduced from 76% to 48% and was achieved after 4 to 5 weeks. And the first significant reduction was observed after 3 weeks.

Discussion

Our results show that the microinjection of 6-OH-DA into the nigrostriatal bundle has developed motor activity disorders in rats characterized by a reduction of 44% in locomotion (spontaneous movement of rats) and a reduction in percentage change in body weight of 95%. Furthermore, it reduced the positive forward pushing by 77%. On the other hand, it has developed significantly motor disorders such as head bobbing, rotation and rearing.

Similar results were found previously. The microinjection of 6-OH-DA into the nigrostriatal bundle (coordinates: AP = - 1.8; L = ±1.8; V = - 6.1) had produced a classical model for PD (Willis and Kennedy, 2004), partial lesion in the nigrostraital tract was produced by microinjection of 6-OH-DA into substantia nigra pars compacta (Vernon et al., 2005) and striatum (Kirik, et al., 1989).

Different glutamate agonists were found to have a protective function in the neurodegenerative diseases and recent studies have focused on the role of metabotropic glutamate receptors in the nigrostriatal pathways. Murray et al. (2002) found that the intracerebroventricular administration of group II metabotropic glutamate receptor LY379268 produced a dose dependent increase in locomotion after the production of the nigrostriatal tract lesion by 6-OH-DA. 6-OH-Da produced a significant loss of tyrosine hydroxylase-immmunopositive cells in substantia nigra pars compacta and

striatal dopamine. however, the group III metabotropic glutamate receptor agonist LAP4 attenuated these losses (Vernon, et al., 2005).

LAP4 is known as a glutamate pre-synaptic agonist, which inhibits Ca++ uptake to the pre-synaptic membrane (Vázquez et al., 1995) and inhibits the release of glutamate (Hans et al., 2004 and Vernon et al., 2005). Glutamate pre-synaptic receptor has an auto-regulatory role in the release of glutamate. It has been shown that the activation of the pre-synaptic receptors in the rat spinal cord on the monosynaptic excitation of neonatal rat motoneurones by the agonists LAP4 depresses the glutamate release (Cao, et al., 1996 and Jane et al., 1994).

Our results show that the intra-cerebral microinjection of 6-OH-DA to basal ganglia of rats causes motor activities disorder such as reduction in locomotion, rotations, animal rearing and head bobbing. Similar results were reported by Troung, et al., 2006; Chaturvedi, et al., 2006; Phillips et al., 2006; Vernon, et al., 2005; Willis and Kennedy, 2004 and Osborne, et al., 2002. Furthermore, the intra-cerebral microinjection of 6-OH-DA was found to cause eating behaviour disorder and significantly reduce the positive forward pushing.

When LAP4 was intra-cerebrally microinjected 15 minutes before the intra-cerebral microinjection of 6-OH-DA into the same site, it was found to reverse the actions of 6-OH-DA on the body motor activities.

Acknowledgement

This work was supported by a grant from the Academy for Educational Development (AED).

References

[1] Abbott A, Wigmore M. A. and Lacey M. G. (1997). Excitation of rat sub-thalamic nucleus neurons in vitro by activation of a group I metabotropic glutamate receptor ***Brain Research 766 (1-2) 162-167.***

[2] Abdul-Ghani, A-S., Attwell, P. J. E. and Bradford, H. F. (1996). The antiepileptic effect of 3-aminopropylarsonate on electrically kindled amygdala. ***Brain Research, 742, 305-312.***

[3] Abdul-Ghani, A-S., Attwell, P. J. E. Kent, N. S., Bradford, H. F., Croucher, M. J. and Jane, D. E. (1997a). Anti-epileptogenic and anti-convulsant activity of L-2-amino- 4-phosphonobutyrate, a presynaptic glutamate receptor agonist. ***Brain Research, 755, 202-212.***

[4] Attwell, P. J. E., Kaura, S., Sigala, G., Bradford, H. F., Croucher, M. J., Jane, D. E. and Watkins, J. C. (1995). Blockade of both epileptogenesis and glutamate release by (1S,3S)-ACPD, a presynaptic glutamate receptor agonist. ***Brain Research, 698, 155-162.***

[5] Attwell, P. J. E., Koumentaki, A., Abdul-Ghani, A-S., Croucher, M. J. and Bradford, H. F. (1998a). Specific group II metabotropic glutamate receptor activation inhibits the development of kindled epilepsy in rats. ***Brain Research, 787(2), 286-291.***

[6] Bradford, H. F. (1995). Glutamate, GABA and Epilepsy. ***Progress in Neurobiology. 47, 477-511.***

[7] Cao, C.Q., Tse, H.W., Jane, D.E., Evans, R.H. and Headley, P.M. (1996) Antagonism of mGlu receptors and potentiation of EPSCs at rat spinal motoneurones in vitro. ***Neurophamacology, 36: 313-318.***

[8] Chapman, A. G., Graham, J. and Meldrum, B. S. (1990). Potent oral anticonvulsant action of CPP and CPP-ene in DBA/2 mice. European ***Journal Pharmacology, 178(1), 97-99.***

[9] Chaturvedi, R.K., Shukla, S., Seth, K., Chauhan, S., Sinha, C., Shukla, Y. and Agrawal, A.K. (2006) Neuroprotective and neurorescue effect of black tea extract in 6-hydroxydopamine-lesioned rat model of Parkinson's disease. ***Neurobiology of Disease, 22: 421 – 434.***

[10] Coutinho-Netto, J., Abdul-Ghani, A-S., Collins, J. F. and Bradford H. F (1981). Is glutamate a trigger factor in epileptic hyperactivity ***? Epilepsia, 22, 289-296.***

[11] Croucher, M. J. and Bradford, H. F. (1989). Kindling of full limbic seizures by repeated micro-injections of excitatory amino acids into the rat amygdala.. ***Brain Research, 501, 58-65.***

[12] Croucher, M. J., Bradford, H. F., Sunter, D. C. and Watkins, J. C. (1988). Inhibition of the development of electrical kindling of the prepyriform cortex by daily focal injections of excitatory amino acids antagonists. ***European Journal Pharmacology, 152, 29-38.***

[13] Croucher, M. J., Collins, J. F. and Meldrum, B. S., (1982). Anticonvulsant action of excitatory amino acid antagonists. ***Science, 216, 899-901.***

[14] Croucher, M. J., Cotterell, K. L. and Bradford, H. F.(1995). Amygdaloid kindling by repeated focal N-methyl-D-aspartate administration: comparison with electrical kindling, ***European Journal of Pharmacology, 286, 265-271.***

[15] Han, J.S., Bird, G.C. and Neugebauer, V (2004) Enhanced group III mGluR-mediated inhibition of pain-related synaptic plasticity in the amygdale. ***Neuropharmacology, 46: 918-926***

[16] Jane, D. E., Jones, P.L.S., Pook, P.C.K., Tse, H.W. and Watkins, J.C. (1994) Actions of two new antagonists showing selectivity for different sub-types of metabotropic glutamate receptor in the neonatal rat spinal cord. ***Br J. Pharmacol. 112: 809-816.***

[17] Kaatz K. W. and Albin R. L. (1995). Intra-striatal and intra-subthalamic stimulation of metabotropic glutamate receptors. ***Neuroscience 66 (1) 55-65.***

[18] Kaura, S., Bradford, H. F., Young, A. M. J., Croucher, M. J. and Hughes, P. D.(1994). Effects of amygdaloid kindling on the content and release of amino acids from the amygdaloid complex: In vitro and in vivo studies. ***J. Neurochem, 65, 1240-1249***

[19] Kirik, D., Rosenblad, C. and Björklund, A. (1998) Characterization of Behavioral and Neurodegenerative Changes Following Partial Lesions of the Nigrostriatal Dopamine System Induced by Intrastriatal 6-Hydroxydopamine in the Rat. ***Exp.Neurol., 152: 259-277***

[20] Meldrum, B. S., Croucher, M. J., Badman, G. and Collins, J. F. (1983). Antiepileptic action of excitatory amino acid antagonists in the photosensitive baboon, Papio Papio. ***Neuroscience Letters, 39, 101-104.***

[21] Meshul, C.K., Emre N., Nakamura, C.M., Allen, C., Donohue, M.K. and Buckman, J.F. (1999) Time –dependent changes in striatal glutamate synapses following a 6-hydroxydopamine lesion. ***Neuroscience, 88: 1-16.***

[22] Mori N. and Wada J. A. (1987). Bi-directional transfer between kindling induced by excitatory amino acids and electrical stimulation. ***Brain Research. 425, 45-48.***

[23] Mori N., Wada J. A. and Kumashiro H. (1989). Bi-directional transfer between kindling induced either by L-glutamate or L-aspartate and electrical stimulation in rats. ***Brain Research. 498 (1), 163-166.***

[24] Murry, T. K., Messenger, M. J., Ward, M. A., Woodhouse, S., Osborne, D. J., Duty, S. and O'Neill, M. J. (2002) Evaluation of the mGluR2/3 agonist LY379268 in rodent models of Parkinson's disease. ***Pharmacology, Biochemistry and Behavior, 73: 455–466.***

[25] Patel, S., Chapman, A. G., Graham, J. L., Meldrum, B. S. and Fray, P. (1990). Anticonvulsant activity of the NMDA antagonists, D-(-)4-(3 phosphonopropyi) piperazine-2-carboxylic acid (D-CPP) and D-(-)(E)-4-(3-phosphonoprop-2-enyl) piperazine-2-carboxylic acid (D-CPPene) in a rodent and a primate model of reflex epilepsy. ***Epilepsy Research, 7, 3-10.***

[26] Peterson, D. W., Collins, J. F. and Bradford, H. F. (1983). The kindling amygdala model of epilepsy: anticonvulsant action of amino acid antagonists. ***Brain Research, 275, 169-172.***

[27] Peterson, D. W., Collins, J. F. and Bradford, H. F. (1984). Anticonvulsant action of amino acid antagonists against kindled hippocampal seizures. ***Brain Research, 311, 169-176.***

[28] Phillips, J.M. and Brown, V.J (1999) Reaction time performance following unilateral striatal dopamine depletion and lesions of the subthalamic nucleusin the rat. ***Eur. J. Neurosci., 11: 1003-1010.***

[29] Phillips, J.M., Lam, H.A., Ackerson, L.C. and Maidment, N.T. (2006) Blockade of mGluR5 glutamate receptor in the subthalamic nucleus ameliorates motor asymmetry in an animal model of Parkinson's disease. ***European Journal of Neuroscience, 23: 15 –160.***

[30] Sacaan, A.I., Monn, J.A. and Schoepp, D.D. (1991) Intrastriatal injection of a selective metabotropic excitatory amino acid receptor agonist induces contralateral turning in the rat. ***J. Pharmacol. Exp. Ther. 259: 1366-70***

[31] Sacaan, A.I. and Schoepp, D.D. (1992) Activation of hippocampal metabotropic excitatory amino acid receptors leads to seizures and neuronal damage. ***Neurosci Lett. 139:77-82***

[32] Troung, L., Allbutt, H., Kassiou, M. and Henderson, J.M. (2006) Developing a preclinical model of Parkinson's disease: A study of behavior in rats with graded 6-OHDA lesions. ***Behavioral Brain Research, 169: 1 – 9.***

[33] Vázquez, E., Budd, D.C., Herrero, I., Nicholls, D.G. and Sánchez-Prieto, J. (1995) Co-existence and interaction between facilitatory and inhibitory metabotropic glutamate receptors and the inhibitory adenosine A1 receptor in cerebrocortical nerve terminals ***Neuropharmacology 34: 919-927***

[34] Vermon, A.C., Palmer, S., Datla, K.P., Zbarsky, V., Croucher, M.J. and Dexter, D.T. (2005) Neuroprotective effects of metabotropic glutamate receptor ligans in a 6-hydroxydopamine model of Parkinson's disease. ***European Journal of Neuroscience, 22: 1799–1806.***

[35] Vezzani A., Wu H. Q., Moneta E. and Samanin R. (1988). Role of the N-methyl-D- aspartate - type receptors in the development and maintenance of hippocampal kindling in rats. ***Neurosci. lett. 87, 63-68.***

[36] Wichmann, T., Marino, M.J. and Conn P.J. (2002) Dopamine modulates the function of group II and group III metabotropic glutamate receptors in the substantia nigra pars reticulate. ***J. Pharmacol. Exp. Ther., 302: 433-441***

[37] Wilkinski S. I. and Acosta G. B. (1995). Role of excitatory amino acids in neuropathology. ***Medicina (B. Aires) 55 (4) 355-365.***

[38] Willis, G.L and Kennedy, G.A (2004) The implementation of acute versus chronic animal models for treatment discovery in Parkinson's disease. *Reviews* ***in the Neurosciences, 15, 75-87***

[39] Willis, G.L. and Armstrong, S.M. (1999) A therapeutic role for melatonin antagonism in experimental models of Parkinson's disease. ***Physiologial Behavior, 66: 785 – 795.***

European Journal of Scientific Research
ISSN 1450-216X Vol.18 No.3 (2007), pp.551-560

http://www.eurojournals.com/ejsr.htm

Relationship Between Work-Family Conflicts and Work Attitudes among Secondary School Teachers in Southwest Nigeria

Samuel O. Salami
Department of Guidance and Counselling, University of Ibadan, Ibadan, Nigeria
E-mail: drsosalami2002@yahoo.co.uk

Abstract

The purpose of this study was to investigate the relationship between work-family conflict and work attitudes of secondary school teachers in Southwest Nigeria. Sample consists of 420 secondary school teachers (males = 200 females = 220) randomly selected from five states in Southwestern Nigeria. The teachers were administered measures of demographic data form, job involvement, career and organizational commitments. Data collected were analysed using hierarchical multiple regression. The study revealed that significant relationship exist between work-family conflicts and organisational commitment and not with job involvement and career commitment. Also emotional intelligence and self-efficacy moderated the relationship between work-family conflicts and work attitudes. Implications for individual teachers and organisational roles were discussed along with future research directions.

Keywords: Career commitment, organisational commitment, job involvement, self-efficacy, emotional intelligence.

Introduction

It is in the interest of organizations to retain employees, improve their work attitudes and minimize turnover. In both organisational research and practice, work attitudes such as job involvement, career and organisational commitments are important constructs because they are related to work behaviour and performance especially in high-complexity jobs (Judge & Bono, 2001; Kluger & Tikochinsky, 2001). Many authors have searched for relevant determinants of work attitudes (Carmeli, 2003; Mathiew & Zajac, 1990; Van der Velde, Bossink & Jansen, 2003). One important factor that influences work attitudes (job involvement, career and organizational commitments) is work-family conflict.

While most previous studies concern the influence of work-family conflicts or multiple role involvement on the psychological well-being of female or male workers (Allen, Herst, Bruck & Sutton, 2000; Aryee & Luk, 1996; Lee, 2004), few have investigated the relationship between work-family conflict and work attitudes (Kossek & Ozeki, 1998; Roehling, Roehling & Moen, 2001; Wentling, 1998). In this study, the relationship between work-family conflict and work attitudes (job involvement, career and organizational commitments) were investigated. Furthermore, this study investigated the moderating roles of self-efficacy and emotional intelligence in the relationship between work-family conflict and work attitudes of secondary school teachers. Unlike this study, most studies dealing with work-family conflict/multiple roles were concerned more with women in high

level jobs (Amatea & Fong, 1991; Lee, 2004). In the present research, men and women in the teaching profession who hold high level jobs in similar organizations (secondary schools) were studied.

The choice of secondary school teachers as the target population was informed by the fact that they occupy a central position in the Nigerian educational system. There are evidences to show that people join the teaching profession as the last resort when they are unable to get into other professions (Adeyemo, 2001; Salami, 1999). Indeed, the teaching profession in Nigeria is replete with teachers who lack job satisfaction, career commitment and organizational commitment (Adeyemo, 2001; Salami, 1999). High turnover has been reported among Nigerian teachers due to poor salary, intolerable working conditions, low prospects, motivation and prestige (Salami, 1999).

Many of the teachers are over-loaded with work due to the high ratio of pupils to teachers and lack of relevant teaching facilities. These teachers had been reported to be working in stressful environments (Adesoji, 2004). The submission above indicates that the job involvement, career and organisational commitments of the secondary school teachers are likely to be low and deserve being investigated.

Literature Review

Work-family conflict and work attitudes

Work-family conflict is a type of inter-role conflict in which the role demands stemming from one domain (work or family) are incompatible with role demands stemming from another domain (family or work) (Greenhaus & Beutell, 1985). A number of studies have indicated that work-family conflict is a critical factor in the behaviour and performance of workers (Frone, 2003; Kossek & Ozeki, 1998). For example, some negative consequences of extensive work-family conflict have been identified to include ineffectiveness at work and dissatisfaction with work and low commitment to jobs, careers, and organizations (Allen, Herst, Bruck & Sutton, 2000; Frone, 2003). In the present study, the extent to which work-family conflict is linked to work attitudes (job involvement, career commitment and organisational commitment) of secondary school teachers is the major concern.

Job involvement is a cognitive state of psychological identification with job and depends on the degree to which job is perceived to meet one's salient needs be they intrinsic or extrinsic (Gorn & Kanugo, 1980). In this study, job involvement is conceptualized as (a) the degree to which an individual is involved in a particular job and actively participates in it, and (b) a psychological state of identification with work in general relative to other activities (e.g. family, leisure), (Rabinowitz & Hall, 1977). Few studies have reported strong link between work-family conflict and job involvement (Higgins, Duxbury & Irving, 1992). However, Carmeli (2003) found low significant relationship between work-family conflict and job involvement. In the present study, the extent to which work-family conflict is related to job involvement is examined.

Career commitment has been defined as a person's belief in and acceptance of the values in his or her chosen occupation or career in line with work and a willingness to maintain membership in that career or occupation (Vandenberg & Scarpello, 1994). Work-family conflict had been linked with career-related factors (Allen, Herst, Bruck & Sutton, 2000; Frone, 2003; Kossek & Ozeki, 1998); however, Carmeli (2003) did not report such relationship. The concern of the present study was to consider the extent of linkage between work-family conflict and career commitment.

Organizational commitment has been defined as the extent to which an employee demonstrates a strong desire to remain a member of the organisation; the degree of willingness to exert high levels of efforts for the organisastion, belief in and acceptance of the major values and goals of the organisation (Meyer & Allen, 1991; Mowday, Steers & Porter, 1979). Mowday, Steers and Porter (1979) found that employees who exhibit higher organizational commitment are happier at their work, spend less time away from their jobs and are less likely to leave the organization.

Work-family conflict has been linked to organizational commitment by a number of researchers (Carmeli, 2003; Robinson, Simourd and Porporino, 1990). These researchers found that situational factors such as role overload, role conflict and role ambiguity explained most of the variance in commitment to the organization. The present study examines the extent to which work-family conflict is related to organizational commitment.

Moderating roles of emotional intelligence and self-efficacy

Empirical evidence have shown that work-family conflict had negative effects on work attitudes and that it may be moderated by several variables especially individual characteristics such as emotional intelligence, self-efficacy, locus of control and self-esteem (Carmeli, 2003; Martins, Eddleston & Veiga, 2002). However, emotionally intelligent individuals with high self-efficacy are likely to be able to control for family interferences with work and vice-versa or minimize the interferences to an acceptable level (Carmeli, 2003). It is expected that when individuals with high emotional intelligence and high self-efficacy experience high work-family conflict, they will reduce their job involvement, career and organizational commitments to reasonable levels in order to deal with work-family conflict.

Few studies have investigated the moderating roles of emotional intelligence and self-efficacy in the relationship between work-family conflicts and work attitudes (Carmeli, 2003; Martins et al 2002). In this study, the moderating roles of emotional intelligence and self-efficacy in the relationship between work-family conflict and work attitude are examined.

Conceptual framework

The conceptual framework that guided this study was based on Goode's role strain theory (Goode, 1960, cited in Lee, 2004) Goode's role strain theory also called the scarcity hypothesis assumes that the more roles one holds, the more likely it is that one will experience incompatible expectations and/or too many demands upon one's limited time and energy (Lee, 2004). Goode's role strain theory seems appropriate to explain the Nigerian teacher's role strain resulting from working under stress, heavy workloads, inadequate facilities, low salaries and wages outside the home, and within the home such as household task and child rearing. The role strain affects the teachers' well-being as well as their work attitudes.

Purpose of this study

The purpose of this study was to investigate the relationships of work-family conflict to work attitudes (job involvement, career and organizational commitments) of secondary school teachers and to examine the moderating roles of emotional intelligence and self-efficacy in the relationships of work-family conflict to work attitudes.

Hypotheses

(1) There is a significant negative relationship between work-family conflict and job involvement of secondary school teachers.
(2) There is a significant negative relationship between work-family conflict and career commitment of secondary school teachers.
(3) There is a significant negative relationship between work-family conflict and organizational commitment of secondary school teachers.
(4) Emotional intelligence will moderate the relationship between work-family conflict and work attitudes of secondary school teachers.
(5) Self-efficacy will moderate the relationship between work-family conflict and work attitudes of secondary school teachers.

Methodology

Research Design

The study adopted a survey research design that utilized an ex post facto research type in which questionnaires were used to collect data from the respondents.

Participants

The sample for this study was 420 secondary school teachers (males = 200, females = 220) randomly selected from five states in Southwestern Nigeria. The mean age of the teachers was 36.75 years with standard deviation of 4.30 and an age range of 21-55 years. Levels of education of the teachers include: Nigeria Certificate in Education NCE (100, 23.81%), B.A. Ed./B.Sc.Ed/B.Ed. (200, 47.62%), B.A./B.Sc. plus PGDE (75, 17.86%), M.Ed. (45, 10.71%). The teaching experience of the teachers ranged from 2 to 26 years (100, 23.81%), B.A.Ed./B.Sc.Ed/B.Ed. (200, 47.62%), B.A./B.Sc plus PGDE (75, 17.86%), M.Ed. (45, 10.71%). The teaching experience of the teachers ranged from 2 to 26 years.

Measures

Work-family conflict

Work-family conflict was measured by means of the Work-Family Conflict Scale (WFCS) by Hassan (2004). WFCS assessed the extent to which work-related roles interfere with family responsibilities. It consists of three sections. Work and Husband/Wife Subscale (7 items), work and children subscale (7 items), work and in-laws subscale (6 items). WFCS adopted a 5-point Likert type scale ranging from 1 = strongly disagree to 5 = strongly agree indicating the extent to which they agreed, or disagreed with the items on the scale. The Cronbach's alpha for the WFCS was 0.89. The scale correlates highly with Work-family Conflict scale by Netemeyer, Boles and McMurian (1996).

Job Involvement

This measure was based on a 10-item scale developed by Kanugo (1982). "Typical items are: the most important things that happen to me involve my present job" and "Most of my personal life goals are job-oriented". The scale was assessed on a five-point scale ranging from 1 = strongly disagree to 5 = strongly agree. The Cronbach's alpha for this scale was 0.83.

Career commitment

Career commitment was assessed by a 7-item scale developed by Lam, Foong, and Moo (1995). It adopted a five-point scale ranging from 1 = strongly disagree to 5 = strongly agree. The Cronbach's alpha for this scale was 0.75. The demographic and biographical information of the respondents involving age, sex, years of working experience, job position or rank, were obtained as part of the career commitment scale.

Organizational Commitment

Organizational commitment was measured by means of Organizational Commitment Questionnaire (OCQ) by Mowday, Steers and Porter (1979). The OCQ consists of 15 items that measures the individual's identification with and involvement in a particular organization. It adopted a 5-point Likert scale ranging from 1 = strongly disagree to 5 = strongly agree. The Cronbach's alpha of the scale range from .82 to .93. Mowday et al (1979) cited evidence of its convergence, discriminant and predictive validity.

Emotional Intelligence (EI)

Emotional Intelligence was assessed by means of Emotional Intelligence (EI) Scale by Law, Wong and Song (2004) known as Wong and Law EI Scale (WLEIS). This is a sixteen-item scale consisting of four sections: Self-Emotions Appraisal (SEA, 4 items), Others – Emotions Appraisal (OEA, 4 items), Use of Emotions (UOE, 4 items) and Regulation of Emotion (ROE, 4 items) that adopted a 5-point scale ranging from 1 = strongly disagree to 5 = strongly agree. The Cronbach's alphas of the four subscales range from .72 to .89.

Self-Efficacy

Self-efficacy was measured by Generalized Perceived Self-Efficacy Scale (GSE) developed by Schwarzer and Jerusalem (1995). GSES is a 10-item scale that assessed self-efficacy based on personality disposition. The scale was measured on a 4-point Likert scale ranging from 1 = Not at all true to 4 = Exactly true. The Cronbach's alpha of the scale range from .75 to .90 (Schwarzer & Jerusalem, 1995). It has high convergent and discriminant validity as it correlates positively with self-esteem and optimism and negatively with anxiety, depression and physical symptoms.

Procedure

Prospective respondents were administered the questionnaires in their secondary schools by the researcher some research assistants who were three undergraduates and three postgraduate students. The informed consents of the teachers and the school authorities were obtained. Of the 500 questionnaires distributed to the teachers 450 were returned, constituting a return rate of 90%. However, only 420 (84%) questionnaires out of the original distribution were properly filled and used for the analysis while 25 were incompletely filled and were discarded. The confidentiality of the information volunteered by the respondents was guaranteed.

Data Analysis

In order to assess the relationship of work-family conflict to work attitudes (job involvement, career commitment and organizational commitment) three hierarchical regression analyses were performed in three stages for each of the three work attitude measures.

In step 1, the three demographic factors – control variables (age, gender and working experience) were entered. The individual characteristics (emotional intelligence and self-efficacy) and work-family conflict were entered in step 2. To assess the moderating effects of emotional intelligence and self-efficacy on the relationship between work-family conflict and work attitudes, work-family conflict x emotional intelligence and work-family conflict x self-efficacy product terms were entered in step 3. Both variables were mean-centred as suggested for variables that are to be constituents of product terms (Aiken & West, 1991). This is to make the interaction terms more directly interpretable and reduce multicollinearity effects.

Results

Means, Standard Deviations and Intercorrelations of Measures

Table 1 shows means, standard deviations and zero-order correlations for all measures

Table 1: Means, Standard Deviation and Intercorrelation Matrix of all Variables in the Study

	Variables	1	2	3	4	5	6	7	8	9
1	Organizational Commitment	1.00								
2	Career Commitment	.30*	1.00							
3	Job Involvement	.22*	.20*	1.00						
4	Work-family Conflict	-.23*	-.17	-.14	1.00					
5	Gender	.08	.05	.12	.07	1.00				
6	Age	.12	.17	.25	.13	.08	1.00			
7	Working Experience	.12	.11	.09	.12	.08	.21*	1.00		
8	Emotional Intelligence	.25*	.22*	.15	0.23*	.07	.12	.15	1.00	
9	Self-efficacy	.27*	.29*	.24*	-.20*	.16	.14	.10	.21*	1.00
	Mean	52.11	27.87	44.30	48.20	1.5	38.40	8.50	58.43	37.90
	S.D.	6.50	5.25	3.50	5.20	0.45	7.60	4.20	5.90	5.80

Note: N = 420, S.D. = Standard Deviation
* P < .05 (2 Tailed Tests)

Results on Table 1 show that work-family conflict had negative significant correlation with organizational commitment but non-significant correlations with job involvement and career commitment. Emotional intelligence and self-efficacy had significant correlations with each of the work attitude measures with correlations ranging from r = 0.22 to 0.29. However, emotional intelligence did not correlate significantly with job involvement. Age, gender and working experience had no significant correlations with all the work attitudes.

Regression Analyses of Work attitudes in relation to work-family conflict, emotional intelligence and self-efficacy

Table 2: Results of hierarchical regression analysis of the prediction of work attitudes from work-family conflict

Variables Entered	Job Involvement Beta (t)	Career Commitment Beta (t)	Organizational Commitment Beta (t)
Step 1			
Gender	.03(.34)	.02(.50)	.05(.64)
Age	-.17(1.5)	.14(1.2)	.04(.58)
Working Exp.	.05(.60)	.03(.36)	.03(1.0)
R2	.08	.06	.079
F	1.50	1.20	1.30
df	3,416	3,416	3,416
Step 2			
Emotional Intelligence	.04(.50)	.30(3.25*)	.26(2.7*)
Self-Efficacy	.32(3.0*)	.27(2.8*)	.28(2.9*)
Work-family Conflict	-.03(.45)	-.02(.27)	-.20(2.1*)
R^2	.22	.31	.25
R^2_{change}	.14	.25	.18
F_{change}	6.80*	7.00*	5.40*
df	3,413	3,413	3,413
Step 3			
WFC X EI	.04(.45)	.32(3.30*)	.28(2.9*)
WFC X SELF-EFF	.05(.63)	.20(1.98)	.20(2.8*)
R^2	.26	.42	.38
R^2_{change}	.04	.11	.13
F_{change}	1.30	4.80*	5.80*
df	2,411	2,411	2,411

Note: N = 420, Working Exp. = Working Experience, WFC = Work-family Conflict, EI = Emotional Intelligence, SELF-EFF = Self Efficacy, (t) = t-values; * P < .05.

The results on table 2 show that self-efficacy interacts with work-family conflict to significantly predict career commitment (Beta = .20, t = 1.98, P < .05), and organizational commitment (Beta = .20, t = 2.8, P < .05) but not job involvement. These results partially support hypothesis 5.

The results of the hierarchical regression analysis on Table 2 show that none of the demographic factors (gender, age and work experience entered in step 1) significantly correlated with the three work attitudes. Emotional intelligence, self-efficacy and work-family conflict entered in step 2 made significant contributions to the prediction of job involvement (R^2_{change} = .14, $F_{change(3,413)}$ = 6.8, P < .05), career commitment (R^2_{change} = .25, $F_{change(3,413)}$ = 7.00, P < .05) and organizational commitment (R^2_{change} = .18, $F_{change(3,413)}$ = 5.40, P < .05). Of the three independent variables added in step 2 only self-efficacy significantly predicted job involvement (Beta = .32; t = 3.0, P < .05). That work-family conflict did not significantly predict job involvement did not support Hypothesis 1. The results on Table 2 further indicate that emotional intelligence and self-efficacy significantly predicted career commitment. That work-family conflict didn't significantly predict career commitment did not confirm hypothesis 2. Emotional intelligence, self-efficacy and work-family conflict significantly predicted organizational commitment. That work-family conflict negatively and significantly predicted organizational commitment confirms hypothesis 3.

The results of Table 2 further indicated that the interaction of emotional intelligence and work-family conflict significantly predicted career commitment (Beta = .32, t = 3.30, P < .05) and organizational commitment (Beta = .28, t = 2.90, P < .05) however, it did not significantly predict job involvement. These results partially support hypothesis 4.

Discussion

The major goal of this study was to examine the extent to which work-family conflict was related to work attitudes of secondary school teachers. This study was also designed to investigate the moderating roles of emotional intelligence and self-efficacy in the relationship.

The finding that work-family conflict didn't significantly predict job involvement is in line with the work of Carmeli (2003) who found non-significant relationship between work-family conflict and job involvement. The results however contradicted the work of previous researchers (Higgins, Duxbury and Irving, 1992) who reported significant relationship between work-family conflict and job involvement. The result could be explained by the fact that the secondary school teachers' experience of work-family conflict was not of high magnitude as to affect their job involvement. Also the urge to earn more salary to cater fro family financial commitments (economic factors) might have influenced the teachers' job involvement rather than work-family conflict. Similarly, the results from this study revealed that work-family conflict was not significantly related to career commitment. This finding was consistent with previous research findings by Carmeli (2003) who found that work-family conflict was not significantly related to career commitment. An explanation for this finding predicted career commitment and organizational commitment showing that emotional intelligence and self-efficacy moderated the negative effects of work-family conflict on career and organizational commitments. These findings are consistent with the work of Carmeli (2003) and Martins et al. (2002) who reported significant interactive effects of emotional intelligence and self-efficacy and work-family conflict on career commitment and job satisfaction.

A possible explanation for these findings is that teachers who have high emotional intelligence and high self-efficacy who experience work-family conflict are likely to possess the skills and capabilities to resolve work-family conflict such that they are still able to maintain commitments to their careers and organizations at moderate levels that allow them to meet family demands.

By this the negative influence of work-family conflict on career and organizational commitment is moderated by, emotional intelligence and self-efficacy. However, the interaction of work-family conflict and emotional intelligence and self-efficacy did not significantly predict job

involvement. These results might be because the teachers might have been involved in their jobs for economic reasons regardless of their work-family conflicts, emotional intelligence and self-efficacy.

Implications of the Findings

Given that education sector in Nigeria is often faced with the challenge of keeping and retaining qualified teachers, it is perhaps timely to investigate the relationship between work-family conflicts and work attitudes and the moderating roles of emotional intelligence and self-efficacy in the relationship. The results of this study revealed that significant relationships exit between work-family conflicts and organizational commitment of secondary school teachers.

The results of this study have implications for the roles the employing organizations can play in minimising work-family conflicts. For example, organizations could have work-family programmes such as providing family friendly, attractive and conducive working environments that will assist the teachers in balancing the work and family demands so as to resolve any work-family conflicts that may arise.

The results also have implications for the roles the individual teachers could play in attending to family needs and demands in ways that conflicts between work and family demands could be resolved. Since emotional intelligence and self-efficacy interact with work-family conflict in predicting work attitudes, organizational and counselling psychologists should mount intervention programmes designed to foster emotional intelligence and self-efficacy of teachers so as to minimize work-family conflict.

Limitations and Conclusions

One limitation of the study is that only teachers in the secondary schools were involved in the study. Future studies could involve teachers at other levels of education such as primary and tertiary educational levels. Another limitation of this study is that this is a cross-sectional study; perhaps a longitudinal study could be conducted to be able to confirm the results of this study. Despite these limitations, this study has revealed that work-family conflicts are significantly correlated with some work attitudes (career and organizational commitments) and that emotional intelligence and self-efficacy moderate the relationships.

References

[1] Adesoji, F.A. (2004). An analysis of occupational stress among science teachers in *Nigeria. Nigerian Journal of Clinical and Counselling Psychology* 10(1), 17-28.

[2] Adeyemo, D.A. (2001). A test of multiplicative effect of job and life satisfaction on the career commitment of secondary school teachers in Oyo State. *African Journal of Educational Management*, 9(1), 13-19.

[3] Aiken, L.S. & West, S.G. (1991). *Multiple regression: Testing and interpreting interactions*, Sage, Newbury Park, CA.

[4] Allen, T.D., Herst, D.E.L., Bruck, C.S. & Sutton, M. (2000). Consequences associated with work-to-family conflict: A review and agenda for future research. *Journal of Occupational, Health psychology*, 5, 278-308.

[5] Amatea, E.S. & Fong, M.L. (1991). The impact of role stressors and personal resources on the stress experience of professional women. *Psychological of Women Quarterly*, 15, 419-430.

[6] Aryee, S. & Luk, V. (1996). Work and non-work influences on the career satisfaction of dual-earner couples. *Journal of Vocational Behaviour*, 49(1), 38-52.

[7] Carmeli, A. (2003). The relationship between emotional intelligence and work attitudes, behaviour and outcomes. *Journal of Managerial Psychology*, 18(8), 788-813.

[8] Colarelli, S.M. & Bishop, R.C. (1989). Career commitment: Functions, correlates and management. *Group and Organizational Studies*, 15, 158-176.

[9] Frone, M.R. (2003). Work-family balance. In J.C. Quick & L.E. Tetrick (Eds.), *Handbook of Occupational health psychology* (pp. 143-162). Washington, D.C. American Psychological Association.

[10] Frone, M.R., Rusell, M. & Barnes, G.M. (1996). Work-family conflict, gender and health-related outcomes: A study of employed parents into two communities. *Journal of Occupational Health Psychology*, 1, 57-69.

[11] Gorn, G.J. & Kanugo, R.N. (1980). Job involvement and motivation: Are intrinsically motivated managers more job involved? *Organizational Behaviour and Human Performace*, 26, 265-277.

[12] Greenhaus, J.H. & Beutell, N.J. (1985). Sources of conflict between work and family roles. *Academy of Management Review*, 10 (1), 76-88.

[13] Hassan, E.M. (2004). Psychosocial correlates of women occupational commitment and work-family conflict in selected organizations in Ogun and Lagos States of Nigeria. Unpublished Ph.D. Thesis, University of Ibadan, Ibadan.

[14] Higgins, C., Duxbury, L. & Lee, C. (1994). Impact of life-cycle stage and gender on the ability to balance work and family responsibilities. *Family Relations*, 43, 144-150.

[15] Higgins, C.A., Durbury, L.E. & Irving, R.H. (1992). Work-family conflict in the dual-career family. *Organizational Behaviour and Human Decision Processes*, 51, 51-75.

[16] Judge, T.A. & Bono, J.E. (2001). Relationship of core self-evaluation traits – self-esteem, generalized self-efficacy, locus of control, and emotional stability with job satisfaction and performance: A meta-analysis. *Journal of Applied Psychology*, 86, 80-92.

[17] Kanugo, R.N. (1982). Measurement of job and work involvement. *Journal of Applied Psychology*, 67, 341-350.

[18] Kluger, A.N. & Tikochinsky, J. (2001). The error of accepting the "theoretical" null hypothesis: The rise, fall and resurrection of commonsense hypotheses in psychology. *Psychological Bulleting*, 127, 408-423.

[19] Kossek, E.E. & Ozeki, C. (1998). Work-family conflict policies, and the job-life satisfaction relationship: A review and directions for organizational behaviour – human resources research. *Journal of Applied Psychology*, 83, 139-149.

[20] Lam, P., Foong, Y.Y. & Moo, S.N. (1995). Job satisfaction and withdrawal cognition among prospective teachers. *South Pacific Journal of Teacher Education,* 23(2), 217-230.

[21] Law, K.S., Wong, C. & Song, L.J. (2004). The construct and criterion validity of emotional intelligence and its potential utility for management studies. *Journal of Applied Psychology*, 89(3), 483-496.

[22] Lazarus, R.S. & Folkman, S. (1984). *Stress, appraisal and coping*. New York: Sprinher.

[23] Lee, K.J. (2004). Multiple roles of married Korean women: effect on depression. *Sex Roles: A Journal of Research*. October. Retrieved 20th November 2006 from http://www.findarticles.com/particles.

[24] Marshall, N.L. & Barnett, R.C. (1993). Work-family strains and gains among two-earner couples. *Journal of Community Psychology*, 21, 64-74.

[25] Martins, L.L., Eddleston, K.A. & Veiga, J.E. (2002). Moderators of the relationship between work-family conflict and career satisfaction. *Academy of Management Journal*, 108, 171-194.

[26] Mathiew, J.E. & Zajac, D.M. (1990). A review and meta-analysis of the antecedents, correlates, and consequences of organizational commitment. *Psychological Bulleting*, 108, 171-194.

[27] Morrow, P.C. (1983). Concept redundancy in organizational research: the case of work commitment. *Academy of Management Review*, 8, 486-500.

[28] Mowday, R., Steers, R. & Porter, L. (1979). The measurement of organizational commitment. *Journal of Vocational Behaviour*, 14, 224-247.

[29] Netemeyer, R.G.; Boles, J.S. & McMurian, R. (1996). Development and validation of work-family conflict and family-work conflict scales. *Journal of Applied Psychology*, 81(4), 400-410.

[30] Rabinowitz, S. & Hall, D.T. (1977). Organisational research on job involvement. *Psychological Bulletin*, 84(2), 265-288.

[31] Robinson, D., Simourd, L. & Porporino, F. (1990). Research on staff commitment: A discussion paper. Retrieved 7th November 2006 from http://www.csc-scc.gc.ca/text/rsrch/reports/r18/r18e_e.shtmi 7/11/06

[32] Roehling, P.V., Moen, P. & Batt, R. (2003). When work spills over into the home and home spills over into work. In P. Moen (Ed.), *It's about time: Couples and careers*. Ithaca, NY: Cornell University Press.

[33] Roehling, P.V., Roehling, M.V. & Moen, P. (2001). The relationship between work-life policies and practices and employees loyalty: A life course perspective. *Journal of Family and Economic Issues*, 22, 141-170.

[34] Salami, S.O. (1999). Influence of job facets satisfaction, gender, age, marital status, and working experience on withdrawal cognition among some trainee teachers. In J.O. Obemeata, S.O. Ayodele, and M.A. Araromi (Eds.), *Evaluation in Africa*. Ibadan: Stirling Horden.

[35] Schwarzer, R. & Jerusalem, M. (1995). Generalized self-efficacy scale. In J. Weinmanr, S. Wright & M. Johnston (Eds.). *Measures in Health Psychology: A User's Portfolio*. (35-37), Windsor, U.K.: NFER-NELSON.

[36] Van de Velde, M.E.G., Bossink, G.J.H. & Jansen, P.G.W. (2003). Gender differences in the influence of professional tenure on work attitudes. *Sex Roles: A Journal of Research*, August Retrieved 7th November 2006 from http://www.findarticles.com/p/articles/mi_m2294/is_3-4_49/ai_106862382.

[37] Vandenberg, R.J. & Scarpello, V. (1994). A longitudinal assessment of the determinant relationship between employee commitments to the occupation and the organization. *Journal of Organizational Behaviour*, 15, 535-547.

[38] Wentling, R. (1998). Work and family issues: Their impact on women's career development. *New Direction for Adult and Continuing Education*, 80, 15-24.

European Journal of Scientific Research
ISSN 1450-216X Vol.18 No.3 (2007), pp.561-567

http://www.eurojournals.com/ejsr.htm

Hardware Implementation of Higher Data Rate Anti-Collision Algorithm of RFID Systems

Jahariah Sampe
Student at the Department of Electrical, Electronic and System Engineering
Univesity Kebangsaan Malaysia (UKM)
E-mail: jahariah@yahoo.com

Masuri Othman
Professor at Univesiti Kebangsaan Malaysia (UKM)
Head of VLSI design group at the Institute of Microengineering and Nanoelectronic (IMEN) in UKM, Director at the MIMOS research group in Malaysia
E-mail: masuri@vlsi.eng.ukm.my

Mahamod Ismail
Lecturer at Univesiti Kebangsaan Malaysia (UKM)
Head of MECHATOR at the Department of Electrical, Electronic and System Engineering
Univesity Kebangsaan Malaysia (UKM)
E-mail: mahamod@eng.ukm.my

Abstract

This paper presents a proposed hardware implementation of higher data rate Fast Detection Anti-collision Algorithm (higher data rate FDACA) for Radio Frequency Identification (RFID) systems. The proposed higher data rate FDACA is deterministic anti-collision technique and is based on Time Division Multiplexing (TDM). The primary FDACA is novel in terms of a faster identification by reducing the number of iterations during the identification process. The primary FDACA also reads the identification (ID) bits at once regardless of its length. It also does not require the tags to remember the instructions from the reader during the communication process. The proposed system is designed using Verilog HDL. The system is simulated using Modelsim XE II and synthesized using Xilinx synthesis technology (XST). The system has been successfully implemented in hardware using Field Programmable Grid Array (FPGA) board model Virtex II Xc2v250. The output waveforms from the FPGA have been displayed on Tektronix Logic Analyzer model TLA 5201 for real time verification. From the results, its show that the proposed higher data rate FDACA system enables to identify the tags without error until the maximum operating frequency of 160MHz. Therefore the maximum data rate of this hardware implemented anti-collision algorithm is 640 Mbps for eight bit ID length and four input/output lines.

Keywords: Deterministic anti-collision, time division multiplexing, faster identification time, real time verification.

1. Introduction

The Radio Frequency Identification (RFID) system consists of three main components reader, tag and data management software is shown in Figure 1. The reader is to write instructions to and to read data from the tags. The tags are to store data or unique Identification (ID) numbers and are basically attached to the objects to be identified. During the communication process, the tags will transmit data simultaneously to the reader and the reader will receive these data streams by using multi-access procedure. In the RFID system, the Time Division Multiplexing (TDM) procedures are the largest group of anti-collision techniques and a binary tree is one of the examples [1]. In TDM, the implementation cost will be reduced because of higher available bandwidth which is split into channels [9].

Figure 1: RFID System

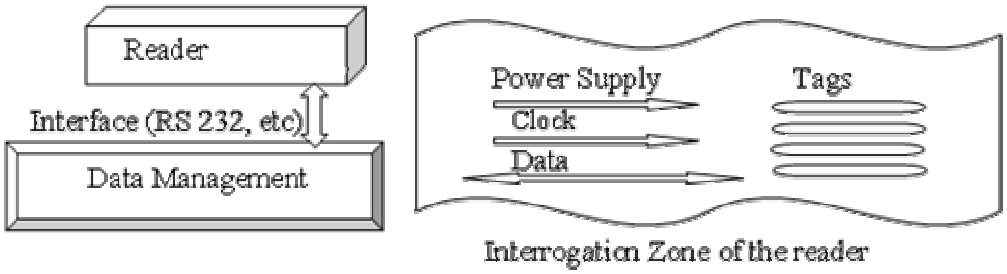

Anti-collision techniques can be classified into two; the deterministic and the stochastic/probability technique. The common deterministic technique is based on the Tree algorithm such as the Binary Tree and the Query Tree algorithms [1]-[4]. The common stochastic techniques are based on the Aloha algorithm such as the Aloha, the slotted Aloha and the frame slotted Aloha. In the Binary Tree algorithm, the identification process will first search the smallest tag's ID until the largest tag's ID follows the Binary Tree sequence. Since this algorithm is a deterministic anti-collision technique, the reader will control the communication between Tags. Therefore simple, small, low cost and low powered consumption tags can be produced. Meanwhile the drawback of the Binary Tree algorithm is its identification time is dependent on two parameters; the number of tags simultaneously exists in the interrogation zone and the length of tag's ID. If either one of these parameters is increased the identification time will increase. This algorithm also requires the tags to remember the previous instructions from the reader during the communication process.

2. FDACA Architecture

Based on the Binary Tree anti-collision algorithm, the primary Fast Detection Anti-collision Algorithm (FDACA) is proposed. The proposed primary FDACA is novel in terms of faster identification time by reducing the number of iterations needed to identify one tag. The powered tags are divided into a group of four for every read cycle in order to reduce the number of iterations during the identification process. In addition, the identification time of the proposed primary FDACA does not dependent on the length of the tag's ID. Instead of sending and receiving the ID bit by bit, the FDACA will read all the ID bits at once regardless of its length. This is performed by using the word-by-word multiplexing or byte interleaving. Meanwhile, this algorithm also does not require the tags to remember the previous instructions from the reader during the identification process. The reader transmits the read command to the tags and the tags will simultaneously backscatter its' ID bits. As a result the tag is treated as an *address carrying device* i.e. the tag only carries its identification bits. Therefore, the memoryless tag which exhibits very low power consumption can be produced [3]. During the identification process, the primary FDACA system will identify four tag's IDs simultaneously in one read cycle. The primary

FDACA will firstly identify the smallest ID bits and finally the largest one follows the two levels Binary Tree with a maximum number of four leaves is illustrated in Figure 2.

Figure 2: One read cycle of primary FDACA system

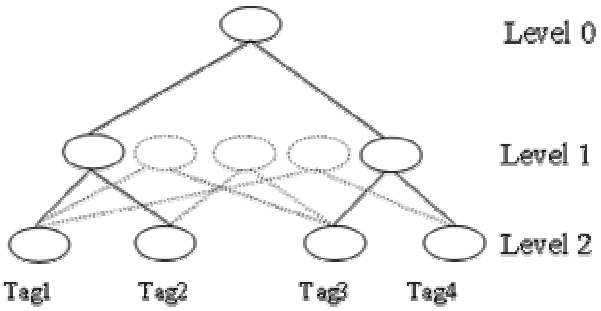

The FDACA system is based on a TDM operation. Therefore three parameters are used to measure the performance of the FDACA system; the maximum data rate (N), the length of ID bits (n) and the number of supported input/output lines (L). The identification time for FDACA system is same regardless of the length of the tag's ID and equal to one cycle of the system clock (T). Therefore, at every T interval n bits of ID is identified via the input or output lines operating at a data rate of N bit per seconds (bps) and represented in Eq. (1) [9].

$$T = \frac{n}{N} \tag{1}$$

The time required to read the input data from the input register and to write the output data to the output register in TDM-based FDACA modules is equal to $T/2$. It is called as access time (t_{acc}) and is represented as in Eq. (2) [9].

$$t_{acc} = \frac{T}{2} \tag{2}$$

Therefore, the relationship between the maximum data rate (N), the length of ID bits (n), the access time (t_{acc}) and the number of input/output lines (L) are given in Eq. (3) [9].

$$N = \frac{n}{L \times t_{acc}} \tag{3}$$

In order to increase the throughput of the primary FDACA system, the number of input/output lines (channels) should be increased. But from equation (3), it shows that if the data rate increases, the number of supported lines will be decreased and vice versa. Therefore, to increase the number of lines supported by the FDACA system per read cycle without decreasing the maximum data rate, a few primary FDACA modules can be multiplexed. For example, two primary FDACA modules are multiplexed to form input/output lines of 8 lines. The two multiplexed primary FDACA modules are called the higher data rate FDACA system.

FDACA Modules

The higher data rate FDACA system consists of one Top module and seven submodules is illustrated in Figure 3. This Top module consists of the Data-generator module, the two Clock-divider modules, the two Fast-search modules, the Select-generator module and the Read-tag module. All these modules are synchronized to a system clock so called synchronous TDM. The higher data rate FDACA system has been designed using the Verilog HDL.

The Fast-search module is the heart of the higher data rate FDACA system. In this module the tags' ID will be manipulated in such a way that there is no collision between them. For every cycle of tag clock, the search process will start by loading the four tag's IDs into four arrays of register. Then the comparators will compare these tag's IDs. The search process is performed by two ICs which use

the conditional statements (*if-else*) for the left and the right branches of the tree respectively. The four identified tag's IDs are loaded simultaneously into the output registers at the negative edge of the tag clock. All these loading processes are through the high speed multiplexing line. The operations are also synchronized by the tag clock which is equal to four times of the system clock.

The Read-tag module is partially based on the TDM operation. Each input data stream is connected to the input registers which store the incoming data from the Fast-search module. When this module is connected to the output of an input register, the contents of this register are rapidly downloaded through the high speed multiplexing line at every cycle of the system clock. Then the Read-tag Module will display the eight identified tags serially; one tag for every cycle of the system clock starts from the smallest tag's ID until the largest one. So, for every two cycles of the tag clock, eight tag's IDs will be displayed. Top module is used to implement the FDACA system in hardware using FPGA. Function of this module is very similar to the Read-tag module but is modified to suit the hardware requirements.

Figure 3: Modules of higher data rate FDACA system

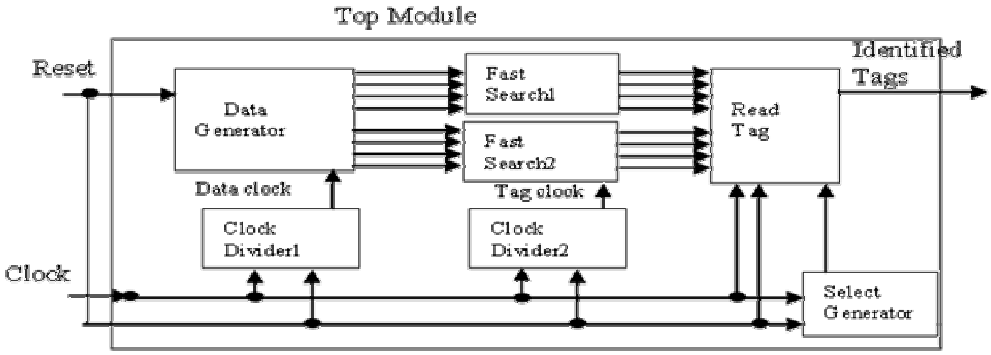

3. Simulation Results

Verilog HDL codes for the higher data rate FDACA system have been successfully simulated and verified using the ModelSim XE II/Starter 5.7g tool. Every FDACA module has been tested on its individual testbench. The FDACA modules have also been simulated and verified at each level of the simulation categories. The following will discuss the output waveforms of the Behavioral simulation for the selected modules of the higher data rate FDACA system.

Figure 4 shows eight input data inside the Data-generator modules for every cycle of the data clock. For example the first frame consists of tags' ID 08_{16}, 01_{16}, 04_{16}, $0C_{16}$, 06_{16}, 03_{16}, $0A_{16}$ and $0E_{16}$ is marked by a circle. These input data will be divided into two, four input data will go to the First Fast-search and the other four will go to the second Fast-search module.

Figure 4: Eight Input data of Data-generator module

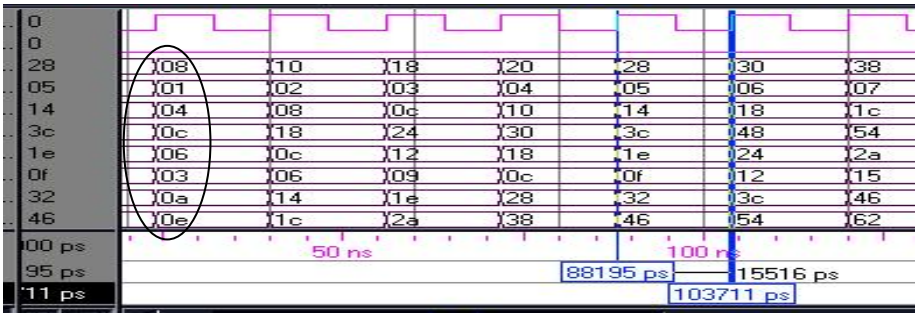

Figure 5(a) shows the output data of the first Fast-search module. For example the identified tags of the first tag clock cycle are; 01_{16}, 04_{16}, 08_{16} and $0C_{16}$ is marked by a circle. Meanwhile, Figure 5(b) shows the output data of the second Fast-search module. The identified tags of the first tag clock cycle for this module are 03_{16}, 06_{16}, $0A_{16}$ and $0E_{16}$ is marked by a circle.

Figure 5: Output of two multiplexed Fast-search Modules

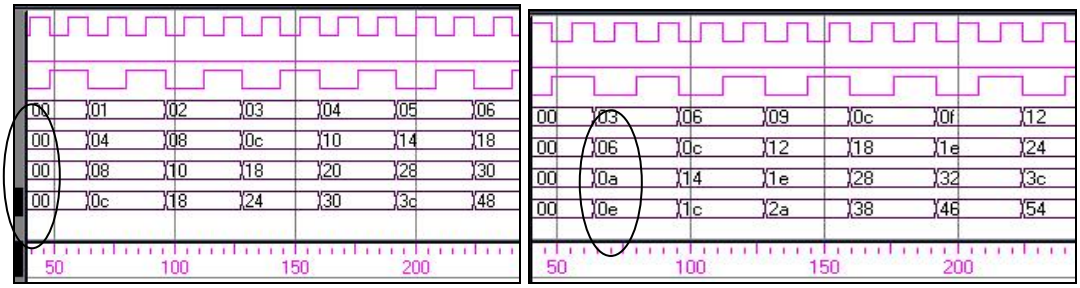

(a) First Fast-search module (b) Second Fast-search module

Figure 6 is the output data of the Read-tag module and its show that two cycles of the tag clock are required to identify eight tags' ID. For example for the input data of the Data-generator module, 0816, 01_{16}, 04_{16}, $0C_{16}$, 06_{16}, 03_{16}, $0A_{16}$ and $0E_{16}$ will be displayed serially as 01_{16}, 03_{16}, 04_{16}, 06_{16}, 08_{16}, $0A_{16}$, $0C_{16}$ and $0E_{16}$ is marked by a circle.

Figure 6: Output of Read-tag Module

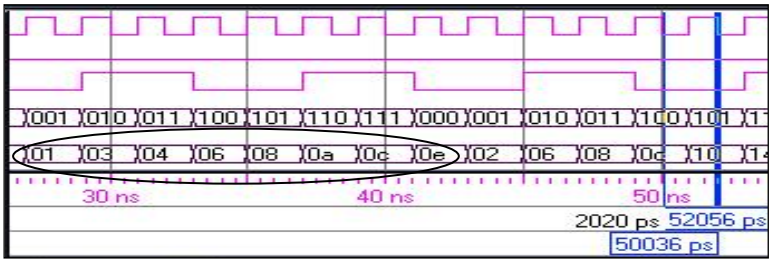

4. Design Implementation

The higher data rate FDACA system has been implemented in hardware using the Field Programmable Grid Array (FPGA) model Virtex II Xc2v250. The output waveforms from the FPGA have been displayed using the Tektronix Logic Analyzer model TLA 5201 for real time verification as shown in Figure 7 and Figure 8. The results show that the higher data rate FDACA system can still identify the tags at the operating frequency of 100 MHz without errors.

Figure 7 shows the tag's IDs have been displayed using Logic Analyzer at the operating frequency of 80MHz. For each cycle of the tag clock the tags have been identified from the smallest ID to the largest ID value. For examples the identified tags of the first tag clock cycle are; 03_{16}, 09_{16}, 10_{16}, 18_{16}, 20_{16}, 28_{16}, 30_{16} and 38_{16} is marked by a circle. The identified tags of the second tag clock cycle are; 04_{16}, $0C_{16}$, 14_{16}, $1E_{16}$, 28_{16}, 32_{16}, $3C_{16}$ and 46_{16} etc.

Figure 7: 80 MHz output waveform

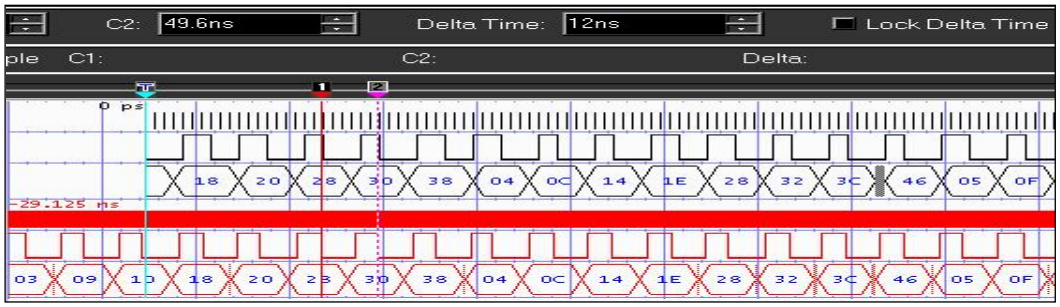

Figure 8 shows at 160 MHz, the higher data rate FDACA system can still identify the tag's IDs correctly for every cycle of the tag clock. For examples the identified tags of the first tag clock cycle are; 01_{16}, 03_{16}, 04_{16}, $0C_{16}$, 10_{16}, 14_{16}, 18_{16} and $1C_{16}$ is marked by a circle. Then, the identified tags of the second tag clock cycle are; 02_{16}, 06_{16}, 08_{16}, 12_{16}, 18_{16}, $1E_{16}$, 24_{16} and 2A16 etc.

Figure 8: 160 MHz output waveform

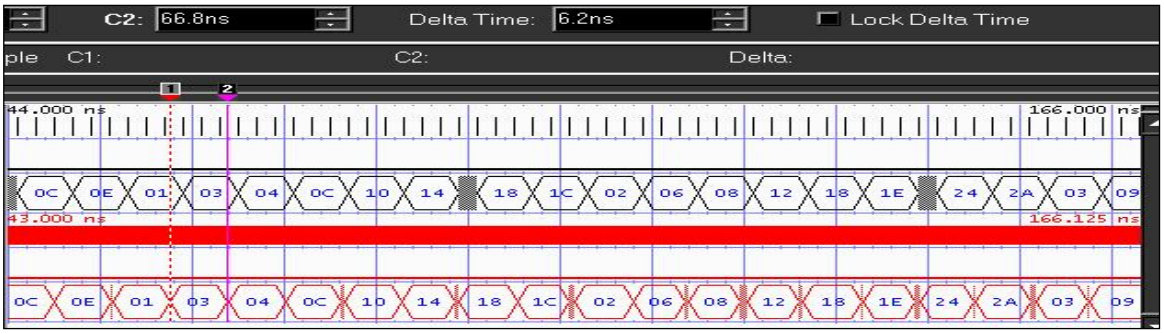

Eventhough the waveform of the tag clock cannot be displayed in this frequency, the operating frequency can be determined by using the ID duration. The identification time (T) of the tag is equal to one cycle (period) of the system clock which is equal to 6.25 ns is shown in Figure 8. Therefore, using the maximum operating frequency from the real time verification results, the maximum data rate of the higher data rate FDACA system can be determined. From the FDACA system parameters; n=8 bits, L = 4 lines and t_{acc}=3.125 ns, the maximum data rate (N) can be determined by using Eq. (3). As a result, the maximum data rate that can be supported by the higher data rate FDACA system on its each input/output line is equal to 640 Mbps. Since the identification time of the tag is same regardless of the length of the ID. Therefore, if the tag's ID length is increased the data rate of FDACA system will increase and vice versa provided the number of lines is constant.

5. Conclusion

A proposed primary Fast Detection Anti-collision Algorithm (FDACA) is presented to minimize the identification time of the deterministic anti-collision technique. The maximum data rate of this primary FDACA system is increased by multiplexing a few primary FDACA modules. A higher data rate of the multiplexed FDACA system has been successfully implemented in hardware using FPGA model Virtex II Xc2v250. The simulation output of the system has been verified in real time using Tektronix Logic Analyzer model TLA 520. From the verification results, its show that the maximum operating frequency of this hardware implemented system is 160MHz. Therefore, the system can support the maximum data rate up to 640 Mbps.

References

[1] K. Finkenzeller, and R. Waddington, "RFID handbook: fundamental and applications in Contactless Smart Cards and Identification" 2nd ed., John Wiley & Sons, 2003, pp.200-219.

[2] F. Zhou, D. Jing, C. Huang and H. Min, "Evaluating and optimizing power consumption of anti-collision protocols for applications in RFID Systems" In Proc. ISLPED'04, Newport Beach, California, USA, pp.357-362, 2004.

[3] C. Law, K. Lee and K. Y. Siu, "Efficient memoryless protocol for tag identification" In Proceedings of the 4th International Workshop on Discrete Algorithms and Methods for Mobile Computing and Communications" Boston, Massachusetts, pp.75-84, 2000

[4] MIT Auto-IDCenter, "Draft protocol specification for a 900 MHz Class 0 Radio Frequency Identification Tag". http://auto-id.mit.edu, 2003

[5] J. Myung and W. Lee, "An adaptive memoryless tag anti-collision protocol for RFID networks" IEEE INFOCOM'05, Poster Session, 2005

[6] Victor P. Nelson, H. Troy Nagle, Bill D. Carroll and J. David Irwin, "Digital logic circuit analysis & design" Prentice Hall, Inc., pp.789-831, 1995

[7] S. Sarma, D. Brock and D. Engels, "Radio Frequency Identification and the Electronic Product Code" IEEE Micro, vol. 21 No. 6, pp. 50-54, 2001

[8] Michael D. Ciletti, "Advanced digital design with the VERILOG HDL" Pearson Education Inc., 2003

[9] Edmond Zahedi "Digital data communication". Prentice Hall, pp.171-177, 2002